The Effect of Synthesis and Post-Synthesis Modifications on the Activity of Zeolite Beta for Cumene Synthesis

By

Sooviraj Hurgobin (Bsc. Chem. Eng.)

Submitted to the University of Cape Town
in fulfilment of the requirements for the degree of
MASTER OF SCIENCE IN ENGINEERING

Department of Chemical Engineering
University of Cape Town
Rondebosch 7701
Cape Town
South Africa

June 1998

ACKNOWLEDGEMENTS

I would like to thank my supervisor Professor Cyril O'Connor for all his assistance and guidance during this work. Special thanks to Leslie Petrik for her invaluable assistance, guidance and training. I would also like to acknowledge the help obtained from Dr Klaus Moller, Dr Sarah Sealy and Frank Heese who were always keen to assist me during hard times.

I am also very grateful to the FRD and the Catalysis Research Unit for financial support during this research. Special thanks to Dr Koos Jansen of the Laboratory of Organic Chemistry and Catalysis at TU Delft and Dr Michael Hunger of the Instituts fur Technische Chemie at the University of Stuttgart for the characterisation of the samples. I would like to extend my gratitude to Natasha Ristic and Marianne Walker for their contributions to this work.

Many thanks to the fellow post-graduate students in the Department of Chemical Engineering, especially the guys in the office, for their help and friendship and to the members of the staff, especially Pam, Lorna, Maria, Bill and Granville from the electronic workshop, Joachim from the workshop and Martin.

I would also like to thank my parents and brother whose support was invaluable and without whom this thesis would not have been possible. Lastly, I would like to thank my friends outside the university for their friendship and support throughout the years.

SYNOPSIS

The isopropylation of benzene to produce cumene is an important petrochemical process since cumene is used as a chemical intermediate for the production of phenol and acetone. In recent years, the good performance of zeolite Beta for this particular reaction has often been reported in the literature (Reddy *et al.*, 1993, Bellussi *et al.*, 1995 and Perego *et al.*, 1996). It is known, from the numerous studies that have been carried out on other zeolite types, that post synthesis modifications such as dealumination of the zeolite framework tend to enhance the activity of these zeolites for catalytic reactions. Moreover, the effect of synthesis parameters on the catalytic activity of zeolite Beta is an important issue that has not been thoroughly investigated in the literature.

In this study, a commercial parent zeolite Beta catalyst (sample A) was modified by post synthesis modifications such as steaming, acid washing or steaming followed by acid washing. A series of zeolite Beta catalysts were also synthesised by different techniques. The samples were characterised with respect to structure, morphology, particle size, number of acid sites, co-ordination state of aluminium and the environment of silicon atoms. The isopropylation of benzene to cumene was used as a test reaction to evaluate the effect of post-synthesis modifications and synthesis procedure on the catalytic activity of the zeolite Beta catalysts.

Steaming of the commercial zeolite Beta catalyst led to the formation of three types of extra framework aluminium (EFAl) species. XRD and XPS studies indicated that the EFAl species are most likely to be present in the pores of the zeolites as there was a decrease in the relative % crystallinity of the catalysts, no loss of bulk Al and no Al enrichment at the zeolite surface, following steaming. Hydrothermal treatment at a temperature of 600°C resulted in a greater decrease in acid site density (TPD) and bridging hydroxyl group concentration (^{1}H MAS NMR) compared to steaming at 400°C. The catalysts that were steamed at 400°C also had a higher total surface area (BET) compared to the parent catalyst and the samples steamed at 600°C. No activity enhancement for the isopropylation of benzene was observed as a result of the hydrothermal treatment and in fact, the activity of the steamed catalysts was lower compared to the parent sample. The catalysts that were steamed at 400°C performed

better that those steamed at 600°C during the course of the reaction. A fairly good correlation was obtained between the cumene yield and the number of acid sites present in the catalysts. Although no bridging hydroxyl groups and hence no Bronsted acid sites were present in one of the steamed catalysts, it was still active for the isopropylation of benzene indicating that Lewis acid sites might have played a role in this reaction. However, the presence of Lewis acid sites in the catalysts could not be confirmed as no pyridine infrared studies were carried out.

Synthesising zeolite Beta using a molar regime which resulted in rapid crystallisation, in a static medium, produced a catalyst which had the highest number of acid sites as well as the highest mesopore and total surface area among the samples synthesised by different techniques. In addition, crystals of a well-defined shape were obtained from the static synthesis. Longer synthesis times resulted in crystals with an average size of 500 nm as opposed to 200 nm crystals that were produced from rapid synthesis. The optimisation of a molar regime for lower template and hydroxide concentrations led to a longer synthesis time, which resulted in a catalyst with a higher relative % crystallinity. On the other hand, the lower relative % crystallinity of the samples synthesised by different techniques compared to sample A was attributed to a higher degree of faulting in these zeolites as ^{27}Al MAS NMR studies showed the absence of EFAl in these samples. Reaction studies showed that the catalysts which had longer synthesis times performed better during the isopropylation of benzene. A distinct splitting of the peak present at 60 ppm in the ^{27}Al MAS NMR spectra of the catalysts has been attributed to the presence of two different types of Al environments. It is proposed that the acid site associated with one of the Al environment, present in a higher concentration in the more active samples, was conducive to the isopropylation of benzene to form cumene. Furthermore, the catalysts that were synthesised by different techniques had a lower activity compared to sample A for this alkylation reaction. Diffusional constraints resulting from stacking faults and local defects in the zeolites might have resulted in the lower activity observed.

Acid washing of sample A with nitric acid of different concentrations also resulted in the formation of EFAl. However, not all three types of EFAl, as observed for the steamed catalysts, were present in all the acid washed samples. The complete removal of EFAl from one of the steamed catalysts was not achieved, after it was acid leached

with 0.01N nitric acid. The total surface area of the acid washed catalysts was higher compared to sample A and the mesopore area was found to increase with an increase in the strength of acid washing. There was no enhancement in the activity of the acid washed catalysts for the isopropylation of benzene. However, the samples that were acid washed with 0.01N, 0.1N and 1N nitric acid performed better than the catalyst subjected to a 10N acid wash and the steamed/acid leached sample during the reaction. Since the acid washed catalysts were not fully characterised, the interpretation of the reaction data with respect to their physico-chemical properties was not possible.

In general, n-propylbenzene was formed in trace amounts during the reaction and was most probably formed via the secondary isomerisation of cumene. Since very little or no o-DIPB was observed during the reaction, m-DIPB was most likely formed via the isomerisation of the primary p-DIPB isomer.

Due to the rapid deactivating nature of the catalysts, their intrinsic activity could not be properly evaluated. Since the presence of soft aliphatic coke species was detected in the coked catalysts, it was proposed that the oligomerisation of propene was favoured initially leading to the formation of coke precursors on the acid sites resulting in rapid deactivation.

TABLE OF CONTENTS

APPENDICES

LIST OF FIGURES

LIST OF TABLES

NOMENCLATURE

AAS	atomic absorption spectroscopy
Al-5	penta co-ordinated aluminium
Al/uc	number of aluminium atoms per unit cell
$(Al/uc)_{fr}$	number of framework aluminium atoms per unit cell
BEA	zeolite Beta
BET	Brunauer Emmett Teller
BJH	Barrett Joyner Halenda
CSD	crystal size distribution
D4R	double four ring
DIPB	diisopropyl benzene
DRIFTS	diffuse reflectance Fourier transform infrared spectroscopy
EDTA	ethylenediamine tetra-acetic acid
EFAl	extra-framework aluminium
EFAl-4	four co-ordinated extra-framework aluminium
EFAl-6	six co-ordinated extra-framework aluminium
EFAl-x	unknown extra-framework aluminium species
FID	flame ionisation detector
FTIR	Fourier transform infrared
GC	gas chromatograph
I_0	intensity of 0 ppm peak in ^{27}Al MAS NMR spectrum
I_{60}	intensity of 60 ppm peak in ^{27}Al MAS NMR spectrum
I_n	intensity of Si(nAl) peaks in ^{29}Si MAS NMR spectrum
IR	infrared
MAS NMR	magic angle spinning nuclear magnetic resonance
MTBE	methyl *tert*-butyl ether
Na/Al	sodium to aluminium ratio
O/T	oxygen to T atom ratio
PONA	paraffins, olefins, naphthenes and aromatics
SBU	secondary building unit
SEM	scanning electron microscopy
Si/Al	silicon to aluminium ratio

$(Si/Al)_{fr}$	framework silicon to aluminium ratio
$(Si/Al)_{gel}$	silicon to aluminium ratio of synthesis gel
Si(nAl)	silicon attached to n aluminium atoms via oxygen
SPA	solid phosphoric acid
TCD	thermal conductivity detector
TEA	tetraethylammonium ions
TEABr	tetraethylammonium bromide
TEOS	tetraethyl orthosilicate
TIPB	triisopropyl benzene
T_{max}	maximum peak temperature of TPD spectrum
TMS	tetramethoxysilane
TPD	temperature programmed desorption
USY	ultra stable Y zeolite
WHSV	weight hourly space velocity
XPS	X-Ray photoelectron spectroscopy
XRD	X-Ray diffraction

CHAPTER ONE

Introduction

1.1 ZEOLITES

Zeolites are three-dimensional crystalline aluminosilicates. They consist of corner linked tetrahedra in which the so-called 'T atoms' (Al, Si and also others such as Ga, Ge and P) lie at the centres of the tetrahedra, with oxygen atoms at the corners. Each apical oxygen atom is shared between two adjacent tetrahedra giving a framework ratio of O/T = 2 (Davis *et al.*, 1992). Pure silicate materials (SiO_2) do not contain framework charge since silicon is tetravalent. However, aluminosilicates have negatively charged oxide frameworks (one charge per framework Al^{3+}) that require charge balancing, extra-framework positive ions. Typical cations in natural zeolites are alkali metal ions, e.g Na^+ and K^+, and alkaline earth metal ions, e.g Ca^{2+} and Ba^{2+}.

The arrangement of the tetrahedral units in the macroscopic crystal results in the formation of open channels in the zeolite structure. Different arrangements yield the various zeolite types and it is this intracrystalline array of pores which confers on zeolites their remarkable properties.

In the zeolite bulk, in addition to the cations needed to neutralise the framework charge, there is room in the channels and cavities for water molecules. The open framework of zeolites also provides an environment in which cations and water molecules have a high degree of mobility, resulting in good ion exchange properties and the capacity for reversible hydration.

1.1.1 The Structure of Zeolites

The primary building units of zeolites are the tetrahedra shown in Figure 1.1. These tetrahedra (primary units) can link up in various ways to form secondary building units. The number of these so-called secondary building units (SBU's) amounts to 16 and these are shown in Figure 1.2. All zeolites can be reduced to combinations of secondary building units.

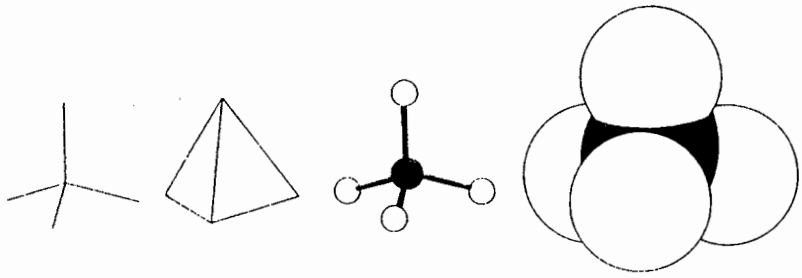

Figure 1.1. Representations of TO_4 tetrahedra.

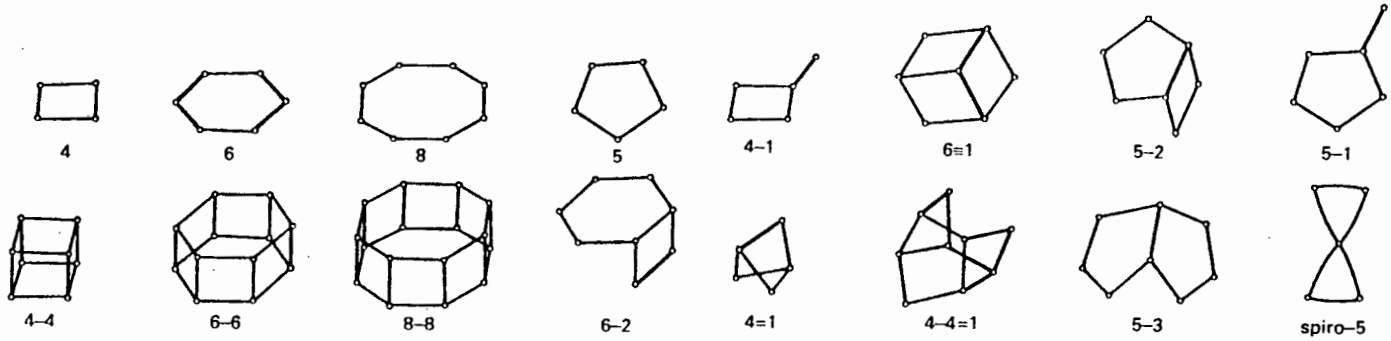

Figure 1.2. Secondary building blocks (Meier *et al.*, 1996). The T atoms are at the corners and the lines represent the O atom linkages.

These SBU's can be interconnected to give rise to a wide range of polyhedra (tertiary units). An example of such a tertiary unit is shown in Figure 1.3 and is referred to as the sodalite unit, which is found in Zeolite A and faujasitic zeolites (types X and Y).

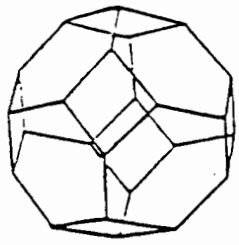

Figure 1.3a. The sodalite unit.

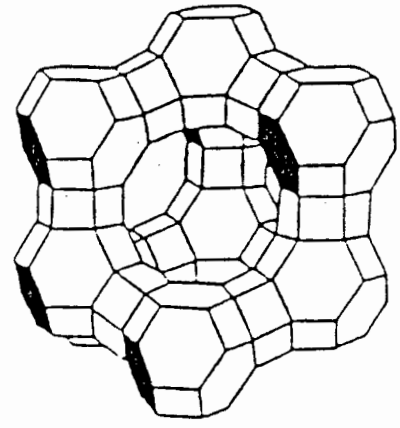

Figure 1.3b. Structure of faujasite.

The tertiary units in turn combine to form the attached frameworks of various zeolites. Since there are many different types of secondary and tertiary units, thousands of theoretical zeolite structures are possible. As shown in Figure 1.3, sodalite units and hexagonal prisms form the faujasite structure (X and Y), which has large cavities interconnected by 12 sided windows

(these large cavities are called supercages). In this way, a 3-D network of channels and cavities is formed. However, not all zeolites have cavities, many only have channels which may consist of straight parallel channels as in mordenite, or of an intersecting network as in ZSM-5.

The 3-D networks of some zeolites are shown in Figure 1.4.

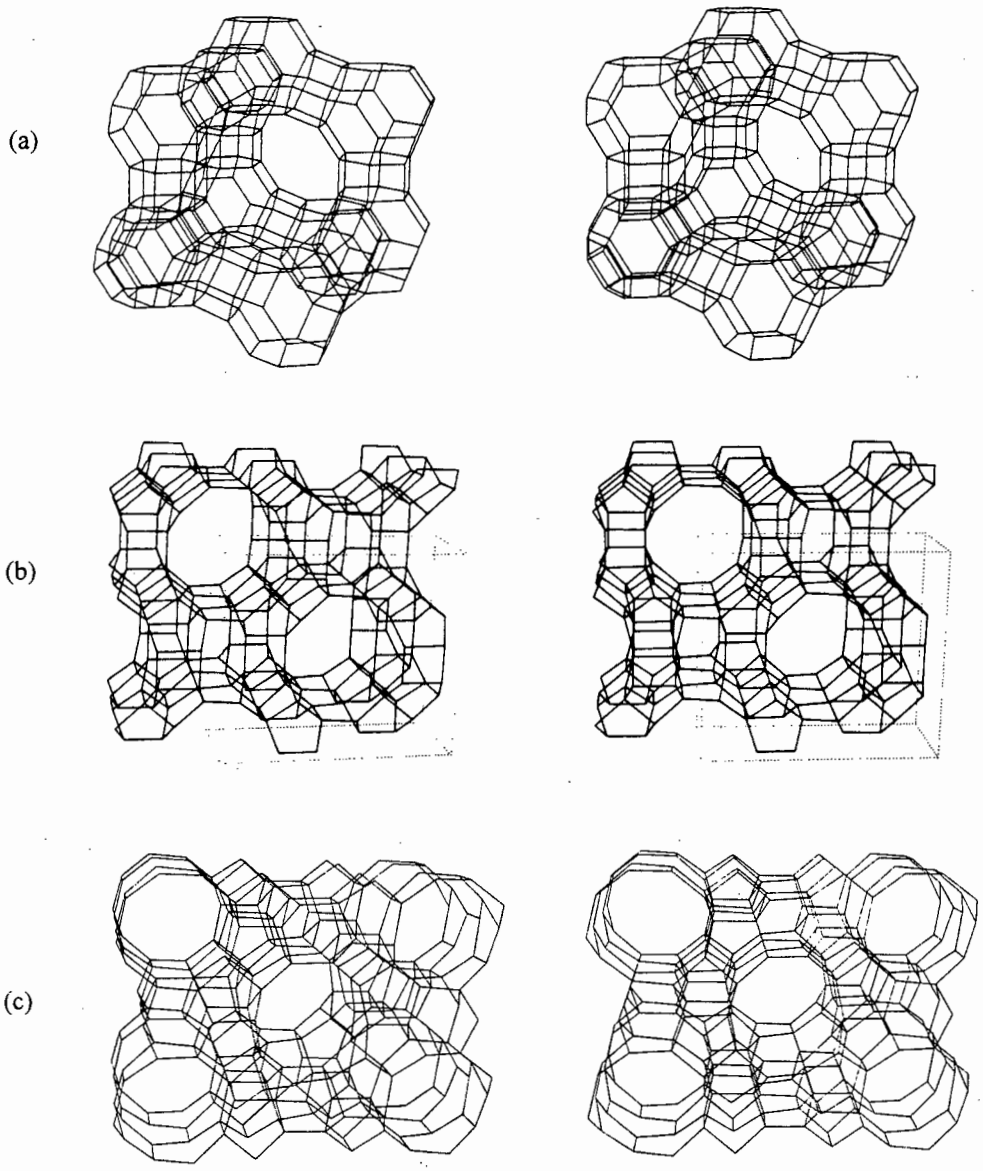

Figure 1.4. Stereoscopic representations of zeolite topologies (a) faujasite, (b) mordenite and (c) ZSM-5 (Meier *et al.*, 1996).

1.1.2 Acidity of zeolites

As it has been mentioned, zeolites are composed of tetrahedrally bound silicon and aluminium ions, joined by bridging oxygen ions. When Al^{3+} is substituted for Si^{4+} in the SiO_2 framework to form the aluminosilicate (zeolite) structure, a net negative charge results. This charge needs to be compensated and is done so by 'non-framework' cations such as Na^+. The Na^+ is not 'boxed' into the framework by oxygen atoms as are the Si and Al ions. As a result, the charge balancing cation is therefore quite mobile and is readily exchanged for other cations, e.g Ca^{2+}, Mg^{2+}, K^+ and NH_4^+.

If the Na^+ ions are exchanged for NH_4^+ ions and the zeolite subsequently calcined, NH_3 is driven off leaving protons behind. This is shown in Figure 1.5 below.

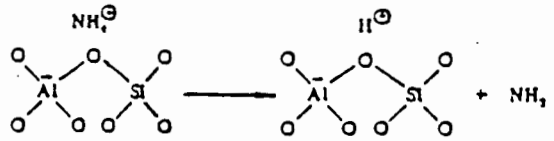

Figure 1.5. The formation of the proton form of zeolites.

Thus, the zeolites become acidic and as such are excellent solid acid catalysts. On calcining at higher temperatures (above 500°C), these 'Bronsted' acids can be converted to 'Lewis' acids as depicted in Figure 1.6 below.

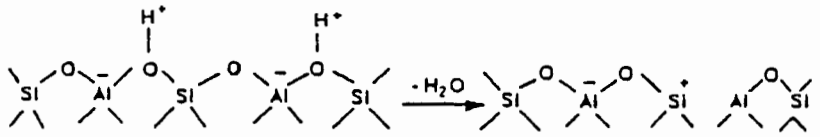

Figure 1.6. The formation of Lewis acid sites by dehydroxylation.

Lewis acid sites, which are electron acceptors, are associated with the positively charged Si. Bronsted acid sites, which are proton donors, are often the acid sites responsible for catalytic activity. The two acid sites can be distinguished by studying the infrared bands of pyridine adsorbed on the zeolite. The interaction of pyridine with the two types of acid sites is

different, thus yielding two different IR bands and thus the relative amount of the two types of acid sites can be estimated from the intensity of the bands.

1.1.3 Zeolite Beta

Zeolite Beta is a wide-pore, high silica, crystalline aluminosilicate, first synthesised by Wadlinger *et al.* (1967). The unit cell formula of the sodium form of zeolite Beta is shown below, with n being less than 7 (Meier *et al.*, 1996).

$$Na_n [Al_n Si_{64-n} O_{128}] \quad n < 7$$

The zeolite usually crystallises as an intergrowth of two polymorphs (A and B) and has a total pore volume of around 0.2 ml/g. Both polymorphs are formed from the same centrosymmetrical tertiary building unit arranged in layers. This arrangement results in a high density of stacking faults in the zeolite structure since successive layers interconnect in either a left-handed or right-handed fashion (Ratnasamy *et al.*, 1989). Polymorph A has tetragonal symmetry and exists as two enantiomorphs with either a RRRR- or a LLLL- stacking sequence. Polymorph B has monoclinic symmetry and is obtained when a recurrent alternation of right and left stacking sequence is formed (RLRLRL-). The framework structures of the two polymorphs are shown in Figure 1.7a. The disordered stacking of layers does not obstruct the micropores or affect the micropore volume (Jansen *et al.*, 1997). Furthermore, the random degree of stacking also accounts for the high concentration of framework hydroxyl groups which are formed by interplanar defect groups that arise from the stacking faults (Newsam *et al.*, 1988). On the other hand, Jansen *et al.* (1997) have stated that local defects, which arise from stacking faults, comprise of partially co-ordinated aluminium atoms that give rise to Lewis acidity in zeolite Beta.

It is proposed that the pore structure of zeolite Beta consists of channels of 12-membered rings interconnected by cages constituted by the intersections of the channels (Newsam *et al.*, 1988). The secondary building blocks that form the tertiary unit are two single 4-rings and a S-3. The 12-ring viewed from the 001 and 100 planes are shown in Figure 1.7b. The channels formed by the 12-membered ring along the 001 plane have a diameter of 7.6×6.4 Å whereas

the channels formed by the 12-membered ring along the 100 plane have a diameter of 5.5×5.5 Å. The lattice constants for zeolite Beta have been evaluated as a = 12.7 Å and c = 26.4 Å, from X-ray diffraction (Newsam *et al.*, 1988).

Furthermore, zeolite Beta is an active alkylation (Corma *et al.*, 1994 and Mitra *et al.*, 1997) and isomerisation (Ratnasamy *et al.*, 1989, Perez-Pariente *et al.*, 1991 and Boulet *et al.*, 1993) catalyst. The disproportionation of m-xylene (Perez-Pariente *et al.*, 1991) and toluene (Ratnasamy *et al.*, 1989) have also been carried out on zeolite Beta. This zeolite can behave as a bifunctional catalyst when loaded with a noble metal in the catalytic hydrodewaxing of petroleum oils, where it is able to lower the pour point of the oil (LaPierre *et al.*, 1985). Recent applications of zeolite Beta include the vapour phase nitration of fluorobenzene with N_2O_4 (Germain *et al.*, 1996) and the selective benzoylation of naphtalene to 2-benzoylnaphtalene (Bhattacharya *et al.*, 1997).

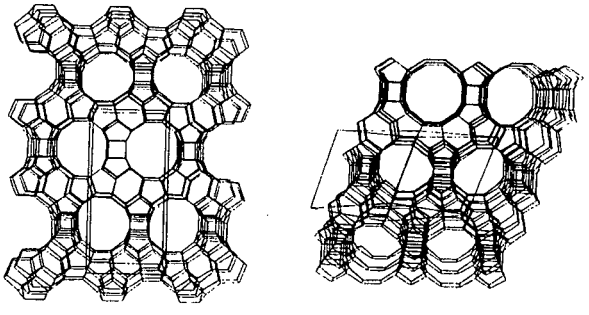

A B

Figure 1.7a. Framework structures of polymorphs A and B (Newsam *et al.*, 1988).

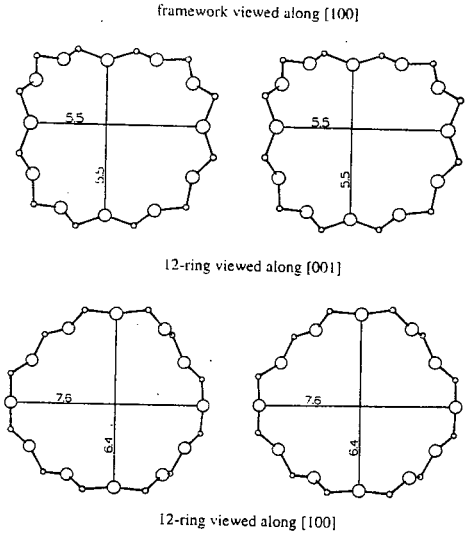

Figure 1.7b. 12-ring structure of zeolite Beta (Meier *et al.*, 1996).

1.2 SYNTHESIS OF ZEOLITE BETA

The crystallisation of high-silica zeolites such as zeolite Beta from aluminosilicate gels in hydrothermal conditions is a very complex process. Several parameters such as the nature of the organic template, the silica source, the alkali cations, the molar composition of the synthesis gel, the basicity and the synthesis temperature affect the kinetics of nucleation and crystal growth of the zeolitic phase (Perez-Pariente *et al.*, 1987). The above mentioned parameters further impact on the phase, the relative crystallinity, the crystal size and morphology, the Si/Al ratio, the acidity and the activity of the final zeolite product. Zeolite Beta is usually prepared from a synthesis mixture containing sodium aluminate, silica, tetraethylammonium (TEA) hydroxide and water.

1.2.1 Effect of Silica Source

The silica source is an important parameter in the synthesis of zeolite Beta. The degree of dissolution of the silica and therefore the concentration of monomeric silica in the solution is determined by the degree of depolymerisation of the silica source and the pH. Since the formation of zeolite Beta follows a liquid phase transformation, the dissolution of the silica may be the rate controlling step during the synthesis of Beta (Perez-Pariente *et al.*, 1988). The most common silica source used in the synthesis of zeolite Beta is tetraethyl orthosilicate (TEOS).

The reactivity and the degree of polymerisation of the silica source determine whether other crystalline phases co-crystallise with zeolite Beta or if a completely different phase is formed (Ernst and Weitkamp, 1994). The study of Bhat and Kumar (1990) on silica gel having different surface areas has revealed that only silica with the highest surface area (400 m^2/g) led to the formation of pure zeolite Beta. Silica gels having surface areas of 120 and 200 m^2/g respectively, produced zeolite Beta that was contaminated with ZSM-12.

The degree of framework defect sites present in zeolite Beta might also depend on the silica source used in the synthesis procedure. When tetraethyl orthosilicate was used by Gabelica *et al.* (1989) in the synthesis of zeolite Beta, the Na^+ concentration in the final product was low.

These authors attributed this to the fact that $Si(OH)_4$ species were progressively being released by hydrolysis and had time to form the adequate TEA^+ aluminosilicate precursors. As a result, few Si-O-Na defect sites were formed. However, when Aerosil was used as a silica source, a highly defective structure was obtained. This was probably due to the fact that Aerosil, being highly reactive, makes silica readily available for addition and thus, the silica anion is randomly neutralised by either TEA^+ or Na^+.

Moreover, when zeolite Beta was synthesised using TEOS as silica source, a more active, stable and selective catalyst was obtained than when using Aerosil as silica source. Corma *et al.* (1994) attributed this observation to a better incorporation of Si into the zeolite framework, thus leading to a higher stability towards dealumination.

1.2.2 Effect of Molar Regime

In the hydrothermal synthesis of zeolites, the alkalinity (pH) of the synthesis gel plays a key role as a mineralising agent (Feijen *et al.*, 1994). The part played by the mineralising agent during synthesis involves bringing the Si and Al oxides or hydroxides into the solution at an adequate rate. Often an optimum range of pH is required for the crystallisation of a pure zeolite phase. This behaviour has also been observed for zeolite Beta for which an optimum OH^-/SiO_2 exists, above which the zeolite nuclei redissolve and thus the crystallisation rate is decreased (Bhat and Kumar, 1990). At high pH values, the crystal size increases indicating a slower nucleation rate (Perez-Pariente *et al.*, 1987).

The basic building blocks of any zeolite structure are silicon and aluminium. Therefore, the SiO_2/Al_2O_3 ratio of the synthesis gel has an important effect on the actual synthesis and on the properties of the zeolite. As the aluminium content of the gel increases, the incorporation of silicon in the zeolite framework is more efficient, resulting in a higher yield of the zeolite (Bhat and Kumar, 1990, Eapen *et al.*, 1994 and Corma *et al.*, 1994). Also, the SiO_2/Al_2O_3 ratio of the gel has an influence on the type of phase that is formed during the synthesis of zeolite Beta. Eapen *et al.* (1994) have found that below a SiO_2/Al_2O_3 ratio of 15, an analcime phase was formed whereas ZSM-12 was formed above a SiO_2/Al_2O_3 ratio of 58, in the molar regime they used to synthesise zeolite Beta. Moreover, both the induction period and the

crystallisation rate are affected by the Si/Al ratio of the gel. As the concentration of SiO_2 in the gel increases, the induction period is shortened whereas the crystallisation rate increases (Bhat and Kumar, 1990 and Eapen *et al.*, 1994). However, Camblor *et al.* (1991) have found that a high SiO_2/Al_2O_3 ratio resulted in a decrease in both the crystallisation and nucleation rates. These authors have also reported that the average crystal size increased with higher ratios, but fewer crystals were produced per unit mass of gel.

Another important parameter that influences the overall synthesis time and/or the crystallinity of the final zeolite Beta product is the water content of the synthesis gel. A slight increase in the induction/nucleation period of the synthesis has been observed with an increase in dilution (high H_2O/SiO_2 ratio) of the synthesis gel (Perez-Pariente *et al.*, 1988, Bhat and Kumar, 1990 and Eapen *et al.*, 1994). Although a faster rate of crystallisation has been reported by Bhat and Kumar (1990), Camblor *et al.*, (1991), Leu *et al.*, (1991) and Eapen *et al.*, (1994) for a more concentrated (low H_2O/SiO_2 ratio) gel, Perez-Pariente *et al.*, (1988) have not observed any significant effect of the water content on the crystallisation rate. On the other hand, the zeolite that crystallises from a more concentrated gel has a lower average crystal size (Camblor *et al.*, 1991).

It should however be noted that the results from the various studies that are being compared in this literature review, were obtained using different molar regimes. These are shown in Table 1.1.

Table 1.1. Molar concentrations of reagents (normalised with respect to Al_2O_3) and temperature used for zeolite Beta synthesis in the literature.

Paper	Na_2O	K_2O	SiO_2	TEAOH	H_2O	Temp./°C
Perez-Pariente et al. (1987)	1.6	0.36	20	10	240	100
	1.5	0.54	30	15	360	
	3.0 (+ NaCl)	0.54	30	15	360	
	1.8	0.54	30	15	360	
	2.5	0.49	30	13.6	360	
	7.8	0.11	30	3	360	
	3.0	0.54	30	15	360	
	4.5	0.54	30	15	360	
	2.4	1.08	60	30	720	
	3.2	1.8	100	50	1200	
Perez-Pariente et al. (1988)	1.5	0.54	30	15	360	100
Bhat and Kumar (1990)	3	-	60	10	1500	150
Camblor et al. (1991)	x	y	50 (static)	25	1500	135
		y/(x+y)= 0.47	50	25	1500	
			50	25	750	
		y/(x+y)= 0.33	30	15	450	
			50	25	750	
			100	50	1500	
			400	200	6000	
			50	20	750	
			50	15	750	
Leu et al. (1991)	1.0	-	13.6	4.6	220	152
Eapen et al. (1994)	3.1	-	35	10 TEA 15 $(NH_4)_2O$	656	100-142
Corma et al. (1994)	1.98	0.77	50	25	750	135
	3.94	1.94	100	50	1500	135
	1.6	1.42	50	25	750	135
	2.94	0	50	25	750	135
	1.45	0	50	25	600	120

1.2.3 Effect of Agitation

In order to ensure the homogeneity of reactants, the synthesis gel is stirred while being mixed. Once the gel is in the synthesis autoclave, it does not need to be agitated in order for zeolite Beta to form (Wadlinger *et al.*, 1967). Hence, the formation of zeolite Beta in the

crystallisation phase does not depend on agitation. However, agitation of the gel during synthesis shortens the induction time and the overall crystallisation time.

Although agitation affects the crystal size distribution (CSD) of the final zeolite product, the average crystal size is not affected. Figure 1.8 shows the effect of agitation on the crystal size distribution of zeolite Beta. When the synthesis gel is stirred, a wider distribution is obtained unlike the static system where no small or large crystals are formed. Camblor *et al.* (1991) attributed the difference in the CSD's to changes in the relative rates of nucleation and growth. The bimodal CSD obtained as a result of agitation is an indication that nucleation takes place during crystal growth (Camblor *et al.*, 1991).

Furthermore, agitation was found to have little or no influence on the framework Si/Al ratio of zeolite Beta (Camblor *et al.*, 1991). However, the cation content is affected by agitation as the zeolite produced in an agitated system has a higher Al/(Na + K) ratio than that produced without agitation (Camblor *et al.*, 1991).

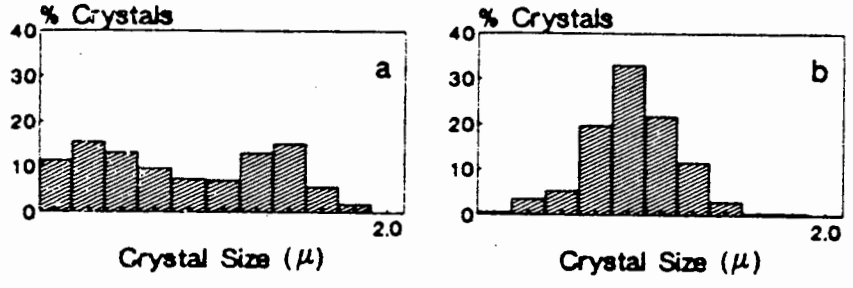

Figure 1.8. CSD of zeolite Beta under (a) agitation and (b) static synthesis (Camblor *et al.*, 1991).

1.3 DEALUMINATION OF ZEOLITES

The acid properties and resultant catalytic activity of zeolite materials are known to be related to the degree of substitution of aluminium for silicon in the framework (Campbell *et al.*, 1996_a). It has been established that high silica (aluminium deficient) zeolites possess remarkable thermal stability (e.g McDaniel and Maher, 1968) and catalytic activity (e.g Lago *et al.*, 1986). Silica-rich zeolites can be prepared in two different ways. Firstly, synthesis conditions can be chosen in such a way that a zeolitic material with a high Si/Al ratio is obtained. Alternatively, a zeolite with a low Si/Al ratio can be chemically or thermally treated, to remove part of the aluminium from the zeolite framework, in a process known as dealumination. In the first decades after the discovery of zeolite catalysis, efforts were directed towards the synthesis of high silica zeolites. But, through the years, dealumination has become a common procedure to increase the Si/Al ratio of zeolites in general.

1.3.1 Methods of Dealumination

Barrer and Makki (1964) were the first to report zeolite dealumination. They removed aluminium from clinoptilolite by treating the zeolite with hydrochloric acid of different strengths. In the literature, dealumination studies have been mostly carried out on zeolite Y, ZSM-5 and mordenite. However, the dealumination of zeolite Beta has only been investigated in recent years. Zeolite dealumination can be achieved by hydrothermal treatment, treatment with mineral acids, a combination of both hydrothermal treatment and acid leaching and reactions with a variety of reagents including chelating agents, $SiCl_4$ vapour and $(NH_4)_2SiF_6$.

1.3.1.1 Hydrothermal Treatment

This method of dealumination involves the calcination of the zeolite at relatively high temperatures in the presence of steam (Scherzer, 1984). Also, the hydrothermal treatment can be carried out under the so-called "self steaming" conditions where the wet zeolite is calcined in a static atmosphere. The latter procedure has been used by McDaniel and Maher (1968) to prepare two types of ultra stable Y zeolite (USY). However, Kerr (1969) has shown that the calcination environment and the bed geometry (deep bed v/s shallow bed calcination) play a significant role in the formation of USY zeolites. On the other hand, Ward (1970) was able to

prepare USY zeolites by treating an ammonium Y zeolite in steam. These samples had the same characteristics as the self steamed ones.

Scherzer (1984) has reported that hydrothermal treatment results in the expulsion of tetrahedral aluminium from the framework into non-framework positions, but the aluminium is not necessarily removed from the zeolite bulk. The process leads to the formation of neutral and cationic species referred to as extra-framework aluminium (EFAl). It has also been shown that during hydrothermal treatment of zeolites, a structural rearrangement of the zeolite framework occurs. The defect sites, formed as a result of dealumination, are filled to a large extent by silicon, giving rise to a very stable siliceous framework. Hydroxyl nests normally occur at defect sites that do not undergo silicon insertion. These nests however are not thermally stable. Figure 1.9 shows a schematic representation of the physical phenomena that occur during the steaming of a crystal of NH_4-Y zeolite.

The effect of various parameters on the degree of dealumination during the hydrothermal treatment of zeolite NH_4NaY has been investigated by Wang *et al.* (1991). The percentage of dealumination increases rapidly with time during the first 2-3 hours of treatment, subsequently slowing down. An increase in temperature and water vapour pressure have also been found to increase the degree of dealumination. A loss in crystallinity was observed in all the above mentioned cases.

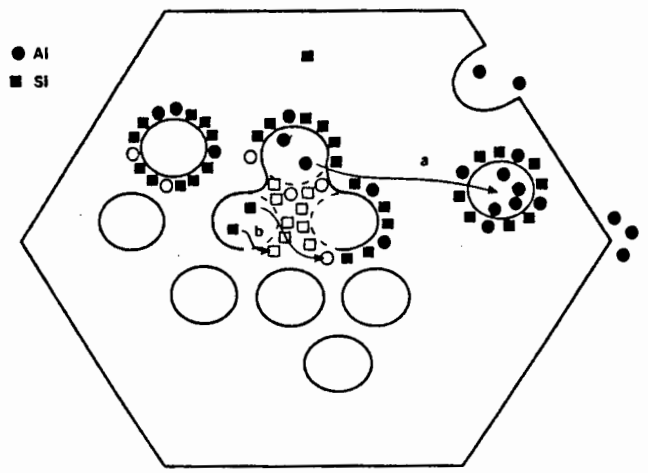

Figure 1.9. Schematic representation of the physicochemical phenomena occuring during the steaming of a crystal of NH_4-Y zeolite: (a) Dislodging and migration of framework Al towards the crystal surface; (b) Annealing with silicon of the vacancies left in the framework (Martens *et al.*, 1997).

1.3.1.2 Acid Leaching

Acid leaching has been used in the early days by Barrer and Makki (1964) to extract aluminium from clinoptilolite. In the literature, work on acid leaching has been mostly carried out on mordenite. Usually, the starting material is stirred in a solution of nitric or hydrochloric acid. The degree of dealumination depends on the temperature, concentration of the mineral acid, the zeolite/acid ratio, treatment time and the number of extraction steps. Coutanceau *et al.* (1997) have reported the presence of two distinct periods in the dealumination of zeolite Beta using hydrochloric acid as dealuminating agent. A rapid initial period corresponds to the elimination of the aluminium species that are partially disconnected from the framework. The second period is attributed to the removal of normal framework aluminium and occurs at a much slower rate. The same authors have also reported that the reaction order with respect to the number of framework aluminium per unit cell is 1.

1.3.1.3 Combined Steaming and Acid Leaching

Combined steaming and acid leaching is a two step process in which thermal or hydrothermal treatment is usually followed by acid leaching. High temperatures and steam enhance the expulsion of aluminium from the framework. The acid leaching in the two-step process involves the solubilisation of primarily non-framework aluminium formed during the thermal/hydrothermal treatment (Scherzer, 1984). Acid leaching after steaming can however remove more framework aluminium. This observation has been made by Hays *et al.* (1984) and Lohse *et al.* (1987) on dealuminated mordenite and Y zeolite respectively. Furthermore, Patzelova *et al.* (1989) have reported that acid leaching does not cause any further loss in crystallinity following the hydrothermal treatment.

If the two-step process is repeatedly carried out on the same material, the thermal treatment following acid leaching results in further expulsion of framework aluminium. The solubilisation of the non-framework aluminium from the initial acid treatment appears to ease further dealumination of the zeolite framework during subsequent thermal treatment due to altered steric and electrostatic parameters in the zeolite channels (Scherzer, 1984). An additional acid treatment can be used to solubilise the newly formed non-framework aluminium species. This cyclic method can be used to achieve the complete removal of aluminium from a zeolite framework. Kornatowski (1992) reports that the best way to obtain

the most open pore structure in dealuminated ZSM-5 is by leaching with acid followed by steaming and final leaching.

1.3.1.4 Dealumination using Chelating Agents

Chelating agents such as EDTA have been mainly used for the partial dealumination of faujasite type zeolites. This method of dealumination was first reported by Kerr (1968), who used it to prepare aluminium deficient Y zeolites. A degree of dealumination of up to 50% has been achieved without any significant loss in crystallinity following the EDTA treatment. Beaumont and Barthomeuf (1972) used acetylacetone as chelating agent to dealuminate zeolite X. More recently, the extraction of aluminium from zeolite Beta has been carried out using oxalic acid (Apelian *et al.*, 1996). The oxalic acid removes framework aluminium and transports it out of the zeolite as a water soluble aluminium-oxalate species. The features of the oxalic acid treatment are a contraction of the zeolite lattice structure and retention of crystallinity. Furthermore, organic sulphonic acids such as methanesulphonic acid have been used for the dealumination of zeolite Beta and a high degree of aluminium removal was achieved without significant loss in crystallinity (Saxton *et al.*, 1996).

1.3.1.5 Dealumination using Fluoride Containing Compounds

Skeels and Breck (1984) were the first to report the successful dealumination of zeolites using $(NH_4)_2SiF_6$ as dealuminating agent. The degree of dealumination varied between 40 and 60%. This method has subsequently been used by Karge *et al.* (1991), Das *et al.* (1996) and Silva *et al.* (1996) to dealuminate zeolite Y, zeolite Beta and mordenite respectively. On the other hand, Parikh *et al.* (1994) and Corma *et al.* (1996) used $(NH_4)_2SiF_6$ to selectively remove extra-framework aluminium from the pores of zeolite Beta and USY respectively, following hydrothermal treatment. Moreover, Sur and Bryant (1996) used a solution of potassium fluoride to extract aluminium from NaY.

1.3.1.6 Dealumination using Other Compounds

Beyer and Belenykaia (1980) were able to dealuminate zeolite Y by a silicon tetrachloride vapour treatment. The product of this dealumination procedure, $AlCl_3$, is volatile under the treatment conditions (730 to 830 K). The degree of dealumination achieved in this case is

about 26% without significant loss in crystallinity. The use of a chromium chloride solution for the dealumination of zeolites has also been reported in the literature.

1.3.2 Mechanisms of Dealumination

Studies on the mechanisms of dealumination have been mainly carried out on Y zeolites and mordenite. These can be applied to zeolites in general as they do not depend on crystal structure. Wang *et al.* (1991) have reported a mechanism for the hydrothermal dealumination of NH_4Y zeolite. The procedure consists of a high temperature hydrolysis of Si-O-Al bonds and leads to the formation of neutral and cationic aluminium species as shown below.

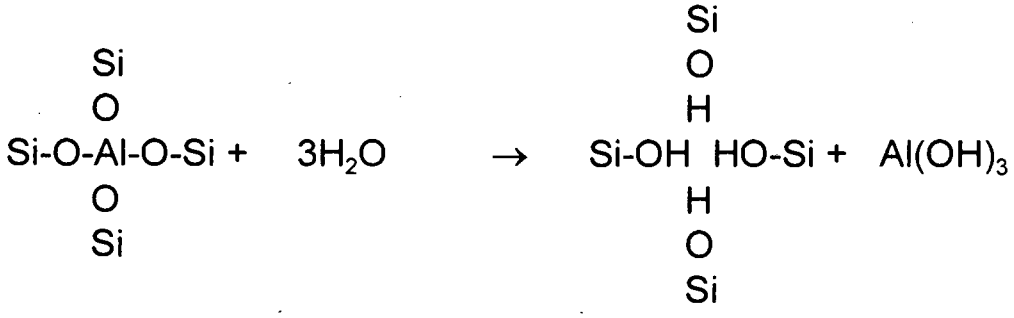

XPS data supports the fact that the extra-framework aluminium, that are formed during hydrothermal treatment, tend to migrate to the zeolite surface. The defect sites created by dealumination are subsequently repaired by undergoing silicon insertion as shown below.

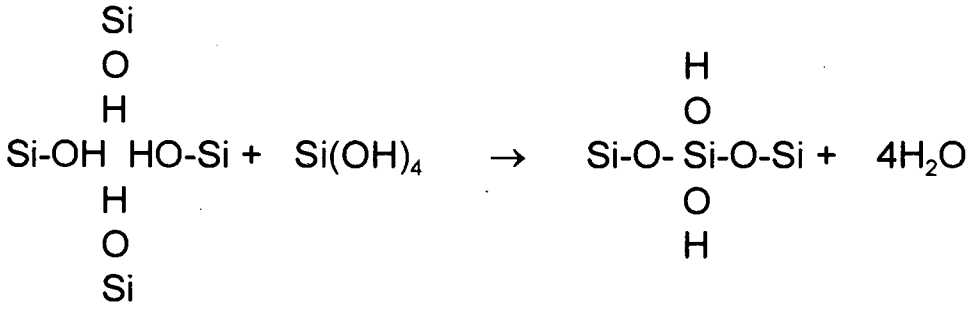

Wang *et al.* (1991) have reported that during conditions of self-steaming, the filling of the defect sites by silicon is slower than the dealumination process. This can be explained by the fact that since the amount of water is small during such dealumination, the migration of hydroxylated silicic species, occurs more slowly than the dealumination steps. Moreover, some collapse of the zeolite framework during dealumination is necessary in order to create the extra-framework silicic species needed to repair the defect sites.

Wang *et al.* (1991) have also stated that steaming can be divided into two periods. In the initial period (first 3 hours of treatment), dealumination occurs rapidly with a reaction order with respect to water of about 0.5. This period is characterised by the fact that the repair of the defect sites through silicon insertion is more rapid than the dealumination. However, there follows a period in which the dealumination is slower with a reaction order with respect to water of 1. This can be attributed to increased diffusion limitations for the water molecules due to the deposition of extra-framework aluminium species on the outer zeolite surface or on the walls of the mesopores created during dealumination. Furthermore, the exchange of the protonic zeolite by cationic extra-framework aluminium species can result in the observed slow dealumination rate.

Hydrothermal treatment has been shown to result in the stabilisation of the zeolite framework. Different reaction mechanisms have been postulated in order to explain this observation. The formation of new Si-O-Si bonds at the hydroxyl nests by elimination of water has been proposed by Scherzer (1984). A schematic representation of the mechanism is shown below.

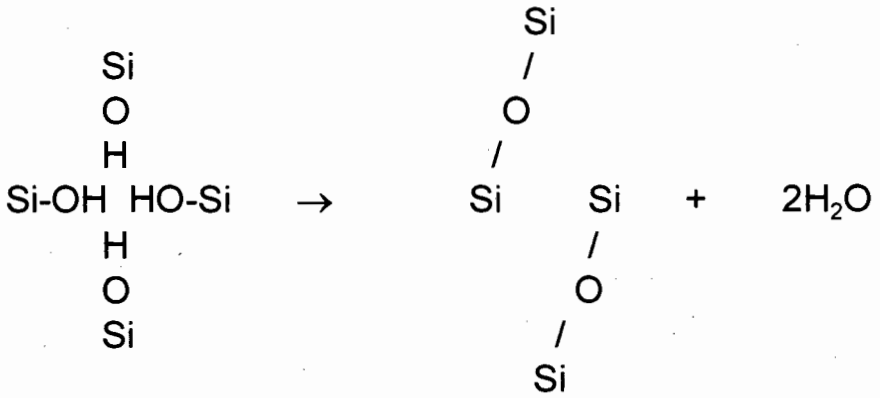

Maher *et al.* (1971) were the first to suggest that the vacancies left by dealumination undergo silica insertion. A similar conclusion was made by Wang *et al.* (1991) and recent sorption studies tend to support this mechanism. It is postulated that the silica required to repair the defect sites originates from those parts of the zeolite framework that collapse during hydrothermal treatment. The freed silicon migrates to the remaining framework vacancies, which undergo silicon insertion. This tends to increase framework stability.

On the other hand, the so-called T-jump mechanism has been proposed by Von Ballmoos (1981) to account for increased framework stability following dealumination. Figure 1.10

represents the T-jump mechanism schematically. This interpretation of framework stabilisation assumes the gradual migration of the vacancies created by framework dealumination from the zeolite interior to its surface, by exchanging places with neighbouring T-atoms (Al or Si). The integrity of the bulk zeolite crystal is thus restored.

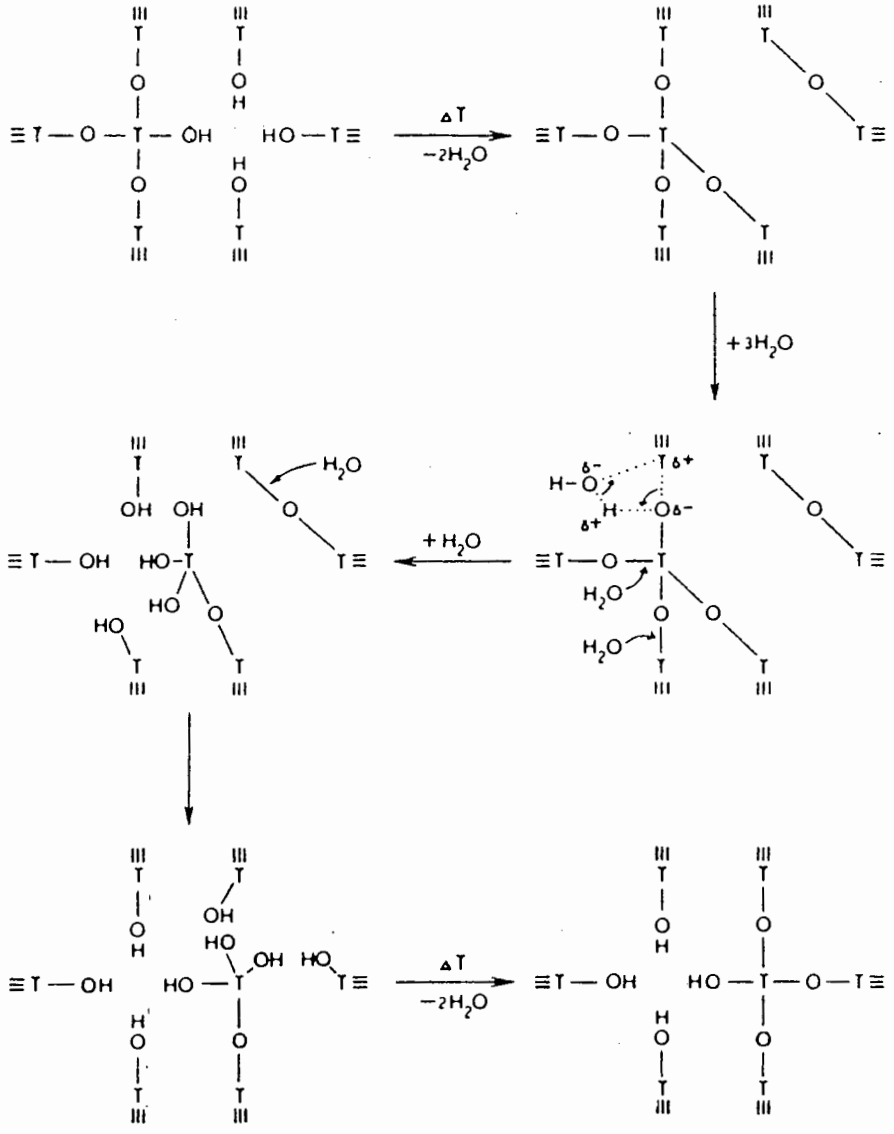

Figure 1.10. "T-Jump mechanism" (from Scherzer, 1984).

Barrer and Makki (1964) were the first to propose a mechanism for the dealumination of clinoptilolite by hydrochloric acid. Aluminium is extracted in a soluble form and is replaced by a nest of four hydroxyl groups as shown below.

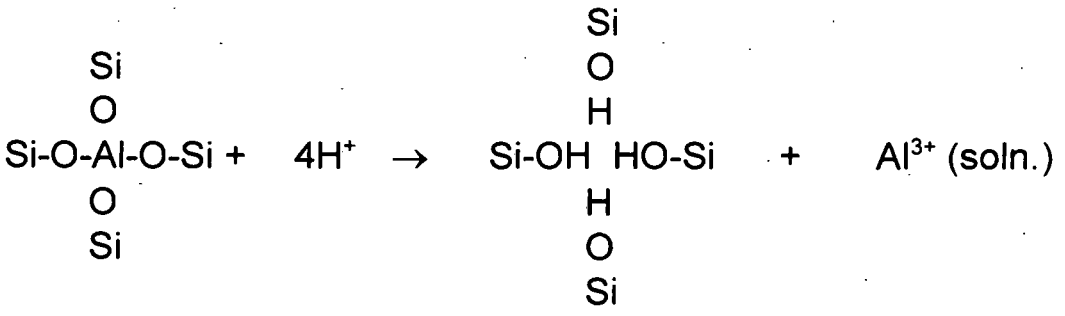

On the other hand, Kerr (1968) postulated that framework dealumination by chelating agents such as EDTA involved a similar mechanism to hydrothermal treatment, that is, the hydrolysis of Si-O-Al bonds. This is followed by the formation of a soluble chelate between cationic extra-framework aluminium and EDTA.

A reaction mechanism for combined hydrothermal and acid leaching of zeolites has been proposed by Scherzer (1984). The mechanism for the hydrothermal treatment has already been discussed. The acid treatment mostly involves the solubilisation of the cationic and neutral extra-framework aluminium species created during steaming. This is illustrated by the following reactions:

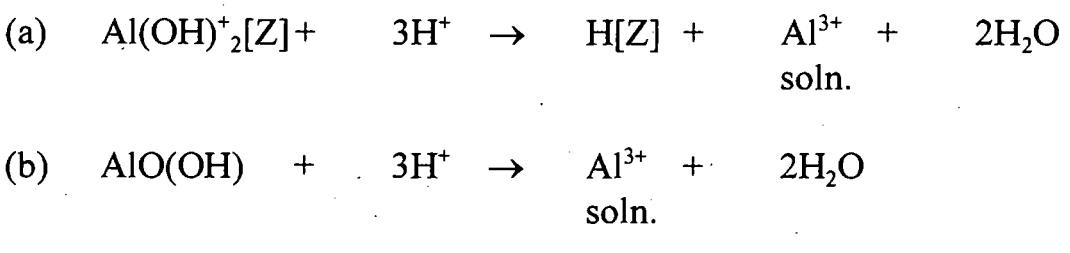

[Z] refers to the zeolite

Reaction (a) involves the ionic exchange and solubilisation of the cationic extra-framework aluminium species, where as in reaction (b), solubilisation of the neutral species takes place. If the solubilisation of some framework aluminium occurs during the two-step dealumination procedure, the reaction whereby aluminum is extracted in a soluble form and replaced by a nest of four hydroxyl groups, also takes place.

1.3.3 Physical and Chemical Characteristics of Dealuminated Zeolites

The structural changes that take place within a zeolitic material upon dealumination have been investigated by a number of characterisation techniques.

1.3.3.1 X-Ray Diffraction (XRD)

X-Ray diffraction has been used to identify particular zeolites since each zeolite has a unique XRD pattern. Furthermore, this technique can provide information about the unit cell parameters, hence unit cell volume and crystallinity of a zeolite.

In general, dealumination of zeolites has no significant effect on crystallinity. Scherzer (1978) has reported that Y zeolite retained its crystallinity after being hydrothermally treated and acid leached. Similar observations have been made by Kim *et al.* (1995) on dealuminated mordenite, Sur and Bryant (1996) on fluoride treated NaY, Rakiewicz *et al.* (1996) on a highly dealuminated faujasite, Apelian *et al.* (1996) on zeolite Beta dealuminated by oxalic acid treatment and Coutanceau *et al.* (1997) on acid treated zeolite Beta. However, Meyers *et al.* (1986) have shown that at high steaming temperatures (850°C), the crystallinity of USY decreased by 50% after 1 hour time on stream. The zeolite was completely destroyed after a 5 hour treatment in steam at 850°C. No crystallinity losses were observed at 650°C and only a moderate loss in crystallinity was found at 750°C. On the other hand, the studies of Vedrine *et al.* (1986) revealed that the crystallinity of offretite decreased significantly after being subjected to a hydrothermal treatment at 597°C for 3 hours.

Moreover, the unit cell parameters of a zeolite decrease upon dealumination due to the removal of aluminium from the framework. This leads to a decrease in the unit cell volume and hence, a contraction in the zeolite lattice structure. This observation has been made by Sun *et al.* (1991) on dealuminated zeolite Y and Hong and Fripiat (1995) on dealuminated zeolites Y, ZSM-5 and mordenite. Although all three unit cell parameters tend to decrease initially upon dealumination, only a_o continues a very slow contraction with progressive dealumination, whereas there is no further contraction in b_o and c_o. This finding was confirmed by the studies of Meyers *et al.* (1988) on dealuminated mordenite, Vedrine *et al.* (1986) on offretite and Meyers *et al.* (1986) on USY.

A 2θ shift in position towards higher angles, upon dealumination, is indicative of the removal of framework aluminium, resulting in a less ordered framework structure and a contraction in the lattice (Vedrine *et al.*, 1986, Apelian *et al.*, 1996). However, Kornatowski *et al.* (1992) and Long *et al.* (1996) have shown that a combination of steaming and acid leaching on ZSM-5 led to a better ordering in the zeolite framework. This observation seems to be particular to ZSM-5.

1.3.3.2 Elemental Analysis

The use of AAS (Atomic Absorption Spectroscopy) to determine the molar ratio of zeolites is a well-known technique. However, the accuracy of this method in determining the amount of Si in particular has been questioned over the years.

1.3.3.3 X-Ray Photoelectron Spectroscopy (XPS)

XPS is a well established surface analysis technique. The dealumination of zeolites by different methods and the subsequent migration of the extra-framework aluminium species has been monitored by XPS. In the literature, most studies have been carried out on zeolite Y and mordenite.

Meyers *et al.* (1986) concluded, from their studies on USY, that aluminium expelled from the zeolite lattice, following hydrothermal treatment, migrated to and enriched the zeolite surface, most likely as a thin amorphous aluminium oxide/hydroxide layer. The migration of aluminium towards the zeolite surface creates an aluminium gradient throughout the structure (*Corma et al., 1990*). Meyers *et al.* (1986, 1988) have also postulated that steam is absolutely essential for aluminium migration. However, aluminium is not necessarily lost from the zeolite bulk during steaming. On the other hand, Remy *et al.* (1996) have reported that the acid leaching of steamed H-Y resulted in a depletion of aluminium at the outer zeolite surface due to the dissolution of extra-framework aluminium species and part of the remaining framework aluminium. A similar observation has been made by Sawa *et al.* (1989) for acid leached mordenite and Pellet *et al.* (1995) for steamed and acid washed ferrierite. In a later study, Sawa *et al.* (1992) reported that the concentration of aluminium at the external surface of acid dealuminated mordenite had a strong dependence on the temperature of the dealumination procedure. There was an enrichment of aluminium at the zeolite surface when

treatment temperatures were in the range 77-93°C. Above 93°C, a decrease in the aluminium concentration at the surface was noticed. However, an increase in the surface aluminium concentration was observed by Silva *et al.* (1996) for mordenite dealuminated by NH_4SiF_6. Studies carried out by Campbell *et al.* (1996_b) and Datka *et al.* (1996) on H-ZSM5 revealed that the zeolite surface had been enriched with aluminium after dealumination. On the contrary, the study of Namba *et al.* (1986) on H-ZSM5 dealuminated by $SiCl_4$ vapour has shown that the Si/Al ratios of the external layers of the dealuminated zeolites were higher than the bulk Si/Al ratios.

1.3.3.4 BET Studies

The BET equation can be used to treat adsorption and desorption isotherms of nitrogen on zeolites such that information about the texture of these materials can be obtained. This technique has also been used to study the effect of dealumination on the total surface area and porosity of zeolites.

Generally, dealumination causes a decrease in the micropore volume, but also an increase in the ultramicropore and/or mesopore volume (Coutanceau *et al.*, 1997). These workers also report a decrease in the micropore volume of zeolite Beta, which had been dealuminated by a treatment with hydrochloric acid. A similar finding has been made by Zukal *et al.* (1986) on dealuminated zeolite Y. The latter attributed the decrease in micropore volume with increasing degree of dealumination to the partial destruction of the zeolite lattice on the surface of the mesopores.

However, Meyers *et al.* (1988) have reported an increase in the micropore volume and total surface area of mordenite after it had been subjected to thermal and acid dealumination. Such an observation has also been made by Dutartre *et al.* (1996) on steamed and acid leached mazzite. An increase in micropore volume of as high as 50% was observed for one of the dealuminated mazzites. On the other hand, Constantinescu and Blum (1995) have shown that the micropore volume of acid leached mordenite increased up to a Si/Al ratio of 100, thereafter decreasing with higher Si/Al ratio.

The generation of a secondary mesoporous network after dealumination is a well known phenomenon. Mesopores are formed by coalescence of the atomic vacancies created by aluminium extraction during the hydrothermal treatment. This process involves re-crystallisation of the zeolite and migration, by lattice diffusion, of a large amount of material. Dutartre *et al.* (1996) have shown that mesopores in mazzite, were essentially formed during the initial period of steaming, between 500 and 750°C. Subsequent treatment with acid did not have a significant effect on the mesoporous network although further dealumination occured. The mesopore volume was found to increase with the severity of steaming. An increase in the formation of mesopores with increasing degree of dealumination has been confirmed by the work of Zukal *et al.* (1986) on Y zeolite. Moreover, Constantinescu and Blum (1995) found that mesoporosity in dealuminated mordenite is not influenced by the increase in Si/Al ratio up to 37, but the mesoporous network subsequently develops with higher degrees of dealumination. In contrast to the above studies, the work of Coutanceau *et al.* (1997) revealed that the mesopore volume of acid treated zeolite Beta decreased with increasing degree of dealumination. This was attributed to the fact that the decrease in the intercrystalline volume, caused by the acid treatment, was more significant than the usual increase caused by dealumination.

1.3.3.5 ^{29}Si MAS NMR

Silicon atoms in the three-dimensional structure of zeolites are connected via oxygen bridges to four other T atoms (Si or Al). As a result, only five different structural units of type $Si(OSi)_{4-n}(OAl)_n$, with n = 0-4 [conventionally designated as Si(nAl)] can exist (Engelhardt, 1991). Therefore, the ^{29}Si MAS NMR spectrum of a zeolite may consist of one to five peaks each corresponding to the five possible Si(nAl) environments in the framework of the zeolite. As the number of aluminium atoms in the second co-ordination sphere of the central silicon atom increases, the peaks in the ^{29}Si NMR spectrum shift to low fields. Thus, the chemical shift is a function of the degree of aluminium substitution for silicon in the zeolite framework. However, the chemical shift is also dependent on the bonding geometry (SiO bond length and SiOT bond angle) around the silicon atom. Consequently, chemically equivalent but crystallographically inequivalent silicon atoms can have different chemical shifts.

Fyfe *et al.* (1988) have shown that the ^{29}Si NMR spectrum of highly dealuminated zeolite Beta consisted of nine peaks, corresponding to nine crystallographically inequivalent tetrahedral sites in the unit cell of the zeolite. Furthermore, Harvey *et al.* (1996) obtained three well-resolved peaks corresponding to three crystallographically non-equivalent sites in mordenite. A similar observation was made by Meyers *et al.* (1988) on highly dealuminated mordenite. On the other hand, Perez-Pariente *et al.* (1990) attributed three signals at -111.5, -113 and -115.7 ppm, in the 29Si NMR spectrum of thermally treated zeolite Beta, to three crystallographically inequivalent sites.

Typical shift ranges for the five Si(nAl) environments are shown in Table 1.2 below. Despite the fact that the ranges tend to overlap, the assignment of well separated peaks to the different Si(nAl) environments is possible.

Table 1.2. ^{29}Si chemical shift assignments (Fyfe *et al.* 1981).

Structural Type	^{29}Si chemical shift (ppm from TMS)
Si(4Al)	-80 to -87
Si(3Al)	-88 to -95
Si(2Al)	-93 to -100
Si(1Al)	-97 to -106
Si(0Al)	-102 to -115

The relative intensities of the peaks in the ^{29}Si NMR spectrum of a zeolite are directly proportional to the relative concentrations of the different Si(nAl) environments in the zeolite structure. Given that the Lowenstein Rule (no Al-O-Al linkages are possible in the zeolite framework) holds and the ^{29}Si NMR spectrum is correctly interpreted in terms of the Si(nAl) environments, the framework Si/Al ratio of the zeolite can be calculated using the following equation (Engelhardt, 1991):

$$(Si / Al)_{fr} = \sum_{4}^{0} I_n / \sum_{4}^{0} 0.25 n I_n$$

where I_n are the intensities of the Si(nAl) peaks.

This equation is not dependent on zeolite structure and therefore can be applied to any zeolite type.

The application of ^{29}Si NMR is particularly useful in the study of dealuminated zeolites as it can provide information about the framework composition independently of non-framework aluminium species. Thus, the dealumination of the framework can be monitored using this technique. The intensities of all the peaks, except for the Si(0Al) signal, are found to decrease following dealumination by thermal, acid or thermal plus acid treatments. An increase in the resolution of the Si(0Al) peak provides evidence of dealumination (Meyers *et al.*, 1988). Such an observation has been made by Campbell *et al.* (1996_a) on dealuminated H-ZSM5, Perez-Pariente *et al.* (1990) on thermally treated zeolite Beta and Meyers *et al.* (1988) on dealuminated mordenite.

However, some complications may arise owing to the fact that silicon atoms bonded to OH groups, normally located at framework defects created by dealumination, give rise to peaks that tend to overlap with those due to Si(n-1)Al signals (Engelhardt, 1991). Those silicon atoms associated with OH groups are of the type $Si(OH)(OSi)_{3-n}(OAl)_n$. Nevertheless, SiOH peaks can be clearly identified by their intensity enhancement using cross-polarisation MAS NMR. Rakiewicz *et al.* (1996) have identified two different silanol sites in mildly dealuminated zeolite Y. A peak at a chemical shift of -90 ppm has been assigned to a site of structure $Si(OSi)(OAl)_2OH$ where as another peak at -95 ppm has been attributed to a site of structure $Si(OSi)_2(OAl)OH$. Moreover, two new signals at -102 and -104 ppm were observed by the same authors for highly dealuminated zeolite Y. Both signals were attributed to framework silicon sites directly bonded to silanol groups. On the other hand, Engelhardt *et al.* (1982) showed the presence of $Si(OSi)_3OH$ groups in the vacancies left by the framework dealumination of acid leached USY.

1.3.3.6 ^{27}Al MAS NMR

^{27}Al NMR is capable of investigating the distribution of both framework and non-framework aluminium species, the latter being generated by dealumination. Extra-framework aluminium species generally act as Lewis acid sites. Brunner *et al.* (1988) have reported that in dealuminated mordenites, all non-framework aluminium can be observed by ^{27}Al MAS NMR.

However, in dealuminated zeolite Y, the majority of non-framework aluminium is present on sites of non-cubic symmetry and as a result, they are "NMR invisible". The reason being that the heavy distortion of the tetrahedral or octahedral symmetry around the aluminium atom causes a strong electric field gradient at the place of the nucleus and therefore, broadens the ^{27}Al signal so strongly that it becomes "NMR invisible" (Brunner *et al.*, 1991).

In general, three signals are visible in the ^{27}Al NMR spectrum of dealuminated zeolites. A line at 60 ppm is assigned to four co-ordinated framework aluminium. However, Freude *et al.* (1994) claim that in strongly dealuminated zeolites, non-framework aluminium also contributes to the signal at 60 ppm although this contribution is considered negligible for mildly dealuminated zeolites. This is in agreement with the work of Long *et al.* (1996) on hydrothermally treated H-ZSM5. The treatment of the zeolite at high temperatures (greater than 777°C) resulted in the transformation of extra-framework aluminium to a different form that possesses the same chemical shift as framework aluminium. The newly formed species has been attributed to a Si-O-Al species dispersed on the zeolite surface. Meyers *et al.* (1988) have reported that the extent of dealumination of a given sample can be followed by measuring only the intensity of the peak at 60 ppm. The intensity of the peak is found to decrease as elemental aluminium decreases showing progressive dealumination.

Six co-ordinated non-framework aluminium, in the form of the hexa-aquo complex $Al(H_2O)_6^{3+}$ (Scherzer *et al.*, 1984), is responsible for a signal at 0 ppm. However, Bourgeat-Lami *et al.* (1991) have suggested from their studies of the state of the aluminium species in zeolite Beta that the signal at 0 ppm could also be generated by aluminium atoms in framework positions linked to four lattice oxygens, the oxygen of a hydronium ion and the oxygen of a water molecule. Accordingly, these atoms are not part of non-framework aluminium species, but despite their octahedral symmetry, they belong to the zeolite framework.

A broad peak at 30-40 ppm is assigned to four co-ordinated non-framework aluminium although some authors, e.g Gilson *et al.* (1987), have also reported a contribution from a penta-coordinated non-framework aluminium species. The four co-ordinated non-framework aluminium has been reported by Brunner *et al.* (1989) to be due to non-framework AlOOH in

which aluminium is in tetrahedral co-ordination through its proximity to two framework oxygens and the proton weakly interacts with a further framework oxygen. Yang and Truitt (1996) have shown that two additional peaks at 72 and 66 ppm, respectively, were observed for NH_3 treated zeolites Y, Beta and ZSM-5. These peaks have been attributed to distorted tetrahedral sites, with hydroxonium ions partially replaced by NH_3, that are more acidic than the framework aluminium sites.

The relative proportions of framework and non-framework aluminium species can be directly derived from the intensities of the signals at 60 and 0 ppm in the ^{27}Al NMR spectrum of a dealuminated zeolite. However, the condition that all aluminium is visible must hold (Engelhardt, 1991). Moreover, if the bulk Si/Al ratio of the zeolite is known from chemical analysis, the framework Si/Al ratio can be calculated from the following equation:

$$(Si/Al)_{fr} = Si/Al\ (I_{60} + I_0)/I_{60}$$

where I_{60} and I_0 are the intensities of the peaks at 60 and 0 ppm respectively.

The results from this method should be compared to those obtained from ^{29}Si NMR since non-framework aluminium is often underestimated from ^{27}Al NMR.

1.3.3.7 Infrared Studies

Infrared spectroscopy has been extensively used to characterise zeolites before and after post synthesis modifications.

Several authors have made use of IR spectra in the framework vibration region, to follow the progress in crystallinity of zeolites with increasing period of crystallisation. Kiricsi *et al.* (1994) have reported that the bands at 575-590 and 525 cm^{-1} are characteristic for zeolite Beta. The band in the 575-590 cm^{-1} range has been found by Bhat *et al.* (1990) and Eapen *et al.* (1994) to narrow and increase in intensity as the crystallisation period increases. These authors have also reported that the band exhibits a direct correlation with XRD crystallinity.

The influence of synthesis parameters on the crystal structure of zeolite Beta has also been investigated in the literature by using FTIR. Lohse *et al.* (1996) studied the effect of using

TEAOH/TEABr with addition of chelates as templating agents in the synthesis of zeolite Beta. These parameters however did not have a significant effect on the IR spectra of framework vibrations for the samples. Similarly, Maache *et al.* (1993) found that changing the synthesis medium (alkaline or fluoride) for zeolite Beta had a negligible effect on the IR spectra of framework vibrations for the samples.

However, the influence of post-synthesis modifications on the crystal structure of zeolite Beta has not been extensively reviewed in the literature. According to the work of Flanigen *et al.* (1976) on other zeolites, some bands are sensitive to the framework Si/Al ratio, that is, their wavenumber increases when framework dealumination occurs. Similar observations have been made by several authors for dealuminated zeolite Beta. Szostak *et al.* (1993) found that the symmetric stretching frequency appearing at 767 cm^{-1}, increases in intensity and shifts to 789 cm^{-1} for steamed Beta. For their part, Kiricsi *et al.* (1994) and Coutanceau *et al.* (1997), have reported that the bands in the 525 to 575 cm^{-1} region are influenced by framework dealumination and that the band at 952 cm^{-1} becomes larger upon removal of aluminium from the framework. Furthermore, Corma *et al.* (1987) and Maache *et al.* (1993) found that the asymmetric stretching vibration situated in the 1075-1090 cm^{-1} region shifts to higher wavenumbers after dealumination. This observation has been confirmed by the work of Coutanceau *et al.* (1997) on acid treated zeolite Beta.

1.3.4 Acidity of Dealuminated Zeolites

1.3.4.1 TPD Studies

The temperature programmed desorption of ammonia from zeolites is a well-known technique used to probe the acidity of such materials. Information about the number and strength of acid sites in the zeolite can be obtained from TPD studies.

Aluminium is removed from the zeolite framework during the dealumination process and since it is postulated that every framework aluminium atom is associated with an acid site, it is expected that the density of acid sites decreases during dealumination. An increase in the severity of the dealumination procedure causes a further decrease in the number of acid sites present. Such a phenomenon has been observed by Parikh *et al.* (1994) on zeolite Beta

dealuminated by a combination of steaming and treatment with NH_4SiF_6, Das *et al.* (1996) on NH_4SiF_6 treated zeolite Beta and Apelian *et al.* (1996) on zeolite Beta dealuminated via dicarboxylic acid treatment.

It has been reported that the maximum peak temperature of the TPD response curve of zeolite Beta is an indication of the strength of the acid sites present (Leu *et al.*, 1991). However, the use of the maximum peak temperature to characterise acid strength represents only a semiquantitative measure (Kapustin *et al.*, 1988 and Dima and Rees, 1990) since it is dependent on a number of factors including particle size and readsorption effects. Karge and Dondur (1990) have revealed the presence of four distinguishable acidic sites viz., strong and weak Bronsted and Lewis acid sites, by the deconvolution of the ammonia TPD spectra of dealuminated mordenite. They also observed that the temperature of the peak maximum shifted to higher values for the dealuminated mordenite as compared to the unmodified mordenite catalyst, indicating an increase in the strength of acid sites with dealumination. However, the work of Meyers *et al.* (1988) on dealuminated mordenite only showed the presence of two types of acid sites in the zeolite. They also concluded that both the acid site density and the acid strength decreased upon dealumination. These observations have been confirmed by various studies on dealuminated mordenites e.g. Sawa *et al.* (1989), Chumbale *et al.* (1992) and Kim *et al.* (1995).

TPD studies have also been conducted on other zeolites such as partially dealuminated HY (Kogelbauer *et al.*, 1994) and steamed and acid washed H-ZSM5 (Kornatowski *et al.*, 1992). In both cases, it was found that the acid site concentration decreased as a result of dealumination. However, the dealumination procedure was accompanied by an increase in the strength of acid sites.

1.3.4.2 ^1H MAS NMR

^1H MAS NMR has mostly been used to probe the different types of hydroxyl groups that are present in dealuminated zeolites. Since these different types of hydroxyl groups may influence the catalytic properties of zeolites, their detailed study is essential for a thorough understanding of the behaviour of zeolites in catalysis (Hunger *et al.*, 1996). In general, four

distinct types of protons can be identified in the ^{1}H MAS NMR spectrum. The typical chemical shift ranges of these protons are detailed in Table 1.3.

Table 1.3. ^{1}H MAS NMR chemical shift assignments (Brunner *et al.*, 1988).

Hydroxyl Group	^{1}H MAS NMR chemical shift/ppm
Terminal SiOH	1.8-2.3
Non-Framework AlOH	2.6-3.6
Bridging SiOHAl	3.8-4.4
NH_4^+	6.5-7.0

The ^{1}H NMR chemical shifts can be considered to be a measure of the acid strength of the protons.

Quantitative information about the changes in the concentration of bridging hydroxyls, terminal silanol groups and non-framework Al hydroxyls following dealumination can be derived from the ^{1}H NMR spectra of zeolites. The intensity of the line at 4 ppm is a direct measure of the number of strong acid sites (Bronsted acid sites) in a zeolite (Engelhardt, 1991). Furthermore, information about the formation of lattice defects or amorphisation of the zeolite and the extent of hydroxylation of the non-framework aluminium species can be obtained from the intensities of the signals due to terminal SiOH and AlOH groups respectively.

Freude *et al.* (1987) have concluded, from their studies on H-ZSM5, that the magnitude of the chemical shift of bridging hydroxyl groups is a measure of their acid strengths and it has been found to increase up to a Si/Al ratio of 10. Thereafter, the chemical shift remains at a constant value of 4.3 ± 0.1 ppm. A different study by Freude *et al.* (1994) has enabled the comparison of the acid strengths of zeolites H-X, H-Y and H-ZSM5 on the basis of their chemical shifts, corresponding to bridging hydroxyl groups, from their respective ^{1}H NMR spectrum.

Brunner *et al.* (1988) have stated that a peak with a chemical shift of 6.5 ppm can be found in the ^{1}H NMR spectra of zeolites after water adsorption on Lewis acid sites. However, Freude *et al.* (1994) only observed this signal in the ^{1}H NMR spectrum of dealuminated zeolite H-Y

and not in the spectrum of dealuminated H-ZSM5. As a result, they concluded that the zeolite structure must be important for the formation of the species causing the signal at 6.5 ppm. Hunger *et al.* (1996) have reported the presence of three different types of silanol groups corresponding to signals at 1.2, 1.7 and 2.1 ppm in the ^{1}H NMR spectrum of H-Beta. Moreover, Brunner *et al.* (1995) has shown that internal silanol groups, i.e SiOH groups bonded to neighbouring framework oxygen atoms, exhibit a chemical shift at about 6 ppm in the ^{1}H NMR spectrum of zeolites. A signal at about 5 ppm has been reported by several authours, e.g Freude *et al.* (1986) for zeolite H-Y and Brunner *et al.* (1995) for H-ZSM5. This peak has been assigned to perturbed bridging hydroxyl groups, i.e bridging OH groups influenced by an electrostatic interaction with the zeolite framework. Brunner *et al.* (1995) has stated that these perturbed bridging hydroxyl groups exhibit the same acid strength as unperturbed bridging OH groups.

1.3.5 Catalytic Activity of Dealuminated Zeolites

The catalytic activity of dealuminated zeolites has been thoroughly reviewed in the literature. Various hypotheses, often conflicting, have been put forward by several authors in order to account for the changes in catalytic activity that are brought about by the dealumination of zeolites. Most of the research carried out in this field has claimed that the mild steaming of zeolites tends to enhance their catalytic activity (Haag, 1983). However, a few studies have proved that mild steaming has no effect on or may even reduce catalytic activity (Miller *et al.*, 1992, Bamwenda *et al.*, 1994, and O'Donovan *et al.*, 1995).

The work of Haag (1983) on mildly steamed H-ZSM5 has shown that the activity of this catalyst for n-hexane cracking is strongly dependent on the temperature, time and partial pressure of steam used in the hydrothermal treatment of the zeolite, prior to reaction. These authors found a narrow band of conditions in which the catalytic activity of the zeolite showed a four-fold increase for n-hexane cracking. A plot of the relative activity of the catalyst against water vapour pressure is shown in Figure 1.11. A later study by Lago *et al.* (1986) has shown that sites of enhanced activity are created as a result of mild steaming. As a model of the enhanced site, they proposed that one member of a paired Al region is modified during steaming by partial hydrolysis and thus acts as a strong electron withdrawing centre

for the remaining tetrahedral Al, producing a stronger Bronsted acid site. The number of enhanced sites that are created is a strong function of the Al content and these sites can be 45 to 75 times more active than conventional acid sites. Enhanced activity sites that are created in H-ZSM5 by mild steaming display remarkably high activity in the hydrogen transfer steps during n-hexane cracking (Luk'yanov, 1991).

However, ^{29}Si and ^{27}Al NMR studies of Brunner *et al.* (1989) on H-ZSM5 failed to confirm the existence of the proposed structure by Lago *et al.* (1986) for the enhanced activity sites. ^{29}Si NMR spectra showed that the concentration of Si(2Al) groupings in H-ZSM5 was too low to allow for the required number of paired Al sites per unit cell, that contribute towards enhanced activity sites. Furthermore, ^{27}Al NMR patterns of hydrated H-ZSM5 samples did not support the existence of partially hydrolysed framework aluminium, as proposed by Lago *et al.* (1986). Instead, Brunner *et al.* (1989) proposed that a suitable spatial arrangement of a bridging hydroxyl group and extra-framework aluminium species might be considered as the enhanced activity site for n-hexane cracking.

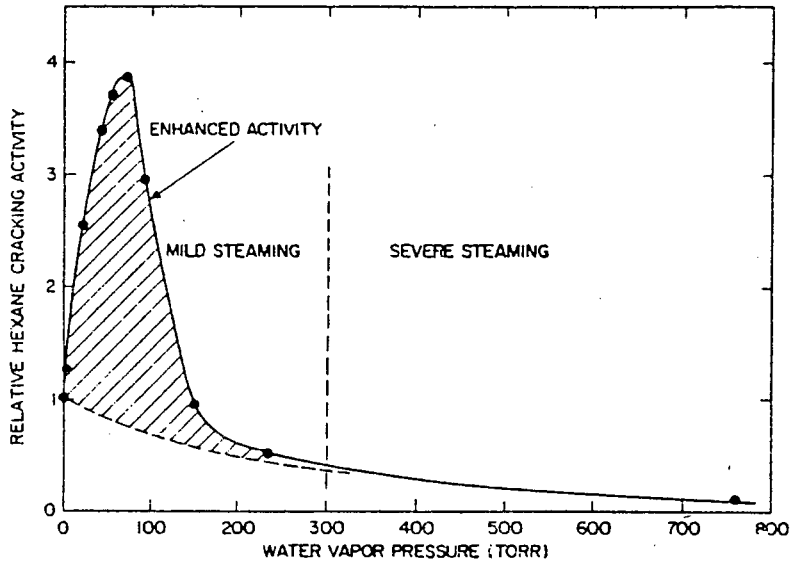

Figure 1.11. Dependence of the activity of H-ZSM5 for n-hexane cracking on the vapour pressure of water used during hydrothermal treatment (Lago *et al.*, 1986).

The role of EFAl in the catalytic activity of dealuminated zeolites has been a subject of much debate in the literature. From the studies that have been carried out, no definite conclusions

have been reached on the exact nature of catalytically active EFAl species. Fritz and Lunsford (1989) have postulated that the isolation of Al atoms is a necessary but an insufficient condition for strong activity and that an additional factor, in the form of EFAl, is required for strong acidity. This argument is supported by Beyerlein *et al.* (1997), who have reported that the presence of some EFAl species is essential for the enhanced activity exhibited by high silica H-Y zeolites for various reactions. Depending on the dealumination conditions used, various types of extra-framework aluminium species can be formed (Corma, 1989). The types of EFAl can be divided into different categories:

(i) monomeric, partially hydrolysed, cationic aluminium species such as Al^{3+}, $Al(OH)^{2+}$, or $Al(OH)_2^+$ that are completely extracted from the framework and neutralise framework charges. These species usually act as strong Lewis acid sites.

(ii) monomeric aluminium species that are coordinated to less than four framework oxygen atoms.

(iii) oligomeric aluminium oxyhydroxides.

(iv) polymeric aluminium oxyhydroxides or oxides.

(v) an amorphous silica-alumina phase that is occluded in the zeolite.

Various hypotheses have been proposed in order to explain the role of EFAl in the catalytic activity of dealuminated zeolites. Mirodatos and Barthomeuf (1981) attributed the high activity of steamed mordenite to the presence of superacidic sites in these catalysts. The model that was proposed for the superacidic site consisted of a partial electron transfer from a bridging hydroxyl group to an EFAl species, which by decreasing the OH bond strength of the site would increase the proton liability and hence the acid strength of the site. The increase in the catalytic activity of steamed H-ZSM5 for n-heptane cracking has also been explained by an increase in the acidic strength of Si-OH-Al groups (Datka *et al.*, 1996). However, microcalorimetry results of Biaglow *et al.* (1994) failed to find evidence for superacidic sites in steamed samples.

The synergism between Bronsted acid sites and Lewis acid sites (EFAl) has often been proposed in the literature as the cause of enhanced activity in dealuminated zeolites. Sendoda and Ono (1988) attributed the enhanced activity of dealuminated H-ZSM5 for propane

cracking to an interaction of dislodged aluminium species (EFAl) with acidic OH groups. A similar explanation has been proposed by Kubelkova *et al.* (1989) for the increased activity of steamed Y zeolite during ethylene oligomerisation, Kogelbauer *et al.* (1994) for the enhanced activity of steamed Y zeolite in the synthesis of MTBE and Parikh *et al.* (1994) for the improved activity of steamed zeolite Beta in the synthesis of DIPB. On the other hand, Fritz and Lunsford (1989) have ascribed the enhanced activity of hydrothermally dealuminated Y zeolite for hexane cracking to an interaction of a non-framework cationic species of the form $[Al(OH)_2Al]^{4+}$ or $Al(OH)^{2+}$ with a Bronsted acid site. A similar argument has been used by Sun *et al.* (1991) to explain the enhanced activity of mildly steamed H-ZSM20 for the same reaction.

According to Wu *et al.* (1996), the local environment and the siting of EFAl species might play a significant role in the enhancement of zeolite activity. From their work on aluminated mordenite, they have concluded that only the EFAl species present inside the channels of mordenite interacted with structural OH groups in their vicinity to enhance the activity of the catalyst for toluene disproportionation and o-xylene conversion.

Other authors have attributed the enhancement of activity in dealuminated zeolites to the fact that the EFAl species, themselves, can act as strong Lewis acid sites. Zholobenko *et al.* (1990, 1991) have postulated that these strong Lewis acid sites in mildly steamed H-ZSM5 polarise the C-H bonds in n-hexane, initiating cracking of that molecule. Remy *et al.* (1996) have ascribed the increased activity of dealuminated Y zeolite for the hydroisomerisation of heptane and decane to the presence of active EFAl species.

Furthermore, Wang *et al.* (1991) have observed that in steamed Y zeolite, having a high number of framework aluminium atoms, EFAl species had a promoting effect on the rates of isomerisation, cracking and hydrogen transfer during n-heptane cracking. These authors assigned the promoting effect of EFAl species to an inductive influence of the Lewis acid sites (EFAl species) on the protonic sites of the zeolite. However, in steamed samples of Y zeolite having less than 15 Al atoms per framework unit cell, EFAl species had no effect on the reaction rates, owing to the fact that they were too far from the protonic sites. The inactivity of EFAl species has also been reported by Miller *et al.* (1992) for dealuminated

mordenite in the cracking of n-hexane and Bamwenda *et al.* (1994) for steamed zeolite Y in the cracking of 2,3 dimethylbutane. It has even postulated that the presence of pentacoordinate EFAl species in steamed mordenite decreased the acid strength of the catalysts by an interaction with framework acid sites (Miller *et al.*, 1992). The study of Corma *et al.* (1996) on USY supports the fact that EFAl can have a negative effect on catalytic activity. The elimination of EFAl from steamed USY by treatment with $(NH_4)_2SiF_6$ increased the initial cracking and alkylation activities of the catalyst during isobutane/2-butene alkylation. Moreover, the removal of EFAl species from steamed ferrierite has been shown to result in an increase in isobutene selectivity in the isomerisation of n-butene (Pellet *et al.*, 1995). Also, the presence of EFAl in the zeolite pores can block access of reactants to the internal acid sites and thus decrease catalytic activity (Silva *et al.*, 1996).

Usually, in dealuminated zeolites, mesoporosity and EFAl co-exist and most of the time, changes in catalytic properties are attributed to the presence of EFAl, thus ignoring the contribution of mesoporosity. However, several authors have reported that the enhancement in catalytic activity as a result of dealumination is not due to the presence of EFAl or Bronsted sites of increased acid strength, but simply due to a decrease in diffusion limitations through the zeolite pores, following the formation of mesopores (Chumbale *et al.*, 1992, Meima *et al.*, 1993, Fernandes *et al.*, 1994, and Leiras Gomes *et al.*, 1997). Since dealumination is known to decrease acid site density, some authors have attributed the enhancement in activity, following dealumination to the suppression of coke deposition on strong acid sites (Sawa *et al.*, 1989, and Kim *et al.*, 1995).

1.4 CUMENE SYNTHESIS

Cumene is produced via the alkylation of benzene with propylene. This reaction is an important petrochemical process since cumene is used as a chemical intermediate in the production of phenol and acetone. The classical cumene process was developed by UOP in the 1940's and commercial production began in May 1942 to supply high-performance fuel for military aircraft. Post-war production of phenol and acetone by oxidation of cumene, based on a new process, provided a growing need for large-scale production (Kaeding *et al.*, 1988).

1.4.1 Catalysts used for Cumene Synthesis

At present, most of the world's cumene requirement is commercially produced using technologies based on the use of catalysts other than zeolites. However, due to the disadvantages of these conventional catalysts, much effort is being put into developing alternative catalysts, especially zeolite-based ones. Some of these disadvantages will be mentioned in the ensuing section.

1.4.1.1 Non-Zeolites

Since the 1940's, " solid phosphoric acid " or SPA has been the major catalyst used in the production of cumene. It consists of phosphoric acid impregnated onto a diatomaceous earth (Kieselguhr). The main advantage of the SPA-catalysed process is that the operating cost is low, due to the fact that a high cumene selectivity is obtained with a relatively cheap catalyst. On the other hand, the polyalkylated byproducts (DIPB's and TIPB's) that are formed cannot be transalkylated back to cumene over the SPA catalyst, thus causing a yield loss. Also, the process requires large quantities of catalyst that cannot be regenerated, leading to increased disposal costs. Furthermore, the catalyst is very difficult to remove from the reactors. In order to activate the SPA catalyst, small quantities of water need to be added to the feed. Hence, phosphoric acid is released and this tends to cause corrosion problems downstream (Meima *et al.*, 1996).

However, in the 1980's an $AlCl_3$-catalysed process was developed based on the well-known $AlCl_3$ process for the production of ethylbenzene. The $AlCl_3$-catalysed process can transalkylate the polyalkylates back to cumene. However, in this case also, the catalyst suffers from certain drawbacks. It is extremely corrosive, thus requiring the use of special and expensive equipment. Cumene manufacturers have to consider the ever-increasing costs for the catalyst and the environmental disposal thereof. Moreover, the process must be operated at relatively low temperatures since the high acidity of the anhydrous $AlCl_3$ causes excessive formation of unwanted n-propylbenzene.

Other non-zeolites that have been studied in the literature for the isopropylation of benzene include a nickel/γ-alumina catalyst (Jian *et al.*, 1992). This catalyst showed a good performance for the alkylation reaction.

1.4.1.2 Zeolites

In the last decade, various authors have reported the use of zeolites to catalyse the isopropylation of benzene to cumene. However, zeolite-based technology has only recently been used on a commercial scale. Georgia Gulf Corporation has claimed the world's most advanced cumene process technology, based on MCM-22. The catalyst's high selectivity minimises olefin oligomerisation reactions that result in unwanted by-products (Kane *et al.*, 1996).

Zeolites offer the advantages of being regenerable, non-toxic, non-corrosive and stable over a wide range of temperatures. Moreover, in the case of alkylation reactions, they are active in the transalkylation of the polyalkylated products, therefore giving the possibility of increasing, under particular conditions, the selectivity to cumene (Cavani *et al.*, 1993). On the other hand, the main disadvantage of zeolitic systems is that they tend to have short lifetimes. The heavy by-products formed during the course of the reaction deactivate the catalyst by either blocking the zeolite pores or by being deposited as coke on the outer zeolite surface. In the literature, various zeolites have been studied for the alkylation of benzene to produce cumene. Most of the work has been carried out on large pore zeolites, e.g MCM-41, zeolite Beta, USY and mordenite, although medium pore zeolites, e.g HZSM-5 , ferrisilicate of MFI

structure and EU-1 have also been studied. For their part, Parikh *et al.* (1993) and Pradhan *et al.* (1991) have investigated the use of metal substituted zeolites to catalyse the reaction.

1.4.2 Mechanism of Cumene Synthesis

The isopropylation of benzene to cumene is an electrophilic substitution on the aromatic ring. The origin of zeolite activity in the isopropylation reaction is found in the ability of the Bronsted acid sites to attack the double bond of the propene molecule to form a carbenium ion as shown below.

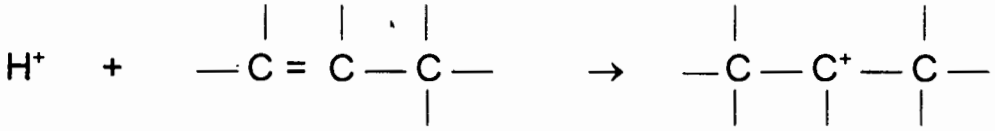

The carbenium ion that is formed, being the active species in the reaction, can follow two major routes. It can react with benzene to produce cumene, which itself reacts with the carbenium ion, to produce mainly diisopropyl benzenes (ortho, meta and para isomers) and to a lesser extent triisopropyl benzenes. The diisopropyl benzenes formed can transalkylate back to cumene by reaction with benzene. Furthermore, the cumene formed can isomerise to n-propylbenzene.

The alternative route leads to the formation of a C_6 species by the reaction of the carbenium ion with a propene molecule. This species can be further transformed through oligomerization, cracking, isomerization and alkylation to produce olefins and other alkylbenzenes (Bellussi *et al.*, 1995). Bellussi *et al.* (1995) proposed that the isopropylation of benzene be represented by the schematic model shown in Figure 1.12.

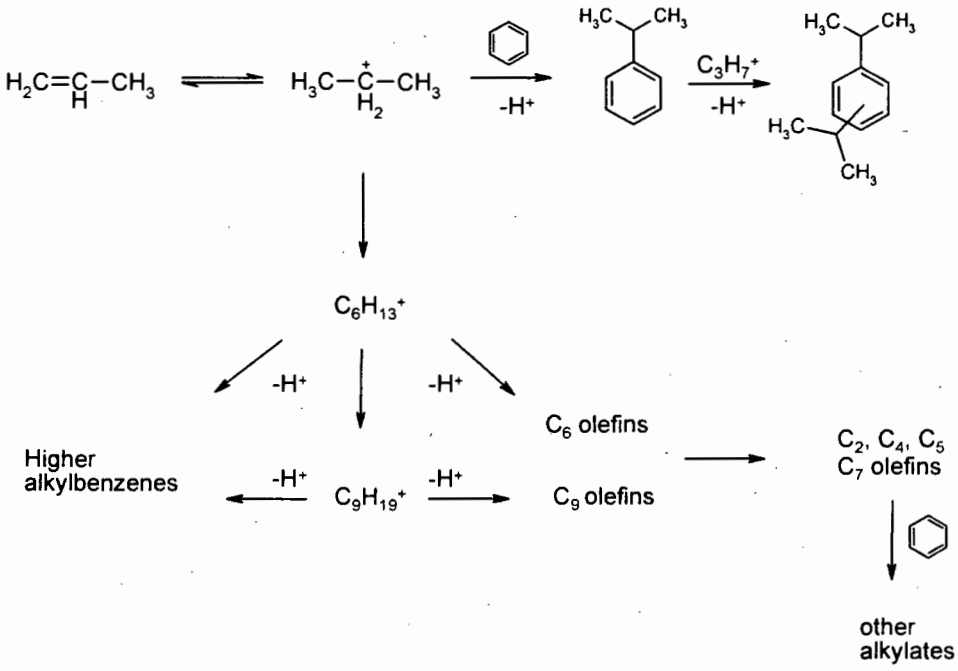

Figure 1.12. Schematic model representing the isopropylation of benzene (Bellussi *et al.*, 1995).

1.4.3 Factors Influencing Cumene Synthesis

The main factors affecting the synthesis of cumene are the temperature of the reaction, the molar ratio between the benzene and the propene and the residence time in the reactor.

Much work has been done, in the literature, to investigate the effect of the reaction temperature on cumene selectivity. Kaeding *et al.* (1988) found that at temperatures in the range 175°C to 200°C, conversion of the starting materials was low using H-ZSM5 as catalyst. But at these temperatures, the selectivity to cumene was more than 90%. However, at higher temperatures (250-300°C), significant reductions in cumene selectivity (69 to 38%) was observed. This was attributed to the fact that at high temperatures, disproportionation, dealkylation and oligomerisation reactions become important. Moreover, the selectivity to n-propylbenzene increases to about 36% at 300°C, most probably due to the subsequent isomerisation of cumene. Similar observations have been made by Chandavar *et al.* (1984), Pradhan *et al.* (1991), Reddy *et al.* (1993) and Parikh *et al.* (1993) on H-ZSM5, EU-1, zeolite Beta and a ferrisilicate equivalent of MFI structure respectively. In addition, Pradhan *et al.* (1991) and Reddy *et al.* (1993) observed that the formation of diisopropyl benzene (DIPB)

decreases at high temperatures, due to the transalkylation of DIPB with benzene to cumene. They also report an optimum temperature of 210°C for cumene selectivity.

Cumene selectivity tends to increase with higher benzene/propene mole ratios (Meima *et al.*, 1993). On the other hand, at lower benzene/propene mole ratios, the concentration of propene increases over the catalyst resulting in the preferential alkylation of cumene, rather than benzene, to form DIPB (Pradhan *et al.*, 1991). Consequently, the selectivity to cumene decreases. Also, at lower ratios, propene oligomerisation reactions can take place to a larger extent, which undesired by themselves can lead to the formation of additional by-products like ethylbenzene, butylbenzenes and C6-benzenes (Meima *et al.*, 1996). In general, low benzene/propene mole ratios give rise to lower catalyst lifetimes, due to propene oligomerisation leading to the formation of coke and poisoning of acid sites.

The effect of contact time on the synthesis of cumene has been well reviewed in the literature. At low contact times (high WHSV), the selectivity to cumene decreases. Accordingly, the selectivity to cumene increases at high contact times (low WHSV), due to the transalkylation of DIPB with benzene. However, at low WHSV, cumene tends to isomerise to n-propylbenzene (Reddy *et al.*, 1993).

1.4.4 Thermodynamics

Accurate thermodynamic data are scarce for the isopropylation of benzene to cumene. The reaction is highly exothermic (ΔH_r = -98 kJ/mol), and is therefore favoured at relatively low temperatures. The equilibrium conversion of propene to cumene during the isopropylation of benzene as a function of temperature is shown in Figure 1.13. The transalkylation of DIPB to cumene is an equilibrium-controlled reaction that can form three different DIPB isomers (Meima *et al.*, 1996). Calculated thermodynamic equilibria of Kaeding *et al.* (1988) for diisopropyl benzene at 100°C indicates a para/meta/ortho ratio of roughly 33/58/9, showing that the meta isomer is the most stable and the ortho isomer is the least stable. However, at 225-230°C, the observed values of 60/31/8 show a strong preference for the para isomer. The latter statement has been contradicted by the work of Medina-Valtierra *et al.* (1998), who have shown that in a temperature range of 150-300°C, selectivity to the para isomer remained

very low while meta and ortho DIPB were the dominant isomers. In fact, the meta/ortho ratio changed from 0.99 at 150°C to 1.35 at 300°C. On the other hand, Perego *et al.* (1996) have stated that large pore zeolites like mordenite and zeolite Beta allow the meta/para ratio to reach thermodynamic equilibrium.

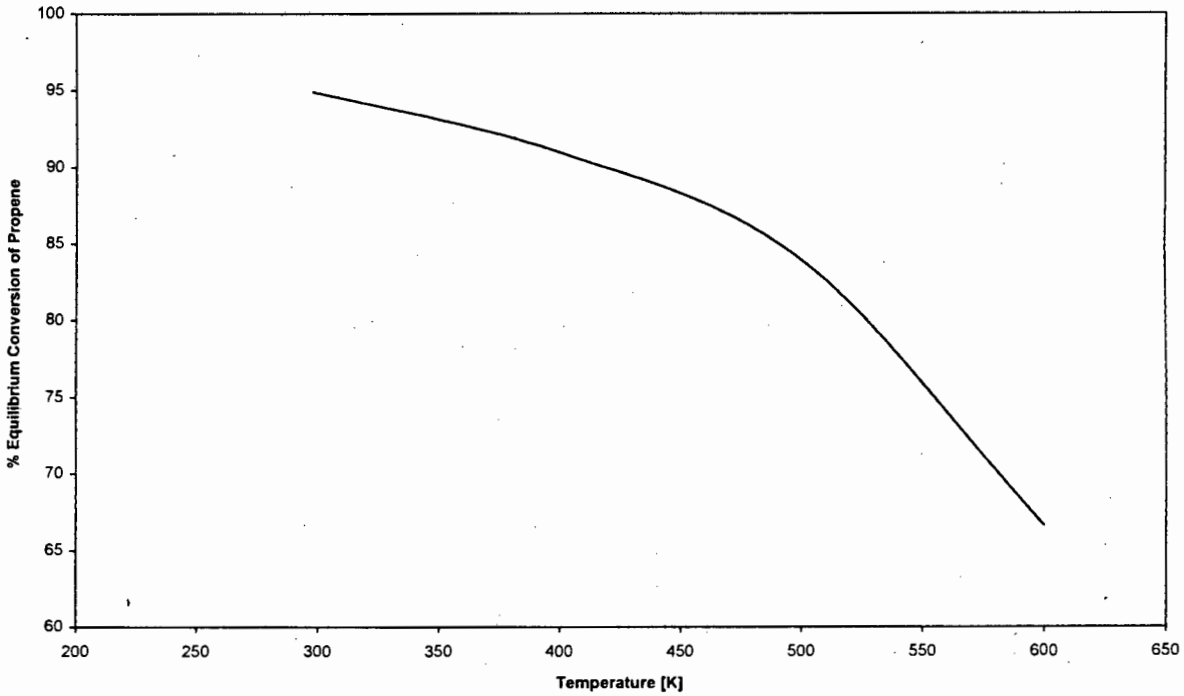

Figure 1.13. % Equilibrium conversion of propene as a function of temperature.

Based on thermodynamics, the formation of n-propylbenzene by isomerisation of cumene is favoured at high temperatures. The thermodynamic equilibrium values of cumene and n-propylbenzene reported by Taylor *et al.* (1946) vary from 53.3:46.7 at 25°C to 31.1:68.9 at 427°C. Although the values are high for the temperatures at which the isopropylation of benzene has been studied in the literature, only small amounts of n-propylbenzene have been reported in the products. Reddy at al. (1993) have attributed this effect to the higher stability of the secondary carbenium ion compared to the primary carbenium ion on the zeolite catalyst. Therefore, the n-propylbenzene in the products is formed via the alkylation of benzene only, at the temperatures at which the reaction has been studied.

1.4.5 Kinetics

Parikh *et al.* (1993) have studied the kinetics of cumene synthesis over a ferrisilicate equivalent of MFI structure using a feed of benzene and isopropanol. They proposed a reaction scheme consisting of three main reactions viz. benzene isopropylation to cumene, cumene isomerisation to n-propylbenzene and cumene alkylation to isobutylbenzene. A simple stoichiometric model was fitted to their kinetic data. The evaluated intrinsic activation energies for the different reactions taking place during alkylation indicated that the main alkylation is faster than isomerisation of the primary product cumene, to n-propylbenzene. Their data also show that the isopropylation of benzene to cumene takes place in the transition regime whereas the other two reactions occur in strongly diffusion hindered regime.

1.5 OBJECTIVES OF RESEARCH

The good performance of zeolite Beta in the isopropylation of benzene to cumene has often been reported in the literature over recent years. It is known, from the numerous studies that have been carried out on other zeolite types, that post synthesis modifications such as dealumination of the zeolite framework tend to enhance the activity of these zeolites for catalytic reactions. Moreover, the effect of synthesis parameters on the catalytic activity of zeolite Beta is an important issue that has not been thoroughly investigated in the literature.

The objectives of this research were:

1. To modify zeolite Beta by direct synthesis techniques in order to change mesoporosity without a significant change in number of acid sites and without any extra-framewrok aluminium.

2. To modify a commercial parent zeolite Beta catalyst by post synthesis modifications such as steaming, acid washing or steaming followed by acid washing in order to generate extra-framework aluminium.

3. To characterise the samples with respect to structure, morphology, particle size, number of acid sites, coordination state of Al and the environment of Si atoms.

4. To use the isopropylation of benzene to cumene as a test reaction to evaluate the effect of items 1 and 2 above on the catalytic activity.

CHAPTER TWO

Experimental Methods

2.1 CATALYST SYNTHESIS

The parent catalyst used in this study is a zeolite Beta sample obtained from a commercial supplier, hereafter referred to as A. Four other samples, referred to as B, C, D and E were synthesised according to the methods described below. A commercial H-BEA standard, referred to as F, was also used in this work.

2.1.1 Reagents and Molar Regimes Used

2.1.1.1 Reagents

The reactants required for the synthesis of zeolite Beta are Si, Al, Na, OH^-, H_2O, Br^- and the template ion tetraethylammonium (TEA^+). These reactants were respectively obtained using fumed silica (silicon dioxide) and a silica source supplied by Syncat (Pty) Ltd., sodium aluminate, sodium hydroxide, tetraethylammoniumhydroxide, deionised water and tetraethylammoniumbromide. The source and purity of these reagents are shown in Table 2.1.

Table 2.1. Reagents used in the preparation of zeolite Beta.

Reagents	Source Catalogue No.	Purity
Silica, fumed (mean dp 0.007 μm)	Aldrich 38-126-8	99.8% SiO_2
Silica	Syncat	89.8% SiO_2
Sodium hydroxide	Saarchem 5823160	97% NaOH
Sodium aluminate	Saarchem 582-110	56% Al_2O_3 37% Na_2O
Tetraethylammoniumhydroxide	Fluka Chemicals	20% and 40% aqueous solution
Tetraethylammoniumbromide	Merck-Schuchardt 17-780-6	>99% TEABr

2.1.1.2 Molar Regimes

The molar regimes used in the synthesis of samples B, C, D and E , as normalised to silica, are described in Table 2.2. Information about the synthesis procedures used in the preparation of the commercial materials, samples A and F, was unavailable. Sample D has a different molar regime as compared to samples B, C and E and was synthesised without NaOH and with a lower template concentration.

Table 2.2. Molar regimes used in the preparation of samples B-E.

Sample	Si	Al	Na^+	TEA^+	OH^-	Br^-	H_2O
B^+	1.0	0.091	0.19	0.29	0.38	0.0014	9.7
C	1.0	0.091	0.19	0.29	0.38	0.0014	9.7
D	1.0	0.085	0.093	0.15	0.15	0.00075	9.7
$E^•$	1.0	0.091	0.19	0.29	0.38	0.0014	9.7

$^+$Static Synthesis, $^•$ Proprietary silica source

2.1.2 Pre-synthesis Mixing

2.1.2.1 Order of Addition

The order in which the reagents were mixed together was kept unchanged throughout the course of the syntheses. Most of the water was added to the template, followed sequentially after thorough mixing by the sodium hydroxide and TEABr. The sodium aluminate, which was dissolved separately in the rest of the water, was then added with thorough mixing. This solution was stirred to allow the reagents to dissolve completely before the addition of the silica source, which was added at a rate of approximately 5g/minute.

2.1.2.2 Mixing Time

The first addition of silica was taken as the start of the mixing time, which in general lasted about 1 hour.

2.1.3 Synthesis Equipment

2.1.3.1 Static synthesis

The static synthesis of zeolite Beta was carried out in Parr bombs. These are fitted with an inner Teflon lining which is corrosion resistant, and an outer stainless steel casing. They have a capacity of 23ml and were filled to about 40% with the pre-synthesis mixture. The operating specifications are a maximum pressure of 8 MPa and a recommended maximum temperature of 150°C.

A Varian model 3700 gas chromatography oven was used for the static synthesis of zeolite Beta. The temperature of this oven was maintained at 160 ±1°C or at 150 ±1°C as required. The heating rate of the Parr bombs, loaded with synthesis gel and placed in this oven, was approximately 2°C/min. The oven was preheated to the required temperature before heating of autoclaves commenced.

2.1.3.2 Agitated synthesis

A mechanically stirred autoclave fitted with a centrally mounted magnedrive, a pitched blade turbine impeller and heated with a band heater was used in all agitated syntheses. The total volume of the autoclave is 400ml and the autoclave was filled to 23-26 % capacity with the gel prepared in the pre-synthesis stage. The heating period required to reach the required synthesis temperature was approximately one hour.

2.1.4 Synthesis Conditions

The synthesis of zeolite Beta was carried out in a number of different ways. These synthesis conditions are summarised in Table 2.3.

Table 2.3. Pre-synthesis and synthesis conditions for samples B-E.

Sample	Pre-synthesis mixing	Synthesis time (hrs)	Synthesis Conditions
B	manual	7	static
C	mechanical	3	agitated
D	manual	30	agitated
E	mechanical	3	agitated

The synthesis temperature used for all samples was 160°C except for D, in which case a temperature of 150°C was used. A heating time of one hour was allowed for the gel to reach the synthesis temperature which was taken as time = 0. The autoclaves were quenched with cold water to prevent further crystallisation after the required synthesis time had elapsed.

After synthesis, the contents of the synthesis vessel were washed with 100ml deionised water. The samples were then centrifuged in a Beckman GPR centrifuge at 4000rpm for 20 minutes in order to separate the solids from the liquid. The supernatants were retained for future analysis. The samples were washed with a further 90ml deionised water and centrifuged again. This was repeated once more before placing the solids in an oven heated to 80°C to dry overnight.

Detemplation and ion-exchanging of the dried catalyst was performed as described in section 2.2.

2.2 POST-SYNTHESIS MODIFICATIONS

2.2.1 Detemplation

The aim of detemplation is to remove any organic compounds, used in the synthesis of the zeolite, from its framework so as to open up its porous structure. Due to the restricted size of the reactor used for detemplation, only about 5 g of catalyst could be detemplated at one time. This amount was loaded in a plug flow reactor, which was then heated up to 500°C under a nitrogen gas flow of 60 ml/min at 3°C/min. The nitrogen was allowed to flow for 8 hours, after the reactor had reached temperature. After this time, air was passed over the catalyst bed at 60 ml/min, keeping the temperature at 500°C, for a further 8 hours. The reactor was then allowed to cool down to room temperature under a nitrogen atmosphere.

2.2.2 Ion-Exchange

Method 1:

The Na-form of the zeolite, following the detemplation procedure, was ion exchanged to the NH_4-form. The catalyst was carefully added to 1 litre of 2M ammonium nitrate solution in a round bottomed glass vessel. The solution was then stirred under reflux at 90°C for 24 hours. The resulting mixture was allowed to settle before decanting the supernatant, leaving the catalyst as the residue in the glass vessel. The zeolite was then washed several times with deionised water, before being filtered using a Buchner funnel. After this, it was dried in an oven at 80°C for 16 hours. This method was used to ion-exchange all the catalysts except samples A_2 and A_3.

Method 2:

In order to test the effectiveness of the above ion-exchange procedure, two additional methods were used to ion-exchange sample A. The first procedure is similar to the method described above with the exception that a reflux time of 8 hours was used. After this time, the catalyst was allowed to settle before the supernatant was decanted. 1 litre of 2M ammonium nitrate was then added, and the solution refluxed for a further 8 hours. This process was

repeated one more time, giving a total ion-exchange time of 24 hours. Sample A_2 was ion-exchanged using this procedure.

Method 3:

The second ion-exchange procedure was carried out at room temperature on 0.5 grams of catalyst in a 50ml beaker containing 0.19 grams of NH_4NO_3 in 2.5 ml of deionised water. The solution was stirred for 2 hours and then filtered using a Buchner funnel. This process was repeated a second time, after which the catalyst was dried in an oven at 80°C for 16 hours. This method was used to ion-exchange sample A_3.

2.2.3 Calcination

All catalyst samples were activated prior to reaction by calcination in air. Calcination of the NH_4-form of the catalyst produced after ion-exchange, yields the active form (H-form) of the catalyst. The required amount of catalyst was loaded in a plug flow reactor, which was then heated under nitrogen gas flow (90 ml/min) to 500°C. At this temperature, air was allowed to flow over the catalyst bed at 90 ml/min for 16 hours. The reactor was then cooled down to room temperature under nitrogen.

2.2.4 Hydrothermal Treatment

Catalyst A was subjected to steaming at different temperatures for different times using the experimental rig shown in Figure 2.1. The steaming conditions with respect to time and temperature are shown in Table 2.4.

Table 2.4. Catalyst coding and steaming conditions.

Sample	Steaming Time/hrs	Steaming Temperature/°C
A	0	-
S400	2	400
S600	2	600
S600(1)	2	600
L400	21	400
L600	21	600

Nitrogen gas was saturated with water at 70°C using a single stage saturator. The double walled saturator temperature was controlled by water from a water bath, the temperature of which was kept at the required saturation temperature. The flow of nitrogen was controlled by a needle valve and a bubble meter was used to determine flowrates. Heating tapes were used to maintain a temperature of 130°C, in order to prevent water from condensing in the lines after the saturator exit.

2 g of catalyst was loaded in the fixed bed reactor, which was then heated up to the required steaming temperature under flowing nitrogen. At the same time, the water bath and the heating tapes were set to the desired temperatures. Nitrogen was passed through the saturator once the required steaming temperature was reached, at a flowrate of 200 ml/min, for the desired steaming time. After completion of the steaming procedure, the reactor was cooled down to room temperature under flowing nitrogen.

2.2.5 Acid Washing

Catalyst A was acid washed using nitric acid of different concentrations, viz. 0.01N, 0.1N, 1N and 10N. 2.5 g of catalyst was added to 70 ml of each of the various concentrations of nitric acid, in a glass vessel and the solution was heated under reflux at 70°C and stirred for 4 hours. The acid was then removed by vacuum filtration, after which the catalyst was washed with 1 litre of deionised water and dried at 80°C overnight. A 0.01N acid wash was also carried out on L400, using the above described procedure. The acid washing conditions are shown in Table 2.5.

Table 2.5. Catalyst coding and acid washing conditions.

Sample	Acid Washing Conditions
A0.01	Catalyst A acid washed with 0.01 N HNO_3
A0.1	Catalyst A acid washed with 0.1 N HNO_3
A1	Catalyst A acid washed with 1 N HNO_3
A10	Catalyst A acid washed with 10 N HNO_3
L400/A0.01	L400 acid washed with 0.01 N HNO_3

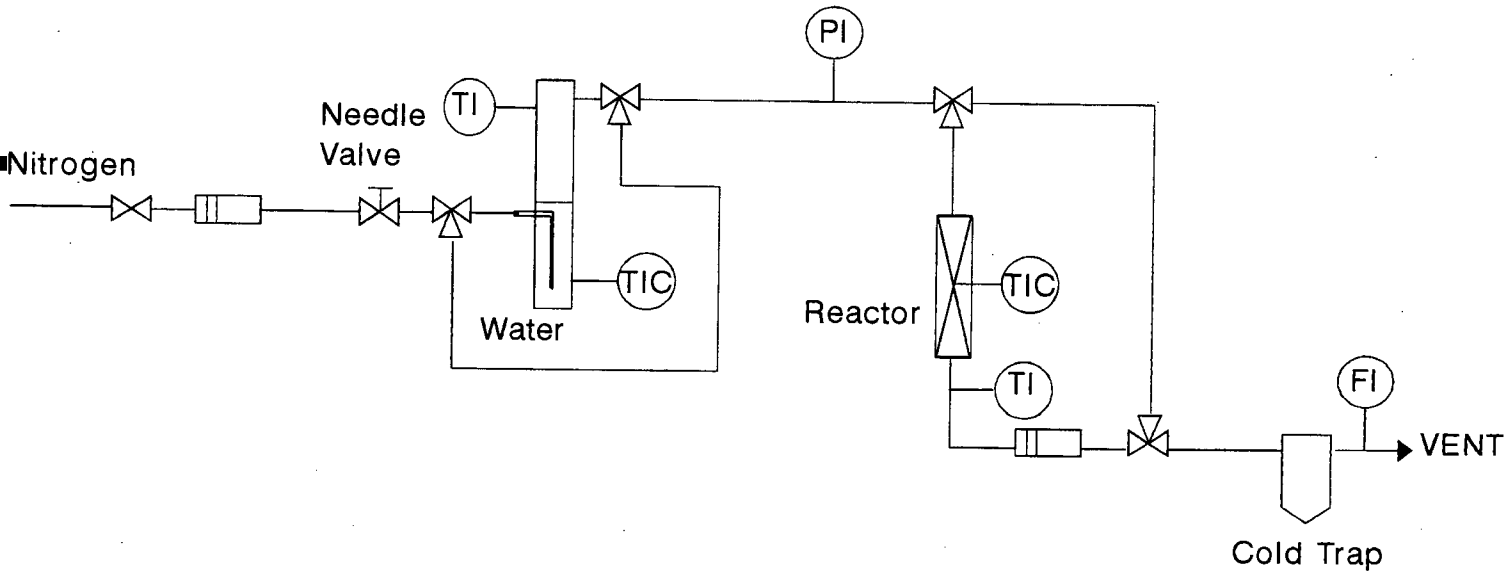

Figure 2.1. Schematic representation of steaming rig.

2.3 CATALYST CHARACTERISATION

All the catalysts were characterised using several techniques. The experimental details of the techniques used are outlined in this section.

2.3.1 Physical and Chemical Characterisation of Catalysts

2.3.1.1 X-Ray Diffraction (XRD)

XRD was used to identify the phase and to detect any change in the crystalline structure of the zeolite as a result of hydrothermal treatment. The scans were performed on a Philips X-Ray Diffractometer using Cu-Kα radiation. The experimental parameters used are as follows:

Voltage	40 kV
Current	25 mA
Time Constant	1
2θ/step	0.1
2θ range	4-47°

2.3.1.2 Elemental Analysis

Elemental analysis was performed on the samples in order to assess the effect of steaming on the bulk Si/Al ratio. 0.1 g of zeolite was digested in concentrated HCl at 150°C for 16 hours. The resulting solution was cooled to room temperature before being vacuum filtered, using ashless filter paper supported on a Buchner funnel. The filtrate consisted of an acidic supernatant while Si was deposited on the ashless filter paper. The filtrate was retained for Al and Na analysis. The filter paper was placed in a weighed crucible and ashed over a bunsen flame. The crucible was then heated to 900°C in a muffle furnace for 3 hours before being cooled and weighed. The difference between the two recorded masses gave the SiO_2 content, from which the percentage mass of Si was calculated. The Si/Al ratio could be calculated using the results from the above procedure and the chemical analysis of the filtrate for Al. Sample calculations are included in Appendix A.

2.3.1.3 X-Ray Photoelectron Spectroscopy (XPS)

The XPS analyses were performed using a PHI 5400 ESCA equipped with a dual anode X-Ray source (Al and Mg), a hemispherical analyser, an omni focus input lens and a 5 keV ion-gun. XPS was used to determine the Na content of some samples. This technique was also used to probe the surface of one of the steamed samples for a possible enrichment in aluminium after hydrothermal treatment. The experimental parameters used are detailed below:

X-Ray anode	Al
Power X-Ray source	300 W
Aperture	#4
Analysis Area	1×3.5 mm
Base Pressure	2×10^{-10} Torr

2.3.1.4 Scanning Electron Microscopy (SEM)

A Cambridge S200 scanning electron microscope was used to take micrographs of the catalyst samples for the purpose of determining the average crystal size and distribution. The samples were mounted on aluminium stubs covered with a mixture of water-based glue and colloidal carbon. The zeolite samples were placed on the carbon mixture and coated with a thin layer of Au/Pd. The crystal size was obtained by determining the average diameter of approximately 150 randomly chosen crystals. The operating parameters are shown below:

Accelerating Voltage	15 keV
Aperture	30
Tilt Angle	30°
Resolution	9
Working Distance	9-22 mm

2.3.1.5 BET Micropore Analysis

Changes in pore volume, pore size distribution and catalyst surface area as a result of steaming were determined using a Micromeritics ASAP 2000. The samples were dried in situ

at 350°C under vacuum. Nitrogen was then adsorbed at liquid nitrogen temperatures at a rate of 3 ml per step until ambient pressure was reached.

2.3.1.6 ^{29}Si and ^{27}Al Nuclear Magnetic Resonance (NMR)

^{29}Si and ^{27}Al spectra were recorded for all the samples. These measurements were made at the University of Stuttgart in Germany. ^{29}Si MAS NMR spectra were recorded for the samples so that any changes in the Si environment within the framework of the zeolite could be detected, as a result of steaming. The experiments were carried out at a resonance frequency of 79.494 MHz with a spinning rate of 3.5 kHz using hydrated samples. The repetition time used was 10 s and the pulse length was adjusted to 4.5 μs.

^{27}Al MAS NMR was performed on the samples so that the effect of the hydrothermal treatment on the co-ordination of the Al atoms within the zeolite could be determined. Also, in this case, hydrated samples were used and the spectra were recorded at a resonance frequency of 104.252 MHz with a spinning rate of 10 kHz. The repetition time used was 0.5 s and the pulse length was adjusted to 0.61 μs. It should be noted that the measurements were carried out in the absolute intensity mode.

2.3.1.7 Fourier Transform Infrared Spectroscopy (FTIR)

FTIR measurements were performed using the NH_4-form of the catalysts in order to detect any changes in the framework vibration region of the infrared spectrum following hydrothermal treatment. Infrared spectra were obtained on a Nicolet 5ZDX spectrometer using KBr discs containing 6 wt% zeolite over a scanning range of 4000-400 cm^{-1}.

2.3.1.8 Diffuse Reflectance Fourier Transform Infrared Spectroscopy (DRIFTS)

The DRIFT spectra were recorded on an Opus Brucker 1FS66 spectrometer using KBr discs containing 10 wt% zeolite over a scanning range of 4000-400 cm^{-1}. Coked samples of catalyst were not diluted with KBr since they had already been mixed with sand. The DRIFT measurements were done in order to determine the type of coke that was present in the samples after reaction.

2.3.2 Catalyst Acidity

2.3.2.1 Temperature Programmed Desorption (TPD)

NH_3-TPD analyses were carried out on the samples in order to determine the effect of synthesis and post-synthesis modifications on the number of acid sites of the zeolites. 0.25 g of catalyst was loaded in a tubular quartz reactor. The sample was first calcined in flowing air at 500°C overnight before ammonia, in a helium carrier gas, was adsorbed for 1 hour at 150° C. Physisorbed ammonia was then allowed to desorb overnight. The actual temperature programmed desorption of chemisorbed ammonia was performed by ramping the temperature to 525°C at a rate of 5°C/min. The concentration of ammonia during the run was measured using a Thermal Conductivity Detector (TCD), connected via an interface to a PC. The experimental data was logged onto disk. Back titration was used to confirm the results obtained using the TCD. A schematic of the experimental rig used to carry out TPD studies is shown in Figure 2.2.

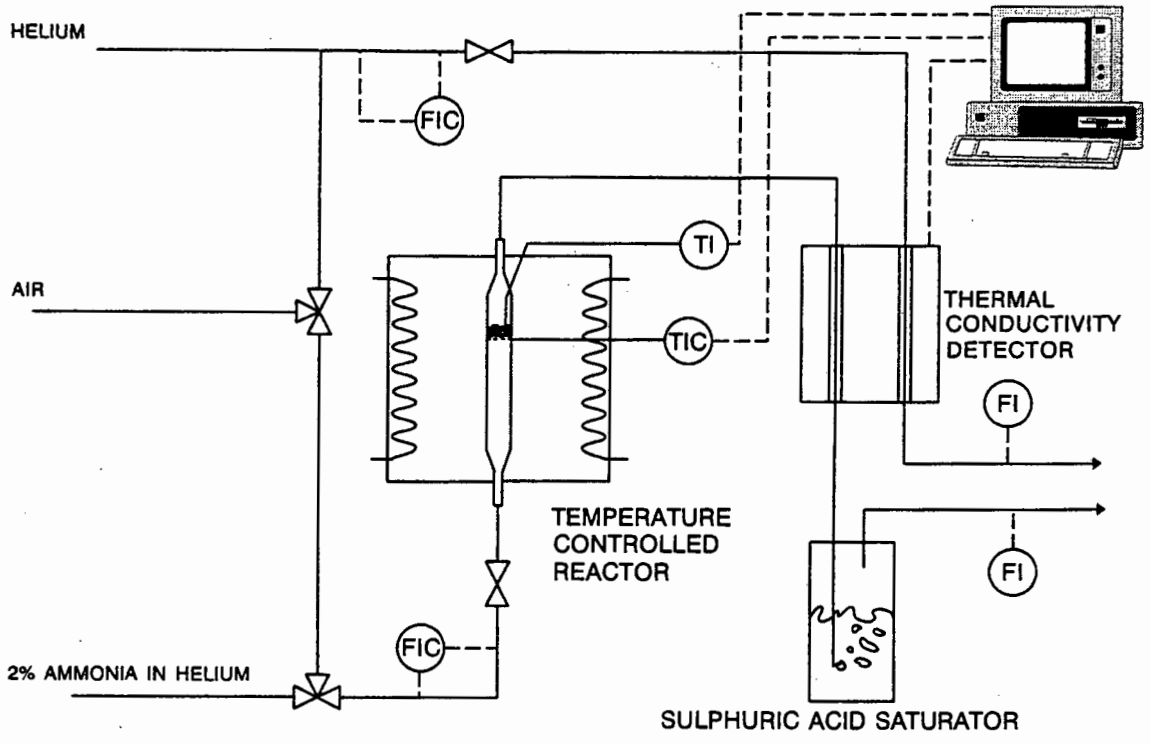

Figure 2.2. Schematic representation of TPD rig.

2.3.2.2 ^{1}H MAS NMR

^{1}H MAS NMR spectra were recorded in order to determine the type of hydroxyl groups present in the samples. Before the measurements were made, all samples were calcined in vacuum for 12 hrs at 673 K. The calcined samples were then filled into the MAS NMR rotors in a glove box under dry nitrogen gas. The spectra were recorded at a resonance frequency of 400.13 MHz with a spinning rate of 10 kHz and a repetition time of 10 s. The absolute intensity mode was again used in this case.

2.4 REACTION STUDIES

The catalytic activity of the samples was tested using the alkylation of benzene with propene as a probe reaction.

2.4.1 Reaction System

The experimental rig used for the reaction is shown in Figure 2.3. Nitrogen fed via a mass flow controller was saturated with benzene at 40°C using a chromosorb saturator, before being introduced to the reactor. The temperature of the saturator was maintained by circulating water being pumped from a water bath. Propene and methane were fed via mass flow controllers to the system from pressurised gas cylinders. Methane was used as an internal standard for carbon balance purposes. The reactor is a stainless steel tube 200 mm long with an internal diameter of 18 mm. The furnace used to heat up the reactor is a brass block with 4 cylindrical heating elements connected to a temperature controller. Temperatures in the reactor were measured using a thermocouple that could be moved along a thermowell axially situated within the reactor. A soap bubble-meter was used to measure flowrates. In-line sampling for analysis was performed using the ampoule sampling technique (Schulz *et al.*, 1986). Samples were subsequently analysed in a gas chromatograph.

2.4.2 Catalyst Preparation

Before the catalyst was loaded into the reactor, it was diluted with sand in order to minimise axial temperature gradients within the reactor. The sand was washed with deionised water and heated to 80°C in an oven for several hours in order to inertise it, prior to being mixed with the catalyst. 0.15 g of catalyst was then mixed with 6 g of sand in a petri dish. A minimal amount of deionised water was added to the mixture to form a slurry. This slurry was dried on a hotplate at 80°C while being continuously stirred with a spatula. The dried mixture of catalyst and sand was then packed into the reactor.

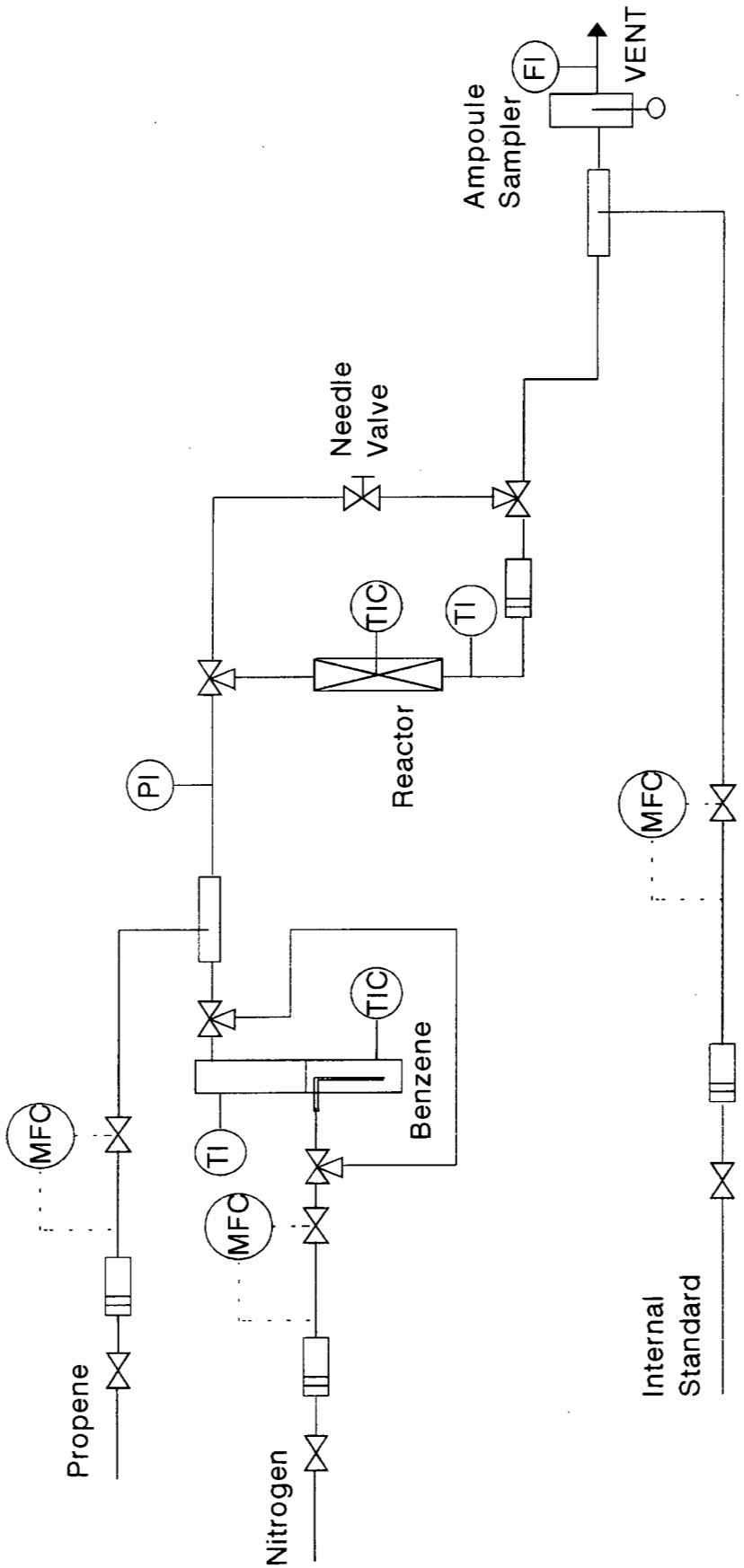

Figure 2.3. Schematic representation of alkylation rig.

2.4.3 Run Procedure

A schematic representation of the packed catalyst bed in the reactor is shown in Figure 2.4. The calcination procedure described in Section 2.1.3 was used to calcine the catalyst before each reaction run. Upon completion of the calcination step, the reactor was cooled down under nitrogen flow to the reaction temperature of 210°C. At the same time, the water bath pump was switched on and the heater was set at the desired temperature (41°C). Heating tapes used to prevent the condensation of benzene in the lines before the reactor inlet and of liquid products after the reactor exit, were also set to the required temperatures (150°C and 200°C respectively) at this stage.

Once the reactor had cooled down and the saturator had reached temperature, the feed consisting of nitrogen saturated with benzene, propene and methane was allowed to flow through the reactor bypass line for half an hour. After this time, the alkylation of benzene with propene was carried out over the catalyst at 210°C and atmospheric pressure. The nitrogen and propene flowrates were set such that a benzene/ propene molar ratio of 5.8 was obtained at a WHSV of 78 hr^{-1} (based on the total mass flowrate of benzene and propene only). Samples of product gas were taken at 1 hour intervals for six hours after which the run was stopped. At this stage, the feed was allowed to flow through the reactor bypass line. Samples were taken by breaking the tip of a heated, evacuated glass ampoule in the ampoule sampler. Once the product gas had entered the ampoule, it was resealed using the flame of a butane burner.

The pressure drop in the reactor was read from a pressure gauge at the reactor inlet during the course of the reaction. A needle valve on the reactor bypass line ensured that the same pressure drop was maintained in both the bypass line and the reactor. After each run, the feed was allowed to flow for half an hour, after which ampoules of the feed were taken.

2.4.4 GC Analysis

Sample analysis was performed in a Varian 3300 gas chromatograph using a flame ionisation detector (FID). A 60 m long PONA capillary column was used to separate the compounds. Peak areas were integrated using a Varian 4270 integrator. An ampoule breaker was used to break the ampoules containing the product and feed gases. Before each GC analysis, the ampoule breaker was flushed for half a minute with nitrogen before the run was started. GC settings and flowrates are shown in Table 2.5.

Table 2.6. Varian 3300 GC parameters.

GC Parameter	Setting
Nitrogen Flowrate	5 ml/min
Hydrogen Flowrate	30 ml/min
Air Flowrate	300 ml/min
Initial Column Temperature	40°C (5 min)
Temperature Program Ramping Rate	5°C/min
Final Column Temperature	230°C (5 min)
Injector Temperature	230°C
Detector Temperature	250°C

An example of the calculation of conversion and selectivity from the raw data is shown in Appendix B. The response factors of all the components that were analysed are presented in the same appendix.

CHAPTER THREE

Results

3.1 CATALYST CHARACTERISATION

3.1.1 Physical And Chemical Characterisation of Catalysts

Different characterisation techniques have been used to detect changes in the physical and chemical nature of the catalysts as a result of steaming and acid washing. The characterisation results of the samples, prepared by different synthesis techniques, are also presented in this section.

3.1.1.1 X-Ray *Diffraction (XRD)*

The X-Ray diffraction pattern of sample A is shown in Figure 3.1 below. The pattern compares well with the simulated X-Ray diffractogram (Figure 3.2a) of zeolite Beta and the patterns reported by several authors, e.g Perez-Pariente *et al.* (1987) (Figure 3.2b), for the zeolite in the literature. The X-Ray diffraction patterns of all other samples are presented in Appendix C.

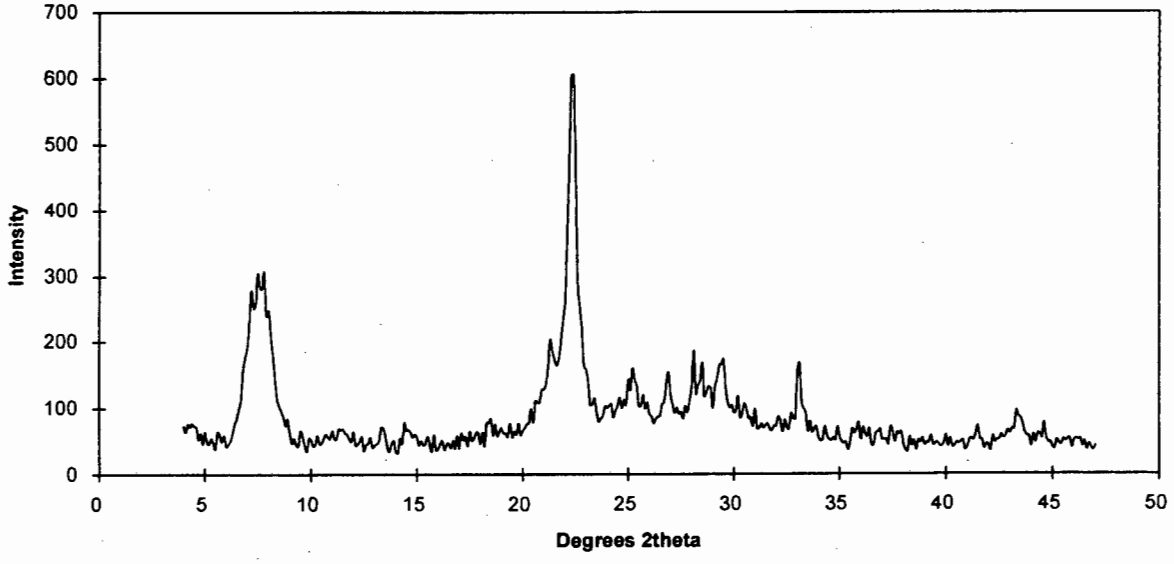

Figure 3.1. X-Ray diffraction pattern of sample A.

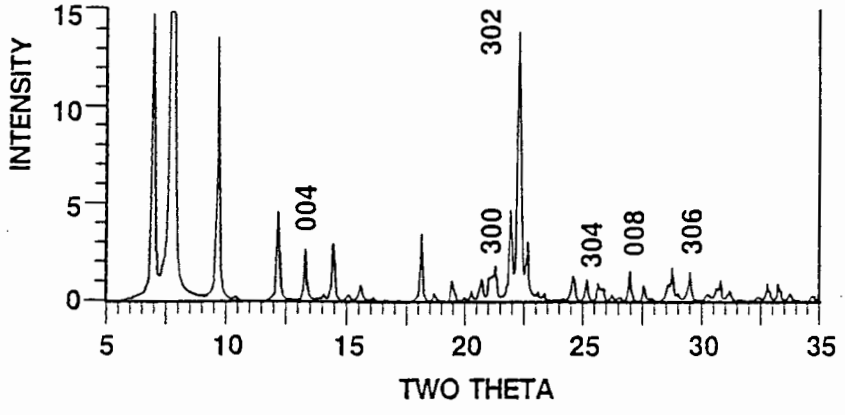

Figure 3.2a. Simulated XRD pattern for zeolite Beta (Szostak, 1992).

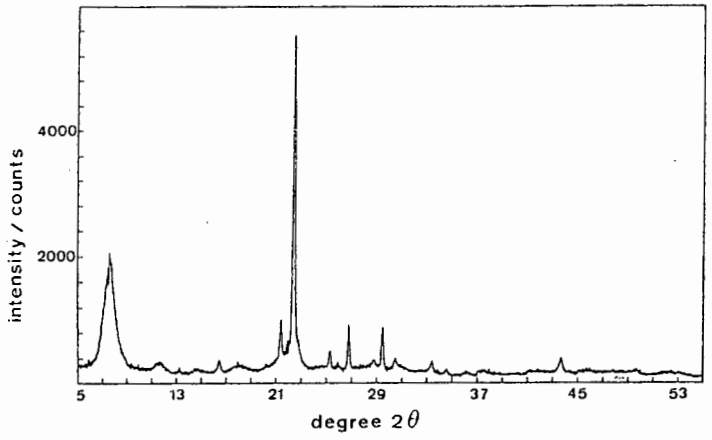

Figure 3.2b. XRD diffraction pattern of zeolite Beta (Perez-Pariente *et al.*, 1987).

The d-spaces and the relative intensities of sample A were comparable to those reported by Szostak (1992), Perez-Pariente *et al.* (1987) and Wadlinger *et al.* (1967) for zeolite Beta, as shown in Table 3.1a.

Table 3.1a. Comparison of relative intensities and d-spaces with literature.

Sample A		Szostak (1992)		Perez-Pariente *et al.* (1987)		Wadlinger *et al.* (1967)	
d-space*	Relative Intensity	d-space*	Relative Intensity+	d-space*	Relative Intensity+	d-space*	Relative Intensity+
1.18	51	1.15	MS	1.13	MS	1.14±0.02	MS
-	-	0.74	W	0.76	W	0.74±0.02	W
-	-	0.69	W	0.67	W	0.67±0.02	W
0.42	29	0.42	W	0.42	W	0.425±0.01	W
0.40	100	0.40	VS	0.40	VS	0.397±0.01	VS
0.30	30	0.30	W	0.30	W	0.30±0.01	W
0.21	18	0.21	W	0.21	W	0.22±0.01	W

*d-spaces are expressed in nm.

+W=weak, MS= medium strong, VS= very strong.

XRD showed that the sample is a single-phase crystalline zeolite Beta. The appearance of both sharp and broad features in the pattern has been ascribed to structural faulting in the zeolite (Newsam *et al.*, 1988). Major peaks at 7.8° and 22.4° 2θ, characteristic of zeolite Beta, constitute important features of the X-Ray diffraction pattern. Other peaks of lesser importance include those at 13.4° and 27.1° 2θ respectively, as reported by Coutanceau *et al.* (1997) for zeolite Beta. Since sample A exhibited the most intense diffractions, it was taken as the 100% crystallinity standard. The crystallinity of the other samples was calculated relative to sample A using the method of Perez-Pariente *et al.* (1987). This involved comparing the area under the most intense diffraction peak situated at 22.4° 2θ, of a particular sample to that of sample A after background subtraction. In order to be able to compare relative % crystallinity data, all the samples were scanned on the same day using identical instrumental set-up parameters. The relative % crystallinity of the samples, as calculated using the method described above, are presented in Table 3.1b.

Table 3.1b. Relative % crystallinity of samples.

Sample	Relative % Crystallinity
A	100
S400	87
S600	87
S600(1)	89
L400	92
L600	84
B	85
C	82
D	85
E	81
F	86

Samples S600 and S600(1) in Table 3.1b, were steamed using identical steaming conditions. The purpose of the duplication is to illustrate reproducibility of the XRD results. Figure 3.3 depicts the X-Ray diffractograms of samples S600 and S600(1). It can thus be assumed that the relative % crystallinity results are reproducible.

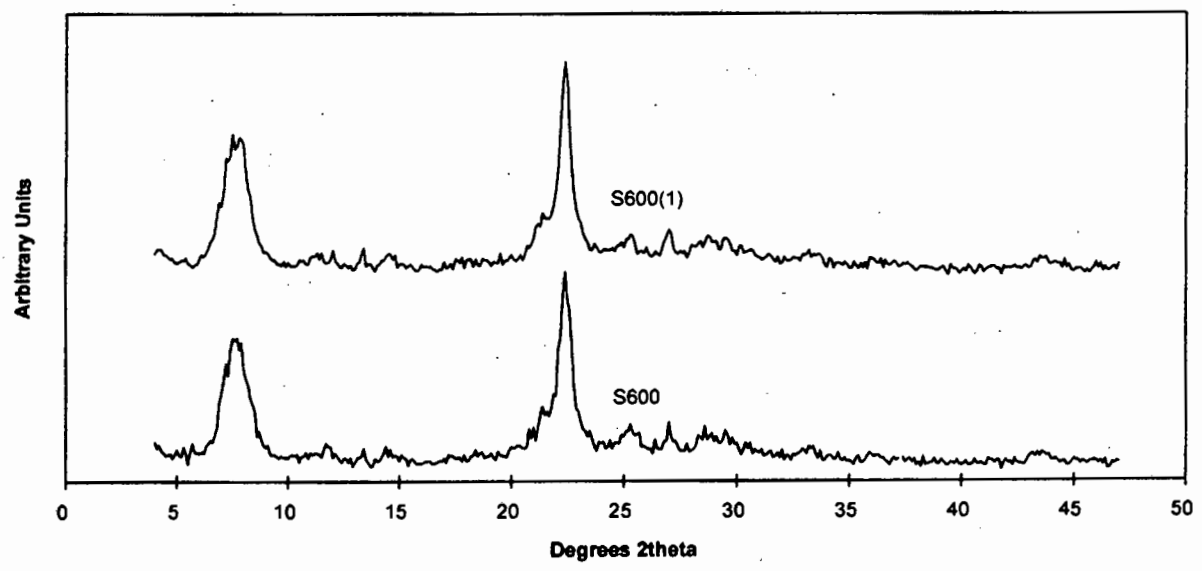

Figure 3.3. Reproducibility of XRD results.

The crystallinity of all the catalysts was generally relatively high (> 80%). From Table 3.1b, it can be deduced that the hydrothermal treatment of sample A resulted in a decrease in

crystallinity. Among the hydrothermally treated catalysts, the most severely steamed sample (L600) had the lowest crystallinity relative to sample A. The differently synthesised catalysts (B, C, D and E) and the commercial H-BEA standard, F, all exhibit relatively lower crystalline phases compared to sample A. Samples C and E, which were both subjected to mechanical pre-synthesis mixing and synthesised in 3 hours, have the lowest relative crystallinity compared to sample A.

3.1.1.2 Elemental Analysis

The elemental analysis of the catalysts was done by a combination of gravimetric analysis and atomic absorption spectroscopy (AAS). The Na and Al contents of the samples are shown in Table 3.2. For comparison purposes, the sodium and aluminium contents of non ion-exchanged sample A as well as the samples ion-exchanged using the three different methods, as outlined in section 2.2.2, are reported.

Table 3.2. Elemental analysis of samples.

Sample	Al content [mol/g]	Na content [mol/g]	Na/Al ratio
NaA	-	0.0018	-
A_1	0.0010	0.0014	1.4
A_2	0.0011	0.0010	0.9
A_3	0.0009	0.0016	1.8
B	0.0012	0.0012	1.0
C	0.0016	0.0017	1.1
D	0.0010	0.0013	1.3
E	0.0014	0.0014	1.0

Samples A_1, A_2 and A_3, that were respectively ion-exchanged using the three methods outlined in Section 2.2.2, had varying sodium contents as determined by elemental analysis. Sample A_2, which was subjected to the most severe ion-exchange procedure contained the least amount of sodium as expected. Conversely, sample A_3, which was treated using the mild ion-exchange procedure had the highest sodium concentration. However, in all cases, the sodium level in the catalysts was unexpectedly high, since all the samples had already been

ion-exchanged before the elemental analyses. Ion-exchange method 1 seems to be the most efficient in substituting ammonium for sodium ions in the zeolite lattice. Although the reason for the poor ion-exchange results could not be established, it can be speculated that the sodium cations are "trapped" in occluded pores, making their removal difficult during ion-exchange. When the zeolite is digested with mineral acid during elemental analysis, the trapped sodium cations are released and their concentration can thus be measured.

The sodium content of the synthesis gel of sample D was half that of the other samples (B, C, and E) (Table 3.2). However, after ion-exchange, the Na/Al ratio for sample D was higher compared to samples B, C and E. Hence, the sodium content after ion-exchange does not have a direct dependence on the sodium content of the synthesis gel.

The bulk Si/Al ratio of the samples are shown in Table 3.3. The $(Si/Al)_{gel}$ ratios of the samples prepared by different synthesis techniques are also presented in Table 3.3.

Table 3.3. $(Si/Al)_{gel}$ and bulk Si/Al ratios of samples.

Sample	$(Si/Al)_{gel}$ ratio	Bulk Si/Al ratio
A	- [1]	14.4
S400	-	10.8
S600	-	12.4
L400	-	9.9
L600	-	12.8
B	11.0	18.6
C	11.0	10.8
D	11.8	17.2
E	11.0	12.3
F	- [1]	14.6

[1] No information was available for these commercially sourced catalysts.

Due to the magnitude of the experimental error (cf. Appendix D) that occurs in the elemental (Al) analysis of zeolites by AAS and gravimetry for Si, it can be deduced that there is not a very significant difference between the bulk Si/Al ratios of the variously steamed samples.

This might be due to the fact that extra-framework aluminium, created during the steaming process, is not removed from the bulk of the zeolite, as proved by XPS analysis (Section 3.1.1.2). This indicates that no significant change would be expected in the bulk Si/Al ratio of the steamed catalysts as compared to sample A. The bulk Si/Al ratio of the differently synthesised samples varied from 10.8 to 18.6. Interestingly, the aluminium incorporation was higher for the samples synthesised in 3 hours (samples C and E) as compared to samples B and D, which were respectively synthesised in 7 and 30 hours respectively.

3.1.1.3 X-Ray Photoelectron Spectroscopy (XPS)

XPS was used to determine the Na content of non ion-exchanged sample A (referred to as NaA) and samples of catalyst A (referred to as A_1, A_2 and A_3) ion-exchanged using methods 1, 2 and 3 respectively, as described in section 2.2.2. Since XPS is a surface analysis technique, it was also used to probe the surface of one of the steamed samples (S600) for a possible enrichment in aluminium, following hydrothermal treatment. The results of the XPS analyses are recorded in Table 3.4 and 3.5. E_b represents the binding energy of the elements and Cmp. is the composition of each element in atom%.

Table 3.4. XPS analysis of sample A ion-exchanged by different methods.

	NaA		$A_1^{(1)}$		$A_2^{(2)}$		$A_3^{(3)}$	
	E_b [eV]	Cmp [at.%]	E_b [eV]	Cmp [at.%]	E_b [eV]	Cmp [at.%]	E_b [eV]	Cmp [at.%]
C	285.4 288.0 289.8	21	 287.3 290.2	12	286.7 288.6	14	285.4 287.7	13
O	535.7	57	534.9	63	534.6	62	535.5	61
Na	1076	0.3	*	0.06*	-#	-#	1080+	0.1+
Al	76.9	2	76.9	2	76.4	2	77.5	2
Si	106.0	20	104.8 106.9	24	104.9	23	105.9	25

(1) Sample A ion-exchanged by method 1.

(2) Sample A ion-exchanged by method 2.

(3) Sample A ion-exchanged by method 3.

+ The content of this element is very low; the peak position is difficult to determine.

The content of this element is below the detection limit.

* The content of this element is below the detection limit, but the element is likely to be present.

Table 3.5. XPS analysis of S600.

	S600	
	E_b [eV]	Cmp [at.%]
C	287.3 290.1	10
O	535.5	64
Na	*	0.05
Al	77.3	2
Si	105.8	25

* The content of this element is very low; the peak position is difficult to determine.

The % composition of sodium in samples A_1, A_2 and A_3 show that ion-exchange methods 1 and 2 seem to be very effective in reducing the sodium in the samples to a very low level. The discrepancy between the two sets of results obtained by XPS and AAS for the sodium content of samples A_1, A_2, and A_3 (Tables 3.2 and 3.4), can be accounted for by the fact that XPS is only a surface analysis technique while AAS is a bulk technique. The depth of analysis in XPS lies between 1.5 and 6 nm and it might have been possible that the ion-exchange procedure more effectively removed sodium at the zeolite surface than from the bulk.

Moreover, the XPS analysis of S600 shows that the % composition of the elements in that catalyst was very similar to that of sample A. Thus, it can be deduced that there was no aluminium enrichment at the surface of S600, in contrast to the findings of most studies carried out on steamed zeolites (Meyers *et al.*, 1986, Campbell *et al.*, 1996_b and Datka *et al.*, 1996).

3.1.1.4 Scanning Electron Microscopy (SEM)

The electron micrograph (Figure 3.4) of sample A shows the presence of 3-4 μm agglomerates of particles ranging in size from 100-200 nm. After hydrothermal treatment, no significant differences were observed in the morphology of the crystals as shown in the micrographs of the steamed samples (Figure 3.5).

The SEM micrographs of the samples prepared by different synthesis techniques are depicted in Figure 3.6. The electron micrographs of samples B and E show the presence of 500 nm and 200 nm oval shaped crystals respectively. 3-4 μm agglomerates of 200 nm particles were present in samples C and F. On the other hand, 1-2 μm agglomerates of 500 nm particles were seen in the SEM micrograph of sample D.

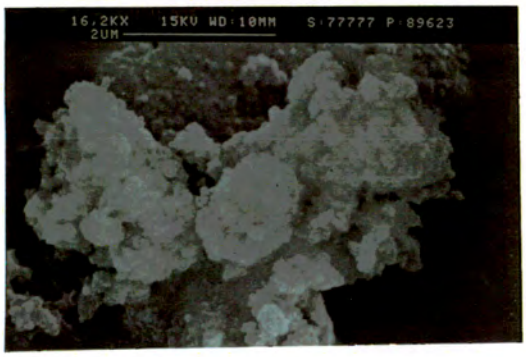

Figure 3.4. SEM micrograph of sample A.

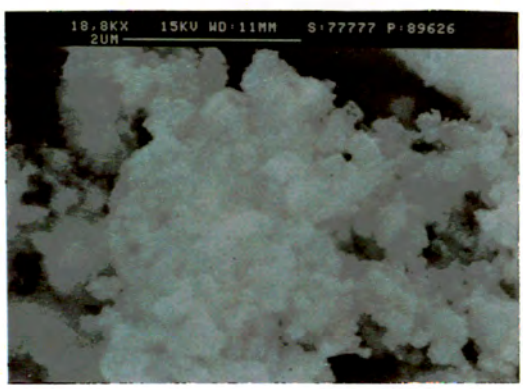

[a]

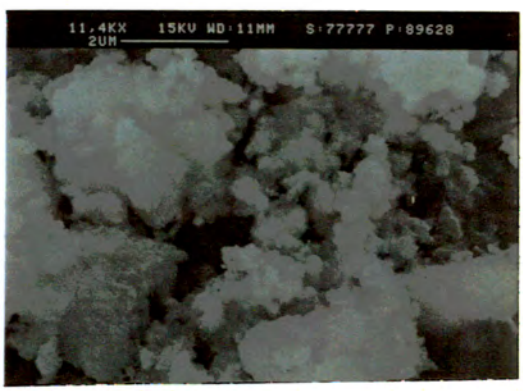

[b]

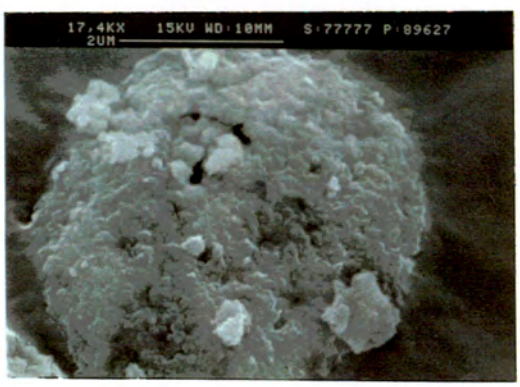

[c]

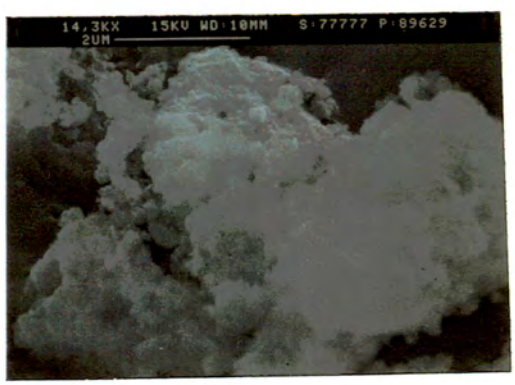

[d]

Figure 3.5. SEM micrographs of steamed samples; [a] S400, [b] S600, [c] L400 and [d] L600.

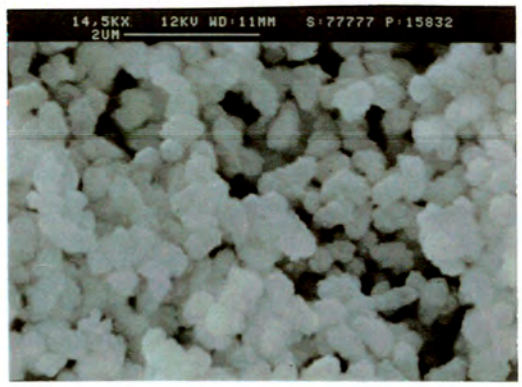

[I]

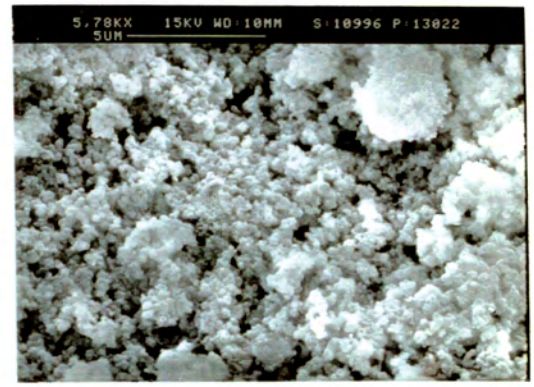

[II]

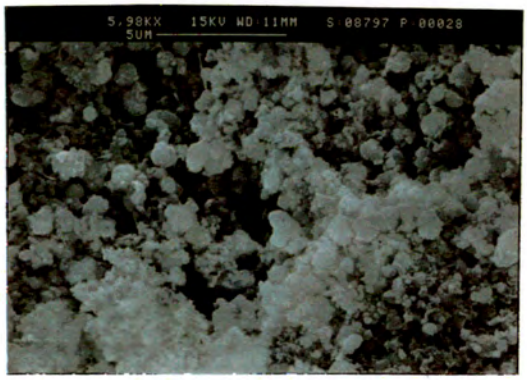

[III]

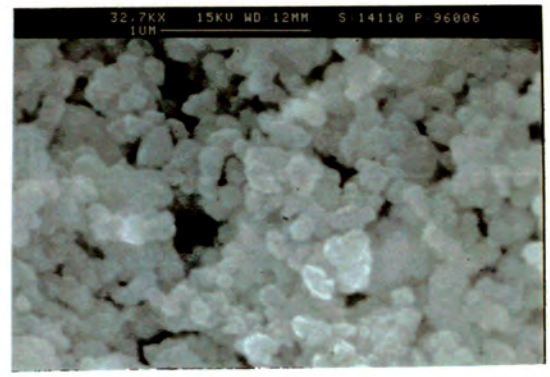

[IV]

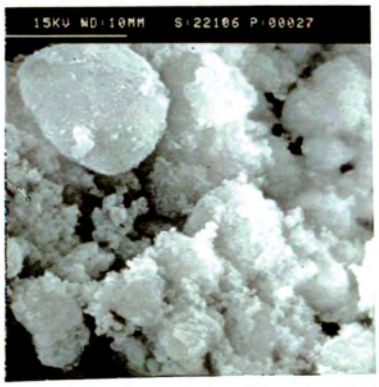

[V]

Figure 3.6. SEM micrographs of differently synthesised samples; [I] B, [II] C, [III] D, [IV] E and [V] F.

3.1.1.5 BET Micropore Analysis

Table 3.6 presents the results of the BET analysis of the samples. Mesopore (20-100 Å) areas were calculated from the BJH desorption plots as shown in Appendix E.

Reproducibility of the technique is shown by the results obtained for samples S600 and S600(1). Hydrothermal treatment at different temperatures and times had no effect on the micropore volume of sample A, indicating that extra-framework aluminium, created by steaming, did not result in any pore blockage of the micropore region of the catalysts. Further evidence is provided by the lack of hysteresis in the isotherm plots of the samples i.e, there was no marked difference between the ease of adsorption and desorption from the pores. However, the influence of hydrothermal treatment on mesopore and total surface area is apparent from Table 3.6. Steaming at a temperature of 600°C decreased both the total surface area and the mesopore area of samples S600, S600(1) and L600 as compared to sample A. There was no significant difference between the mesopore area of the samples steamed at 400°C (S400 and L400) and that of sample A. A slight increase in the total surface area of these samples was observed as compared to sample A, after hydrothermal treatment at 400°C. The change of steaming time from 2 to 21 hours did not have a major effect on the mesopore or the total surface area of the catalysts.

Table 3.6. BET analysis of samples.

Sample	Micropore Volume [ml/g]	Mesopore Area [m^2/g]	Total Surface Area [m^2/g]
A	0.14	188	526
S400	0.15	183	550
S600	0.14	157	501
S600(1)	0.14	136	501
L400	0.15	196	558
L600	0.14	133	478
B	0.14	272	594
C	0.16	110	505
D	0.15	139	505
E	0.14	140	478
F	0.15	184	546
A0.1	0.15	216	615
A1	0.15	206	593
A10	0.14	227	569

The modification of the mesoporosity of zeolite Beta by direct synthesis techniques has been shown to be possible as indicated by the mesopore areas of samples B to E in Table 3.6. B has the highest mesopore area while C has the lowest mesoporosity where as the mesoporosity of samples D and E are almost identical. Interestingly, sample B, the only zeolite that was prepared by static synthesis, has the highest total surface area as compared to the other samples. The mesoporosity and total surface area of the commercial H-BEA standard (sample F) was intermediate between those of sample B and the other zeolites synthesised by different techniques.

An increase in both mesoporosity and total surface area was observed for the acid washed samples (A0.1, A1 and A10) as compared to sample A. A similar observation has been made for other zeolites (Zukal *et al.*, 1986, Meyers *et al.*, 1988 and Dutartre *et al.*, 1996). The strength of the acid used in the leaching procedure was shown to be inversely proportional to the increase in total surface area. The mild acid washing (A0.1) resulted in a greater increase in surface area as compared to the more severe leaching procedures (A1 and A10).

3.1.1.6 ^{29}Si MAS NMR

^{29}Si MAS NMR was used to determine the environment of the Si atoms in the hydrothermally treated and acid washed samples. The framework Si/Al ratio of selected samples was also determined from ^{29}Si MAS NMR by using the following equation (Engelhardt, 1991):

$(Si / Al)_{fr} = \sum_{4}^{0} I_n / \sum_{4}^{0} 0.25nI_n$, where I_n are the intensities of the Si(nAl) peaks. The results were then compared to the values of the framework Si/Al ratio, obtained by a combination of chemical analysis and ^{27}Al MAS NMR by using the following equation (Engelhardt, 1991):

$(Si/Al)_{fr} = (Si/Al)_{bulk}(I_{60} + I_0)/I_{60}$

where I_{60} and I_0 are the intensities of the peaks at 60 and 0 ppm respectively.

The two sets of data are reported in Table 3.7.

Table 3.7. $(Si/Al)_{fr}$ as determined by ^{29}Si NMR and ^{27}Al NMR and chemical analysis.

Sample	^{29}Si MAS NMR		^{27}Al MAS NMR and Chemical Analysis	
	$(Si/Al)_{fr}$	$(Al/uc)_{fr}$	$(Si/Al)_{fr}$	$(Al/uc)_{fr}$
A	14.8	4.1	14.4	4.2
S400	27.0	2.3	24.5	2.5
S600	59.1	1.1	33.6	1.8
L400	32.1	1.9	26.6	2.3
L600	44.7	1.4	40.6	1.5
F	25.0	2.5	40.6	1.5

There exists a fairly good correlation between the two sets of results indicating that very little "NMR invisible" aluminium was present in the samples.

The assignment of the peaks present in a typical ^{29}Si MAS NMR spectrum, to different Si environments, has been previously discussed (Section 1.3.3.7). ^{29}Si MAS NMR revealed that the Si atoms in all the samples (including sample A) only have two different environments, viz Si(1Al) and Si(0Al). The peaks observed at -104 ppm were assigned to Si(1Al), that is silicon atoms tetrahedrally co-ordinated to 1 Al and 3 Si atoms. The peaks in the range -111 to -115 ppm were assigned to Si(0Al), that is silicon atoms tetrahedrally co-ordinated to 4 other Si atoms. The relative % intensities of the peaks corresponding to the different Si environments are shown in Table 3.8.

Table 3.8. Assignment and relative % intensities of peaks in the ^{29}Si MAS NMR spectra.

Sample	-104 ppm – Si(1Al)	-111 ppm – Si(0Al)	-113 ppm – Si(0Al)	-115 ppm – Si(0Al)
A	27	58	-	15
S400	15	73	-	12
S600	7	79	-	14
L400	12	77	-	11
L600	9	62	10	19
F	16	74	-	10

In the case of sample L600, three different peaks corresponding to a Si(0Al) environment were observed. The detection of signals at –111.5, -113 and –115.7 ppm in the ^{29}Si MAS NMR spectrum of thermally treated zeolite Beta has been attributed to the presence of three crystallographically inequivalent sites by Perez-Pariente *et al.* (1990). Moreover, the relative intensities of the different peaks detected in the ^{29}Si MAS NMR spectra of samples F and S400 are comparable.

From Table 3.8, the decrease in the relative intensity of the peak situated at –104 ppm as a result of steaming is about 60% on average, indicating that a considerable amount of aluminium has been extracted from the framework of these zeolites. The effect of the severity (temperature) of the hydrothermal treatment is apparent from the first column in Table 3.8. Accordingly, the relative intensity of the peaks situated in the –111 to –115 ppm range increased by an average of about 22% for the steamed samples as compared to sample A. This observation is in agreement with the fact that during the steaming process, Si insertion at the vacant sites left by framework aluminium takes place, leading to an increase in the concentration of Si environments of the type Si(0Al).

^{29}Si NMR MAS spectra of selected samples are shown in Figure 3.7.

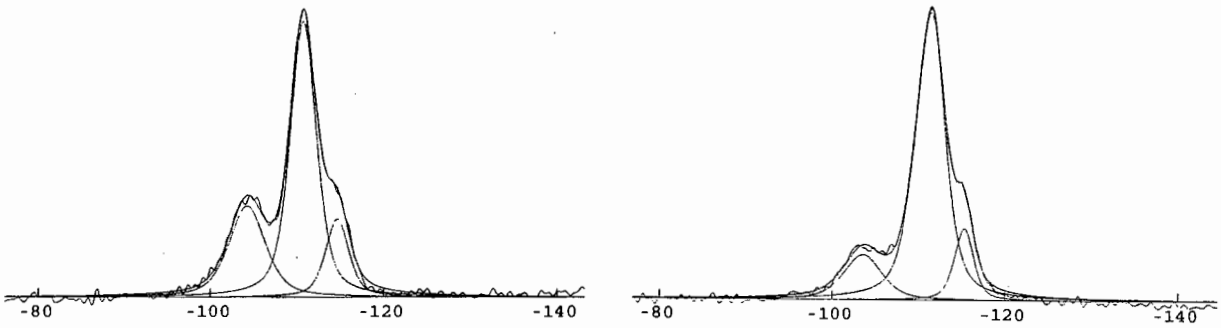

[a] [b]

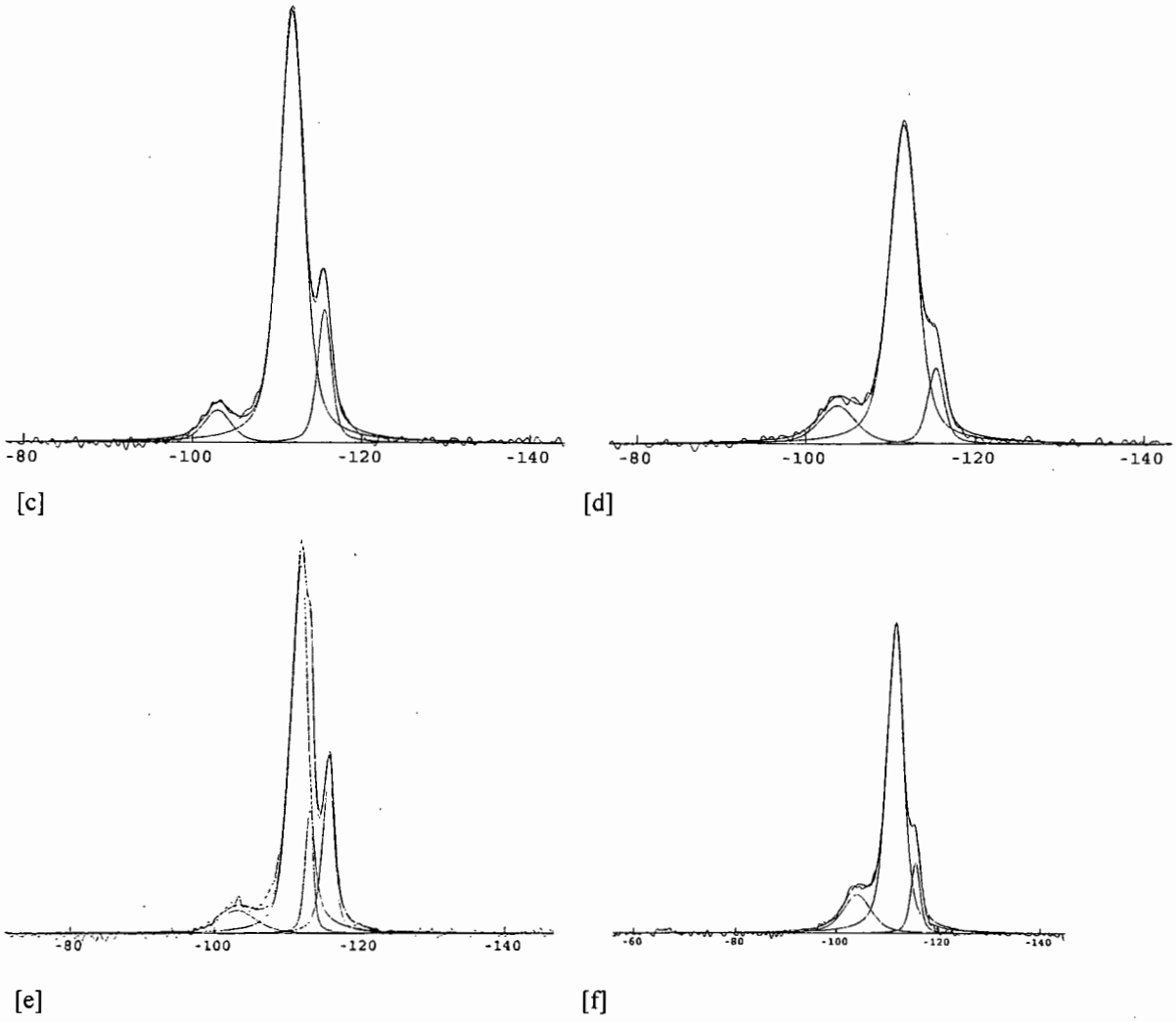

Figure 3.7. ^{29}Si MAS NMR spectra of selected samples: [a] A, [b] S400, [c] S600, [d] L400, [e] L600 and [f] F.

Furthermore, only two different Si environments viz. Si(1Al) and Si(0Al), were detected in the acid washed samples (A0.01, A0.1, A1, A10 and L400/A0.01). The spectra of these samples are presented in Appendix F.

3.1.1.7 ^{27}Al MAS NMR

^{27}Al MAS NMR spectra were recorded in order to determine the co-ordination of the Al atoms in all samples. The relative amounts of each aluminium species (framework and/or non-framework) present in some samples were calculated using a combination of ^{27}Al MAS NMR and chemical analysis results. The ^{27}Al MAS NMR spectra of a range of samples are shown in Figure 3.8. The spectra of all other samples are presented in Appendix G.

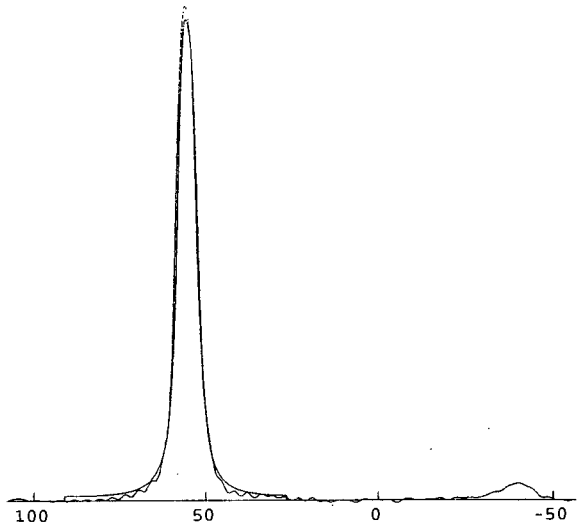

[a]

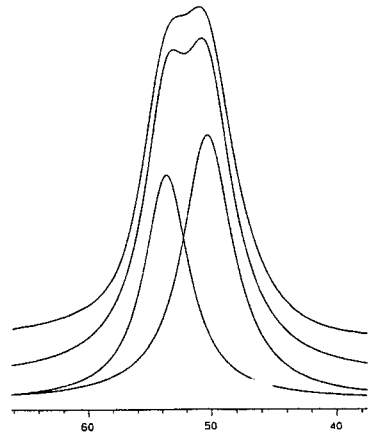

[b]

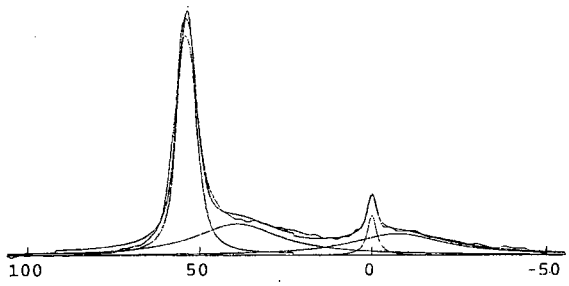

[c]

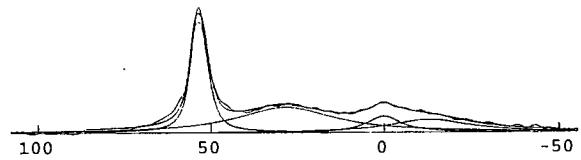

[d]

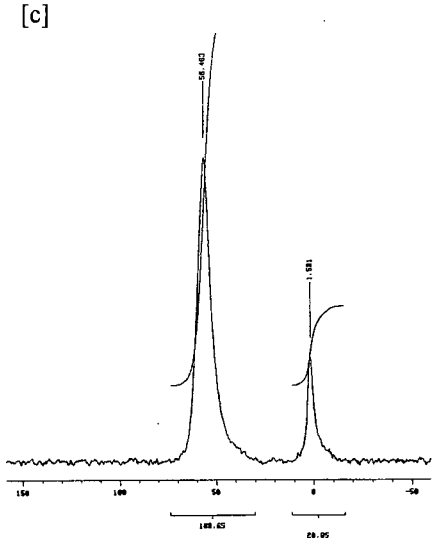

[e]

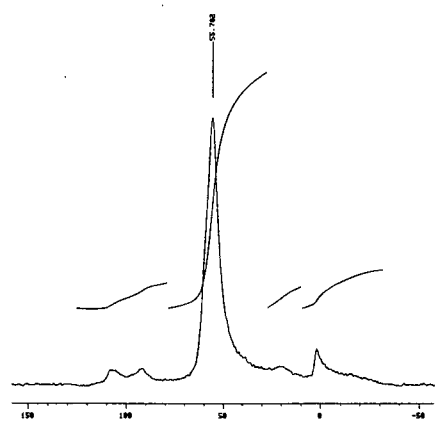

[f]

Figure 3.8. ^{27}Al MAS NMR spectra of selected samples: [a] A, [b] C, [c] S400, [d] L600, [e] A0.1 and [f] L400/A0.01.

The assignment of peaks present in the ^{27}Al MAS NMR spectrum of zeolites in general, to Al atoms of different co-ordinations, has been reviewed in section 1.3.3.6. The ^{27}Al MAS NMR spectra of all samples revealed a major peak located between 50 and 60 ppm. This signal has been previously assigned to four co-ordinated framework aluminium atoms in zeolite Beta (Perez-Pariente *et al.*, 1990).

A peak at a chemical shift of ~0 ppm was exhibited in the ^{27}Al MAS NMR spectra of the steamed and acid washed samples. This signal has been attributed to six co-ordinated extra-framework aluminium (EFAl) species. The presence of a broad shoulder situated at a chemical shift of ~35 ppm was clearly apparent in the ^{27}Al MAS NMR of the steamed and some acid washed samples. Four co-ordinated non-framework aluminium, with a possible contribution from a penta co-ordinated non-framework aluminium species is thought to be responsible for the peak at ~35 ppm (Gilson *et al.*, 1987). Furthermore, a shoulder at ~10 ppm was observed in the ^{27}Al MAS NMR of some samples. However, even though this shoulder has been assigned to EFAl, the exact nature of these species could not be identified. Hence, this type of EFAl will be referred to as EFAl-x.

The samples that were synthesised by different synthesis techniques (B-E) as well as sample A only contained framework aluminium atoms. Interestingly, a distinct splitting of the ^{27}Al MAS NMR signal (50-60 ppm), corresponding to four co-ordinated framework aluminium, was observed for these samples. Similar phenomena have been reported by Chauvin *et al.* (1990) and Hunger *et al.* (1995) for mazzite and dealuminated MCM-22 respectively.

The chemical shifts and the relative intensity of the two types of framework aluminium atoms (herein referred to as types Al[I] and Al[II]) responsible for the splitting of the signal in the 50-60 ppm range are presented in Table 3.9.

Table 3.9. Chemical shifts and relative intensity of Al[I] and Al[II] type atoms present in samples A-E.

Sample	Chemical Shift/ppm		%Relative Intensity	
	Al[I]	Al[II]	Al[I]	Al[II]
A	53.4	50.2	36.9	63.1
B	53.8	50.4	19.7	80.3
C	53.6	50.3	43.3	56.7
D	53.5	50.4	38.4	61.6
E	53.5	50.4	48.4	51.6

Steaming of sample A resulted in the formation of a low concentration of six co-ordinated EFAl species (EFAl-6). However, a significant amount of four co-ordinated EFAl species (EFAl-4), with a possible contribution from penta co-ordinated aluminium species (Al-5), was formed following hydrothermal treatment. Moreover, a substantial amount of EFAl-x species resulted from steaming, except for sample L600 which had the lowest concentration of this type of EFAl. The maximum number of EFAl was attained after sample A was steamed at 600°C for 21 hours (L600). Although the commercial standard (sample F) was not subjected to any hydrothermal treatment, it contained an appreciable amount of EFAl (EFAl-4/Al-5 and EFAl-6 species). The amount of the different aluminium species present per unit cell in samples A and F, as well as in the steamed samples, is shown in Table 3.10. Detailed calculations are presented in Appendix H.

Table 3.10. Amount of different aluminium species per unit cell in samples A, F and steamed samples.

Sample	Framework Al	EFAl-6	EFAl-4/Al-5	EFAl-x	Total Al[(1)]
A	4.2	-	-	-	4.2
S400	2.4	0.2	1.6	1.2	5.4
S600	1.8	0.2	1.3	1.5	4.8
L400	2.2	0.2	1.8	1.7	5.9
L600	1.5	0.4	1.9	0.8	4.6
F	1.5	1.1	1.5	-	4.1

[(1)] Calculated from AAS.

Acid washing resulted in the creation of EFAl-6 species in all these samples. The most severely acid washed sample (A10) contained a significant amount of both EFAl-6 and EFAl-x species, but no EFAl-4/Al-5 species compared to the samples that were leached with lower acid concentrations. Only four co-ordinated framework aluminium atoms and EFAl-6 species were detected in sample A1. On the other hand, all three types of EFAl species and four co-ordinated framework aluminium atoms were present in samples A0.01, A0.1 and L400/A0.01. It was not possible to deconvolute the NMR spectra of the acid washed samples in order to calculate the relative concentrations of the differently co-ordinated aluminium species present in these catalysts.

3.1.1.8 Infrared Spectroscopy

Figure 3.9 shows the framework vibration region spectra of samples A-E. Peaks and/or bands with wavenumbers at 430, 465, 526, 579, 800, 1095 and 1230 cm^{-1} have been observed by Jacobs and Martens (1987) in the FTIR spectrum of zeolite Beta. The peaks and/or bands do not always occur at these wavenumbers but show some variation depending on the composition of the unit cell. All the peaks and/or bands with the above wavenumbers were detected in the spectra of samples A-E. Bands and/or shoulders present at 624 cm^{-1} (Lohse *et al.*, 1996), 730 cm^{-1} (Szostak *et al.*, 1993) and 950 cm^{-1} (Szostak *et al.*, 1993, Kiricsi *et al.*, 1994 and Yang and Xu, 1997) have also been reported in the literature for zeolite Beta. The bands at 624 and 730 cm^{-1} were visible in the spectra of the samples. However, the band at 950 cm^{-1} was not apparent from the infrared spectra of samples A-E. This particular band has been assigned to structural vacancies present in zeolite Beta (Yang and Xu, 1997) and large amounts of surface silanol groups in very small crystals (Szostak *et al.*, 1993). In addition, Vaudry *et al.* (1994) have suggested that silanol defects in zeolite Beta are evidenced by shoulders present at 910 and 970 cm^{-1} in the infrared spectrum. Since the presence of highly defected silanol sites in zeolite Beta is associated with the faulting of layers (Newsam *et al.*, 1988), the absence of the 950 cm^{-1} band indicates that the crystals of samples A-E were not extensively faulted.

Two major bands are present in the asymmetric stretching vibration region (1250-950 cm^{-1}) of samples A-E, as has been previously reported for zeolite Beta (Jacobs and Martens, 1987). While the band present at 1230 cm^{-1} is associated with the asymmetric stretching vibration of

external tetrahedra, the 1095 cm^{-1} band originates from the asymmetric stretching vibration of internal tetrahedra. A band present at a wavenumber of ~1300 cm^{-1} in the infrared spectra of samples A, B and E could not be assigned to any particular vibration.

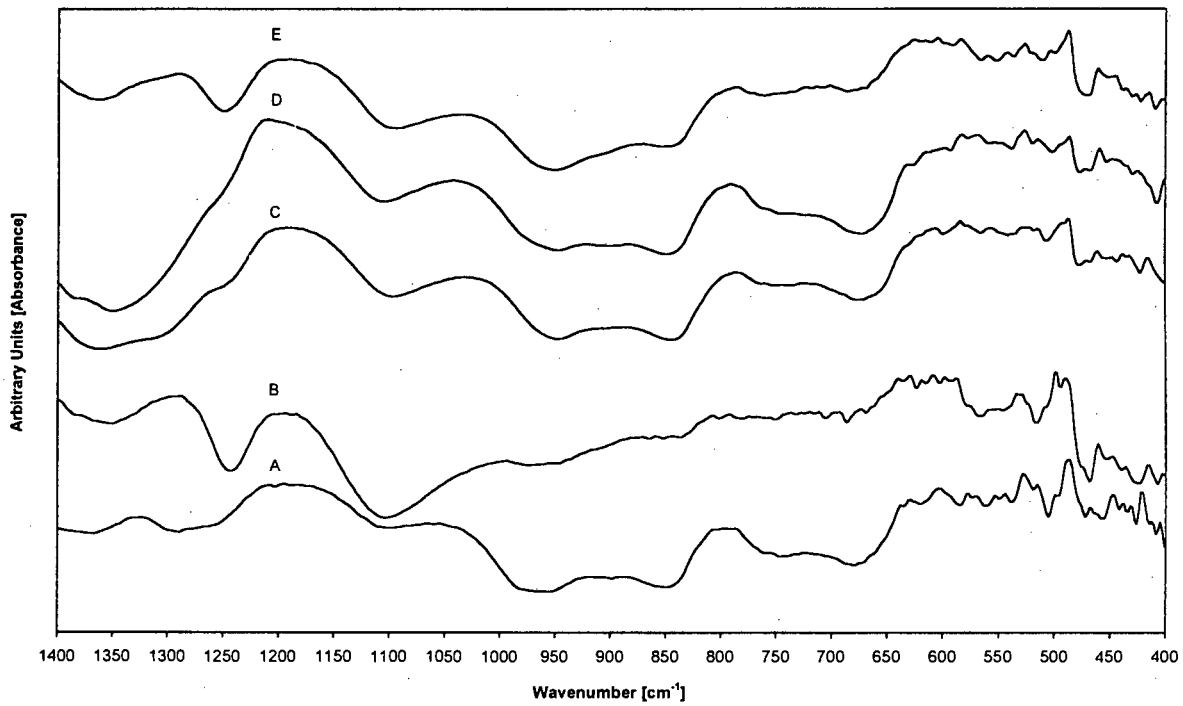

Figure 3.9. Infrared spectra of samples A-E.

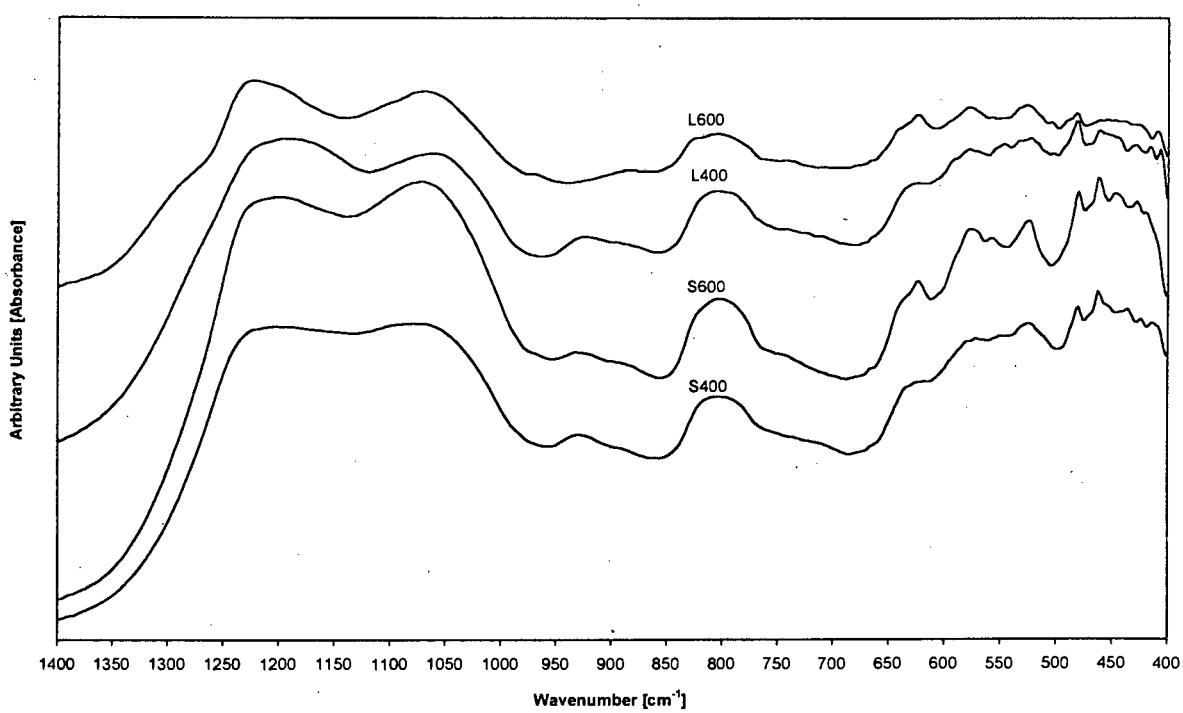

Figure 3.10. Infrared spectra of steamed samples.

The band situated at a wavenumber of 800 cm^{-1} in the symmetric stretching vibration region (950-650 cm^{-1}) of the samples has been attributed to external linkages of AlO_4 tetrahedra vibrations (Jacobs and Martens, 1987). The peaks present at 526 and 579 cm^{-1} are characteristic of zeolite Beta (Perez-Pariente *et al.*, 1987 and Kiricsi *et al.*,1994) and lie within the range of the double ring vibrations of tetrahedra. The peak situated at 526 cm^{-1} has been attributed to the double four ring (D4R) vibrations of zeolite Beta, due to the fact that a large fraction of 4-membered rings is present in the framework of the zeolite (Newsam *et al.*, 1988). Furthermore, the two peaks detected at 430 and 465 cm^{-1} in the infrared spectra of the samples, have been assigned to TO_4 bending vibrations of the internal tetrahedra.

The infrared spectra of the framework vibration region of the steamed samples are presented in Figure 3.10. All the characteristic zeolite Beta peaks and/or bands were present in these spectra. In general, the definition of the peaks present in the spectra of the steamed samples was lower than those present in the spectrum of sample A. The asymmetric stretching vibration at 1076-1095 cm^{-1} has been reported to shift to higher wavenumbers following the dealumination of zeolite Beta (Coutanceau *et al.*, 1997 and Yang and Xu, 1997). In the present case, the band present at 1054 cm^{-1} in the spectrum of sample A was seen to shift to 1080, 1072, 1063 and 1068 cm^{-1} for samples S400, S600, L400 and L600 respectively. Moreover, Szostak *et al.* (1993) have related shifts in the wavenumbers of the bands, in particular the band at 767 cm^{-1}, present in the 400-800 cm^{-1} region of the infrared spectrum of zeolite Beta, to dealumination. The band present at 787 cm^{-1} in the spectrum of sample A shifted to 804 cm^{-1} after hydrothermal treatment. A shoulder at 970 cm^{-1} was apparent from the infrared spectra of the samples steamed at a temperature of 600°C (S600 and L600). As has been previously stated, this particular shoulder has been assigned to structural vacancies in zeolite Beta. Hydrothermal treatment at 600°C might have resulted in the creation of such structural vacancies due to aluminium removal from the framework of the zeolite.

3.1.2 Catalyst Acidity

The temperature programmed desorption of ammonia (TPD) was used to investigate changes in the number of acid sites as a result of dealumination. TPD results of the samples synthesised by different techniques are also reported. ^1H MAS NMR was performed on the

steamed samples in order to investigate the type of hydroxyl groups present in these catalysts. These results are also presented in this section.

3.1.2.1 Temperature Programmed Desorption (TPD)

The number and strength of acid sites present in the samples were determined using ammonia TPD. The results of the TPD studies are detailed in Table 3.11. The experimental error associated with the TPD measurements was calculated to be 8%.

Only one desorption peak was observed in all the TPD spectra of the samples. Steaming of sample A under various conditions reduced its acid site density as evidenced by the data in Table 3.11. This observation is in agreement with the fact that framework aluminium, which is postulated as being associated with an acid site, is removed during the dealumination procedure. A decrease in the number of the acid sites in zeolite Beta as a result of dealumination has been previously reported (Parikh *et al.*, 1994, Das *et al.*, 1996 and Apelian *et al.*, 1996). The density of acid sites decreased with the severity of the steaming procedure, with the steaming temperature having a more significant effect than the steaming time. A similar finding has been made by Kornatowski *et al.* (1992) on steamed ZSM-5.

Sample B, the only zeolite Beta catalyst that was synthesised in a static medium, had the highest density of acid sites. On the other hand, of the differently synthesised catalysts (B-E), sample D, which had the longest synthesis time (30 hours), had the lowest number of acid sites. The density of acid sites in both samples C and D was comparable. Thus, the different silica sources that were used in the synthesis of these samples did not have a significant effect on the number of acid sites. The commercial H-BEA standard (sample F) had a relatively low acid site density (comparable to L600).

Table 3.11. Comparison of AAS and TPD data of samples.

Sample	Al content [mmol/g] (AAS)	Number of Acid Sites [mmol/g] (TPD)	T_{max} [°C]
A	1.00	1.25	375
S400	1.04	0.96	319
S600	0.98	0.84	326
L400	1.02	0.91	335
L600	1.01	0.67	311
B	1.20	1.37	385
C	1.60	1.06	294
D	1.00	0.90	372
E	1.40	1.16	361
F	-	0.70	312

The concentration of aluminium atoms in the samples as determined by AAS was compared to the number of acid sites present. In all cases, except for sample A, the concentration of aluminium atoms was higher than the number of acid sites.

T_{max} (maximum peak temperature) values of the samples are presented in Table 3.11. Leu *et al.* (1991) have suggested that the strength of acid sites in zeolite Beta can be directly correlated to T_{max}. Steaming had the effect of decreasing the strength of the acid sites in sample A. Samples A, B and D had high acid site strengths whereas sample C is the weakest in terms of strength of acid sites. The strength of the acid sites present in the commercial H-BEA standard (sample F) was again comparable to that of sample L600 (low acid site strength).

Figure 3.11 shows the TPD response curves of selected samples. The TPD spectra of the remaining samples are presented in Appendix I.

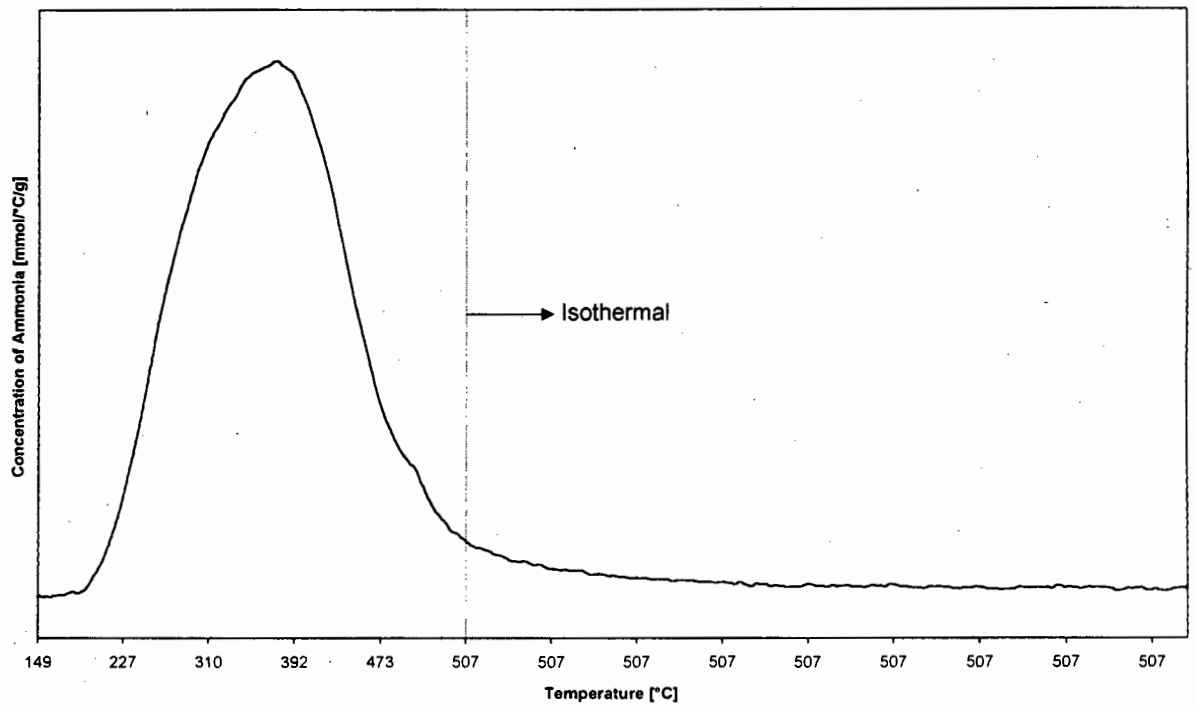
Concentration of Ammonia [mmol/°C/g]
Isothermal
149 227 310 392 473 507 507 507 507 507 507 507 507 507
Temperature [°C]

A

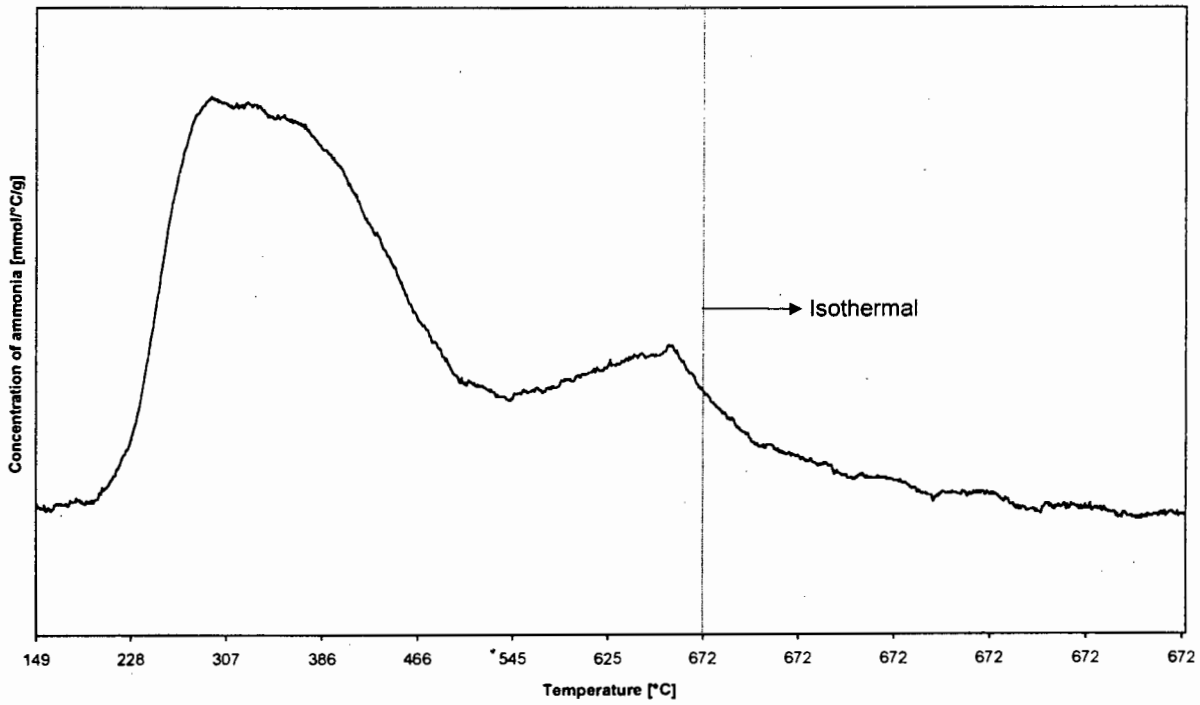
Concentration of ammonia [mmol/°C/g]
Isothermal
149 228 307 386 466 545 625 672 672 672 672 672 672
Temperature [°C]

C

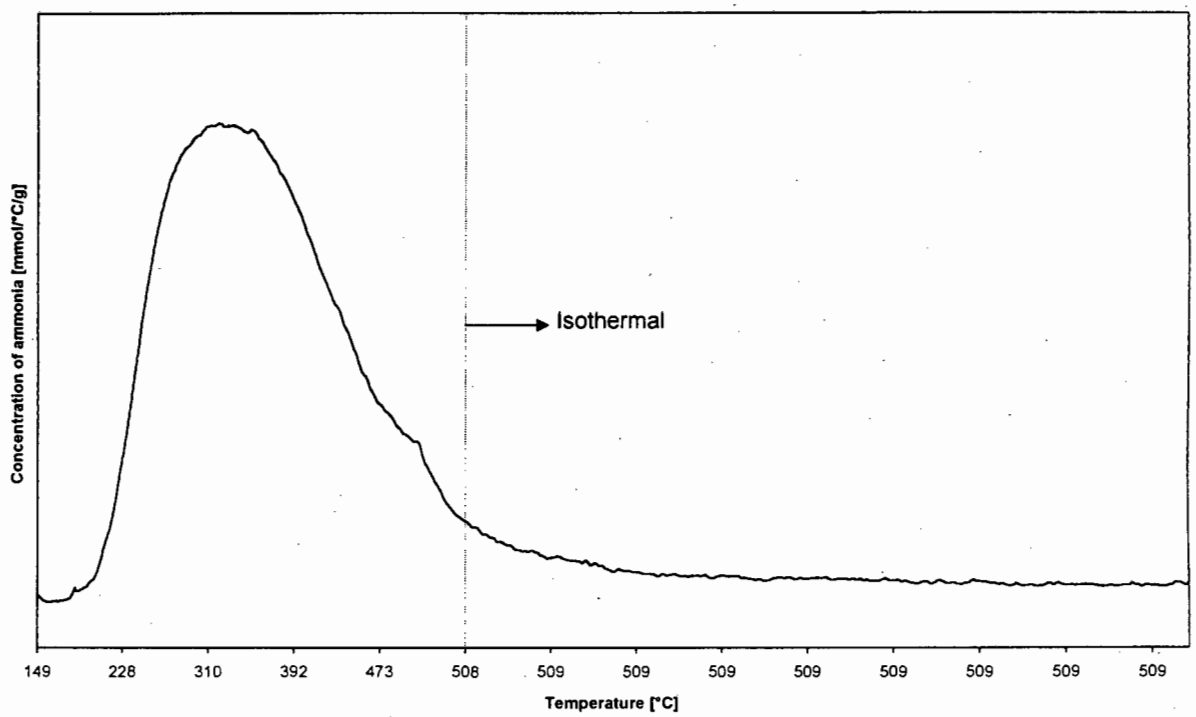

S400

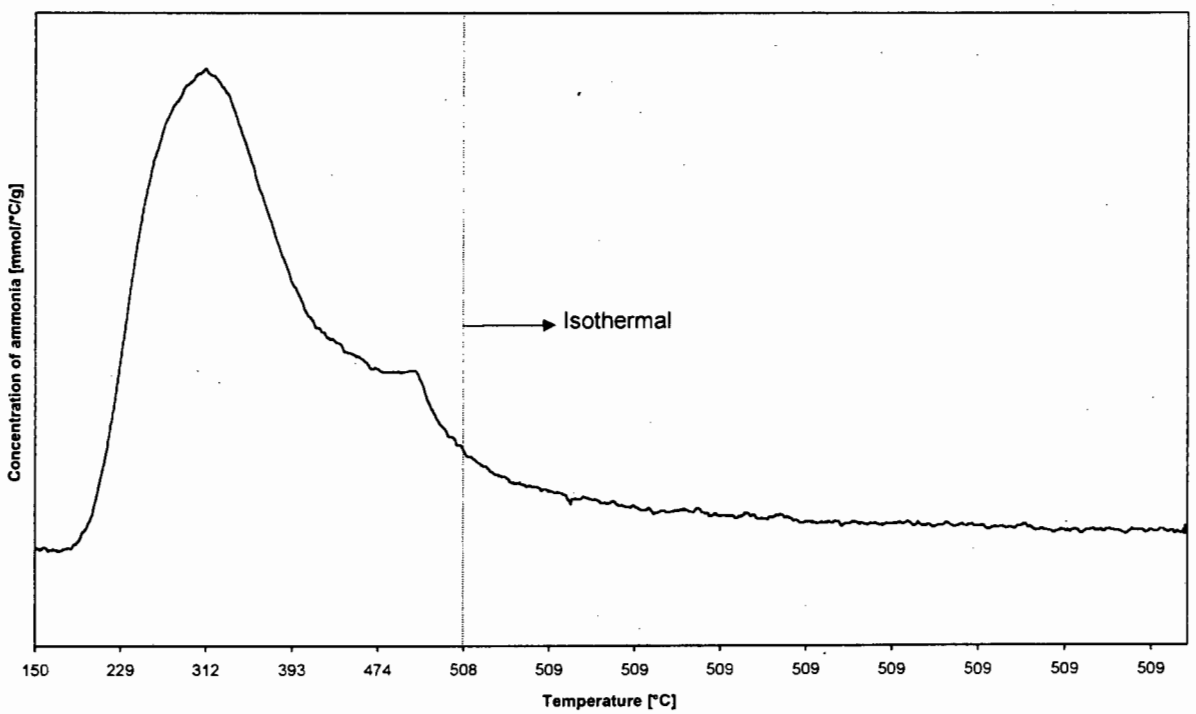

L600

Figure 3.11. TPD spectra of selected samples.

3.1.2.2 ^1H MAS NMR

^1H MAS NMR studies were performed on the steamed samples in order to determine the effect of steaming on the concentration of the different hydroxyl groups present in the zeolite. A table detailing the typical chemical shift ranges, corresponding to the four distinct types of protons that can be identified in the ^1H MAS NMR spectrum of zeolites, is presented in section 1.3.4.1.

In the present study, three types of hydroxyl signals were observed in the spectra of the samples. The signal at ~2 ppm has been assigned to SiOH groups at framework defects and to OH groups associated with extra-framework Al species (AlOH). The signals at ~4 ppm (narrow) and ~4.5-5 ppm (broad) are respectively due to acidic bridging hydroxyl groups and the so-called perturbed bridging OH groups. The broad band due to the perturbed bridging OH groups is explained by weak hydrogen bonds of these hydroxyl protons to neighbouring framework oxygen atoms. It has been reported by Brunner *et al.* (1995) that these groups exhibit the same acid strength as the unperturbed bridging OH groups. The relative concentrations of the different OH groups present in the samples, are presented in Table 3.12.

Table 3.12. Concentration of hydroxyl groups in samples A, F and steamed samples.

Sample	SiOH and AlOH groups (~2 ppm) [mmol/g]	Bridging OH groups (~4 ppm) [mmol/g]	Perturbed bridging OH groups (~4.5-5 ppm) [mmol/g]	Total Concentration [mmol/g]
A	1.01	0.29	0.80	2.1
S400	1.02	0.08	0.50	1.6
S600	1.00	0.00	0.20	1.2
L400	0.83	0.02	0.65	1.5
L600	1.10	0.00	0.00	1.1
F	1.15	0.05	0.10	1.3

The concentration of SiOH and AlOH groups did not change significantly following hydrothermal treatment. On the other hand, there was a marked decrease in the concentration of bridging and perturbed bridging hydroxyl groups as a result of steaming. The decrease was more pronounced for the samples steamed at 600°C (S600 and L600). Interestingly, the ^1H

MAS NMR spectrum of sample L600 did not show evidence of any type of bridging hydroxyl groups even though TPD studies showed that this sample had an appreciable number of acid sites. The amount of desorbed ammonia from TPD investigations was higher than the concentration of acidic (bridging and perturbed bridging) hydroxyl groups present in all samples except for sample A. The commercial HBEA standard has a low concentration of acidic (bridging and perturbed bridging) hydroxyl groups.

The ^{1}H MAS NMR spectra of all the samples are presented in Figure 3.12.

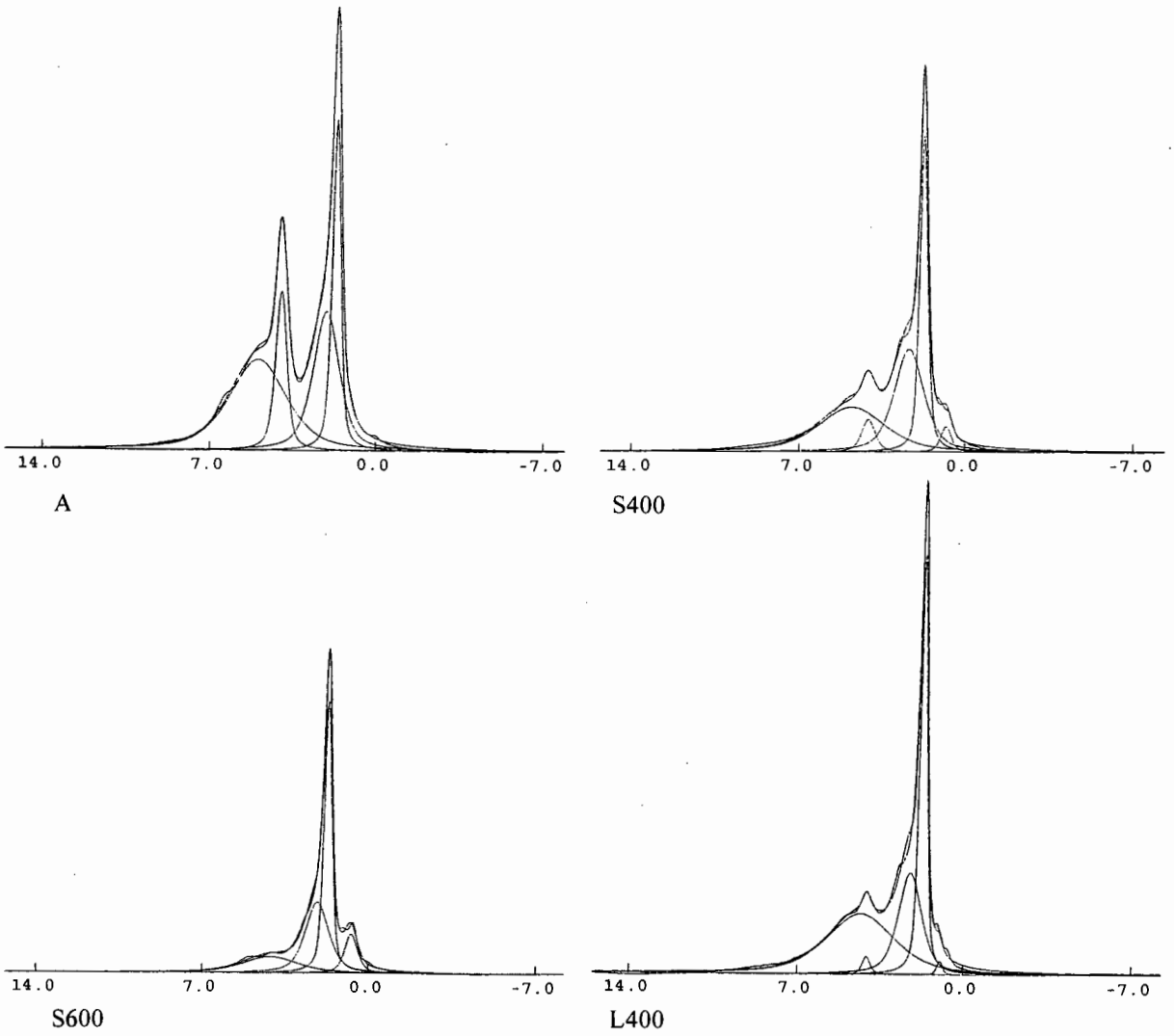

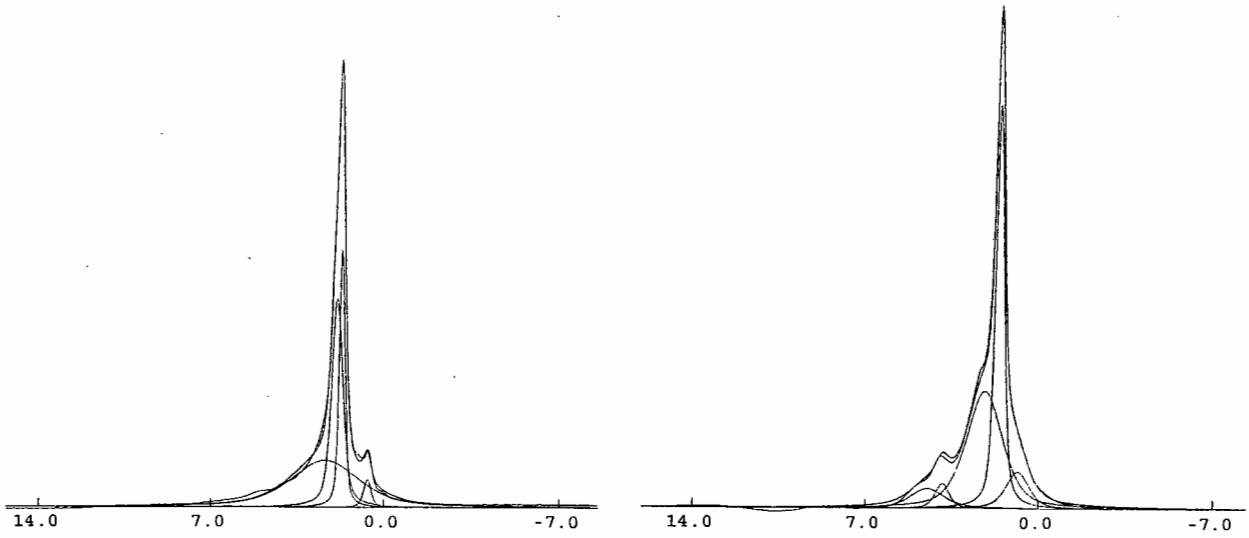

L600 F

Figure 3.12. ^{1}H MAS NMR spectra of samples.

3.2 REACTION STUDIES

In the present study, the activity of the catalysts was tested using the alkylation of benzene with propene. The effects of synthesis technique, steaming and acid washing on the alkylation activity of the catalysts were investigated separately. The experimental conditions that were used in the reaction studies are detailed in section 2.4.3.

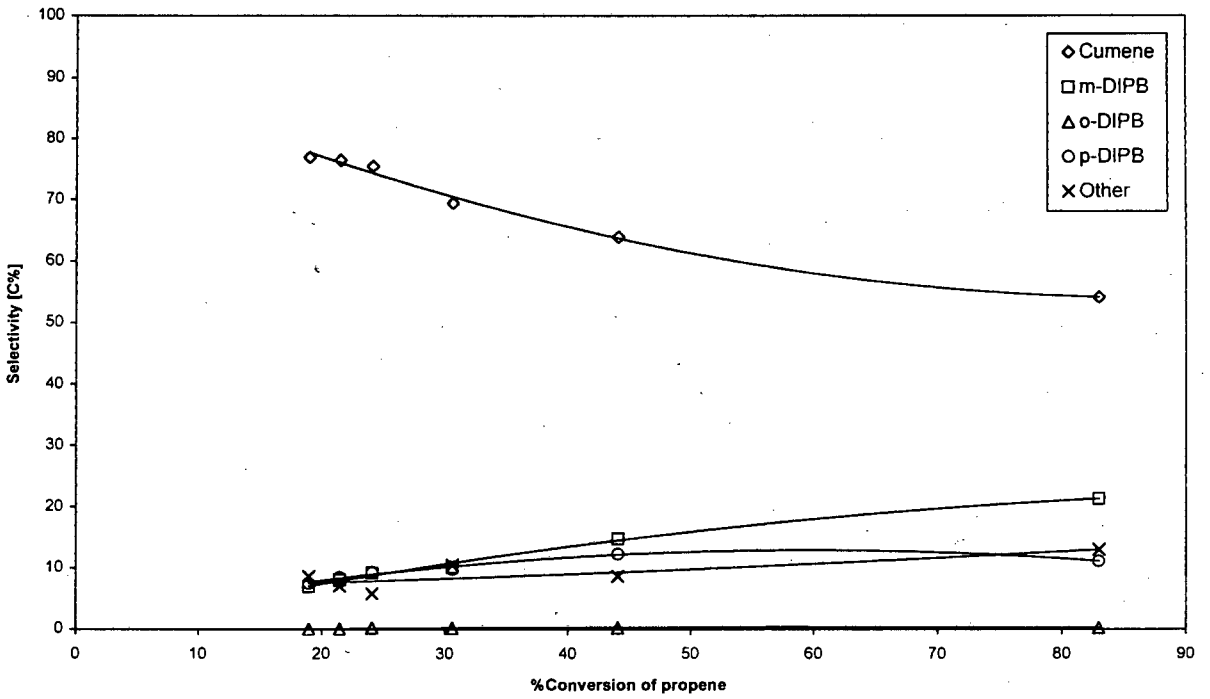

Figure 3.13. Selectivty [C%] to products as a function of % conversion of propene for sample A.

Since the alkylation of benzene with propene is a series reaction, the selectivity to cumene (primary product) increases with decreasing conversion levels of propene. It follows that the selectivity to diisopropyl benzene (DIPB) and triisopropyl benzene (TIPB) decreases with decreasing conversion of propene, as shown in Figure 3.13. In addition to the above products, propene oligomers were formed during the reaction. Moreover, trace amounts of n-propyl benzene were detected in the reaction products. TIPBs, propene oligomers and n-propyl benzene are grouped under "other" products in Figure 3.13. The desired product of this particular alkylation reaction is the primary product, cumene.

3.2.1 Effect of Steaming on Catalytic Activity

The results of the reaction studies that were carried out on the steamed zeolite Beta catalysts are presented in this section. The time on stream conversion data for these catalysts are shown in Figure 3.14.

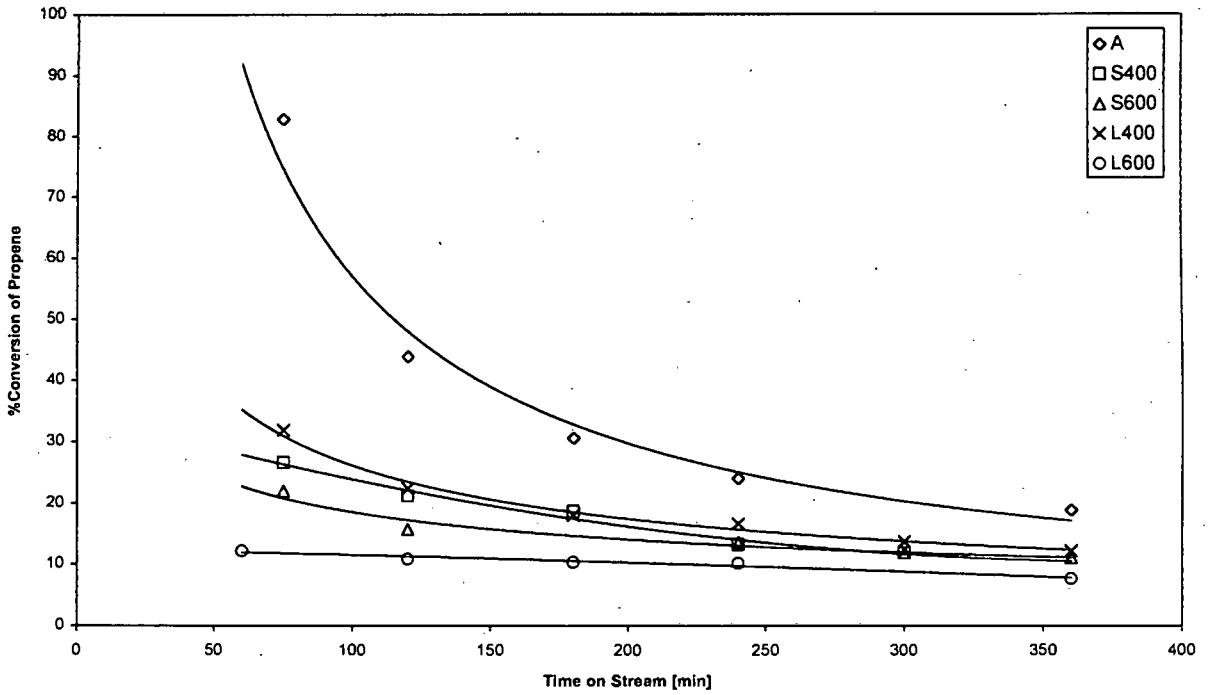

Figure 3.14. Activity of steamed samples.

It can be clearly seen from Figure 3.14 that sample A was the most active catalyst for this particular reaction compared to the hydrothermally treated catalysts. Steaming of sample A using a set of conditions resulted in a significant decrease in its activity for the alkylation of benzene with propene. Among the steamed catalysts, L400 showed the highest activity. However, the rates of conversion of propene molecules over samples S400 and L400 as well as S600 and L600 were comparable during the reaction period. L600, being the least active catalyst, exhibited a stable time on stream behaviour. There was no significant difference between the deactivation rates of samples L400, S400 with time on stream. At pseudo steady state (TOS = 360 min), the activity of the steamed catalysts was similar.

The change in selectivity [C%] to cumene with time on stream for the steamed samples is presented in Figure 3.15.

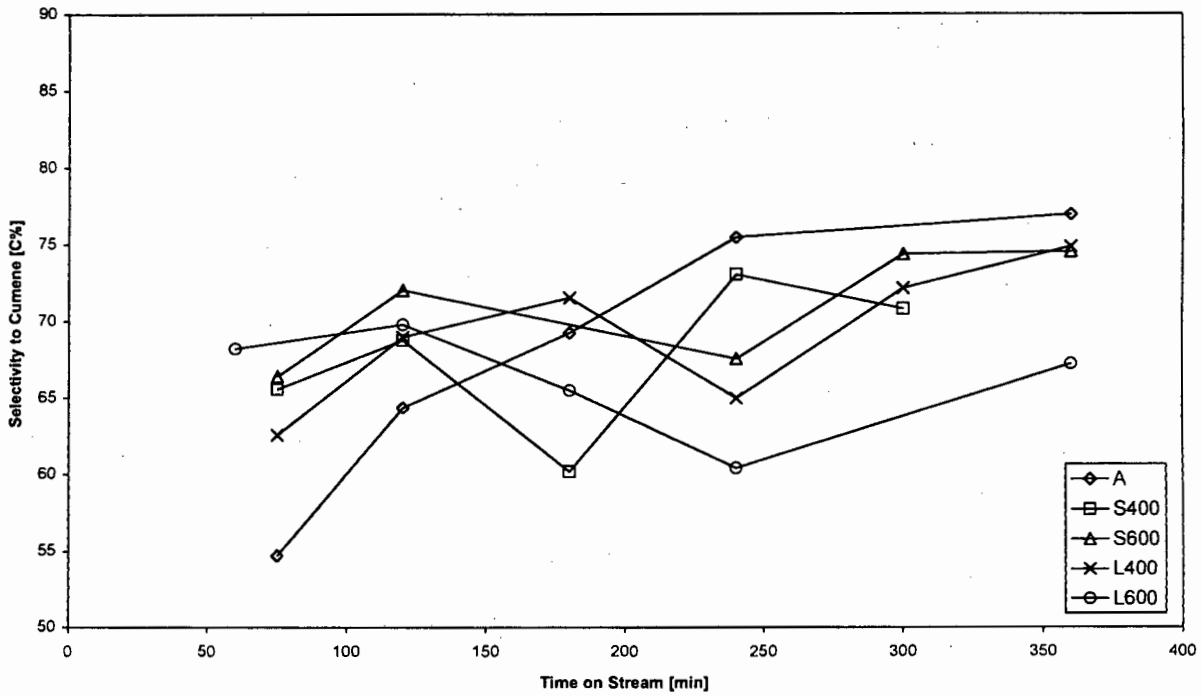

Figure 3.15. Selectivity [C%] to cumene for steamed samples.

Sample A, the most active catalyst, had the highest selectivity (77%) to cumene for this reaction at pseudo steady state (TOS = 360 min). As expected, since the % conversion of propene decreased with time on stream, a general increase in the selectivity to cumene was observed for catalysts A, S400, S600 and L400, although the increase in selectivity for S400 was erratic. Despite the difference in the activity of sample A and that of S400, S600 and L400, the selectivity to cumene over these catalysts were similar at pseudo steady state. On the other hand, there was no major variation in the selectivity to cumene with time on stream for the least active catalyst, L600 as the selectivity to cumene for this catalyst was almost constant at 66%.

Figure 3.16 shows the variation in the % yield of cumene with time on stream for the steamed catalysts.

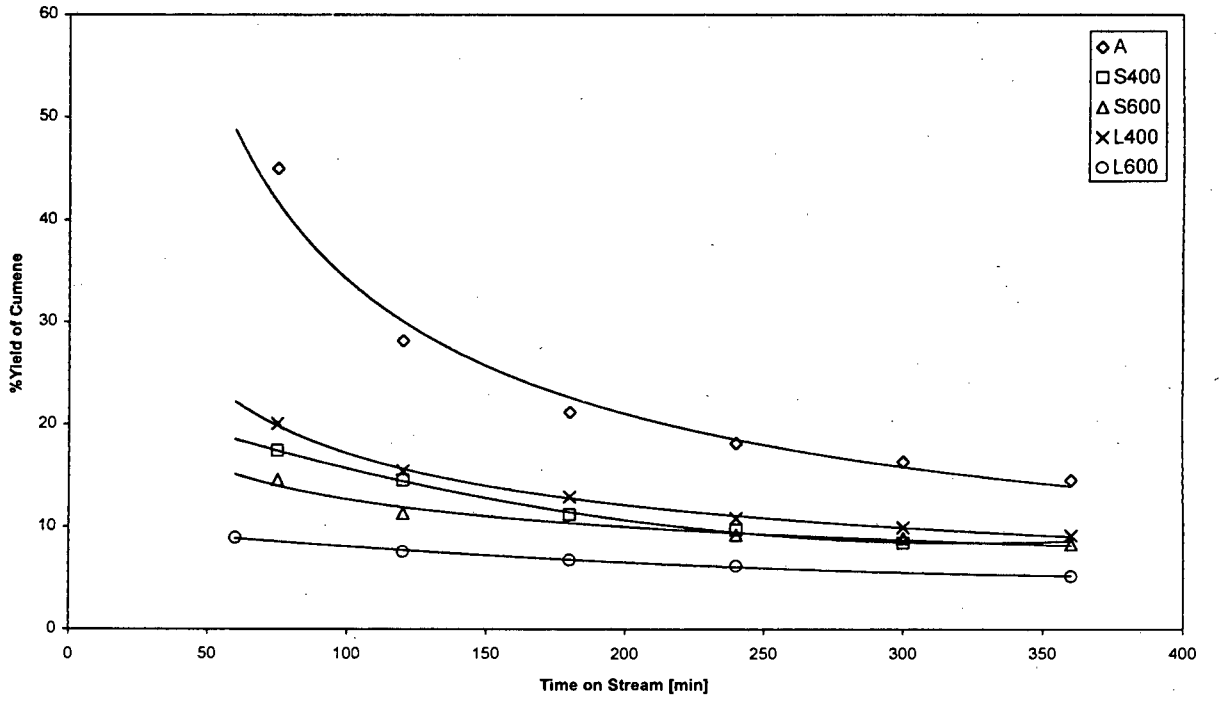

Figure 3.16. %Yield of cumene for steamed samples.

The same trend as for the time on stream conversion data was observed for the change in the cumene yield with time on stream for the steamed catalysts. The effect of steaming temperature was once more apparent from Figure 3.16; the cumene yield for samples S400 and L400 was higher than for S600 and L600 for most of the reaction period. Sample A, being the most active catalyst gave the highest cumene yield. At pseudo steady state (TOS = 360 min), almost identical cumene yields were observed for samples S400, L400 and S600. On the other hand, the % yield of cumene that was obtained for catalyst L600 was constant at about 7% for the entire duration of the reaction. Among the steamed catalysts, sample L600 gave the lowest cumene yield.

Figure 3.17 presents the distribution (selectivity [C%]) of the products that were formed during the alkylation reaction over the steamed catalysts at 4 hours time on stream.

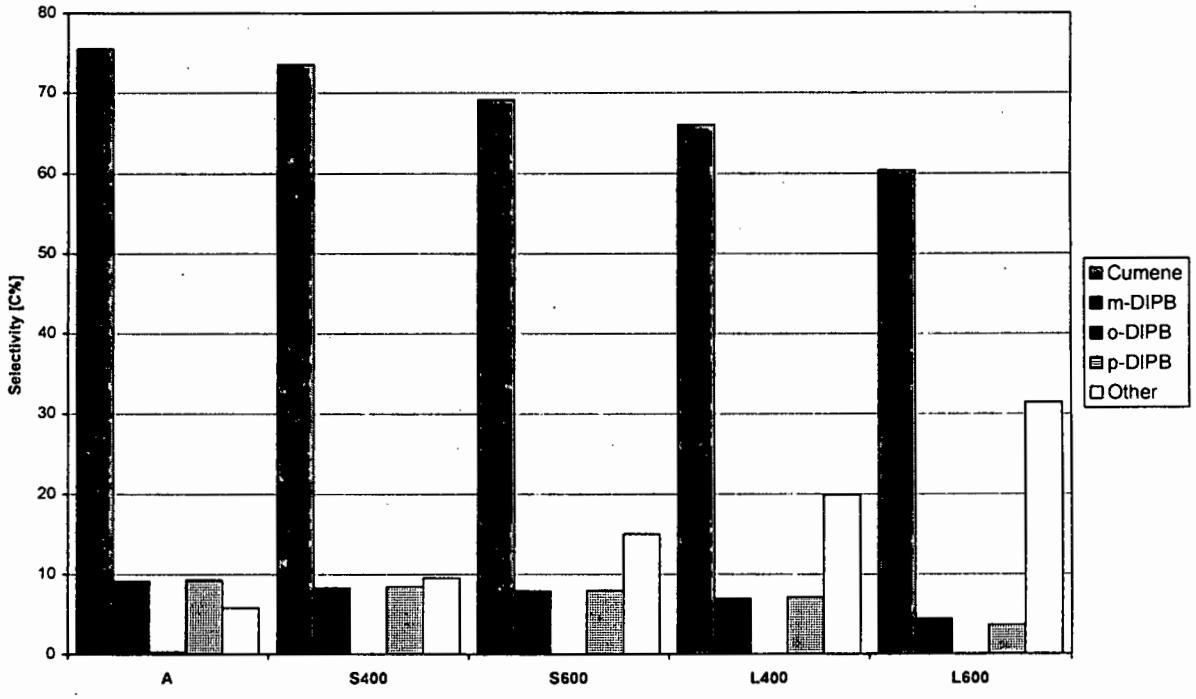

Figure 3.17. Selectivity [C%] to products for steamed samples at TOS = 240 min.

In Figure 3.17, the "other" products that were formed during the reaction include primarily propene oligomers, together with triisopropyl benzene (TIPB) and trace amounts of n-propylbenzene. As has been previously mentioned, catalyst A was the most selective to cumene since it formed the least by-products. From Figure 3.17, it can be deduced that the selectivity to cumene at this particular time on stream (240 min) decreased with the severity of the hydrothermal treatment i.e, L600 having the lowest and S400 the highest selectivity to cumene respectively. A similar trend was observed for the selectivity to diisopropyl benzene (DIPB) over the steamed catalysts. Hence, it followed that the formation of by-products, including triisopropyl benzene (TIPB), propene oligomers and n-propyl benzene, was greatest for L600. A steady increase in the formation of by-products was observed with the severity of the hydrothermal treatment. Moreover, only the para and meta isomers of DIPB were formed over the steamed catalysts.

The variation of the m/p DIPB ratio with time on stream for the steamed samples is shown in Figure 3.18.

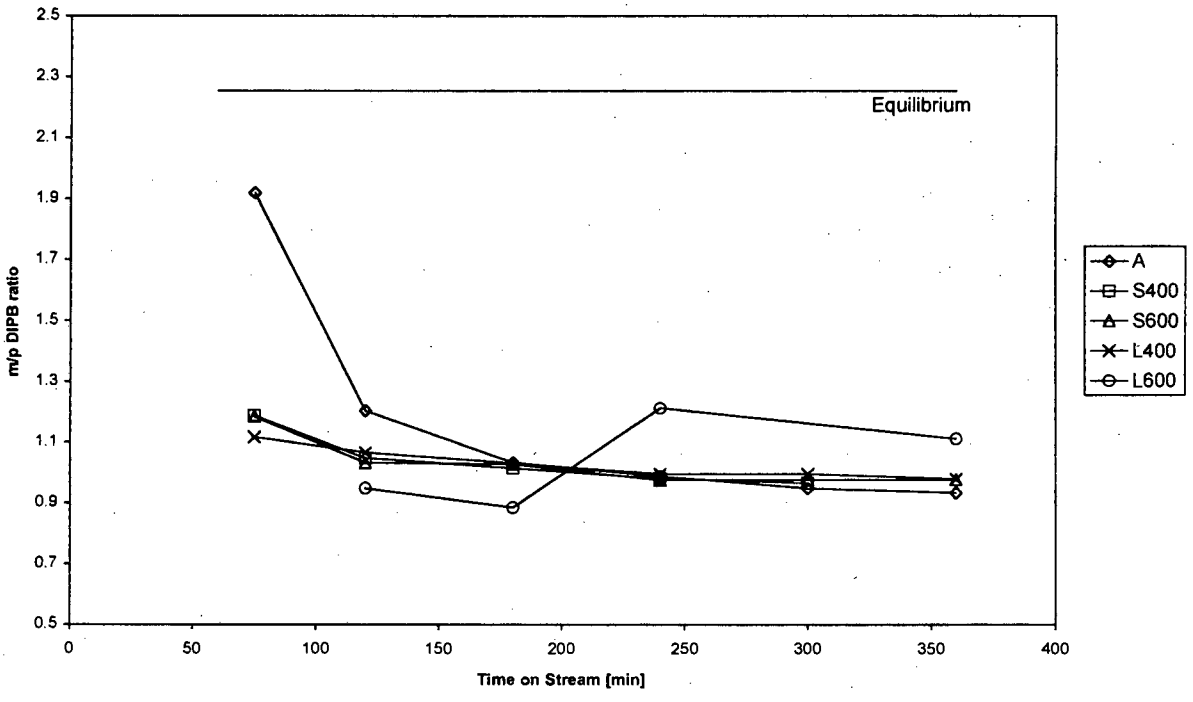

Figure 3.18. m/p DIPB ratio for steamed samples.

A sharp decrease in the m/p DIPB ratio was observed for catalyst A in the first half of the reaction period, after which the ratio remained constant at about 1. On the contrary, only a slight decrease in the m/p DIPB ratio with time on stream was observed for samples S400, S600 and L400. All these catalysts exhibited very similar m/p DIPB ratios during the course of the reaction. Since the meta isomer is thermodynamically more stable than the para isomer, it would be expected that the m/p DIPB ratio would be at the value predicted by equilibrium calculations at the reaction temperature (210°C). However, the fact that the m/p DIPB ratio was below equilibrium indicates a possible influence of the shape selective nature of the catalysts.

3.2.2 Effect of Synthesis Technique on Catalytic Activity

The time on stream behaviour of the catalysts that were synthesised by different techniques, is shown in Figure 3.19.

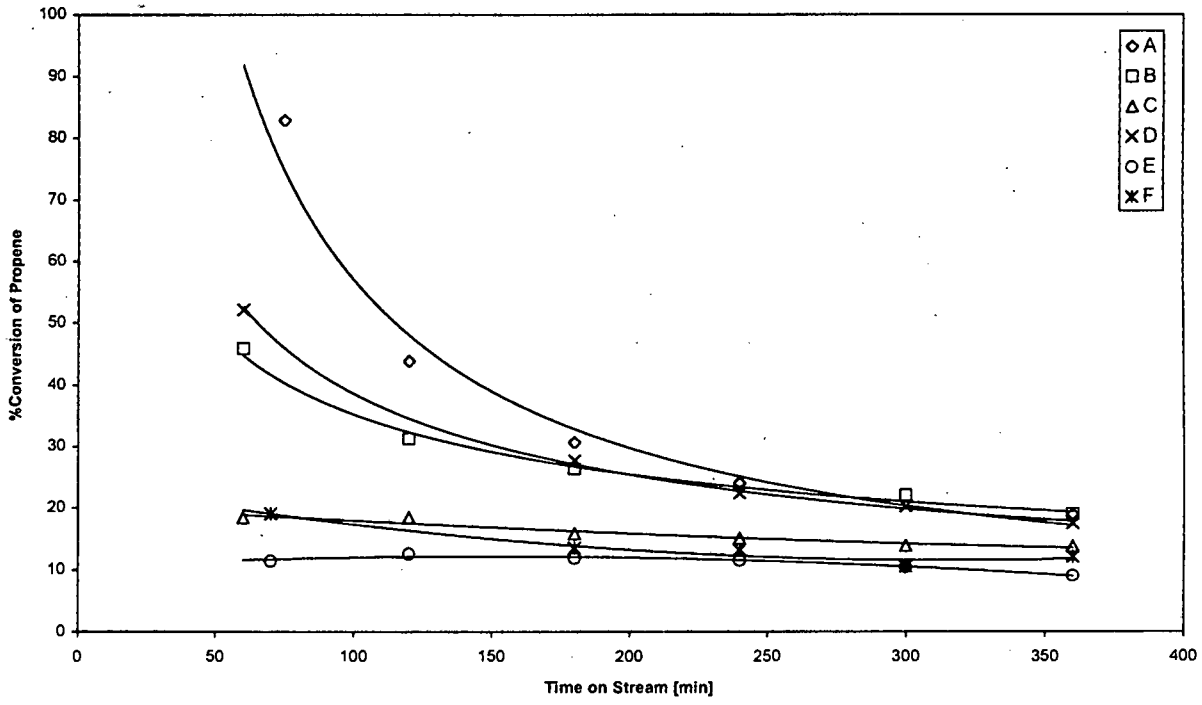

Figure 3.19. Activity of samples A-F.

It can be deduced from Figure 3.19 that sample A was the most active catalyst for the alkylation of benzene with propene. However, although both sample A and the H-BEA standard (sample F) are commercial catalysts, there exists a significant difference in their catalytic activity for this particular reaction. Among the catalysts that were synthesised by different synthesis techniques, samples B and D were the most active, with comparable activity. Moreover, samples C, E and F exhibited similar low catalytic activity. As a result of their low activity, these catalysts had stable time on stream behaviours. On the other hand, the more active catalysts underwent rapid deactivation due to the formation of coke. At pseudo-steady state (TOS = 360 min), there was no marked difference in the rate of conversion of propene molecules to products over the different catalysts.

Figure 3.20 shows the change in selectivity to cumene with time on stream for the differently synthesised zeolite Beta catalysts.

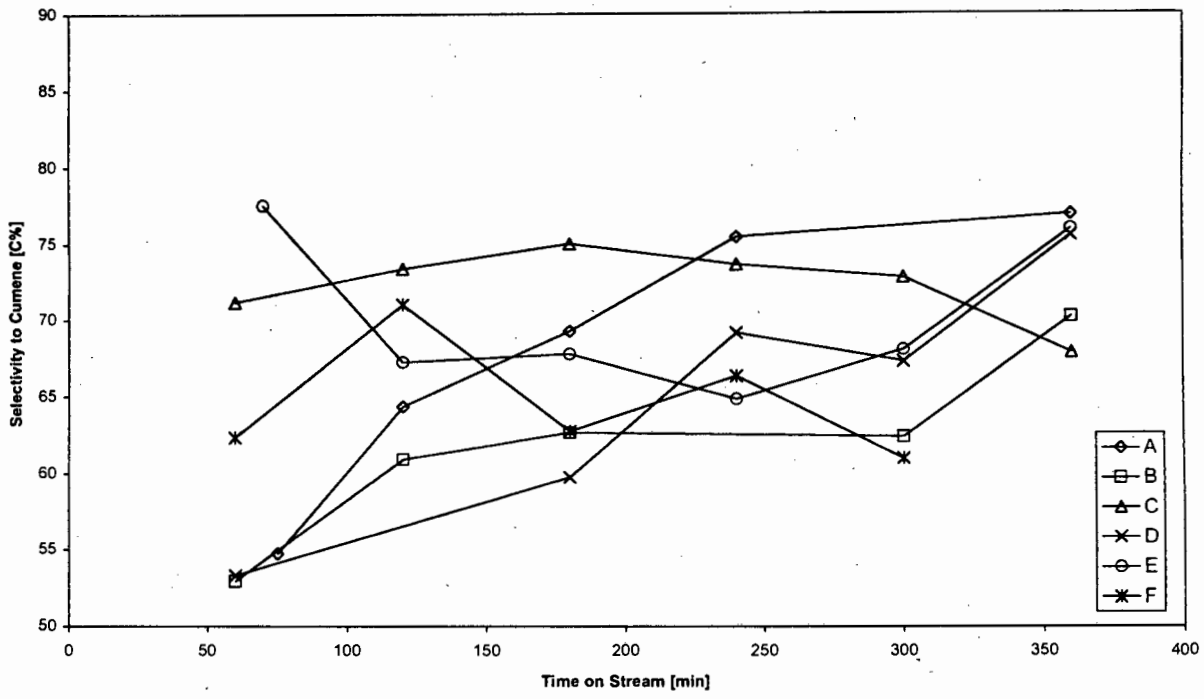

Figure 3.20. Selectivity [C%] to cumene for samples A-F.

The more active catalysts (samples A, B and D) showed a steady increase in selectivity to cumene with time on stream. At pseudo steady state (TOS = 360 min), the selectivity to cumene was highest (77%) for sample A. The selectivity to cumene for both samples A and D was comparable at similar conversion levels at pseudo steady state. However, although sample B had a relatively high activity for this alkylation reaction, it is evident from Figure 3.20 that this particular catalyst did not have a high selectivity to cumene. On the other hand, there were no major differences in the selectivity to cumene with time on stream for the least active catalysts (samples C, E and F). The selectivity to cumene for sample C was constant at about 72% for the entire duration of the reaction. Moreover, the commercial H-BEA standard (sample F) had the lowest selectivity (61%) to cumene at pseudo steady state.

The change in the % yield of cumene as a function of time of stream for samples A-F is shown in Figure 3.21.

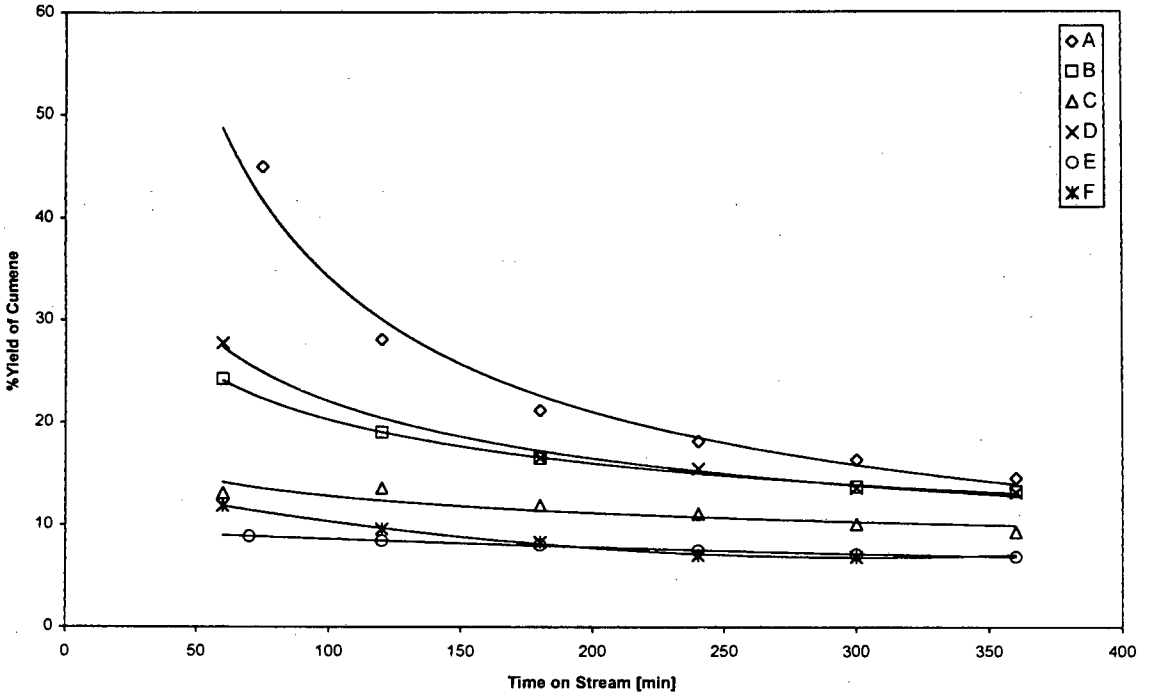

Figure 3.21. %Yield of cumene for samples A-F.

In the present case, three different groups of catalysts could be distinguished in terms of the change in the % yield of cumene with time on stream. The highest cumene yield was obtained for sample A since this catalyst was the most active. The cumene yields for catalysts B and D were very similar for most of the reaction period. Moreover, there was no significant difference in the cumene yields that were obtained for the least active catalysts (C, E and F) during the course of the reaction. At pseudo steady state (TOS = 360 min), the cumene yield was almost identical for samples A, B and D whereas it was comparable for catalysts C, E and F. In addition, the % yield of cumene for catalysts C and E was almost constant at 11.5 and 8% respectively, throughout the reaction period.

The distribution (selectivity [C%]) of the products that were formed during the alkylation of benzene with propene over the differently synthesised zeolite Beta catalysts after 4 hours time on stream, is shown in Figure 3.22.

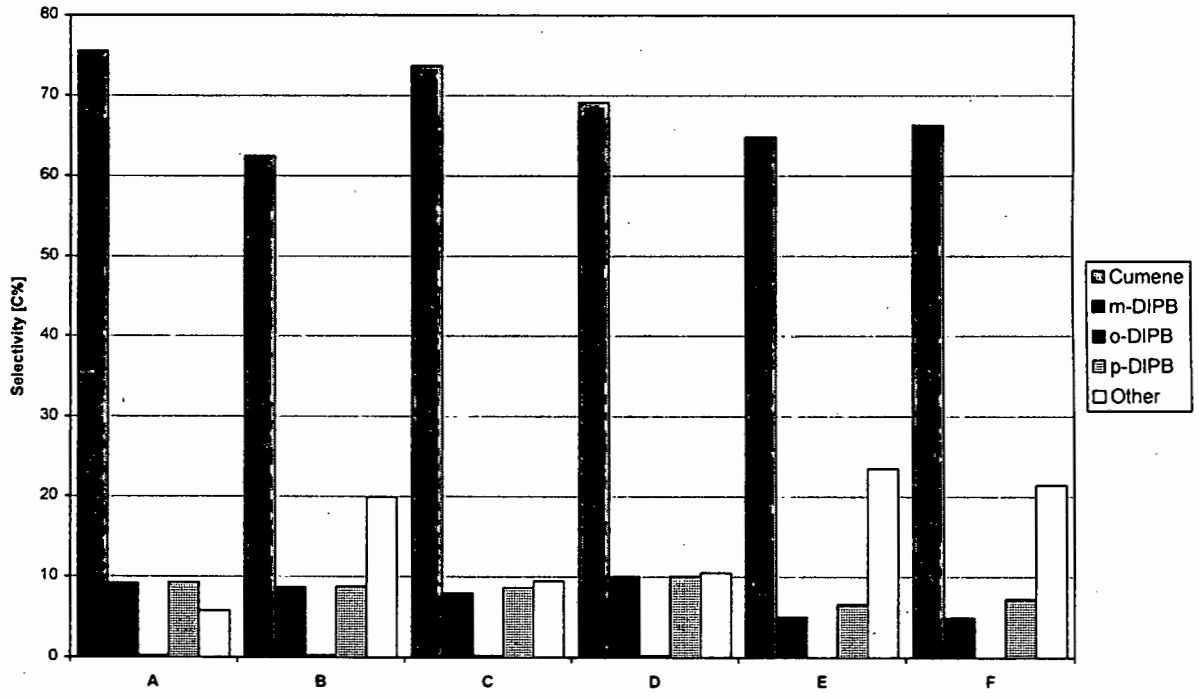

Figure 3.22. Selectivity [C%] to products for samples A-F at TOS = 240 min.

It is evident from Figure 3.22 that the least amount of by-products was formed over sample A, hence reiterating the fact that this catalyst was the most selective to cumene. However, despite the difference in the activity of catalysts A and C for this alkylation reaction, their product distributions after 4 hours time on stream were comparable. Sample B, which had a higher activity compared to samples C, E and F had a lower selectivity to cumene than these catalysts due to the increased formation of by-products. In fact, sample B was the most non-selective to cumene at this particular time on stream. All three diisopropyl benzene (DIPB) isomers were formed during the reaction with the meta and para forms being favoured. The ortho isomer was formed in trace amounts over some catalysts (samples A, B, C and D). In the case of samples E and F, no ortho DIPB was detected in the product spectrum.

Figure 3.23 shows the change in the meta/para (m/p) DIPB ratio with time on stream for the differently synthesised Beta catalysts.

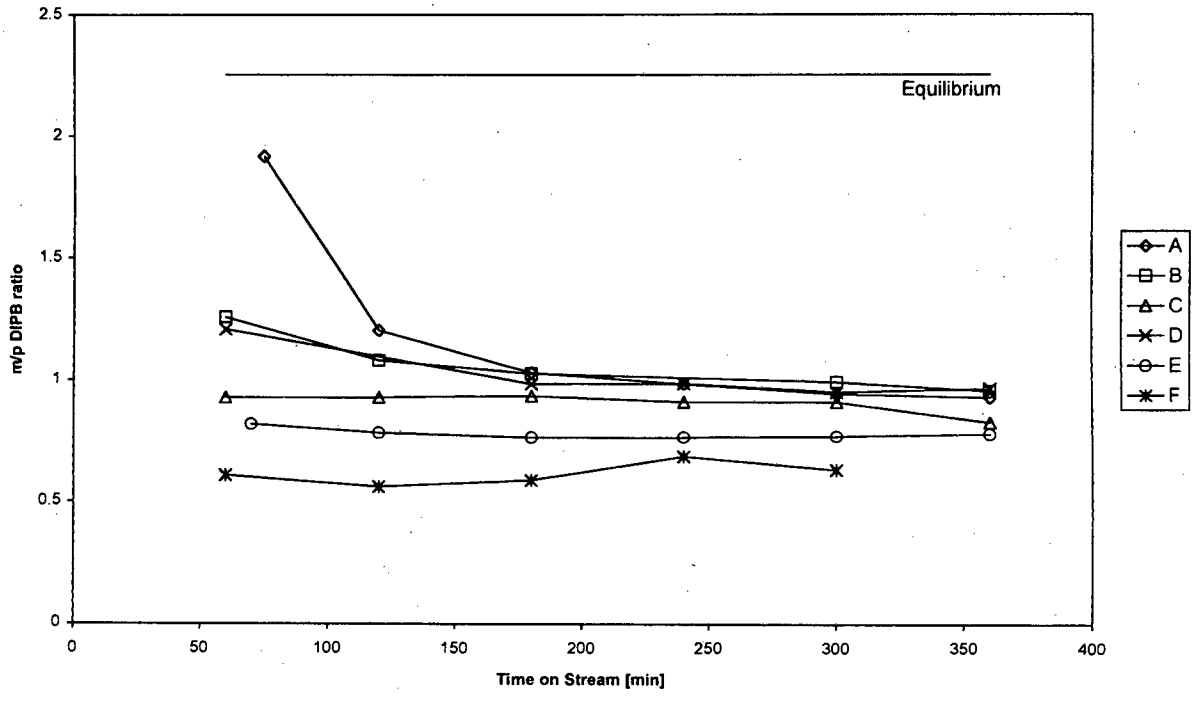

Figure 3.23. m/p DIPB ratio for samples A-F.

The m/p DIPB ratio decreased with time on stream for the more active catalysts (samples A, B and D) where as it was almost constant for samples C, E and F, which were the least active catalysts for this reaction. The most significant decrease in the m/p DIPB ratio, from 2 to 1, was observed for sample A. In the present case, the potential shape selective effects of these catalysts were apparent from the fact that the m/p DIPB ratio was significantly lower than the expected equilibrium value.

3.2.3 Effect of Acid Washing on Catalytic Activity

This section details the results of the reaction studies that were carried out on the acid washed catalysts. The activity of these catalysts, as measured by the change in the conversion of propene with time on stream, are compared in Figure 3.24.

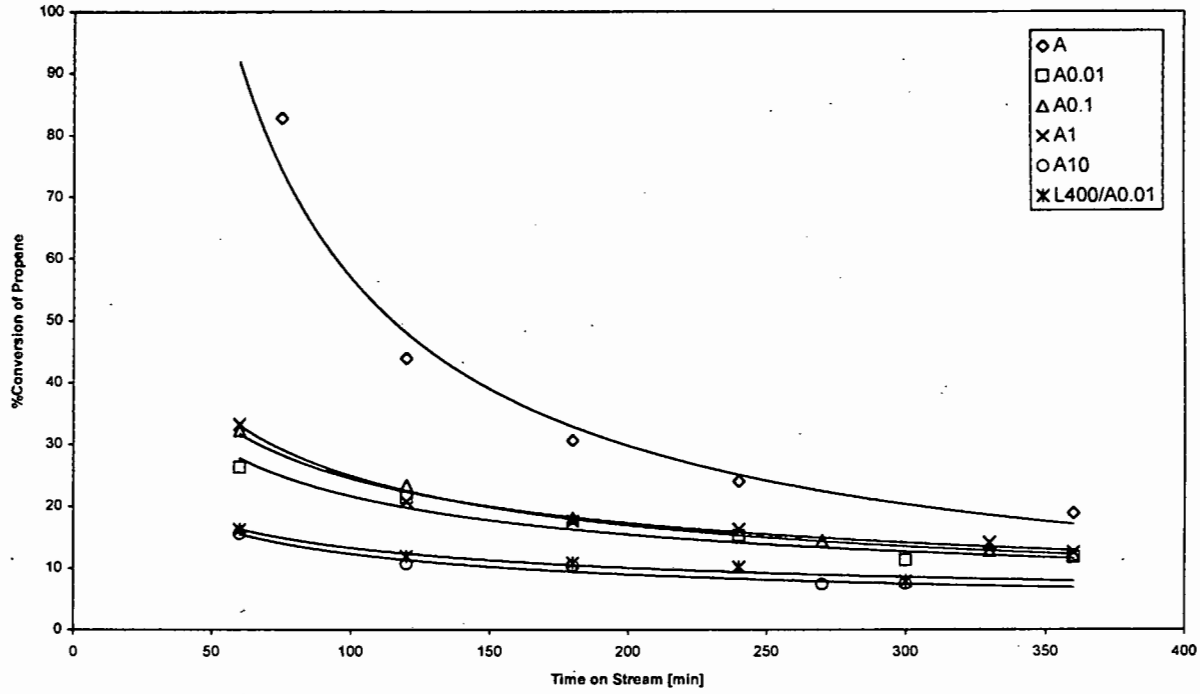

Figure 3.24. Activity of acid washed samples.

In the present case, sample A was the most active catalyst compared to the acid washed samples, similar to the results reported in Sections 3.2.1 and 3.2.2. A major difference in activity between sample A and the acid washed catalysts was observed as shown in Figure 3.24. In terms of time on stream behaviour, the acid washed catalysts could be divided into two groups. Catalysts A0.01, A0.1 and A1 performed in a similar manner during the alkylation reaction. In fact, these catalysts were the most active among the acid washed samples. On the other hand, A10 and L400/A0.01 were the least active catalysts for this reaction. At pseudo steady state, the activity of samples A0.01, A0.1 and A1 were comparable as were those of samples A10 and L400/A0.01.

Figure 3.25 shows the change in selectivity to cumene [C%] with time on stream for the acid washed catalysts.

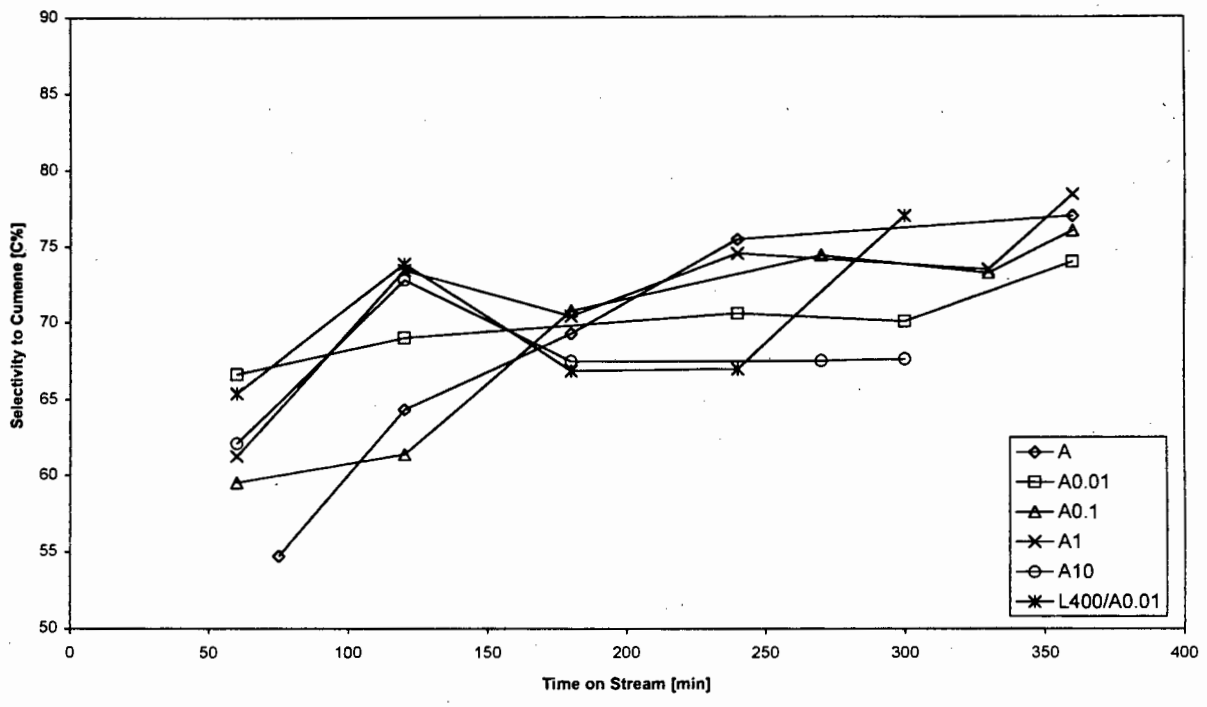

Figure 3.25. Selectivity [C%] to cumene for acid washed samples.

A general increase in the selectivity to cumene with time on stream was observed for the acid washed samples. At pseudo steady state (TOS = 360 min), the selectivity to cumene for sample A1 was marginally higher than that of sample A (78% compared to 77%) in spite of the difference in activity between these two catalysts. At this particular time on stream, the selectivity to cumene for samples A, A0.01, A0.1 and A1 were comparable. Sample A10 had the lowest selectivity to cumene (67%) at pseudo steady state. Acid washing of L400 with 0.01 N nitric acid to yield L400/A0.01, resulted in a slight improvement in the selectivity of that catalyst to cumene (77% as compared to 72%) at pseudo steady state. The catalysts were compared at similar conversion levels.

The variation in the % yield of cumene with time on stream for the acid washed catalysts is presented in Figure 3.26.

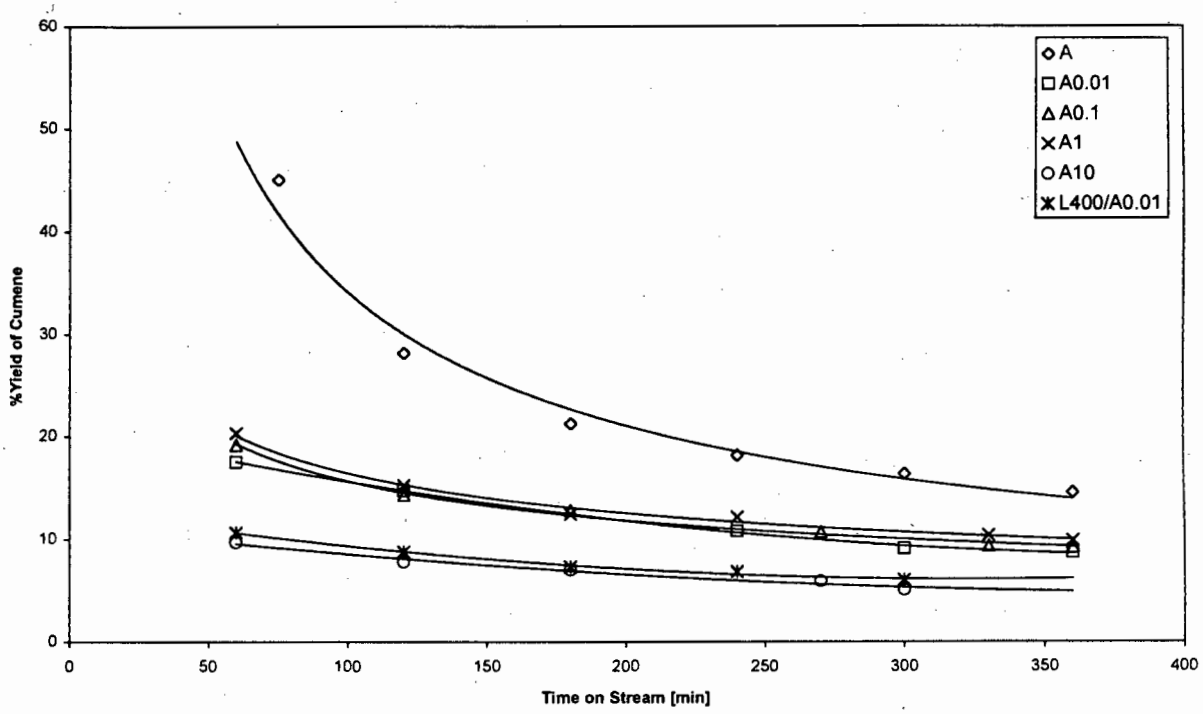

Figure 3.26. %Yield of cumene for acid washed samples.

As it has previously been mentioned for samples A to F (Section 3.2.2), three sets of catalysts could be distinguished in terms of the change in the % yield of cumene with time on stream. This is also the case for the acid washed samples. The % yield of cumene for sample A was much higher compared to the acid washed catalysts. Almost identical cumene yields were observed for samples A0.01, A0.1 and A1 as well as for catalysts A10 and L400/A0.01 for the entire duration of the reaction. Even at pseudo steady state (TOS =360 min), there was a marked difference between the % yield of cumene for sample A and the acid washed catalysts.

Figure 3.27 shows the distribution (selectivity [C%]) of the products formed during the alkylation reaction at 4 hours time on stream for the acid washed catalysts.

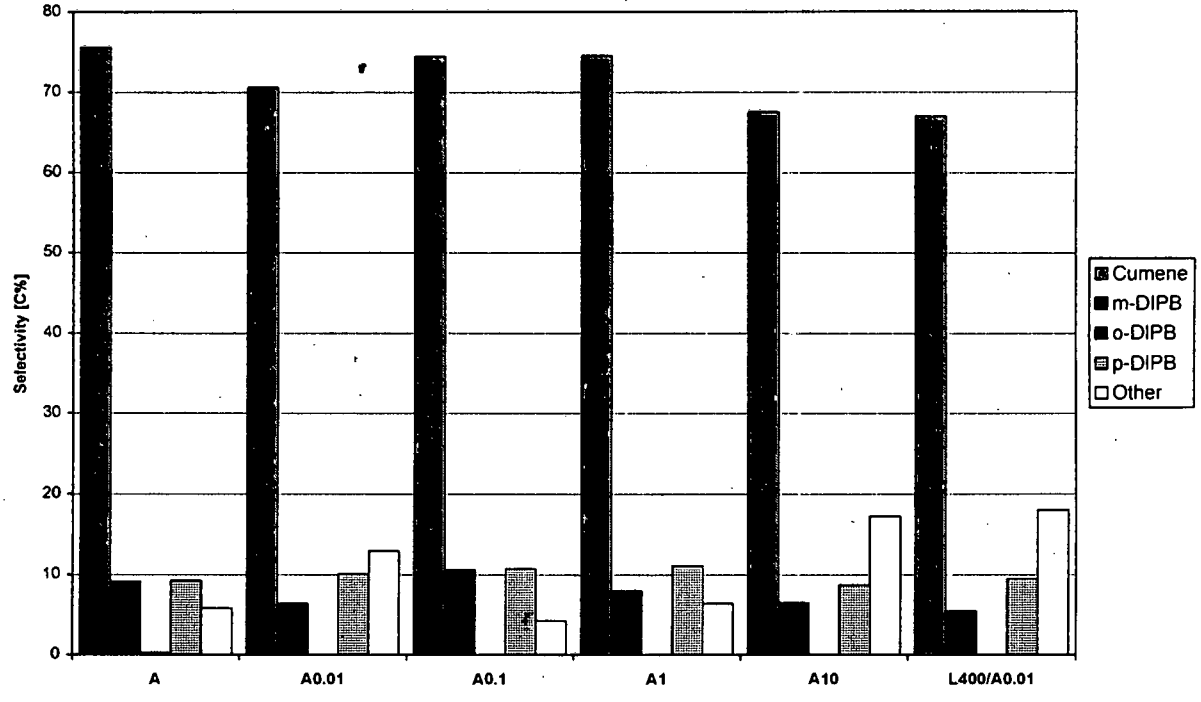

Figure 3.27. Selectivity [C%] to products for acid washed samples at TOS = 240 min.

The distribution of products after 4 hours time on stream was similar for samples A, A0.1 and A1. These catalysts produced the least amount of propene oligomers, triisopropyl benzene and n-propyl benzene. There was no significant variation in the selectivity to cumene (67-75%) at this particular time on stream for the catalysts although a difference in their activity was observed. Furthermore, the product distributions for samples A0.01, A10 and L400/A0.01 were also comparable despite the fact that the activity of sample A0.01 was higher than those of A10 and L400/A0.01 at 4 hours time on stream. Only the para and the meta isomers of DIPB were formed over the acid washed catalysts, similar to the observation made for the steamed samples.

The change in the m/p DIPB ratio with time on stream for the acid washed catalysts is shown in Figure 3.28.

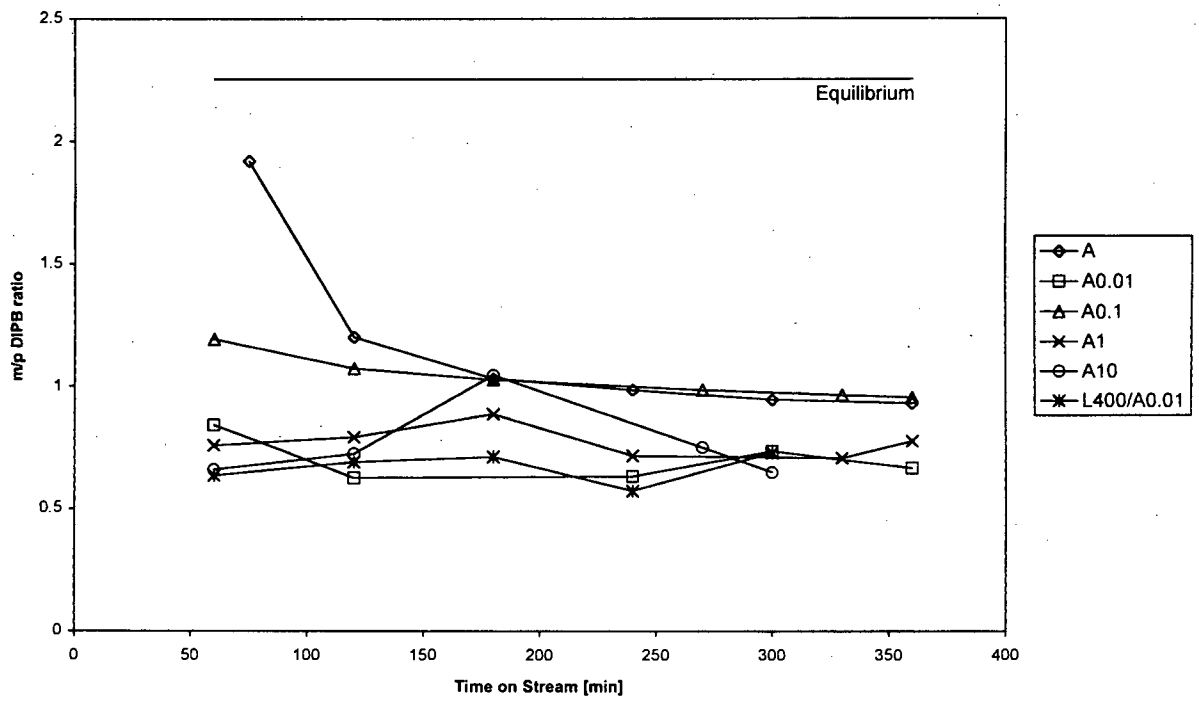

Figure 3.28. m/p DIPB ratio for acid washed samples.

The m/p DIPB ratio decreased slightly during the first half of the reaction period for sample A0.1. The concentration of the two DIPB isomers was very similar for samples A and A0.1 during the second half of the reaction period. Apart from sample A10, the m/p DIPB ratio for all the other acid washed catalysts was almost constant for the entire duration of the reaction. The possible influence of the shape selective effects of the catalysts that were observed in the case of the zeolite Beta samples synthesised by different techniques and the steamed catalysts were also seen in the present case.

In summary, sample A proved to be more active than the zeolite Beta catalysts that were synthesised by different techniques as well as the steamed and acid washed catalysts for the alkylation of benzene with propene. In general, the carbon balances for the reactions ranged between 95 and 105%.

3.2.4 Coke Formation

After the reaction, coked samples of some catalysts (A, S400, S600 and L400) were subjected to infra red analysis (DRIFTS) in order to detect the type of coke that was present in the samples. Figure 3.29 shows the DRIFT spectra of these coked catalysts.

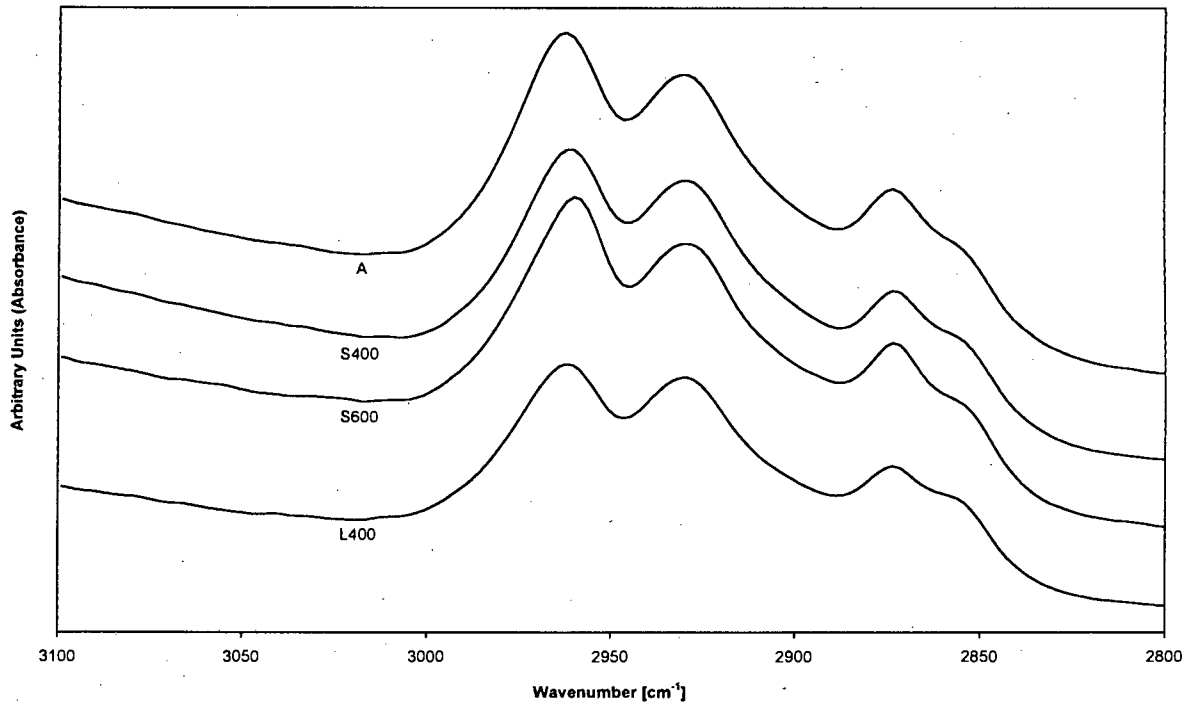

Figure 3.29. DRIFT spectra of coked catalyst samples.

Peaks at 2860, 2875, 2930 and 2960 cm^{-1} were detected in the DRIFT spectra of the coked samples. The bands at 2860 and 2930 cm^{-1} have been assigned to aliphatic CH_2 where as those at 2875 and 2960 cm^{-1} have been attributed to CH_3 groups (Colthup *et al.*, 1990). Thus, the presence of only aliphatic soft coke species was indicated in the samples. The presence of these bands in the region of the C-H stretching vibrations of the infrared spectra of coked zeolite Beta catalysts has been previously reported (Smirnov *et al.*, 1997).

CHAPTER FOUR

Discussion

The discussion of the results of this study is divided into two sections. Section 4.1 deals with the effect of synthesis and post synthesis modifications on the physico-chemical characteristics of the catalysts. This is followed by section 4.2 in which the catalytic properties of the different catalysts are discussed in relation to their physico-chemical characteristics.

4.1 CATALYST CHARACTERISATION

The effect of steaming, synthesis technique and acid washing on the structural and acidic properties of the zeolite Beta catalysts are dealt with in this section of the discussion. The results that are referred to herein can be found in Section 3.1 of this thesis.

4.1.1. Steamed Catalysts

^{27}Al MAS NMR of the steamed samples showed that substantial quantities of extra-framework aluminium (EFAl) species were formed (Table 3.10) as a result of the hydrothermal treatment, but aluminium was not removed from the bulk of the steamed catalysts. This is confirmed by the results obtained from the elemental analysis of the samples, where the bulk chemical composition of the steamed catalysts remained unchanged (within experimental error) compared to sample A (Table 3.3). Meyers *et al.* (1986) and many other researchers have also found that the extra-framework aluminium species that are created as a result of steaming remain in the bulk of the zeolite. Framework dealumination was found to increase with the severity of the hydrothermal treatment and three types of EFAl, namely EFAl-6, EFAl-4/Al-5 and EFAl-x (Section 3.1.1.7), could be detected in the ^{27}Al MAS NMR spectra of the steamed samples. On average, 54% of the framework aluminium was removed after hydrothermal treatment and significant amounts of EFAl-4/Al-5 and EFAl-x were formed compared to EFAl-6.

XRD results indicated that there was a general decrease in the relative % crystallinity of the steamed samples compared to sample A, as shown in Table 3.1b. A decrease in the relative % crystallinity after steaming has been previously reported for other

zeolite types (Meyers *et al.*, 1986 and Vedrine *et al.*, 1986). In the present case, the decrease in crystallinity is due to the formation of amorphous extra-framework aluminium (EFAl) species (as detected by ^{27}Al MAS NMR), as a result of the hydrothermal treatment. These EFAl species are likely to be present in the zeolite pores as XPS studies on one of the steamed samples (S600) revealed that there was no aluminium enrichment at the surface. This observation is in contrast to most XPS studies carried out on steamed zeolites in the literature (Meyers *et al.*, 1986, Campbell *et al.*, 1996$_b$ and Datka *et al.*, 1996), where a higher concentration of aluminium at the zeolite surface was detected compared to the bulk. However, these studies were carried out on mordenite and H-ZSM5.

In addition, the removal of aluminium from the zeolite framework tends to result in a less ordered framework structure. This is evidenced by the presence of a shoulder at 970 cm^{-1} in the infrared spectra of the samples steamed at 600°C (S600 and L600). Vaudry *et al.* (1994) have attributed this particular shoulder to silanol defects in zeolite Beta.

Both the total surface area and the mesopore area of the samples steamed at 600°C (S600 and L600) decreased compared to sample A (Table 3.6). On the other hand, there was almost no change in the mesopore area of samples S400 and L400 whereas the total surface area increased compared to sample A. These observations give an indication that the steaming temperature has an effect on the surface area of the catalysts. This might indicate the formation of amorphous debris in the pores of the zeolites as a result of the high steaming temperature (600°C). This was in turn reflected in the relative % crystallinity of the samples steamed at 600°C. In general, dealumination causes a decrease in the micropore volume (Coutanceau *et al.*, 1997). However, in the present case, no such decrease was observed for the steamed samples.

Only two types of silicon environments viz. Si(1Al) and Si(0Al) were detected in the ^{29}Si MAS NMR spectra of the steamed catalysts (Table 3.8). These correspond to silicon atoms tetrahedrally co-ordinated to 1Al and 3 Si atoms and no Al and 4 Si atoms respectively. The ^{29}Si MAS NMR spectrum of sample A also revealed only these two types of Si environments in contrast to the study of Perez-Pariente *et al.* (1990) on zeolite Beta. These authors observed an additional peak in the ^{29}Si MAS

NMR spectrum of zeolite Beta (Si/Al = 18) at –96 ppm, which they attributed to Si atoms tetrahedrally co-ordinated to 2 Al and 2 Si atoms [Si(2Al) environment]. In addition, they assigned the signal present at –104 ppm in the ^{29}Si MAS NMR spectrum of zeolite Beta to the superposition of Si(1Al) and Si(1OH) components. The latter component corresponds to silicon atoms surrounded by 3 other Si atoms and 1 OH group. In the present case, since an appreciable concentration of SiOH groups was present in all the samples as determined by ^{1}H MAS NMR (Table 3.12), the signal at –104 ppm in the ^{29}Si MAS NMR spectrum of the catalysts can be attributed to a superposition of both Si(1Al) and Si(1OH) components.

The signals detected above –111 ppm in the ^{29}Si MAS NMR spectrum of zeolite Beta have been assigned to crystallographically inequivalent sites in this zeolite by Perez-Pariente *et al.* (1990). These are silicon atoms with no aluminium in the second co-ordination sphere that occupy different structural sites in the zeolite. Two crystallographically inequivalent sites corresponding to signals at –111 and –115 ppm were detected in samples A, S400, S600, L400 and F. A third signal at –113 ppm was only present in the ^{29}Si MAS NMR spectrum of sample L600, corresponding to an additional crystallographically non-equivalent site not detected in the other samples. The severe steaming conditions might have resulted in the appearance of such a signal in the ^{29}Si MAS NMR spectrum of that catalyst.

The reduction in the number of acid sites in the steamed catalysts, as observed from TPD studies, is consistent with framework dealumination as evidenced by ^{27}Al MAS NMR (Table 3.11). There is a direct correlation between the number of acid sites as measured by TPD and the amount of framework Al/uc, as determined by ^{27}Al MAS NMR and chemical analysis. This correlation is shown in Figure 4.1. It is assumed that the framework aluminium atoms are not charge balanced by any positively charged extra framework aluminium species (EFAl) present in the steamed samples.

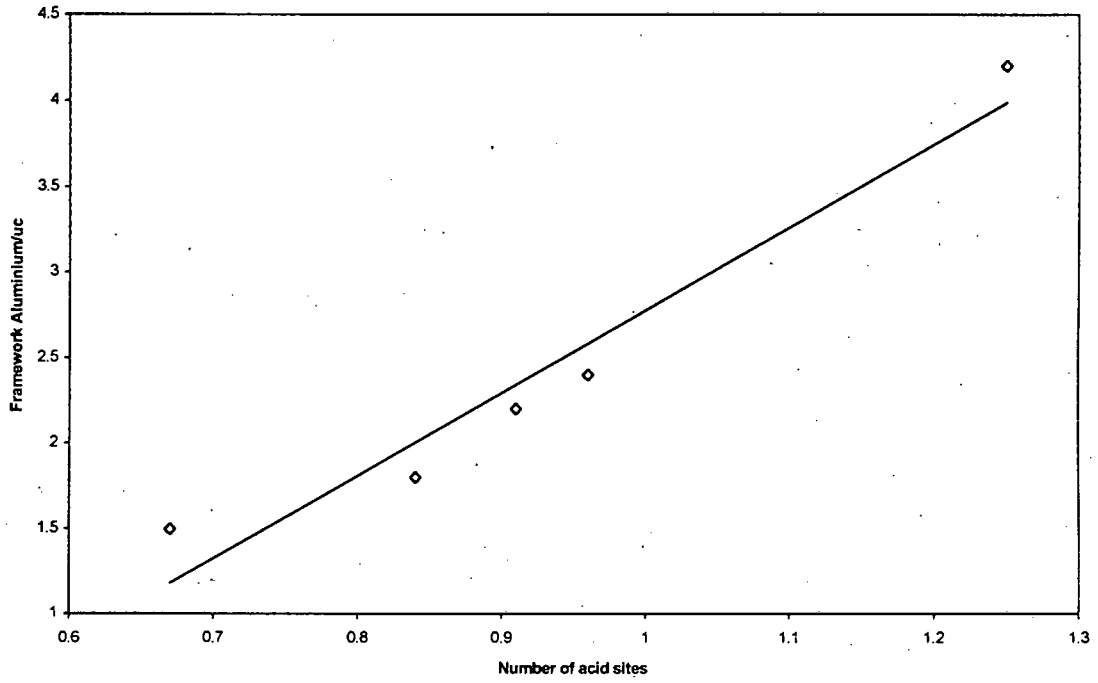

Figure 4.1. Correlation between framework aluminium/unit cell and number of acid sites for steamed samples.

The number of acid sites present in the steamed samples was compared to the concentration of aluminium atoms as determined by chemical analysis (Table 3.11). In every case, except for sample A, the concentration of aluminium atoms from chemical analysis was higher than the number of acid sites. This is in agreement with the work of Miller *et al.* (1992) and Meyers *et al.* (1988) on dealuminated mordenite and could be due to the inaccessibility of the ammonia molecules to some acid sites. Access to these acid sites might be blocked by the presence of amorphous material in the channels of the zeolite, as evidenced by the relative % crystallinity from XRD. Thus, elemental analysis detects the presence of aluminium that may not give rise to measurable acidity. In the case of sample A, it could be that not all the physisorbed ammonia was removed.

The T_{max} value, the maximum peak temperature of the TPD spectrum, for each catalyst is also shown in Table 3.11. It has been proposed by Leu *et al.* (1991) that there is a direct correlation between the strength of acid sites in zeolite Beta and T_{max}. However, some limitations exist as to the interpretation of T_{max} values. As has been suggested by Kapustin *et al.* (1988) and Dima and Rees (1990), T_{max} is affected by a

number of factors including particle size and readsorption effects. Although there was no significant difference in the particle size of the catalysts in the present case, the possibility of readsorption taking place cannot be excluded. Therefore, one can at most obtain an estimate of the strength of acid sites from the data in Table 3.11. As the number of acid sites increases, a general increase can be observed for the T_{max} value from Table 3.11. As more NH_3 molecules are adsorbed onto the acid sites, T_{max} increases due to the lag in the desorption time. It can thus be proposed that all the samples have similar distributions of acid site strength.

Three types of hydroxyl groups were detected in the ^1H MAS NMR spectra of sample A as well as the steamed samples. These were SiOH groups at framework defects and OH groups associated with extra-framework aluminium species (AlOH), bridging hydroxyl groups and perturbed bridging hydroxyl groups (Table 3.12). The effect of the steaming temperature on the concentration of bridging hydroxyl groups is apparent from the data in Table 3.12. No bridging hydroxyl groups were detected in L600 whereas the concentration of these groups in S600 was low.

The number of acid sites, as probed by TPD, was higher than the concentration of acidic (bridging and perturbed bridging) hydroxyl groups present in all the steamed samples, except for sample A. Thus, all the acidic sites present in the samples, as probed by ammonia TPD, cannot be ascribed to Bronsted acid sites except for sample A. There exists no conclusive evidence for the presence of Lewis acidity in the steamed catalysts as no pyridine infrared studies were performed. However, it would appear from ^1H MAS NMR and TPD studies, that Lewis acidity might be associated with the extra-framework aluminium species (EFAl) present in the steamed samples.

4.1.2 Synthesised Catalysts

A distinct splitting of the peak situated at 50-60 ppm in the ^{27}Al MAS NMR spectra of sample A as well as the samples synthesised by different techniques (B-E) was observed (Fig. 3.8 and Appendix G). Similar phenomena have been reported by Chauvin *et al.* (1990) and Hunger *et al.* (1995) for mazzite and dealuminated MCM-22 respectively. The signals were assigned to aluminium atoms present at crystallographically non-equivalent T sites in the framework of the zeolites by these

authors. For their part, Fyfe *et al.* (1986) attributed the splitting of the signal to aluminium atoms with different cations in their vicinity. The presence of two different Bronsted acid sites was even suggested by the studies of Sarv *et al.* (1996) on ZSM-5 to account for the splitting of the peak at 50-60 ppm. The latter explanation appears to be the most plausible in the present case, as will be discussed in Section 4.2.1.

Among the zeolite Beta catalysts that were synthesised by different techniques, samples B and D had the same average crystal size (500 nm) whereas the average crystal size of samples C and E was 200 nm. The rapid and agitated synthesis of these samples increased the degree of supersaturation in the synthesis mixture, resulting in massive nucleation and the formation of small crystals. On the contrary, the slower synthesis of samples B and D favoured crystal growth over nucleation, resulting in the formation of large crystals.

The synthesis time also seemed to have an effect on relative % crystallinity (Table 3.1b). The relative % crystallinity of samples C and E was lower compared to samples B and D. Samples C and E were synthesised in 3 hours whereas samples B and D were synthesised in 7 and 30 hours respectively.

In general, the relative % crystallinity of samples B-E was lower compared to sample A. One would expect this to be due to the presence of amorphous material that is still present in the catalysts as a result of incomplete crystallisation. It is also evident that the lower relative % crystallinity of these catalysts is not due to the presence of extra-framework aluminium (EFAl) species as none were detected by ^{27}Al MAS NMR (Fig. 3.8 and Appendix G). The lower relative % crystallinity of these samples could thus be due to a higher degree of faulting in the lattice of these zeolites. Zeolite Beta is known to contain a considerable amount of faulting due to the disordered stacking of layers (Jansen *et al.*, 1997).

The proprietary silica source that was used in the synthesis of sample E could have influenced the morphology as well as the surface area of this catalyst. Only samples B and E had crystals of a well-defined shape (oval) (Fig. 3.6). Moreover, sample E was found to have the lowest total surface area among the catalysts synthesised by different techniques (Table 3.6). On the other hand, sample B had the highest

mesopore and total surface area. The synthesis of this catalyst in a static medium could have contributed to the high surface area observed and the production of crystals of a well-defined shape. The high mesopore area observed for sample B is odd as a slower crystallisation time (7 hours) usually leads to more perfect crystals. This gives an indication that intergrowth and agglomeration of primary particles was favoured over crystal growth. Furthermore, the BET results showed that there was no significant difference in the micropore volume of the catalysts that were synthesised by different techniques (Table 3.6).

Although sample F, the commercial H-BEA standard, was not subjected to any dealumination procedure, it had an almost identical number of acid sites, as measured by TPD, as the most severely steamed catalyst (L600). This is not surprising as both of these catalysts contained the same number of aluminium atoms per unit cell. It follows, from the correlation shown in Figure 4.1, that L600 and sample F should have similar acid site density. Among the catalysts that were synthesised by different techniques, sample B had the highest number of acid sites. The fact that it was the only catalyst that was synthesised in a static medium could have contributed to its high acid site density. It would appear that the long synthesis time (30 hours) of sample D resulted in the low acid site density of this catalyst. The different molar regime (lower OH^- content) used in the synthesis of this catalyst might have prevented all the aluminium that was loaded into the synthesis mixture from being incorporated into the framework.

4.1.3 Acid Washed Catalysts

In contrast to the steamed samples, the three types of EFAl (Section 3.1.1.7) could not all be detected in all of the acid washed catalysts. The samples that were subjected to a mild acid wash (A0.01, A0.1 and L400/A0.01) contained the three types of EFAl. However, no EFAl-x and EFAl-4/Al-5 were detected in samples A1 and A10 respectively. It is well documented in the literature that acid washing of zeolites tends to remove extra-framework aluminium species from the zeolite bulk (Meyers *et al.*, 1988 and O'Donovan *et al.*, 1995). In the present case, it is possible that the stronger acid washing procedures selectively removed EFAl from the zeolite.

An increase in the mesopore area was observed with increasing strength of acid washing (Table 3.6). A similar observation has also been made by Zukal *et al.* (1986) on dealuminated zeolite Y. There was an increase in the total surface area of the acid leached catalysts compared to sample A. However, the total surface area decreased with increasing strength of acid washing. This might be a result of partial structural collapse as the severity of the dealumination procedure increased. As has been previously mentioned for the steamed catalysts, there was almost no change in the micropore volume after acid washing as well.

In the case of the acid washed catalysts, only two types of Si environments, viz. Si(1Al) and Si(0Al), were also detected. However, since ^{1}H MAS NMR studies were not performed on these catalysts, it is not evident from the ^{29}Si MAS NMR spectrum alone whether the signal present at –104 ppm can be attributed to a superposition of Si(1Al) and Si(1OH) components. The signal at –113 ppm (as observed in the spectrum of L600) was prominent in the ^{29}Si MAS NMR spectra of the acid washed samples (cf. Appendix F). Two crystallographically non-equivalent sites corresponding to signals situated at –113 and –115 ppm in the ^{29}Si MAS NMR spectra of all the acid washed samples could be detected.

4.2 REACTION STUDIES

The effect of steaming, synthesis technique and acid washing on the catalytic properties of the zeolite Beta catalysts are discussed in this section. The catalytic properties of the samples are discussed in relation to their physico-chemical characteristics. The results that are referred to herein can be found in Section 3.2.

The product spectrum for the alkylation of benzene with propene corresponded to those previously observed for zeolite Beta (Perego *et al.*, 1996). At the studied reaction temperature (210°C) no products due to propene cracking were seen. Trace amounts of n-propylbenzene were observed during the reaction period. This is in contrast to studies carried out on medium pore zeolites, e.g H-ZSM5, where shape selective effects and the presence of strong acid sites promote the formation of n-propylbenzene (Chandavar *et al.*, 1984 and Das *et al.*, 1995). Raimondo *et al.* (1997) have compared the activity of different zeolites for the alkylation of benzene and observed that the pore dimension rather than acidity was the controlling factor during the reaction. Chandavar *et al.* (1984) have proposed that the formation of n-propylbenzene on H-ZSM5 is due to the secondary isomerisation of the primary product, cumene. However, later studies by Das *et al.* (1995) and Wichterlova *et al.* (1996) showed that n-propylbenzene was formed from a bimolecular reaction between cumene and benzene over H-ZSM5 as a result of structure directed transition state selectivity. This phenomenon involves the geometrical arrangement of the channel intersections in H-ZSM5 which enables benzene and cumene to approach each other in the most efficient way to form the transition complex (Das *et al.*, 1995). The more open structure of zeolite Beta does not favour the formation of the intermediate in this transalkylation reaction. As a result, the formation of n-propylbenzene on zeolite Beta is more likely to occur via the secondary isomerisation of cumene.

Apart from n-propylbenzene, little or no ortho-diisopropylbenzene (DIPB) was observed during the reaction period. Other authors also found that the formation of ortho-DIPB practically did not occur during the alkylation of benzene catalysed by zeolite Beta (Reddy *et al.*, 1993 and Perego *et al.*, 1996). According to these authors, the formation of the ortho isomer does not occur due to the steric hindrance of the

isopropyl group, prevailing at the ortho position. Furthermore, the para position is favoured by shape selectivity due to a proper pore structure of the zeolite catalyst. The size of the para isomer is smaller than the ortho and meta isomers; the critical diameter of the para isomer being 7.2 Å and the critical size of the meta isomer being 9.0 × 7.4 Å (Pradhan and Rao, 1991). The zeolite Beta pores (7.6 × 6.4 Å) can accommodate both meta and para isomers. p-DIPB diffuses completely unhindered through the 12-membered ring channels as a consequence of the fact that the para substitution does not significantly alter the cross section of the molecule with respect to cumene. The energy barriers for the diffusion of the different DIPB isomers through the 12-membered ring channel of zeolite Beta have been calculated to be 223.5, 57.3 and 14.2 $kJmol^{-1}$ for o-, m- and p-DIPB respectively (Perego *et al.*, 1996).

Sasidharan *et al.* (1995) have reported that the ortho isomer has a very high strain energy compared to the meta and para isomers. In spite of the low strain energy of the meta isomer, it is not expected to be formed as a primary product since the isopropylation of cumene is an electrophilic substitution (ortho-para directing) reaction. Consequently, the thermodynamically favoured meta isomer is formed through the isomerisation of the ortho and para isomers or via the disproportionation of cumene into benzene and DIPB. In the present case, since the m/p ratio generally decreased with decreasing conversion (Figs. 3.18, 3.23 and 3.28) and very little or no ortho-DIPB was observed, it can be proposed that meta DIPB was mainly formed via the isomerisation of the para isomer.

In this study, the zeolite Beta catalysts generally underwent rapid deactivation (Figs. 3.14, 3.19 and 3.24) although a benzene/propene molar ratio of 5.8 was used to partially suppress the oligomerisation of propene. Reddy *et al.* (1993) have observed a faster deactivation of zeolite Beta in the alkylation of benzene when propene was used as the alkylating agent as opposed to isopropanol. Since the smaller propene molecules diffuse much faster than the bulkier benzene molecules during the reaction, they tend to preferentially adsorb onto the acid sites present in the catalysts. These are most probably acid sites that are conducive to the rapid oligomerisation of propene leading to the formation of soft coke. This argument is supported by the detection of peaks at 2860, 2875, 2930 and 2960 cm^{-1} in the DRIFT spectra of coked samples (Fig.

3.29). Thus, the presence of only aliphatic soft coke species was indicated in the samples. The presence of these bands in the region of the C-H stretching vibrations of the infrared spectra of coked zeolite Beta catalysts has been previously reported (Smirnov *et al.*, 1997).

A reduction in the number of acid sites in dealuminated mordenite was found to lower the deactivation rate of the catalyst during the isopropylation of benzene (Meima *et al.*, 1993). However, Bellussi *et al.* (1995) have postulated that zeolite Beta samples with a lower Al content, and hence fewer acid sites, led to the formation of more propene oligomers. These contradictory statements can be explained by the fact that the Si/Al ratio of the catalysts was very different (156 for mordenite and 35 for Beta). Thus, there exists an optimum Si/Al ratio at which the deactivation rate is maximum. In the present case, at pseudo steady state, there was a considerable reduction in the number of active acid sites as shown by the % conversion of propene from Figures 3.14, 3.19 and 3.24 and a corresponding decrease in the deactivation rate. It has been reported that under steady state conditions, the isopropylation behaviour of zeolite Beta is dominated by the strength of a few remaining free acid sites (Smirnov *et al.*, 1997) and this seems to be the case in the present work.

In this study, the intrinsic activity of the catalysts could not be properly evaluated due to the extensive coking nature of this reaction.

4.2.1 Catalyst Related Trends

In the literature, various hypotheses have been put forward concerning the contribution of EFAl towards enhancing the catalytic activity of dealuminated zeolites. The presence of non-framework aluminium may have an inductive effect on protonic sites generating superacidic sites (Mirodatos and Barthomeuf, 1981 and Wang *et al.*, 1991). However, calorimetry experiments have failed to find evidence for the superacidic sites in dealuminated zeolites (Biaglow *et al.*, 1994). It has been postulated that some of the EFAl species are active catalytic species themselves (Kogelbauer *et al.*, 1994). Moreover, it has also been reported that there exists a synergism between EFAl and Bronsted acid sites (Hong *et al.*, 1994). However, in the present study, EFAl did not lead to any enhancement in the activity of dealuminated

zeolite Beta during the isopropylation of benzene. A similar observation has been made by O'Donovan *et al.* (1995) for dealuminated mordenite during isobutane cracking. In fact, the steamed samples had similar concentrations of EFAl (Table 3.10) and the activity of these catalysts was lower compared to sample A. All the acid washed catalysts also contained an appreciable amount of EFAl, but nonetheless did not perform better than sample A during the alkylation reaction. As has been previously reported, other forms of dealumination, including the treatment of zeolite Beta with $(NH_4)_2SiF_6$, also did not result in enhanced activity for the synthesis of cumene (Das *et al.*, 1996).

From Figures 3.14 and 3.16, it can be seen that there are two distinct groups of catalysts in terms of activity and cumene yield among the steamed samples. The samples that were steamed at a temperature of 400°C (S400 and L400) performed better compared to samples S600 and L600 (steamed at 600°C). Interestingly, the physico-chemical characteristics of these two sets of catalysts showed the same trend, with samples S400 and L400 having a higher mesopore and total surface area (Table 3.6) as well as a greater number of framework aluminium atoms per unit cell (Table 3.7) than S600 and L600. In addition, samples S400 and L400 had a higher number of acid sites (Table 3.11) as measured by TPD studies as well as a higher concentration of bridging hydroxyl groups (Table 3.12) compared to S600 and L600. Among the factors that influenced the catalytic activity of the steamed samples, the number of acid sites appeared to have the strongest effect. This is confirmed by the fairly good correlation between the number of acid sites and the initial cumene yield for the steamed samples as shown in Figure 4.2.

The correlation between acid site concentration and activity has frequently been reported in the literature for the isopropylation of benzene. It has been demonstrated that the catalytic activity of HZSM5 in the synthesis of cumene is proportional to the concentration of surface OH groups and acidic sites (Chandavar *et al.*, 1984). Moreover, Smirnov *et al.* (1994) have shown that there is a good proportionality between catalytic activity and the concentration and strength of acid sites in Ga-MFI catalysts for the isopropylation of benzene. A similar correlation has been found by Das *et al.* (1996) for NH_4SiF_6 dealuminated zeolite Beta for this alkylation reaction.

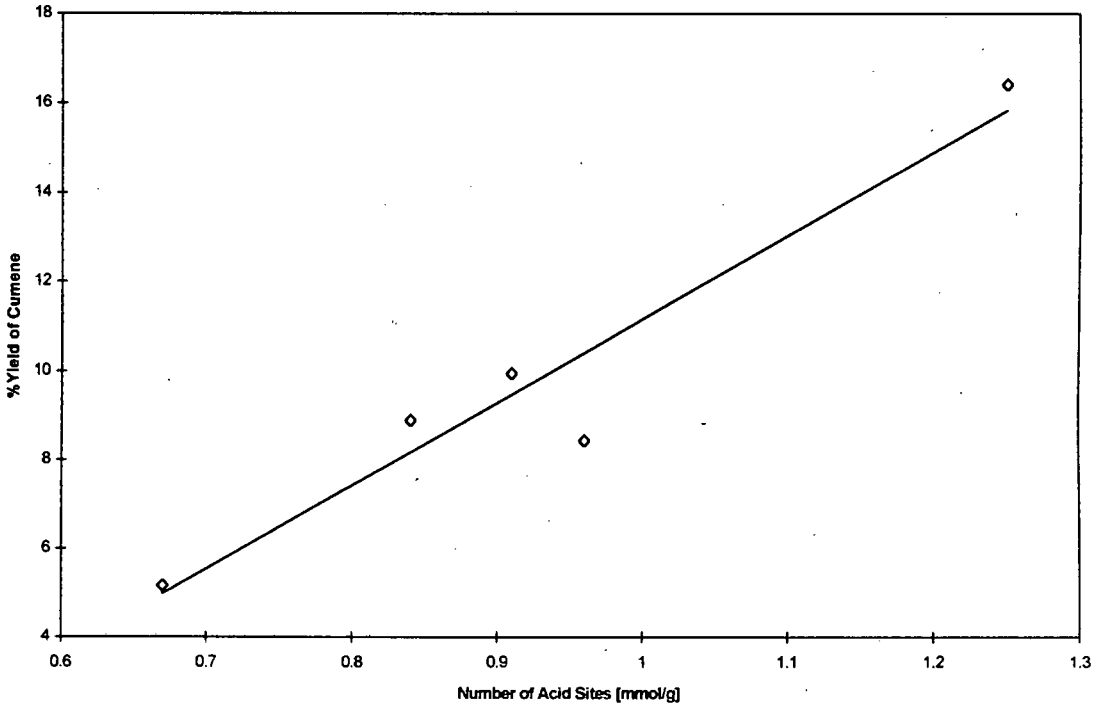

Figure 4.2. Correlation between cumene yield and number of acid sites for the steamed catalysts.

An interesting feature of sample L600 is that although there was no evidence for bridging hydroxyl groups in this catalyst (Table 3.12), it was still active during the isopropylation of benzene. Hence, it would appear that the reaction was also catalysed by Lewis acid sites. As has been previously mentioned, no pyridine infrared studies were carried out on the steamed catalysts to determine the nature of the acid sites present. The contribution of Lewis acidity in the isopropylation of benzene has been emphasised in the literature by Geatti *et al.* (1997) and Medina-Valtierra *et al.* (1998) for cation exchanged aluminium pillared bentonite and MCM-41/γ Al_2O_3.

The activity of the zeolite Beta catalysts (B-E) that were synthesised by different synthesis techniques varied for the isopropylation of benzene (Fig. 3.19). In this case also, there were clearly two groups of catalysts in terms of activity and cumene yield. Samples B and D had a higher overall yield of cumene than catalysts C and E (Fig. 3.21). The presence of charge balancing sodium cations in zeolites is known to lower catalytic activity by reducing the number of acid sites. Although, samples A and E had the same sodium content (Table 3.2), their catalytic activity for the isopropylation of benzene was very different. Hence, the sodium content of the catalysts does not seem to have a significant bearing on catalytic activity for this particular reaction.

^{27}Al MAS NMR studies of samples B-E showed the absence of EFAl in all of these samples as the 0 ppm peak was not evident. Thus the low activity observed for samples C and E cannot be attributed to diffusional resistance caused by the presence of EFAl. Moreover these samples performed similarly and deactivated at approximately the same rate compared to the most severely steamed sample (L600), which had EFAl present. It is also clear that the differences in activity between samples B and D compared to C and E cannot be ascribed to the presence of EFAl generated Lewis acidity as there was no EFAl present in any of these samples.

Furthermore, although sample C had the lowest mesopore area (Table 3.6), it was not the least active catalyst. This indicates that for the present samples, diffusional constraints due to hindered access to the micropore area cannot be the cause of low activity for the isopropylation of benzene. The mesopore area of samples B and D was very different and yet both these catalysts were equally active. Samples D and E had comparable mesopore areas, but yet differed significantly in terms of catalytic activity. Thus, the mesopore area did not correlate with the activity observed for the isopropylation of benzene. Hence, differences in the activity observed for the differently synthesised zeolite Beta samples cannot be attributed to the sodium content of the catalysts or changes in the mesopore area. Also, these differences cannot be due to diffusional constraints caused by the presence of EFAl as none were present in the samples. Contrary to the findings for the steamed catalysts, no correlation was found between the number of acid sites, as determined by TPD, and catalytic activity for samples B-E. However, ^{27}Al MAS NMR spectra of the samples revealed a distinct splitting of the peak situated at around 60 ppm (assigned to tetrahedrally co-ordinated framework Al atoms). Sarv *et al.* (1996) attributed the splitting of the peak to the presence of two types of Bronsted acid sites in ZSM5. In the present case, the catalysts (A, B and D) with the higher Al[II] type aluminium atom concentration (Table 3.9) performed better during the alkylation reaction. Therefore, it is possible that the acid site associated with Al[II] type aluminium atom is conducive to the isopropylation of benzene.

Moreover, it is clear from the literature that stacking faults and local defects are inherent in zeolite Beta (Jansen *et al.*, 1997). It is proposed that diffusional constraints due to these local defects may also have contributed to the observed differences in

activity for the Beta samples synthesised by different techniques. The higher degree of faulting in the lattice of samples B-E was evidenced by their low relative % crystallinity, from XRD studies.

The commercial H-BEA standard (sample F) had an almost identical number of acid sites compared to the most severely steamed catalyst (L600) and as a result, these catalysts had a very similar performance for the isopropylation of benzene. The number of acid sites also explains the significant difference in activity observed for samples A and F, which are both commercial zeolite Beta catalysts.

The acid washed catalysts could also be divided up into two distinct groups in terms of activity and cumene yield. Higher cumene yields (Fig. 3.26) were observed for catalysts A0.01, A0.1 and A1 compared to A10 and L400/A0.01. However, due to the limited physico-chemical characterisation data available for these samples, the difference observed in their catalytic activity could not be properly accounted for. The strength of acid wash clearly has an effect on catalytic activity.

4.2.2 Non-Catalyst Related Trends

There was a general decrease in the selectivity to cumene with an increase in propene conversion over the catalysts as shown in Figures 4.3, 4.4 and 4.5. The scatter in these figures is too large to discriminate between the various sets of data points. As a result, it can be deduced that at the same conversion level, there was no significant difference in the selectivity to cumene between sample A and the other catalysts.

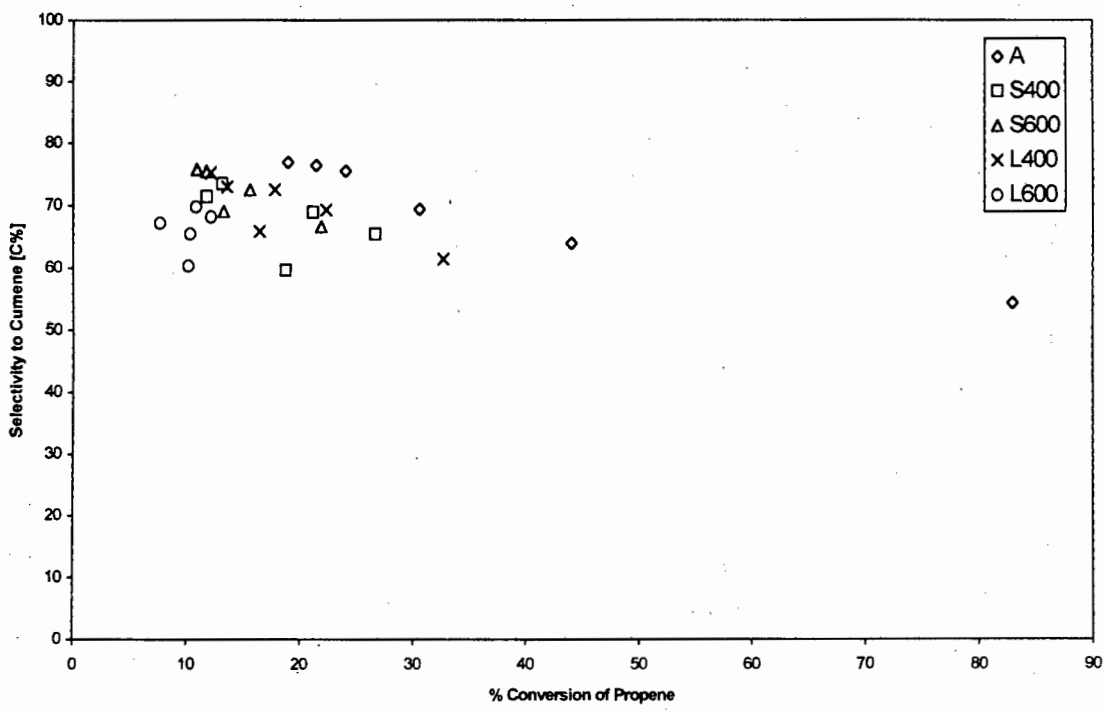

Figure 4.3. Selectivity [C%] to cumene v/s % conversion of propene for steamed catalysts.

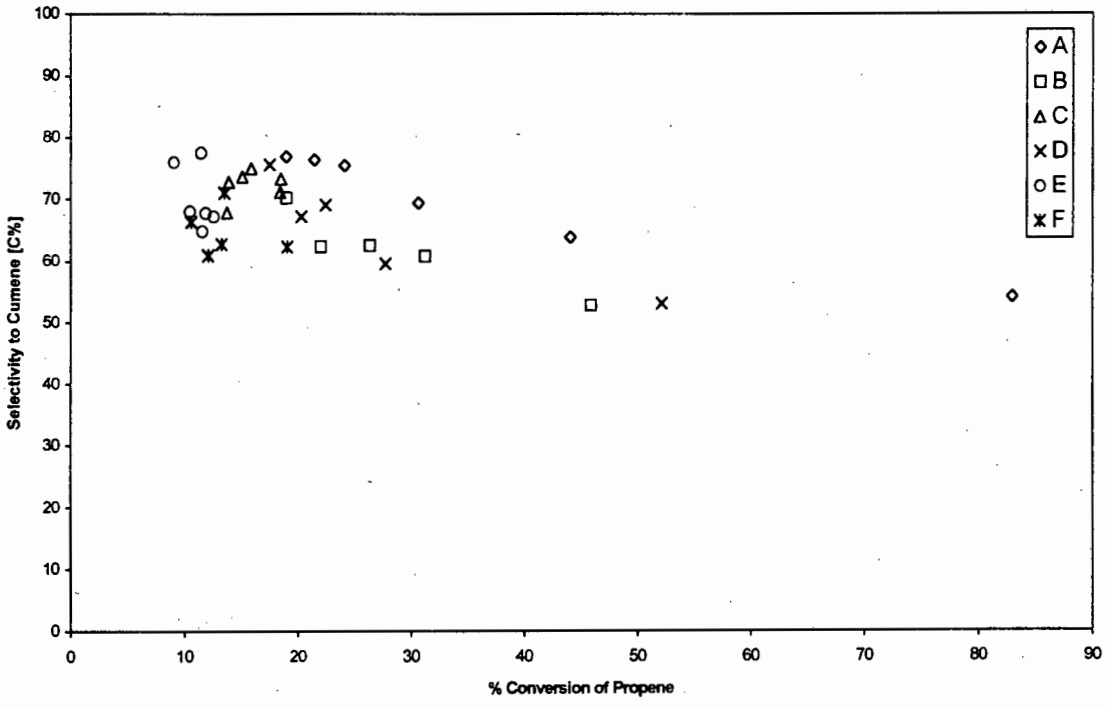

Figure 4.4. Selectivity [C%] to cumene v/s % conversion of propene for samples A-F.

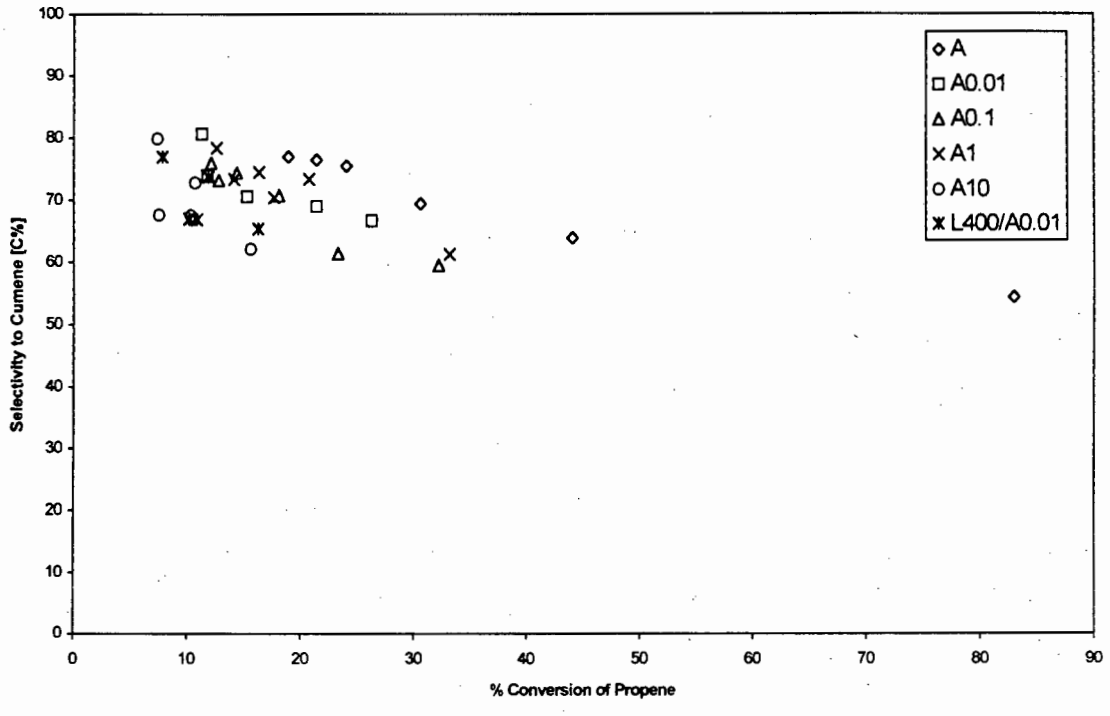

Figure 4.5. Selectivity [C%] to cumene v/s % conversion of propene for acid washed catalysts.

The variation of the m/p DIPB ratio (Figs. 3.18, 3.23 and 3.28) with time on stream appears to be a function of conversion. At the same conversion level, similar m/p DIPB ratio were observed for the different zeolite Beta catalysts. Calculated thermodynamic equilibria for diisopropylbenzene at 100°C indicates a para/meta/ortho ratio of roughly 33/58/9, showing that the meta isomer is the most stable and the ortho isomer is the least stable (Pradhan *et al.*, 1991). It has been shown that large pore zeolites like mordenite and zeolite Beta allow the meta/para ratio to reach thermodynamic equilibrium (Perego *et al.*, 1996). In theory, the equilibrium meta/para DIPB ratio at 210°C is 2.25. The fact that under the reaction conditions used, equilibrium concentrations of the different isomers could not be achieved shows the slight influence of the shape selective nature of the catalysts.

The deactivation studies of Pradhan and Rao (1991) during the isopropylation of benzene over La-H-Y, which has a three dimensional pore structure, have shown that the acid sites in that catalyst were poisoned by site coverage. On the other hand, these authors have observed that for mordenite, which possesses a unidimensional pore structure, the decrease in activity was due to the partial blocking of the pores through coking. The presence of coke deposits in the channels of mordenite induced shape

selectivity by allowing the para DIPB isomer to diffuse out faster than the meta isomer. In the present work, there is no conclusive evidence for coke induced shape selectivity since no adsorption studies were conducted on the coked catalysts.

CHAPTER FIVE

Conclusions

Steamed Catalysts

Steaming of a commercial zeolite Beta catalyst at different conditions (time and temperature) resulted in the formation of extra framework aluminium species (EFAl). Three types of EFAl species were detected by ^{27}Al MAS NMR. These species are most probably located in the zeolite pores as evidenced by the low relative % crystallinity observed for these catalysts. This was supported by XPS studies which revealed that there was no aluminium enrichment at the steamed zeolite surface. Moreover, elemental analysis showed that Al remained in the zeolite bulk after hydrothermal treatment.

The steaming temperature had a more pronounced effect on the physico-chemical characteristics of the catalysts compared to the duration of the steaming procedure. A less ordered framework structure resulted from steaming at 600°C. This was confirmed by the presence of a shoulder at 950 cm^{-1} (assigned to silanol defects) in the infrared spectra of samples S600 and L600. In addition, these catalysts had a lower mesopore and total surface area (BET) as well as fewer acid sites (TPD) and bridging hydroxyl groups (^{1}H MAS NMR) compared to the catalysts steamed at 400°C. The difference in the physico-chemical characteristics of these two groups (S400/L400 and S600/L600) of catalysts was reflected in their catalytic activity for the isopropylation of benzene.

The activity of samples S400 and L400 was higher compared to that of the catalysts steamed at 600°C. In contrast to what has often been reported for steamed zeolites in the literature, there was no enhancement in the activity of the steamed catalysts as compared to sample A. As a matter of fact, the activity of sample A was significantly higher than the steamed catalysts. The number of acid sites present in the steamed samples was the dominant factor that influenced the activity of the catalysts, as shown by the fairly good correlation between the % yield of cumene and the activity of the steamed catalysts.

Furthermore, the fact that sample L600 was active for this reaction although ^{1}H MAS NMR showed the absence of bridging hydroxyl groups and hence Bronsted acid sites, supports the role of Lewis acid sites in the isopropylation of benzene. However, as no

pyridine infrared studies were carried out, the exact nature of the acid sites present in the sample could not be determined.

Synthesised Catalysts

In this study, the synthesis of zeolite Beta by different techniques resulted in catalysts with varying physico-chemical characteristics. Synthesis of zeolite Beta in a static medium (sample B) produced crystals of a well-defined shape. In addition, sample B had the highest mesopore and total surface area as well as the highest number of acid sites. Longer synthesis times resulted in crystals with an average size of 500 nm (samples B and D) as opposed to rapid synthesis which produced 200 nm crystals (samples C and E). A higher relative % crystallinity was also observed for samples with long synthesis times. In general, the relative % crystallinity of samples B-E was lower compared to catalyst A. This was most probably due to the higher degree of faulting in these zeolites as no EFAl, as evidenced by ^{27}Al MAS NMR, was present in the samples. However, ^{27}Al MAS NMR showed a distinct splitting of the peak (60 ppm) corresponding to tetrahedrally coordinated framework aluminium. The splitting of this particular peak might indicate the presence of two Al environments and thus two types of acid sites in the catalysts.

As expected, the catalysts that were synthesised by various techniques performed differently during the isopropylation of benzene. Two sets of catalysts could again be distinguished in terms of their performance for this reaction. Samples B and D had a higher activity compared to samples C and E. However, the activity of these four catalysts was lower compared to sample A. It is possible that diffusional constraints resulting from stacking faults and local defects present in the samples could have contributed to the lower activity observed. The performance of the catalysts showed that one of the types of acid sites assigned to the doublet observed in ^{27}Al MAS NMR could be conducive to the isopropylation of benzene to form cumene.

Acid Washed Catalysts

Acid washing of sample A with nitric acid of different concentrations also resulted in the creation of EFAl. Steaming followed by acid washing (sample L400/A0.01) did not lead to the complete removal of EFAl from the pores of the zeolite. As opposed to the steamed catalysts, not all three types of EFAl were present in all the acid washed samples. An increase in the strength of acid washing resulted in an increase in the mesopore area of the catalysts. The total surface area of the acid washed catalysts was found to be higher compared to sample A. As was the case for the steamed samples, acid washing did not enhance the activity of the catalysts for the isopropylation of benzene. In this particular situation also, the catalysts could be divided into two distinct groups in terms of activity and cumene yield. Samples A0.10, A0.1 and A1 had a higher activity compared to samples A10 and L400/A0.01. However, due to the limited characterisation data available for the acid washed catalysts, the reasons for the difference observed in their activity could not be postulated.

Reaction Studies

Trace amounts of n-propylbenzene, seen in the product spectrum, were most probably formed by the secondary isomerisation of cumene, since the more open structure of zeolite Beta does not allow the formation of the transition complex between benzene and cumene to form n-propylbenzene, as in the medium pore ZSM-5. Furthermore, very little or no o-DIPB was seen in the product spectrum. In addition, there was a decrease in the m/p DIPB ratio with decreasing conversion of propene. These observations tend to show that m-DIPB was most likely formed via the isomerisation of the primary isomer, p-DIPB.

The interpretation of the reaction studies data was problematic due to the rapid deactivating nature of the catalysts. DRIFTS analysis of coked catalyst samples showed the presence of aliphatic soft coke species in the samples. It is proposed that the oligomerisation of propene resulted in the formation of coke precursors during the initial stages of the reaction.

In summary, the creation of EFAl by the steaming and acid washing of zeolite Beta using the conditions described in this study, did not result in the enhancement of the activity of the catalysts for the isopropylation of benzene. The mesoporosity of the zeolite Beta catalysts synthesised by various techniques were different and no EFAl species were detected in these catalysts. However, there was no correlation between the mesoporosity and the activity of the synthesised catalysts during the isopropylation of benzene.

REFERENCES

REFERENCES

Andersen, B., PhD Thesis, Department of Chemical Engineering, University of Cape Town, 1991.

Apelian, M. R., Fung, A. S., Kennedy, G. J., and Degnan, T. F., *Journal of Physical Chemistry* **100**, 16577, 1996.

Bamwenda, G. R., Zhao, Y. X., Wojciechowski, B. W., *Journal of Catalysis* **150**, 243, 1994.

Barrer, R. M., and Makki, M. B., *Canadian Journal of Chemistry* **42**, 1481, 1964.

Bhat, R. N., and Kumar, R., *Journal of Chemical Technology and Biotechnology* **48**, 453, 1990.

Beaumont, R., and Barthomeuf, D., *Journal of Catalysis* **26**, 218, 1972.

Bellussi, G., Pazzuconi, G., Perego, C., Girotti, G., and Terzoni, G., *Journal of Catalysis* **157**, 227, 1995.

Beyer, H. K., and Belenykaia, I., *in* "Catalysis by Zeolites" (B. Imelik., C. Naccache, Y. BenTaarit, J. C. Vedrine, G. Condurrer and H. Praliand, Eds.) Studies in Surface Science and Catalysis Vol.5, p.203, Elsevier, Amsterdam, 1980.

Beyerlein, R. A., Choi-Feng C., Hall, J. B., Huggins, B. J., and Ray, G. J., *Topics in Catalysis* **4**, 27, 1997.

Bhat, R. N., and Kumar, R., *Journal of Chemical Technology and Biotechnology* **48**, 453, 1990.

Bhattacharya, D., Sharma, S., and Singh, A. P., *Applied Catalysis* **150**, 53, 1997.

Biaglow, A. I., Parillo, D. J., Kokotailo, G. T., and Gorte, R. J., *Journal of Catalysis* **148**, 213, 1994.

Boulet, M., Bourgeat-Lami, E., Fajula, F., Des Courieres, T., and Garrone, E., *in* "Proceedings of the Ninth International Zeolite Conference" (R. von Ballmoos, J. B Higgins and M. M. J. Treacy, Eds.) Vol.II, p.389, Butterworth-Heinemann, USA, 1993.

Bourgeat-Lami, E., Massiani, P., Di Renzo, F., Espiau, P., and Fajula, F., *Applied Catalysis* **72**, 139, 1991.

Brunner, E., Ernst, H., Freude, D., Hunger, M., and Pfeifer, H., *in* "Innovation in Zeolite Materials Science" (P. J. Grobet, W. J. Mortier, E. F. Vansant and G. Schulz-Ekloff, Eds.) Studies in Surface Science and Catalysis Vol.37, p.155, Elsevier, Amsterdam, 1988.

Brunner, E., Ernst, H., Freude, D., Hunger, M., Krause, C. B., Prager, D., Reschetilowski, W., Shwieger, W., and Bergk, K. H., *Zeolites* **9**, 282, 1989.

Brunner, E., Ernst, H., Freude, D., Frohlich, T., Hunger, M., and Pfeifer, H., *Journal of Catalysis* **127**, 34, 1991.

Brunner, E., Beck, K., Koch, M., Heeribout, L., and Karge, H. G., *Microporous Materials* **3**, 395, 1995.

Camblor, M. A., Mifsud, A., and Perez-Pariente, J., *Zeolites* **11**, 792, 1991.

Campbell, S. M., Bibby, D. M., Coddington, J. M., Howe, R. F., and Meinhold, R. H., *Journal of Catalysis* **161**, 338, 1996_a.

Campbell, S. M., Bibby, D. M., Coddington, J. M., and Howe, R. F., *Journal of Catalysis* **161**, 350, 1996_b.

Cavani, F., Girotti G., and Terzoni, G., *Applied Catalysis* **97**, 177, 1993.

Chandavar, K. H., Hegde, S. G., Kulkarni, S. B., and Ratnasamy, P., *Journal of Chemical Technology and Biotechnology.* **34A**, 165, 1984.

Chauvin B., Massiani P., Dutartre R., Figueras F., Fajula F., and Des Courieres T., *Zeolites* **10**, 174, 1990.

Chumbale, V. R., Chandwadkar, A. J., and Rao, B. S., *Zeolites* **12**, 63, 1992.

Colthup, N. B., Daly, L. H., and Wiberley, S. E., *in* "Introduction to Infrared and Raman Spectroscopy", Academic Press, San Diego, 1990.

Constantinescu, F., and Blum, J., *Journal of Porous Materials* **2**, 35, 1995.

Corma, A., Fornes, V., Melo, F., and Perez-Pariente, J., *in* "Preprints-Symposia", p.632, Division of Petroleum Chemistry Inc., American Chemical Society, Washington D.C, 1987.

Corma, A., *in* "Zeolites: Facts, Figures and Future" (P. A. Jacobs and R. A. van Santen, Eds) Studies in Surface Science and Catalysis Vol.49A, p.49, Elsevier, Amsterdam, 1989.

Corma, A., Melo, F. V., and Rawlence, D. J., *Zeolites* **10**, 690, 1990.

Corma, A., Gomez, V., and Martinez, A., *Applied Catalysis* **119**, 83, 1994.

Corma, A., Martinez, A., and Martinez, C., *Applied Catalysis* **134**, 169, 1996.

Coutanceau, C., Da Silva, J. M., Alvarez, M. F., Ribeiro, F. R., and Guisnet, M., *Journal de Chimie Physique* **94**, 765, 1997.

Davis, M. E., and Lobo, R. F., *Chemistry of Materials* **4**, 756, 1992.

Das, J., Bhat, Y. S., and Halgeri, A. B., *Catalysis Letters* **32**, 319, 1995.

Das, J., Bhat, Y. S., and Halgeri, A. B., *Indian Journal of Chemistry* **35A**, 690, 1996.

Datka, J., Marschmeyer S., Neubauer, T., Meusinger, J., Papp, H., Schutze, F. -W., and Szpyt, I., *Journal of Physical Chemistry* **100**, 14451, 1996.

Dima, E., and Rees, L. V. C., *Zeolites* **10**, 8, 1990.

Dutartre, R., de Menorval, L. C., Di Renzo, F., McQueen, D., Fajula, F., and Schulz, P., *Microporous Materials* **6**, 311, 1996.

Eapen, M. J., Reddy, K. S. N., and Shiralkar, V .P., *Zeolites* **14**, 295, 1994.

Engelhardt, G., *in* "Introduction to Zeolite Science and Practice" (H. van Bekkum, E. M. Flanigen and J. C. Jansen, Eds.) Studies in Surface Science and Catalysis Vol.58, p.285, Elsevier, Amsterdam, 1991.

Engelhardt, G., Lohse, U., Samoson, A., Magi, M., Tarmak, M., and Lippmaa, E., *Zeolites* **2**, 59, 1982.

Ernst, S., and Weitkamp, J., *Catalysis Today* **19**, 27, 1994.

Feijen, E. J., Martens, J. A., and Jacobs, P. A., *in* "Zeolites and Related Microporous Materials: State of the Art 1994" (J. Weitkamp, H. G. Karge, H. Pfeifer, and W. Holderich, Eds.) Studies in Surface Science and Catalysis Vol.84A, p.3, Elsevier, Amsterdam, 1994.

Fernandes, L. D., Bartl, P. E., Monteiro, J. L. F., da Silva, J. G., de Menezes, S. C., and Cardoso, M. J. B., *Zeolites* **14**, 533, 1994.

Flanigen, E. M., *in* "Zeolites Chemistry and Catalysis" (J.A. Rabo Ed.), ACS Monograph 171, p.80, American Chemical Society, Washington D.C, 1976.

Freude, D., Ernst, H., and Wolf, I., *Solid State Nuclear Magnetic Resonance* **3**, 271, 1994.

Freude, D., Hunger, M., and Pfeifer H., *Zeitschrift. für Physikalische.Chemie Neue Folge* **152**, 2722, 1987.

Freude, D., Hunger, M., Pfeifer, H., and Schwieger, W., *Chemical Physics Letters* **128**, 62, 1986.

Fritz, P. O., and Lunsford, J. H., *Journal of Catalysis* **118**, 85, 1989.

Fyfe, C. A., Gobbi, G. C., Hartman, J. S., Klinowski, J., and Thomas, J. M., *Journal of Physical Chemistry* **85**, 2590, 1981.

Fyfe, C., Kokotailo, G. T., Graham, J. D., Browning, C., Gobbi, G. C., Hyland, M., Kennedy, G. J., and DeSchutter, C. T., *Journal of the American Chemical Society* **108**, 522, 1986.

Fyfe, C. A., Strobl, H., Kokotailo, G. T., Pasztor, C. T., Barlow, G. E., and Bradley, S., *Zeolites* **8**, 132, 1988.

Gabelica, Z., Dewaele, N., Maistriau, L., Nagy, J. B., and Derouane, E. G., *in* "Zeolite Synthesis" (M. Ocelli and H. D. Robson, Eds.) ACS Symposium Series, No.398, p.518, American Chemical Society, Washington D.C., 1989.

Geatti, A., Lenarda, M., Storaro, L., Ganzerla, R., and Perissinotto, M., *Journal of Molecular Catalysis* **121**, 111, 1997.

Germain, A., Akouz, T., and Figueras, F., *Applied Catalysis* **136**, 57, 1996.

Gilson, J. P., Edwards, G. C., Peters, A. W., Rajagopalan, K., Wormsbecher, R. F., Roberie, T. G., and Shatlock, M. P., *Journal of the Chemical Society, Chemical Communications,* p.91, 1987.

Haag, W. O., U.S. Patent 4,374,296, 1983.

Harvey, G., Prins, R., Crockett, R., and Roduner, E., *Journal of the Chemical Society, Faraday Transactions* **92**(11), 2027, 1996.

Hays, G. R., van Erp, W. A., Alma, N. C. M., Couperus, P. A., Huis, R., and Wilson, A. E., *Zeolites* **4**, 377, 1984.

Hong, Y., and Fripiat, J. J., *Microporous Materials* **4**, 323, 1995.

Hunger, M., Ernst, S., and Weitkamp, J., *Zeolites* **15**, 188, 1995.

Hunger, M., Ernst, S., Steuernagel, S., and Weitkamp, J., *Microporous Materials* **6**, 349, 1996.

Jacobs P. A., and Martens J. A., *in* "Synthesis of High Silica Aluminosilicate Zeolites" (P. A Jacobs and J. A. Martens, Eds.) Studies in Surface Science and Catalysis Vol.33, p.16, Elsevier, Amsterdam, 1987.

Jansen, J. C., Creyghton, E. J., Njo, S. L., van Koningsveld, H., and van Bekkum, H., *Catalysis Today* **38**, 205, 1997.

Jian, P., Wang, Q., Zhu, C., and Xu, Y., *Applied Catalysis* **91**, 125, 1992.

Kaeding, W. W., and Holland, R. E., *Journal of Catalysis* **109**, 212, 1988.

Kane, L., Romanow-Garcia, S., and Nakamura, D., *Hydrocarbon Processing* **75**(10), 40, 1996.

Kapustin, G. I., Brueva, T. R., and Klyachko, A. L., *Applied Catalysis* **42**, 239, 1988.

Karge, H. G., and Dondur V., *Journal of Physical Chemistry* **94**, 765, 1990.

Karge, H. G., Dondur, V., and Weitkamp, J., *Journal of Physical Chemistry* **95**, 283, 1991.

Kerr G. T., *Journal of Catalysis* **15**, 200, 1969.

Kerr, G. T., *Journal of Physical Chemistry* **72**, 2594, 1968.

Kim , J-H., Sugi, Y., Matsuzaki, T., Hanaoka, T., Kubota, Y., Tu, X., and Matsumoto, M., *Microporous Materials* **5**, 113, 1995.

Kiricsi, I., Flego, C., Pazzuconi, G., Parker Jr., W. O., Millini, R., Perego, C., and Bellussi, G., *Journal of Physical Chemistry* **98**, 4627, 1994.

Kogelbauer, A., Nikolopoulos, A. A., Goodwin, Jr., J. G., and Marcelin, G., *in* "Zeolites and Related Microporous Materials: State of the Art 1994" (J. Weitkamp, H. G. Karge, H. Pfeifer, and W. Holderich, Eds.) Studies in Surface Science and Catalysis Vol.84C, p.1685, Elsevier, Amsterdam, 1994.

Kornatowski, J., Baur, W. H., Pieper, G., Rozwadowski, M., Schmitz, W., and Cichowlas, A., *Journal of the Chemical Society, Faraday Transactions* **88**(9), 1339, 1992.

Kubelkova, L., Beran, S., Malecka, A., and Mastikhin, V. M., *Zeolites* **9**, 12, 1989.

Lago, R. M., Haag, W. O., Mikovsky, R. J., Olson, D. H., Hellring, S. D., Schmitt, K. D., and Kerr, G. T., *in* "Proceedings of the Seventh International Zeolite Conference" (Y. Murakami, A. Iijima and J. M. Ward, Eds.), p.677, Kodansha Ltd., Tokyo, 1986.

LaPierre, R. B., Partridge, R. D., Chen, N. Y., and Wong, S. S., U.S. Patent 4,501,926, 1985.

Leiras Gomes, A. C., Falabella S-Aguiar, E., Cabral Menezes, S., and Cardoso, D., *Applied Catalysis* **148**, 373, 1997.

Leu, L-J., Hou, L-Y., Kang, B-C., Li, C., Wu, S-T., and Wu, J-C., *Applied Catalysis* **69**, 49, 1991.

Lohse, U., Loffler, E., Hunger, M., Stockner, J., and Patzelova, V., *Zeolites* **7**, 11, 1987.

Lohse, U., Altrichter, B., Donath, R., Fricke, R., Jancke, K., Parlitz, B., and Schreier, E., *Journal of the Chemical Society, Faraday Transactions* **92**(1), 159, 1996.

Long, Y., Jin, M., Sun, Y., Wu, T., Wang, L., and Fei, L., *Journal of the Chemical Society, Faraday Transactions* **92**(9), 1647, 1996.

Luk'yanov, D. B., *Zeolites* **11**, 325, 1991.

Maache M., Janin, A., Lavalley, J. C., Joly, J. F., and Benazzi, E., *Zeolites* **13**, 419, 1993.

Maher, P. K., Hunter, F. D., and Scherzer, J., *Advances in Chemistry Series* **101**, 266, 1971.

McDaniel, C. V., and Maher, P. K., *in* "Proceedings of the First International Conference on Molecular Sieves" (R. M Barrer Ed.), p.186, London, 1968.

Medina-Valtierra, J., Zaldivar, O., Sanchez., M. A., Montoya, J. A., Navarrete, J., and de los Reyes, J. A., *Applied Catalysis* **166**, 387, 1998.

Meier, W. M., Olson, D. H., and Baerlocher, Ch., Atlas of Zeolite Structure Types, Fourth Revised Edition, Elsevier, New York, 1996.

Meima, G.R., van der Aalst, M. J. M., Samson, M. S. U., Garces, J. M., and Lee, J. G., *in* "Proceedings of the Ninth International Zeolite Conference" (R. von Ballmoos, J. B. Higgins and M. M. J. Treacy, Eds.) Vol.II, p.327, Butterworth-Heinemann, USA, 1993.

Meima, G. R., van der Aalst, M. J. M., Samson, M. S. U., Garces, J. M., and Lee, J. G., *in* "Proceedings of the DGMK Conference: Catalysis on Solid Acid and Bases" (J. Weitkamp and B. Lucke, Eds.), p.125, DGMK, Hamburg, 1996.

Meyers, B. L., Fleisch, T. H., and Marshall., C. L., *Applied Surface Science* **26**, 503, 1986.

Meyers, B. L., Fleisch, T. H., Ray, G. J., Miller, J. T., and Hall, J. B., *Journal of Catalysis* **110**, 82, 1988.

Miller, J. T., Hopkins, P. D., Meyers, B. L., Ray, G. J., Roginski, R. T., Zajac, G. W., and Rosenbaum, N. H., *Journal of Catalysis* **138**, 115, 1992.

Mirodatos, C., and Barthomeuf, D., *Journal of the Chemical Society, Chemical Communications*, p.39, 1981.

Mitra, A., Subramanian, S., Das, D., Satyanarayana, Chilukuri, V. V., and Chakrabarty, D. K., *Applied Catalysis* **153**, 233, 1997.

Moon, G. C., MSc Thesis, Department of Chemical Engineering, University of Cape Town, 1995.

Namba, S., Inaka, A., and Yashima, T., *Zeolites* **6**, 107, 1986.

Newsam, J. M., Treacy, M. M. J., Koetsier, W. T., and De Gruyter, C. B., *Proceedings of the Royal Society of London, Series A.* **420**, 375, 1988.

O'Donovan, A. W., PhD Thesis, Department of Chemical Engineering, University of Cape Town, 1995.

O'Donovan, A. W., O'Connor, C. T., and Koch, K. R., *Microporous Materials* **5**, 185, 1995.

Parikh, P. A., Subrahmanyam, N., Bhat, Y. S., and Halgeri, A. B., *Journal of Molecular Catalysis* **88**, 85, 1994.

Parikh, P. A., Subrahmanyam, N., Bhat, Y. S., and Halgeri, A. B., *Canadian Journal of Chemical Engineering* **71**, 756, 1993.

Patzelova, V., Drahoradova, E., Tvaruzkova, Z., and Lohse, U., *Zeolites* **9**, 74, 1989.

Pellet, R. J., Casey, D. G., Huang, H. -M., Kessler, R. V., Kuhlman, E. J., O'Young, C. -L., Sawicki, R. A., and Ugolini, J. R., *Journal of Catalysis* **157**, 423, 1995.

Perego, C., Amarilli, S., Millini, R., Bellussi, G., Girotti, G., and Terzoni, G., *Microporous Materials* **6**, 395, 1996.

Perez-Pariente, J., Martens, J. A., and Jacobs, P. A., *Applied Catalysis* **31**, 35, 1987.

Perez-Pariente, J., Martens, J. A., and Jacobs, P. A., *Zeolites* **8**, 46, 1988.

Perez-Pariente, J., Sanz, J., Fornes, V., and Corma, A., *Journal of Catalysis* **124**, 217, 1990.

Perez-Pariente, J., Sastre, E., Fornes, V., Martens J. A., Jacobs, P. A., and Corma, A., *Applied Catalysis* **69**, 125, 1991.

Pradhan, A. R., and Rao, B. S., *Journal of Catalysis* **132**, 79, 1991.

Pradhan, A. R., Kotasthane, A. N., and Rao, B. S., *Applied Catalysis* **72**, 311, 1991.

Raimondo, M., Perez, G., De Stefanis, A., Tomlinson, A. A. G., and Ursini, O., *Applied Catalysis* **164**, 119, 1997.

Rakiewicz, E. F., Mueller, K. T., Jarvie, T. P., Sutovich, K. J., Roberie, T. G., and Peters, A. W., *Microporous Materials* **7**, 81, 1996.

Ratnasamy, P., Bhat, R. N., Pokhriyal, S. K., Hegde, S. G., and Kumar R., *Journal of Catalysis* **119**, 65, 1989.

Remy, M. J., Stanica, D., Poncelet, G., Feijen, E. J. P., Grobet, P. J., Martens, J. A., and Jacobs, P. A., *Journal of Physical Chemistry* **100**, 12440, 1996.

Reddy, K. S. N., Rao, B. S., and Shiralkar, V. P., *Applied Catalysis* **95**, 53, 1993.

Sarv, P., Fernandez C., Amoureux, J-P., and Keskinen, K., *Journal of Physical Chemistry* **100**, 19223, 1996.

Sasidharan, M., Reddy, K. R., and Kumar, R., *Journal of Catalysis* **154**, 216, 1995.

Sawa, M., Niwa, M., and Murakami., Y., *Applied Catalysis* **53**, 169, 1989.

Sawa, M., Niwa, M., and Murakami., Y., *Zeolites* **12**, 175, 1992.

Saxton, R. J., Crocco, G. L., and Zajacek, J. G., Eur. Pat. Appl. EP 690,024.

Scherzer, J., *in* "Catalytic Materials" (T. E. Whyte Jr., R. A. Dalla Betta, E. G. Derouane and R. T. K. Baker, Eds.), p.157, American Chemical Society, Washington D.C, 1984.

Scherzer, J., *Journal of Catalysis* **54**, 285, 1978.

Schulz, H., and Nehren, S., *Erdol und Kohle- Erdgas – Petrochemie* **39**, 93, 1986.

Sendoda, Y., and Ono Y., *Zeolites* **8**, 101, 1988.

Silva, J. M., Ribeiro, M. F., Ramoa Ribeiro, F., Benazzi, E., Gnep, N. S., and Guisnet, M., *Zeolites* **16**, 275, 1996.

Skeels, G. W., and Breck, D. W., *in* "Proceedings of the Sixth International Conference on Zeolites" (D. Olson and A. Bisio, Eds.), p.87, Butterworths, London, 1984.

Smirnov, A. V., Romanovsky, B. V., Ivanova, I. I., Derouane, E. G., and Gabelica, Z., *in* "Zeolites and Related Microporous Materials: State of the Art 1994" (J. Weitkamp, H. G. Karge, H. Pfeifer and W. Holderich, Eds.) Studies in Surface Science and Catalysis Vol.84C, p.1797, Elsevier, Amsterdam, 1994.

Smirnov, A. V., Di Renzo, F., Lebedeva, O. E., Brunel, D., Chiche, B., Tavolaro, A.,

Romanovsky, B. V., Giordano, G., Fajula, F., and Ivanova, I. I., *in* "Progress in Zeolite and Microporous Materials" (H. Chon, S. -K. Ihm, and Y. S. Uh, Eds.) Studies in Surface Science and Catalysis Vol.105, p.1325, Elsevier, Amsterdam, 1997.

Sun, Y., Chu, P-J., and Lunsford, J. H., *Langmuir* **7**, 3027, 1991.

Sur, S. K., and Bryant, R. G., *Zeolites* **16**, 118, 1996.

Szostak, R., *in* "Handbook of Molecular Sieves", Van Nostrand Reinhold, New York, 1992.

Szostak, R., Lillerud, K. P., and Stocker, M., *in* "Preprints-Symposia" Vol. 38(3), p.552, Division of Petroleum Chemistry Inc., American Chemical Society, Washington D.C., 1993.

Taylor, W. J., Wagman, D. D., Williams, M. G., Pitzer, K. S., and Rossini, R. D., *Journal of Research of the National Bureau of Standards* **37**, 95, 1946.

Vaudry F., di Renzo, F., Fajula, F., and Schulz, P., *in* "Zeolites and Related Microporous Materials: State of the Art 1994" (J. Weitkamp, H. G. Karge, H. Pfeifer, and W. Holderich Eds) Studies in Surface Science and Catalysis Vol.84A, p.163, Elsevier, Amsterdam, 1994.

Vedrine J. C., Fernandez, C., Grosmangin, J., and Szabo, G., *Zeolites* **6**, 484, 1986.

Von Ballmoos, R., *in* "The ^{18}O-exchange method in zeolite chemistry", p.185, Salle and Sauerlander, Frankfurt am Main, 1981.

Wadlinger, R. L., Kerr, G. T., and Rosinski, E. J., U.S. Patent 3,308,069, 1967.

Wang, Q. L., Giannetto, G., Torrealba, M., Perot, G., Kappenstein, C., and Guisnet, M., *Journal of Catalysis* **130**, 459, 1991.

Ward, J. M., *Journal of Catalysis* **18**, 348, 1970.

Weber, R. W., MSc Thesis, Department of Chemical Engineering, University of Cape Town, 1993.

Wichterlova, B., Cejka, J., and Zilkova, N., *Microporous Materials* **6**, 405, 1996.

Wu, P., Komatsu, T., and Yashima, T., *Journal of the Chemical Society, Faraday Transactions.* **92**(5), 861, 1996.

Yang, X., and Truitt, R. E., *Zeolites* **16**, 249, 1996.

Yang, C., and Xu, Q., *Journal of the Chemical Society, Faraday Transactions* **93**(8), 1675, 1997.

Zholobenko, V. L., Kustov, L. M., Kazansky, V. B., Loeffler, E., Lohse U., Peuker, Ch., and Oehlmann, G., *Zeolites* **10**, 304, 1990.

Zholobenko, V. L., Kustov, L. M., Kazansky, V. B., Loeffler, E., Lohse U., and Oehlmann, G., *Zeolites* **11**, 132, 1991.

Zukal, A., Patzelova, V., and Lohse, U., *Zeolites* **6**, 133, 1986.

APPENDIX A

Sample calculation of Si/Al ratio from AAS and gravimetric analysis

Sample calculation of Si/Al ratio (S400)

Determination of Si content (Gravimetric Analysis):

Mass of crucible	=	18.4573 g		
Mass of crucible + SiO_2	=	18.5248 g		
Mass of SiO_2	=	0.0675 g		
Moles of SiO_2/Si	=	0.0675/MW	=	0.0675/[28.09 + 2(16.00)]
	=	0.001123		

Determination of Al content (Atomic Absorption Spectroscopy):

Al content/ppm	=	28.0		
Al content/μg	=	2800		
Moles of Al	=	0.0028/MW	=	0.0028/26.98
	=	0.0001038		

Si/Al ratio	=	0.001123/0.0001038
	=	10.8

MW in the above calculations stands for molecular weight.

APPENDIX B

Sample calculation of conversion and selectivity for the isopropylation of benzene

A typical GC trace of the products from the isopropylation of benzene is shown below.

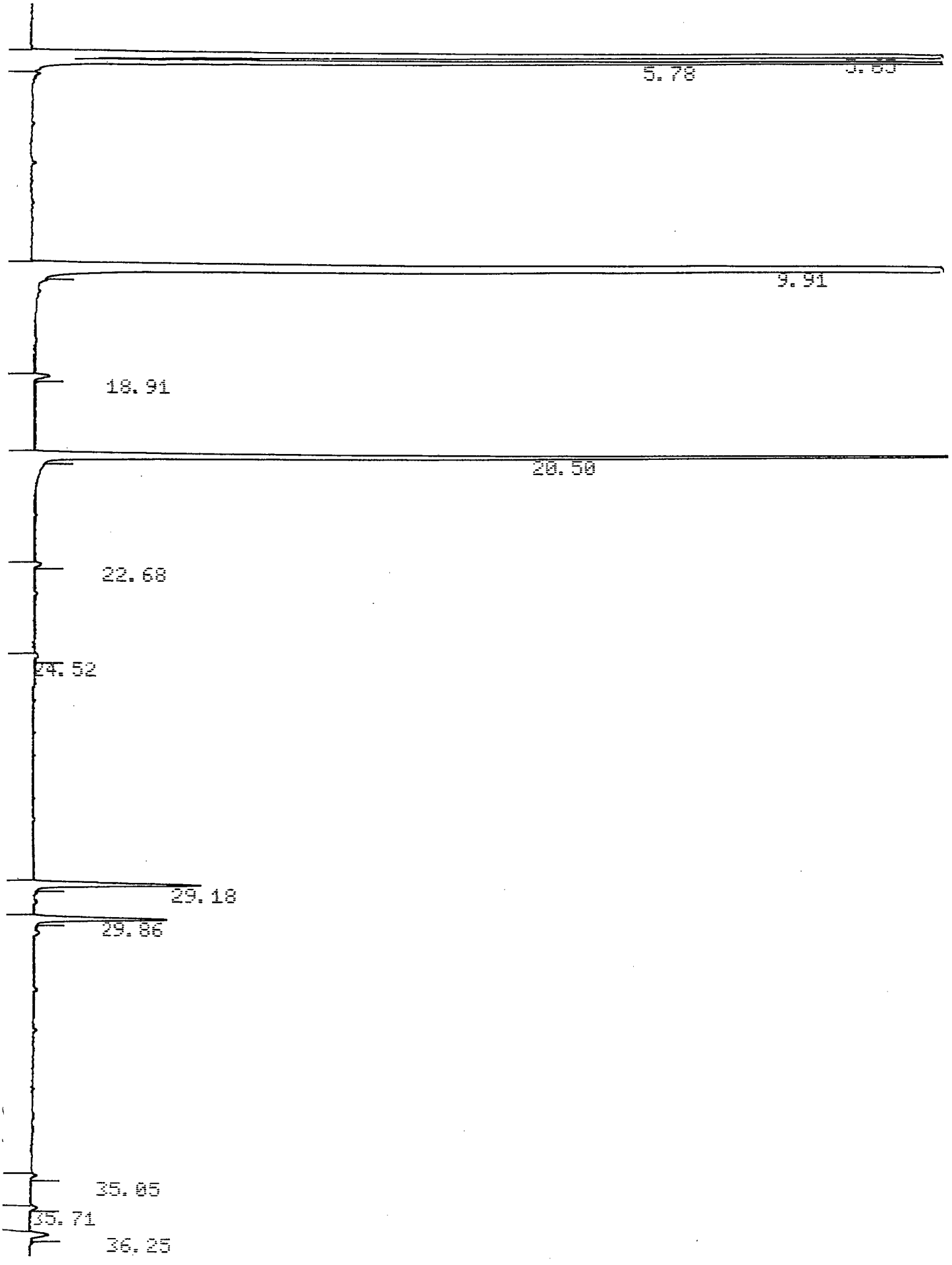

The peak assignments based on the observed retention times with corresponding % areas and response factors are shown in Table B.1.

Table B.1. Calculation of the relative amounts of each species in the product stream.

Time [min]	Component	% Area	Response Factor [Mass Basis]	Mass%	Number of moles	Carbon Number	Number of carbons from propene converted to product [N]
5.65	Methane	20.43	0.97	22.41	1.40	1	-
5.78	Propene	7.80	0.98	8.46	0.20	3	-
9.91	Benzene	64.81	1.12	61.55	0.79	6	-
-	C6's	0	1	0	0	6	6
18.91	n-propylbenzene	0.074	1.01	0.078	0.00065	6	3
20.50	Cumene	5.24	0.97	5.74	0.0448	9	3
22.68	C9's	0.066	1	0.077	0.00065	9	9
24.52							
29.18	m-DIPB	0.78	1	0.83	0.0051	12	6
-	o-DIPB	0	1	0	0	12	6
29.86	p-DIPB	0.66	1	0.70	0.0043	12	6
-	C12's	0	1	0	0	12	12
35.05	TIPB's	0.15	1	0.16	0.012	15	9
35.71							
36.25							
-	C15's	0	1	0	0	15	15

Methane was not formed during the reaction, but was used as an internal standard for carbon balance purposes. The % area of each component from GC analysis was divided by the respective response factors and normalised to give the mass% of that component.

$$(Mass\%)_n = \frac{(\%Area)_n / RF_n}{\sum_{i=C1}^{C15}\left[(\%Area)_i / RF_i\right]}$$

A basis of 100 grams of product stream was taken in order to calculate the number of moles of each component. MW_n refers to the molecular weight of component *n*.

$$(Moles)_n = \frac{(Mass\%)_n \times 100}{MW_n}$$

A carbon balance was performed by comparing the number of moles of carbon in the feed to the number of moles of carbon in the product stream. C_i and C_n refer to the number of carbon atoms present in the molecules.

$$\sum_{i=C1}^{C6}\left[(Moles)_i C_i\right]_{feed} \approx \sum_{n=C1}^{C15}\left[(Moles)_n C_n\right]_{product}$$

In this particular case, the values for the expressions on the left-hand and right-hand side of the above equation were 4.17 and 4.22 mols respectively, thus giving a carbon balance of 101%.

The conversion was based on the number of moles of carbon from propene that were converted into products.

$$Conversion = \frac{\sum_{n=C6's}^{C15's}(Moles)_n N_n}{3(Moles)_{propene} + \sum_{n=C6's}^{C15's}(Moles)_n N_n}$$

Selectivity to the different products was calculated on a carbon basis in order to ensure that the selectivity calculated for each product represented the amount of propene converted to that product.

$$(Selectivity)_n = \frac{(Moles)_n N_n}{\sum_{n=C6's}^{C15's}(Moles)_n N_n}$$

APPENDIX C

XRD patterns

X-Ray Diffraction Patterns

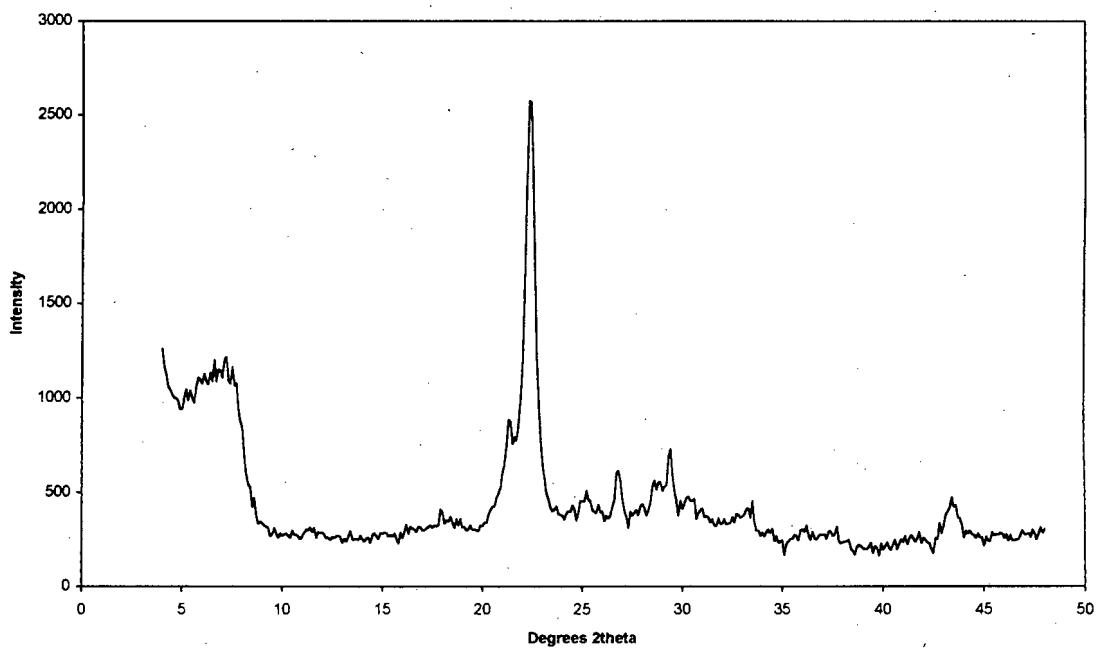

Sample B

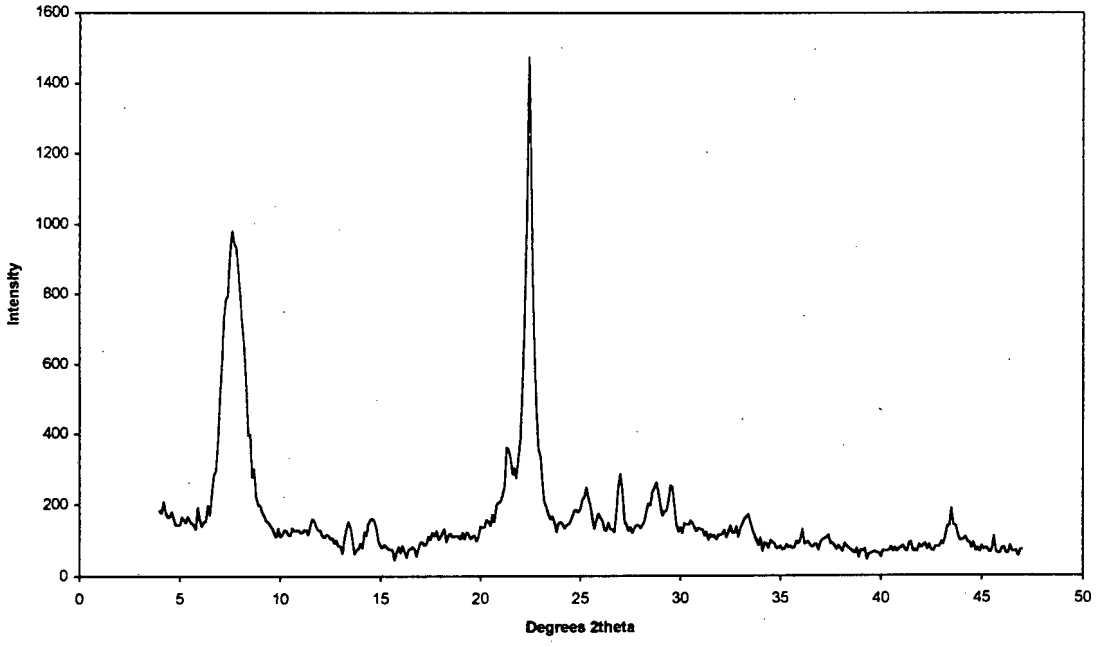

Sample C

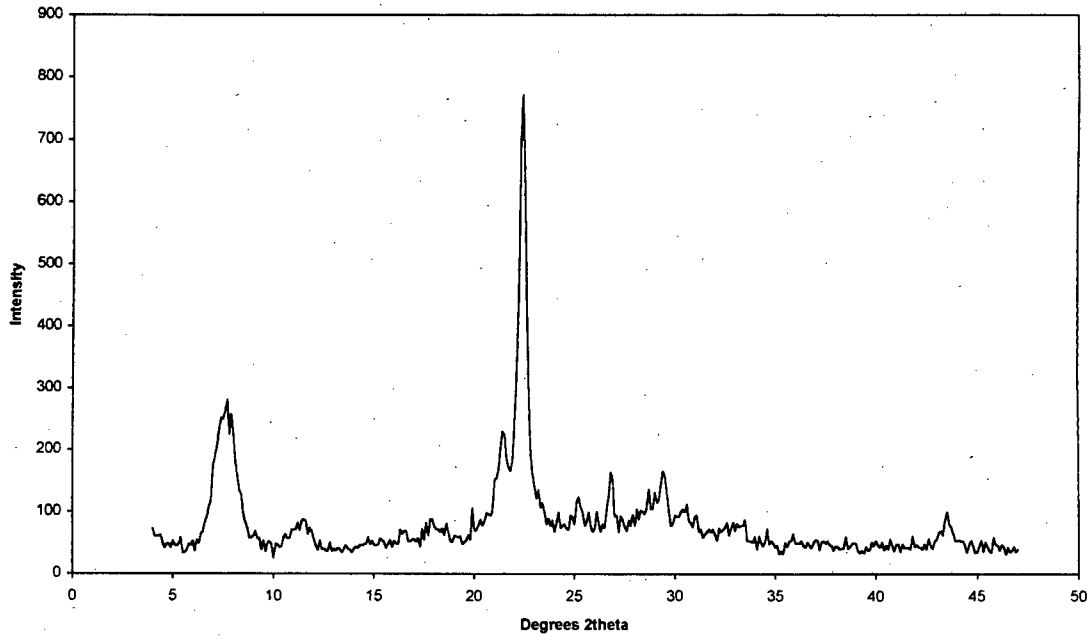

Sample D

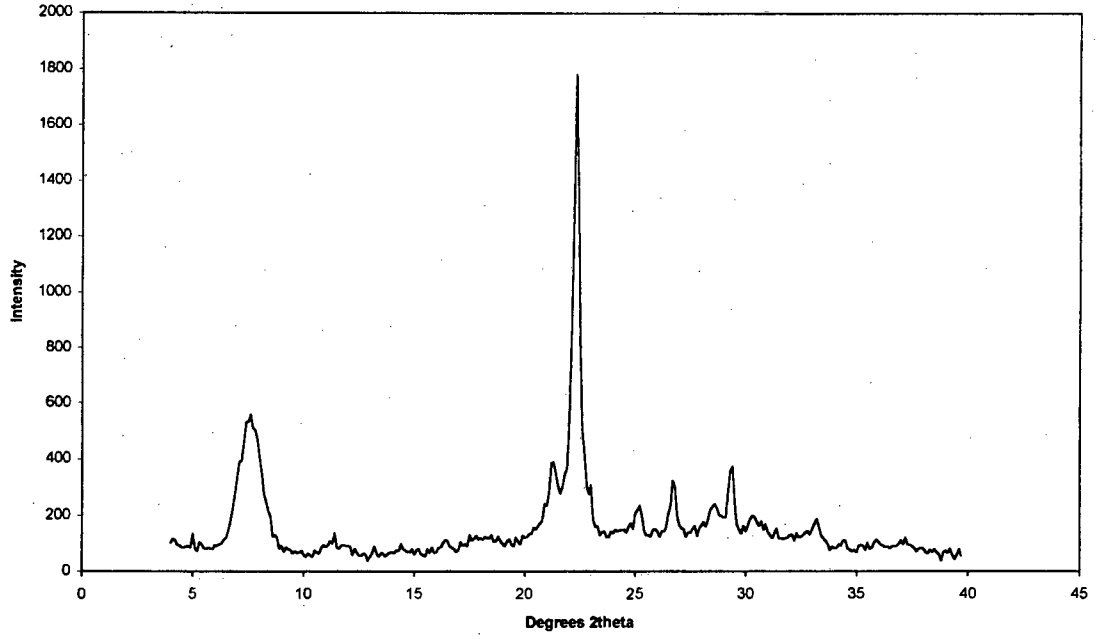

Sample E

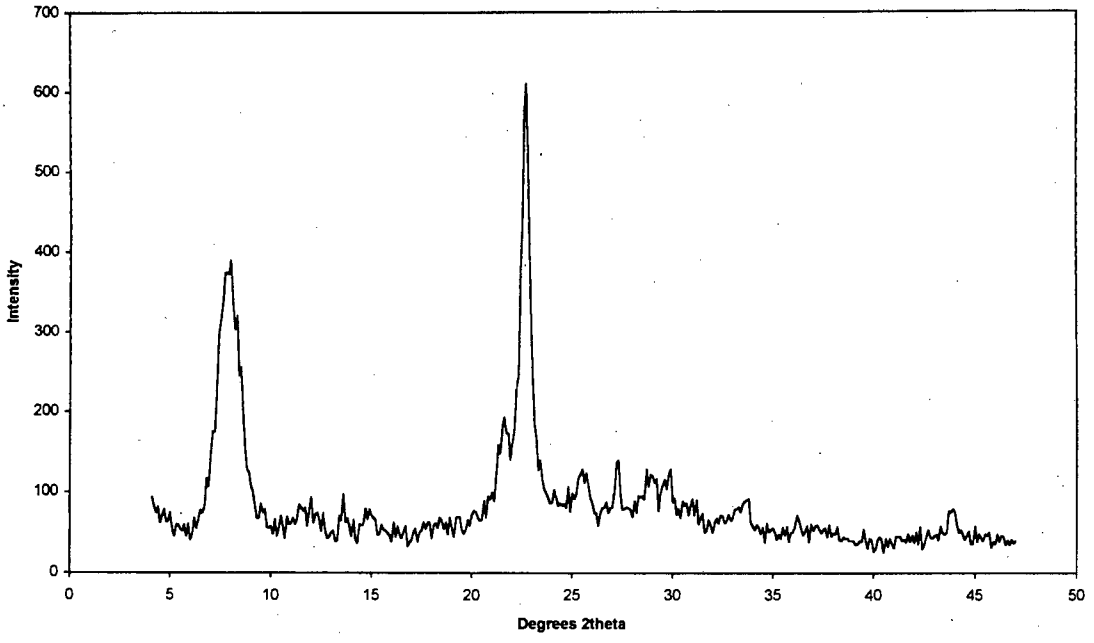

Sample F

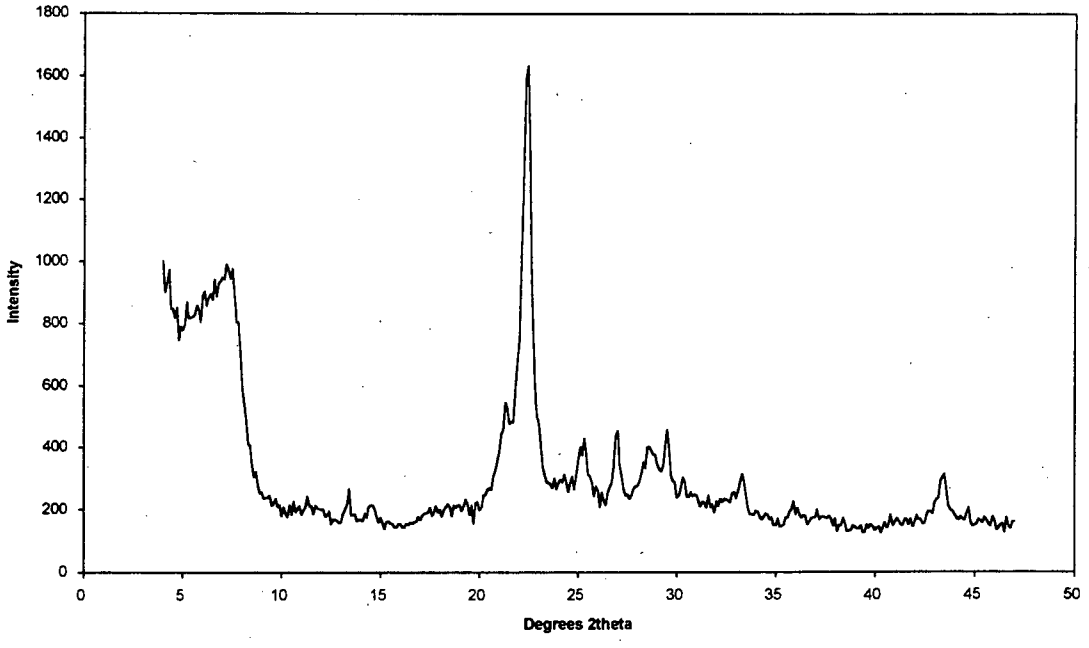

Sample S400

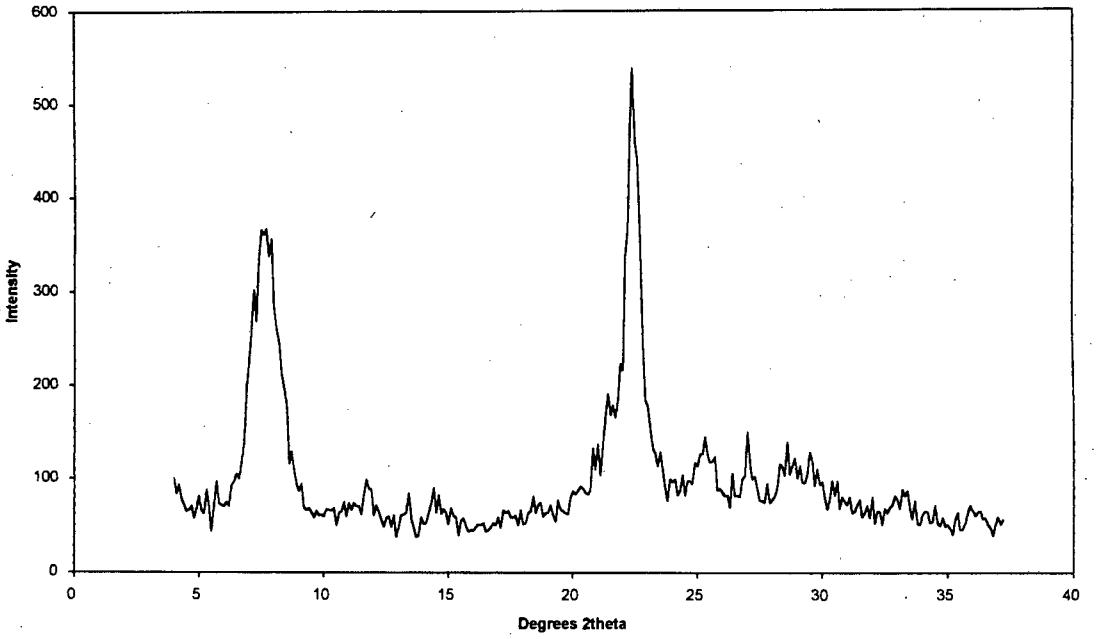

Sample S600

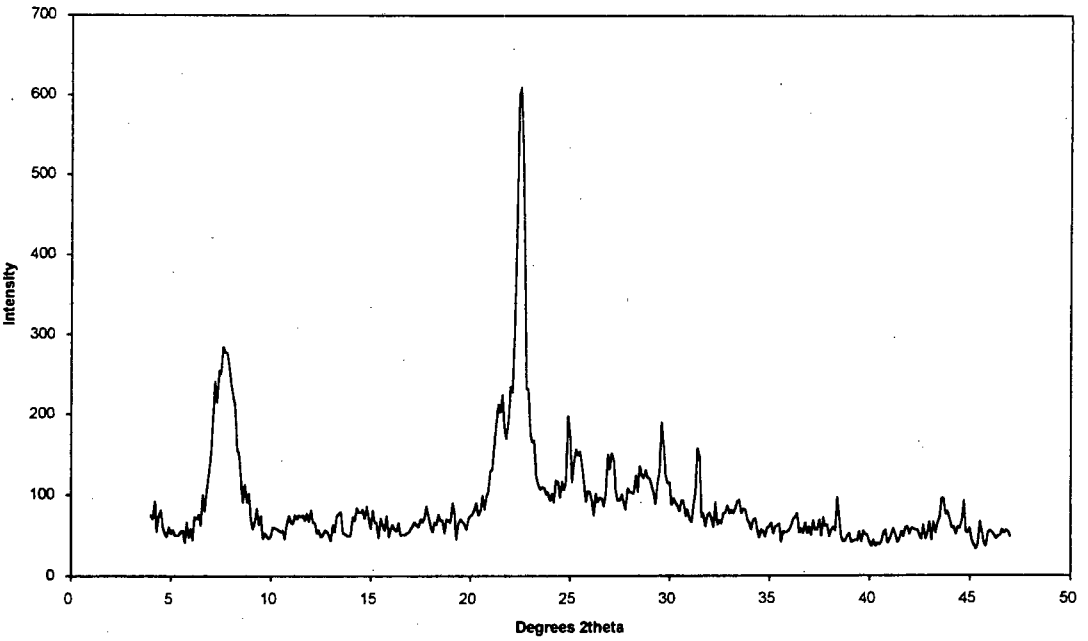

Sample L400

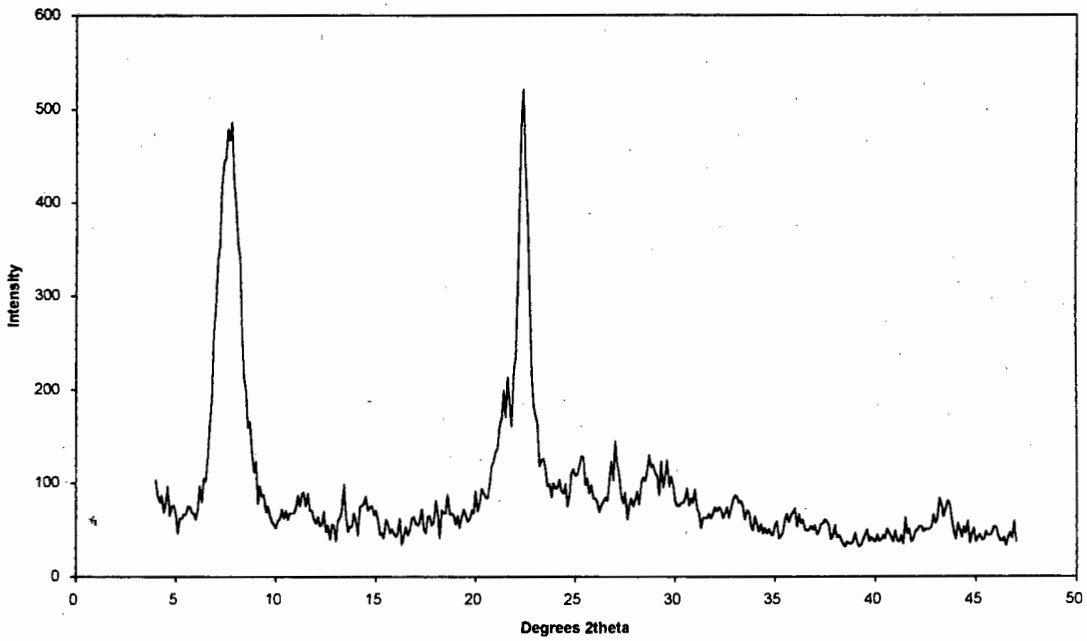
600
500
400
300
200
100
0
Intensity
0
5
10
15
20
25
30
35
40
45
50
Degrees 2theta

Sample L600

APPENDIX D

Error analysis of AAS technique and gravimetric method

Error analysis of AAS technique and gravimetric method

1. Sensitivity analysis of AAS

Table D.1. The AAS results of a sample of zeolite Beta.

Sample	Si ppm	Al ppm	Si/Al
1	65.7	6.35	10.34
2	68.8	6.4	10.75
3	68	6.62	10.27
4	69.6	6.7	10.43
5	57	6.55	8.70

A sensitivity analysis of the Si/Al ratio to errors in the Si and Al AAS readings is given in Figures D.1 and D.2. Sample 1 in the above table was taken as a basis.

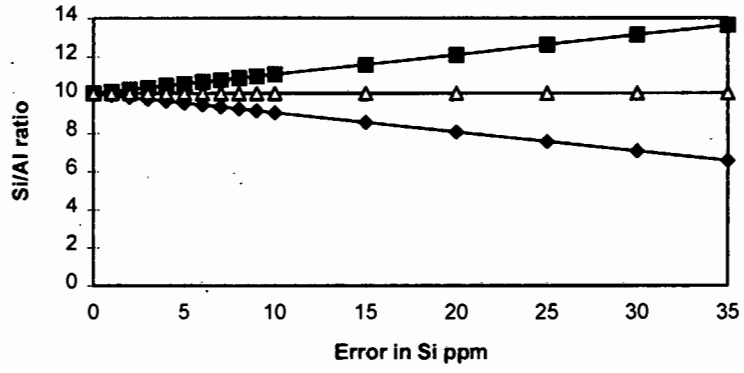

Figure D.1. The sensitivity of Si/Al ratio of zeolite Beta to the error in the Si AAS reading.

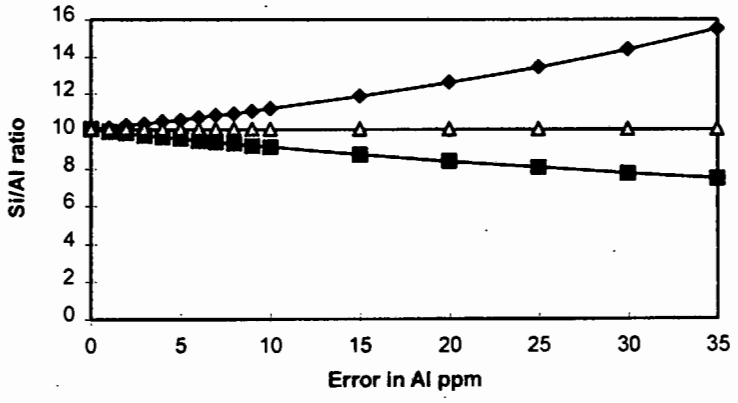

Figure D.2. The sensitivity of Si/Al ratio of zeolite Beta to the error in the Al AAS reading.

2. Confidence levels

We want a 95% confidence level i.e. we want to say that the samples are x ± y % with 95% confidence.

For a small-sample confidence interval for μ:

$$\bar{x} - t_{\alpha/2} \cdot \frac{s}{\sqrt{n}} < \mu < \bar{x} + t_{\alpha/2} \cdot \frac{s}{\sqrt{n}}$$

where: $\bar{x}$ is the mean given by $\bar{x} = \frac{\sum x_i}{n}$

$t_{\alpha/2}$ is the t-distribution

s is the standard deviation given by $s = \sqrt{\frac{\sum (x_i - \bar{x})^2}{n-1}}$

n is the number of samples

μ is the mean of the probability distribution.

The $t_{\alpha/2}$ value depends on the degrees of freedom. The degrees of freedom are generally given by (n-1) where n is the number of samples (Melville and Goddard, 1996). Thus for zeolite Beta there are 4 degrees of freedom. The following table gives the $t_{\alpha/2}$ used (Miller and Freund, 1985).

Table D.2. The $t_{\alpha/2}$ values zeolite Beta.

Degrees of freedom	$t_{0.95}$	$t_{0.99}$
4	2.776	3.747

2.1 Confidence levels for the AAS

Thus for a 95% confidence level:

Si ± 4.87%

Al ± 1.39%

And for a 99% confidence level:

Si ± 6.54%

Al ± 1.88%

2.2. Confidence levels for the gravimetric determination of Si

The following graph shows the sensitivity of the mass% of SiO_2 to the error in the gravimetric method.

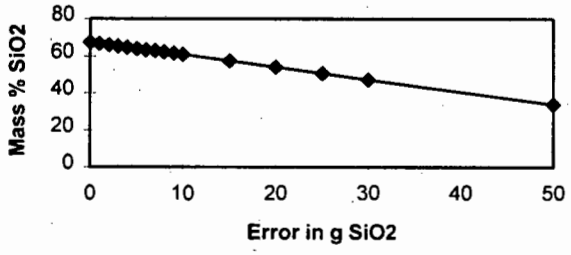

Figure D.3. The sensitivity of the mass % SiO_2 to the error in the weight of SiO_2.

Table D.3. The gravimetric determination of Si.

Mass of SiO_2 in [g]	Mass of full crucible [g]	Mass of empty crucible [g]	SiO_2 [g]	SiO_2 [mass%]
0.1011	17.8722	17.804	0.0682	67.458
0.1512	18.1284	18.0265	0.1019	67.394
0.0902	17.8721	17.8126	0.0595	65.965

Thus a value of $t_{0.95} = 4.303$ gives,

Si ± 2.22%

and a value of $t_{0.99} = 6.965$ gives,

Si ± 2.4%

3. The F-Test

The F-test is the statistical test for determining the equality of two variances of two populations sampled. If independent random samples of size n_1 and n_2 are taken from normal populations having the same variance, it follows that

$$F = \frac{s_1^2}{s_2^2}$$

is a value of a random variable having the F distribution with (n_1-1) and (n_2-1) degrees of freedom. Thus, if the null hypothesis $\sigma_1^2 = \sigma_2^2$ is true, the ratio of the sample variance s_1^2 and s_2^2 provides a statistic on which tests of the null hypothesis can be based.

Table D.4. Critical regions for testing $\sigma_1^2=\sigma_2^2$ (normal populations) (Miller and Freund, 1985).

Alternative hypothesis	Test statistic	Reject null hypothesis if
$\sigma_1^2 < \sigma_2^2$	$F = \frac{s_2^2}{s_1^2}$	$F > F_\alpha(n_2 -1, n_1 -1)$
$\sigma_1^2 > \sigma_2^2$	$F = \frac{s_1^2}{s_2^2}$	$F > F_\alpha(n_1 -1, n_2 -1)$
$\sigma_1^2 \neq \sigma_2^2$	$F = \frac{s_M^2}{s_m^2}$	$F > F_{\alpha/2}(n_M -1, n_m -1)$

Thus, using the results from AAS and the gravimetric method of Si determination we obtain the following results:

s = 0.05968, n= 3, Si gravimetric determined
s = 3.80142, n=5, Si AAS determined
s = 0.09765, n=4, Al AAS determined.

For a confidence level of 95% and taking into account the Si and Al determined by AAS; $F_{0.025}(4,3)$ = 15.1 and F = 1518. Thus $F>F_\alpha$ and so the null hypothesis is rejected and the alternative hypothesis is accepted i.e. $\sigma_{Si}^2 > \sigma_{Al}^2$ [$F_\alpha(n_1-1, n_2-1)$ obtained from Davis and Goldsmith, 1980]. For the gravimetric determined Si and the AAS Al readings, $F_{0.025}(2,3)$ = 16.0 and F= 0.37. Thus, $F<F_\alpha$ the null hypothesis is

accepted i.e. $\sigma_{Si}^2 = \sigma_{Al}^2$. Considering the Si determined by AAS v/s the Si determined by gravimetric method, $F_{0.025}(4,3) = 15.1$ and $F = 4056$. Thus, $F > F_\alpha$ and the null hypothesis is rejected and the alternative hypothesis is accepted i.e. σ_{Si}^2 (AAS) > σ_{Si}^2 (gravimetrically).

The conclusion of the F-test is that the variance of the Si determined either by AAS or gravimetrically is larger than the variance of the Al. Also the variance of the Si determined by AAS is larger than the variance of the Si determined by gravimetric method.

References

Davis O. L. and Goldsmith P. L., "Statistical Methods in Research and Production", 4th revised edition, Longman Group Ltd, London, 1980.

Melville S. and Goddard W., "Research Methodology", Juta & Co Ltd, South Africa, 1996.

Miller I. and Freund J. E., "Probability and Statistics for Engineers", 3rd edition, Prentice/Hall International, USA, 1985.

APPENDIX E

BJH desorption plots

BJH Desorption Plots

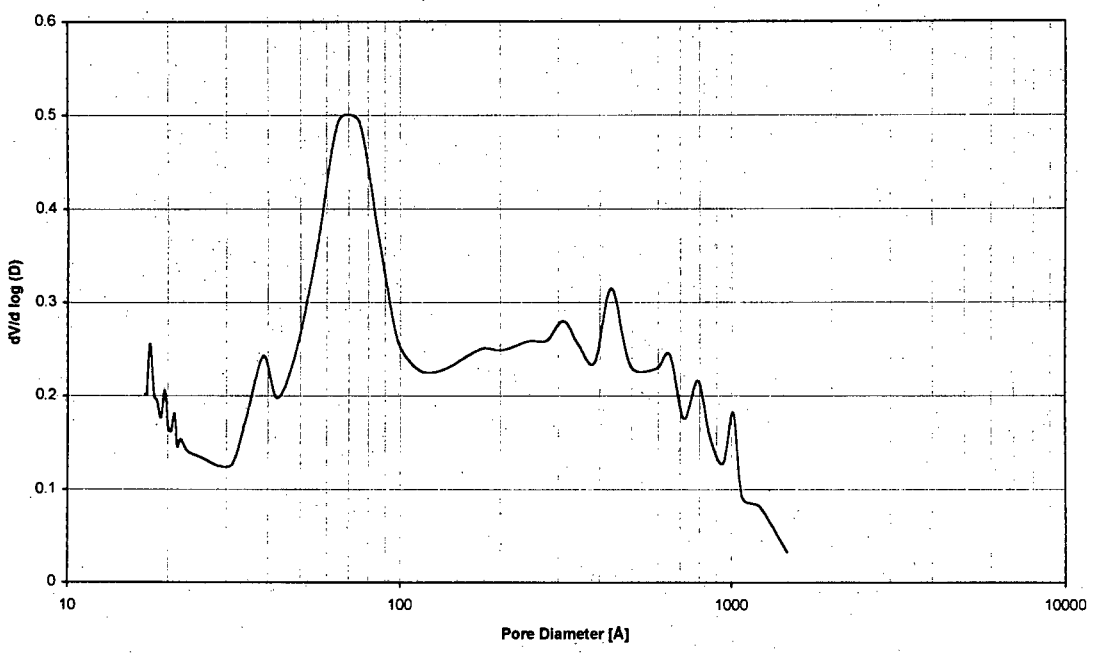

Sample A

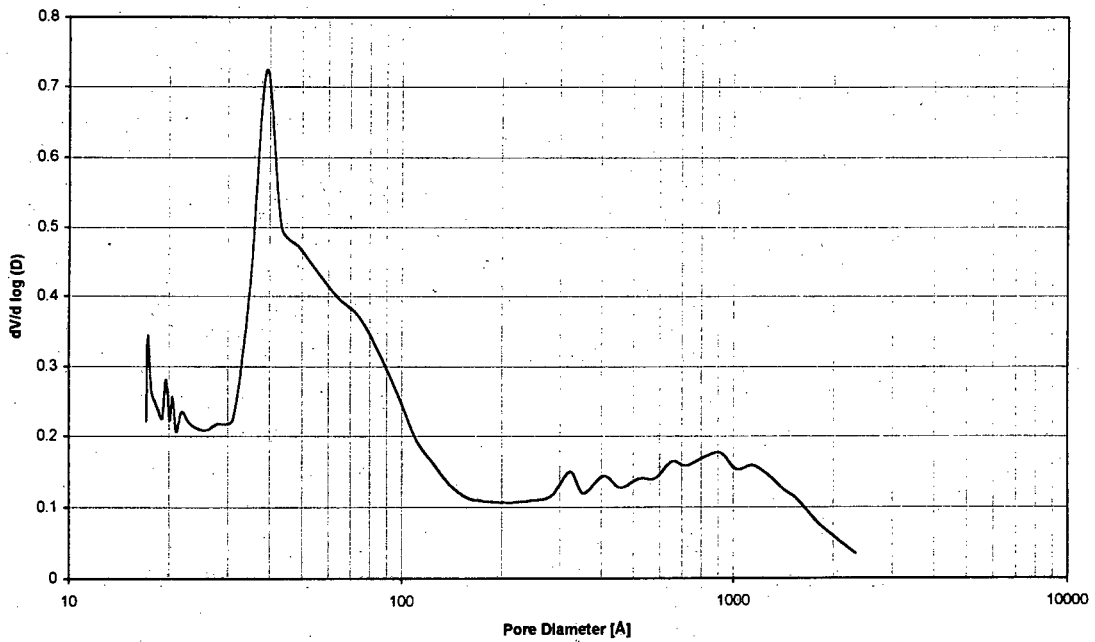

Sample B

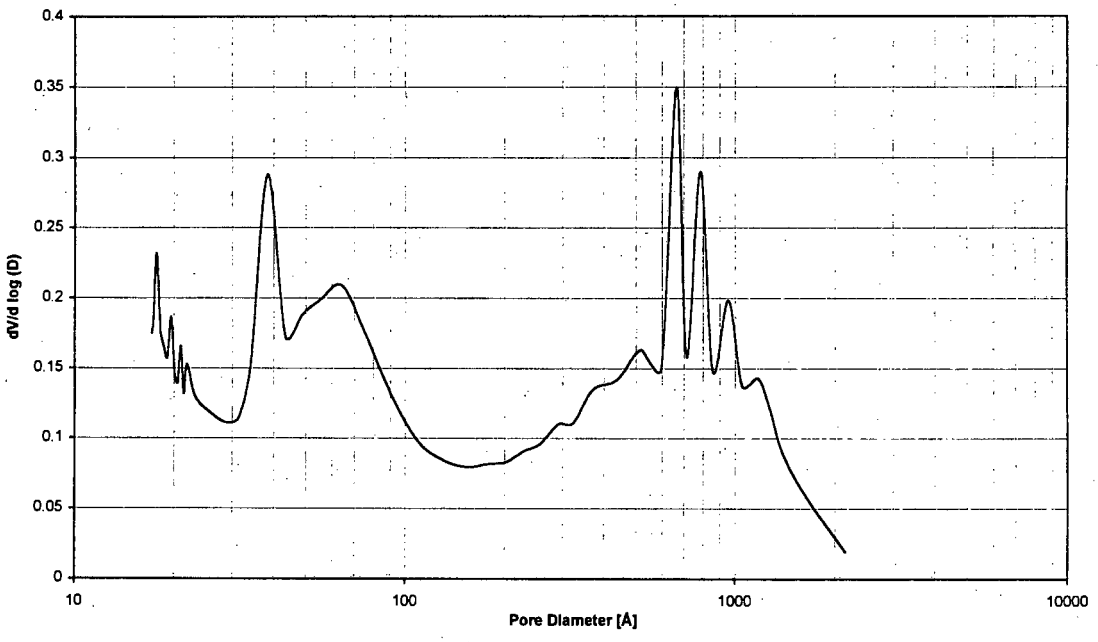

Sample E

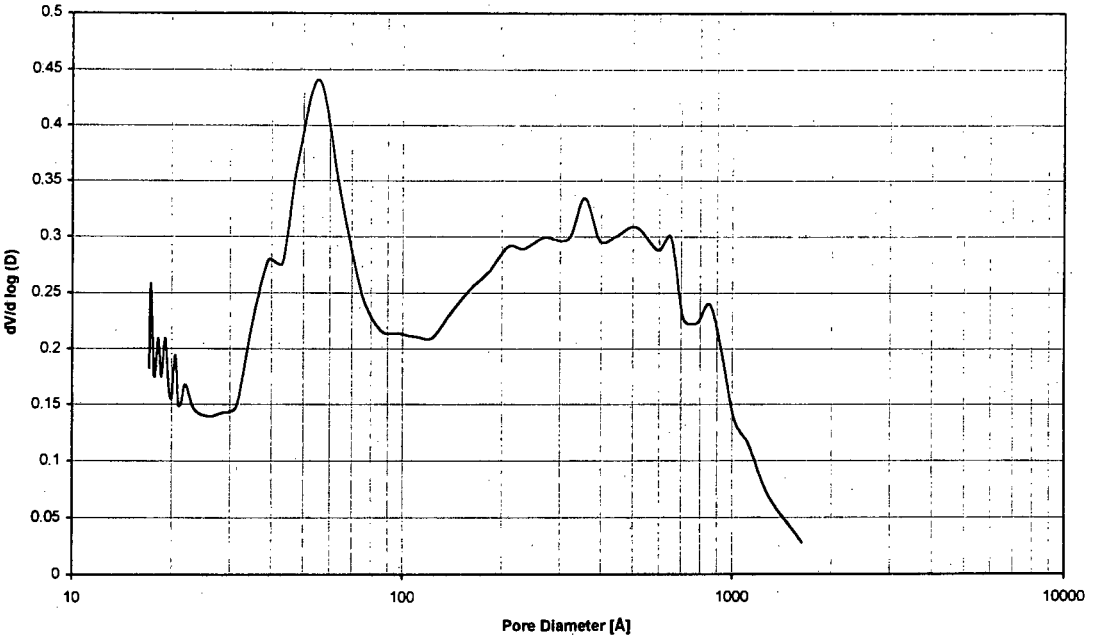

Sample F

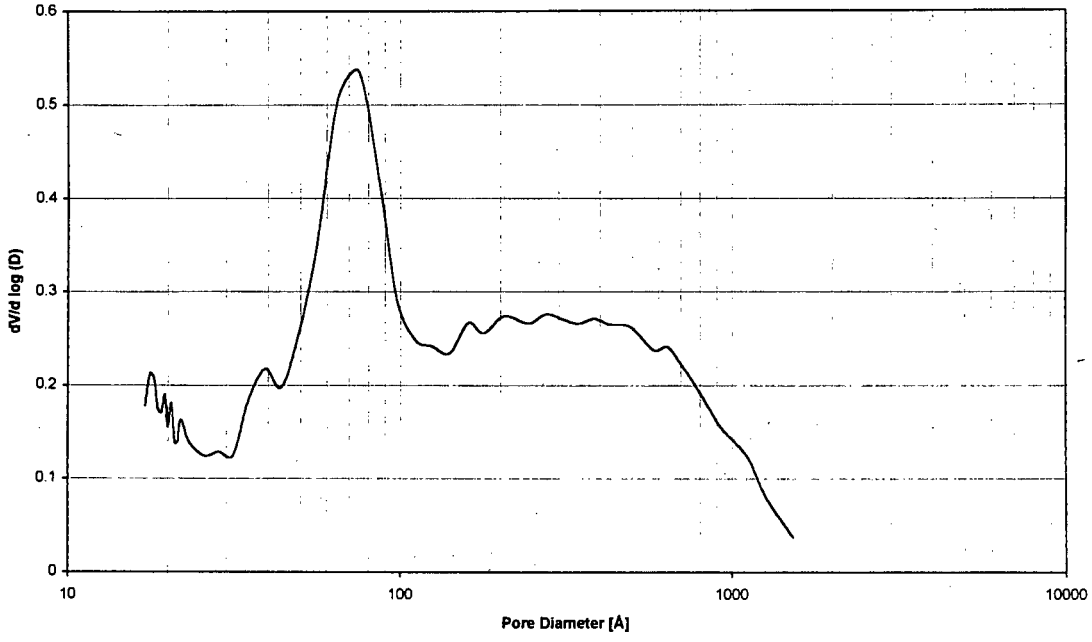

Sample S400

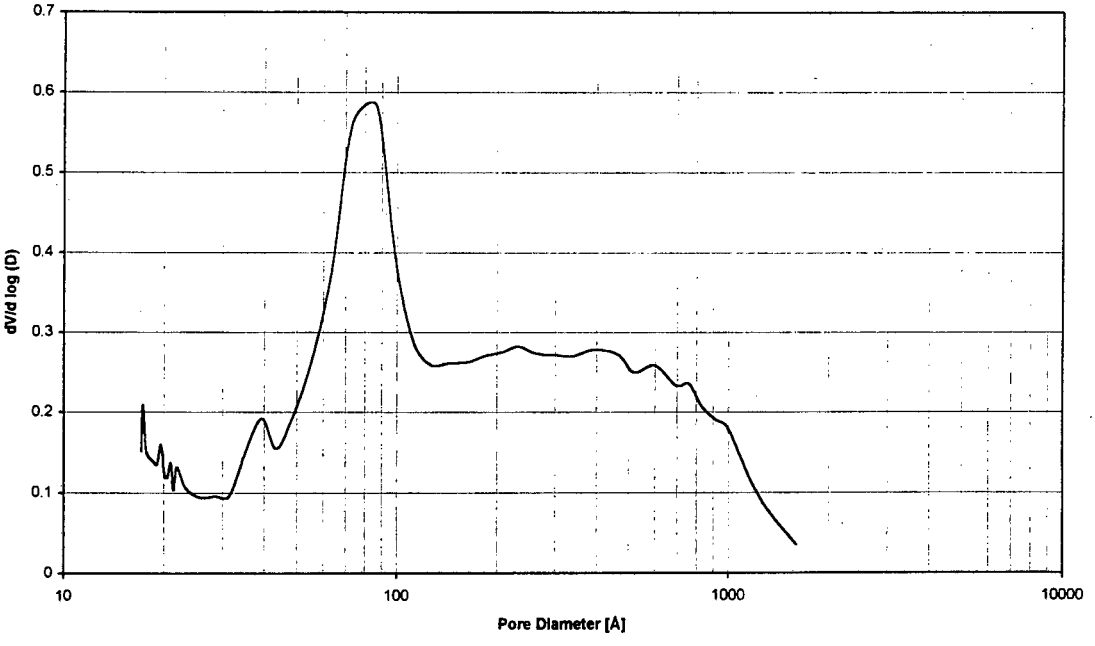

Sample S600

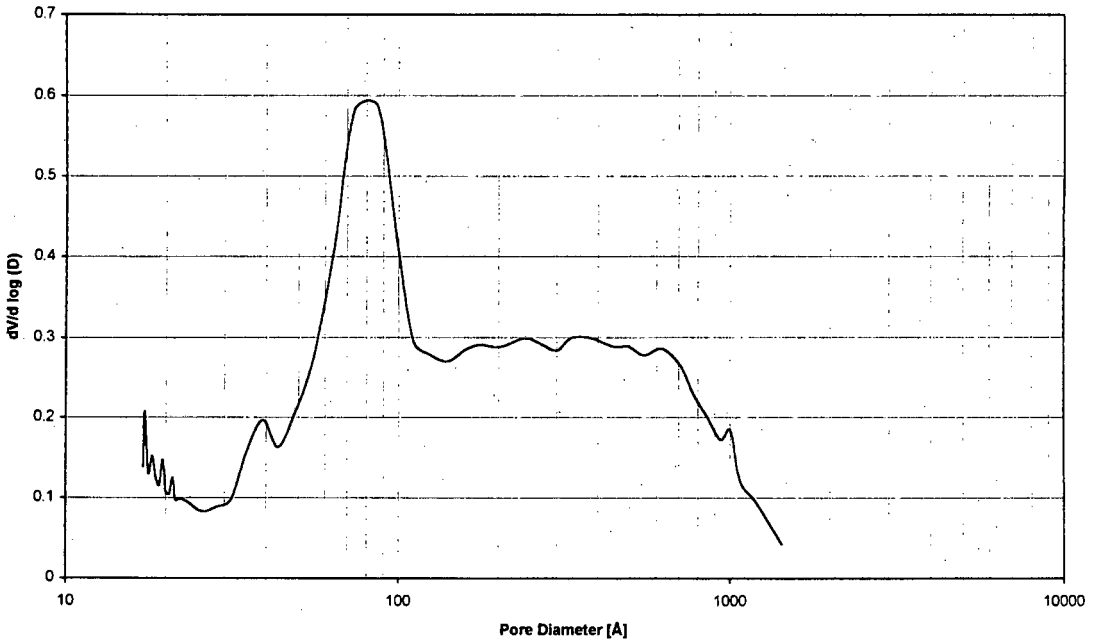

Sample S600(1)

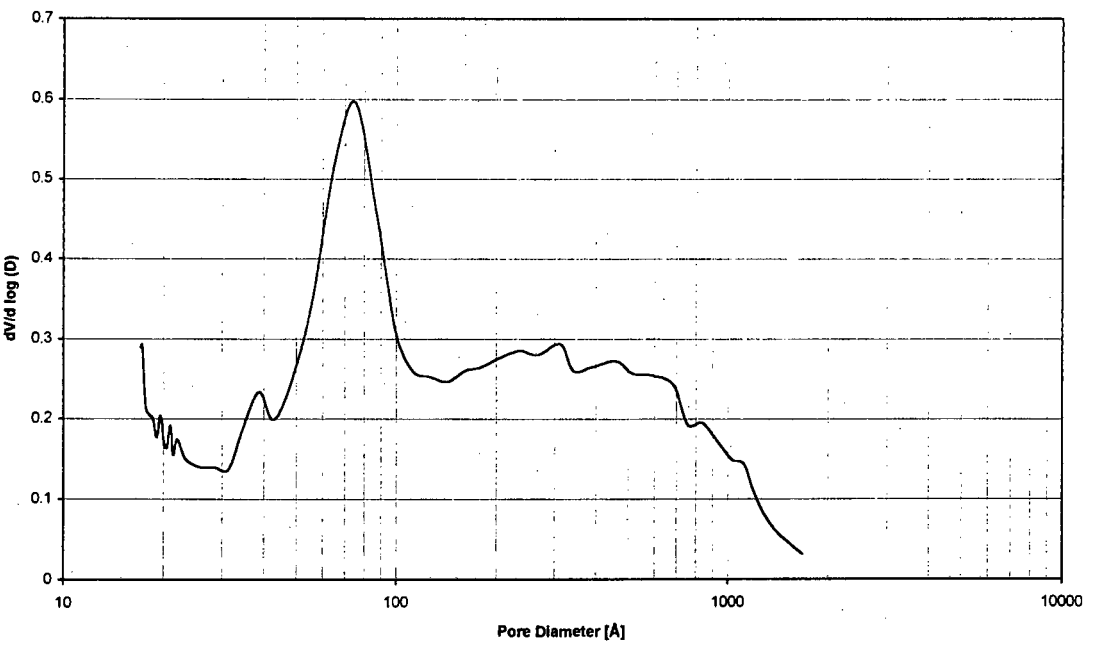

Sample L400

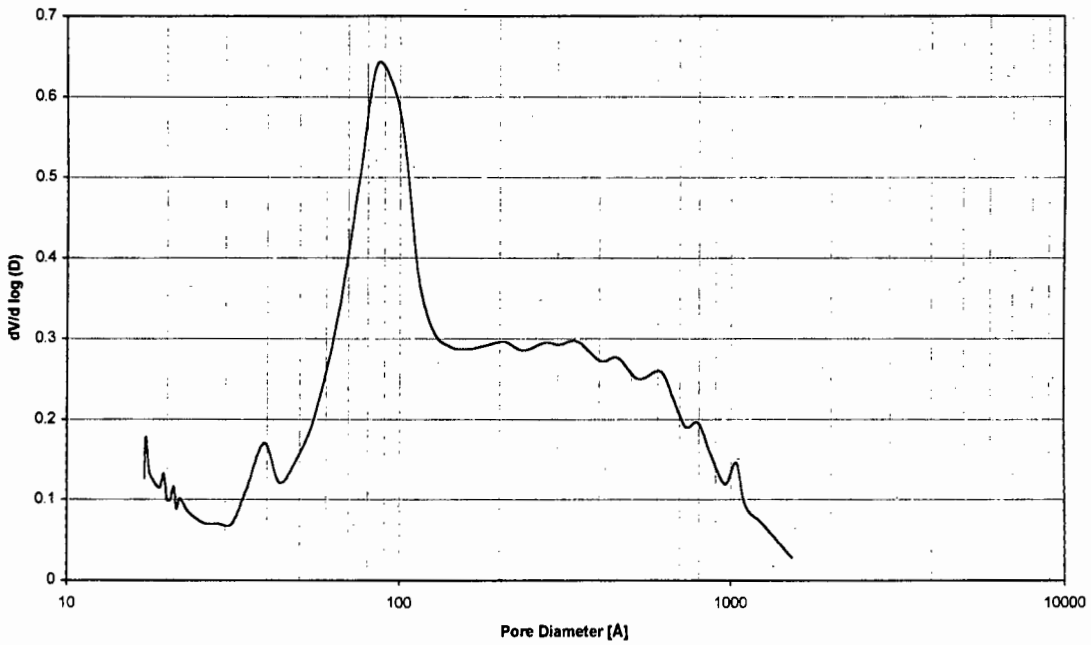

Sample L600

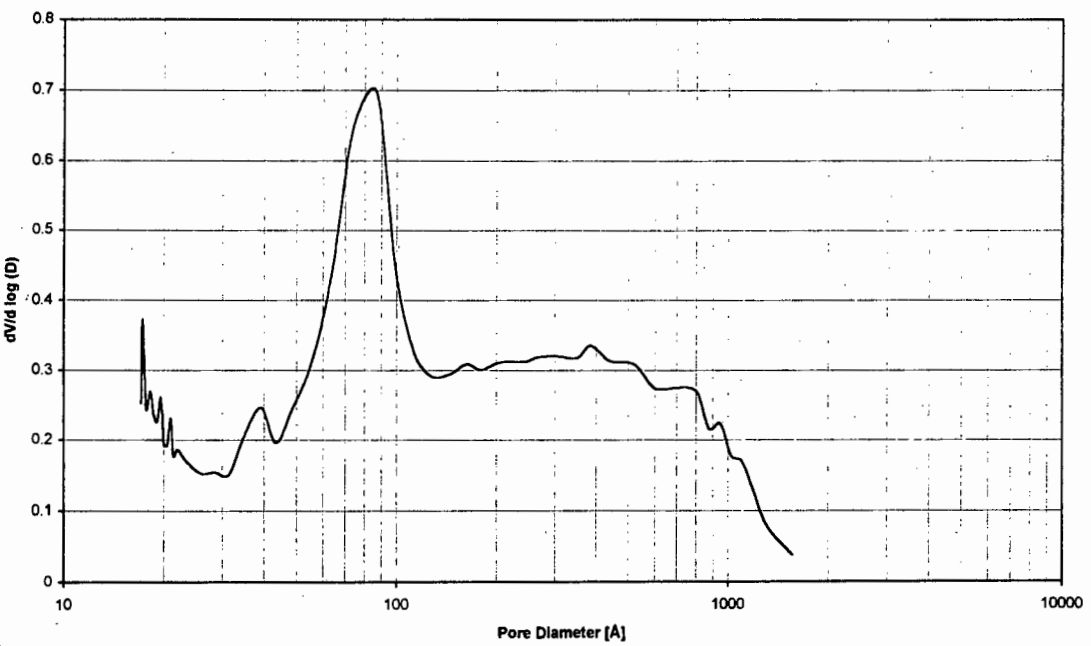

Sample A0.1

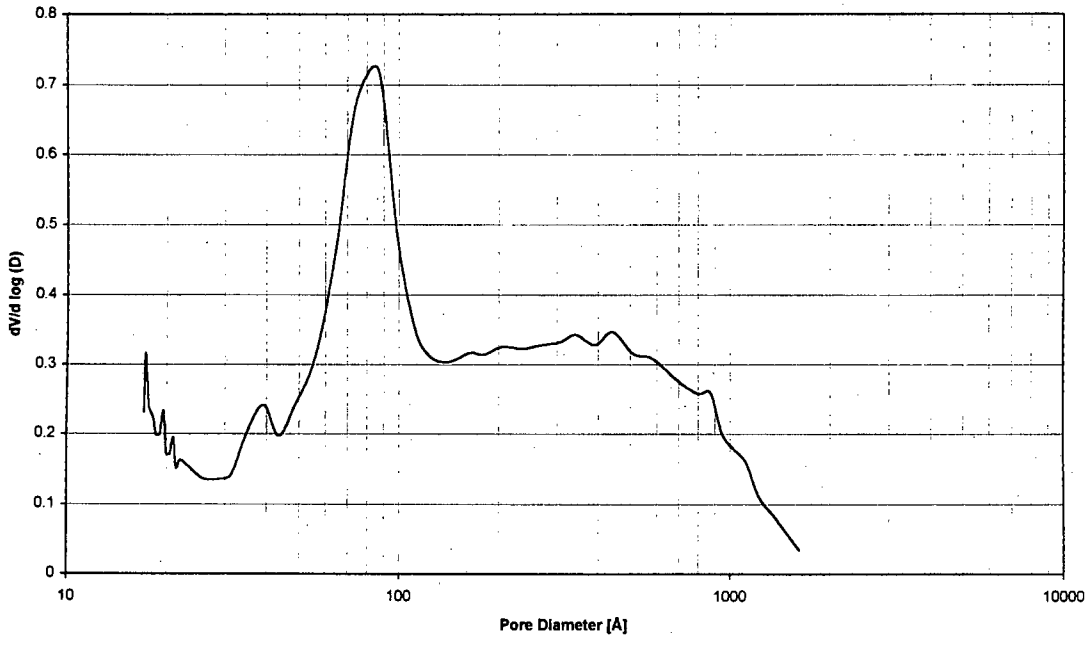

Sample A1

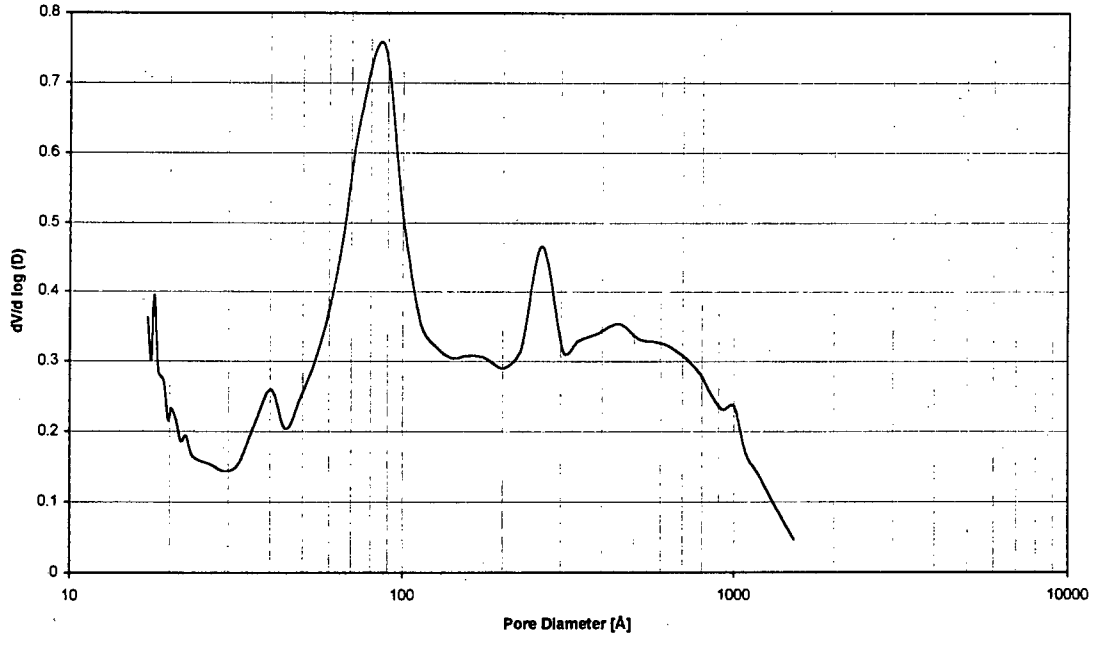

Sample A10

APPENDIX F

^{29}Si MAS NMR spectra

^{29}Si MAS NMR Spectra

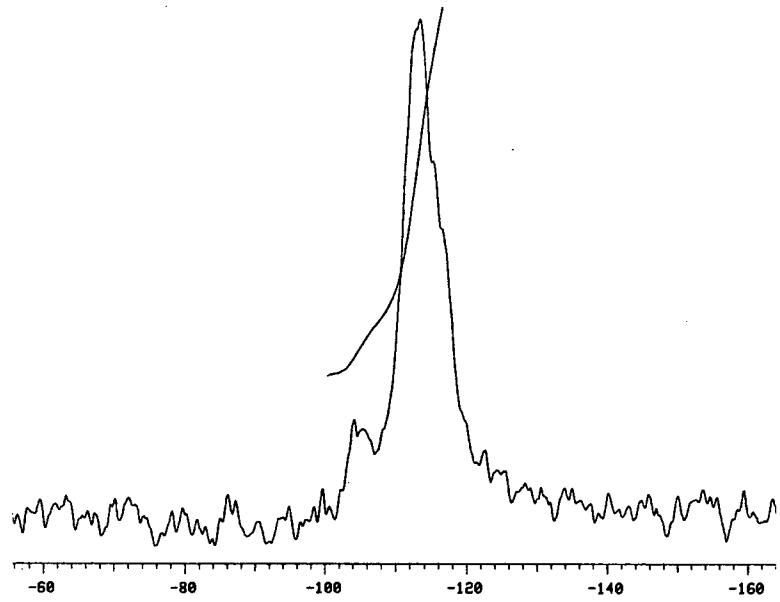

Sample A0.01

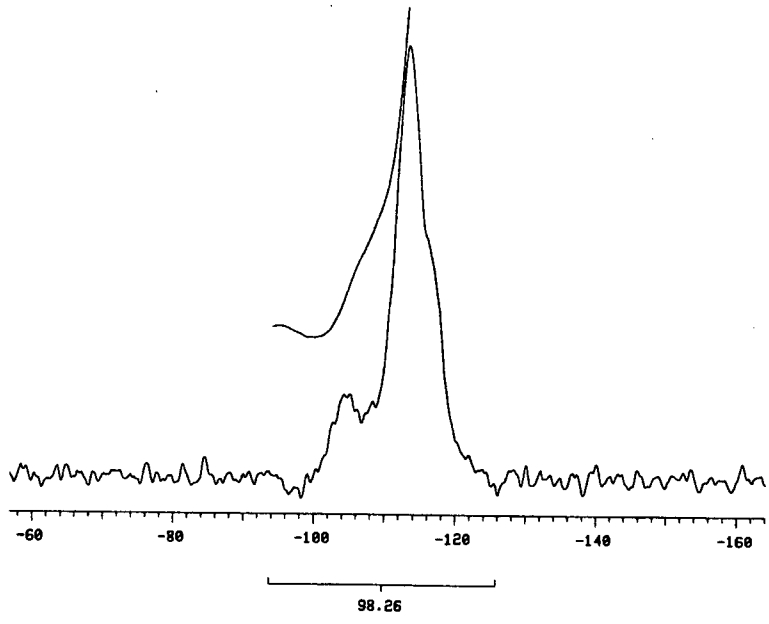

Sample A0.1

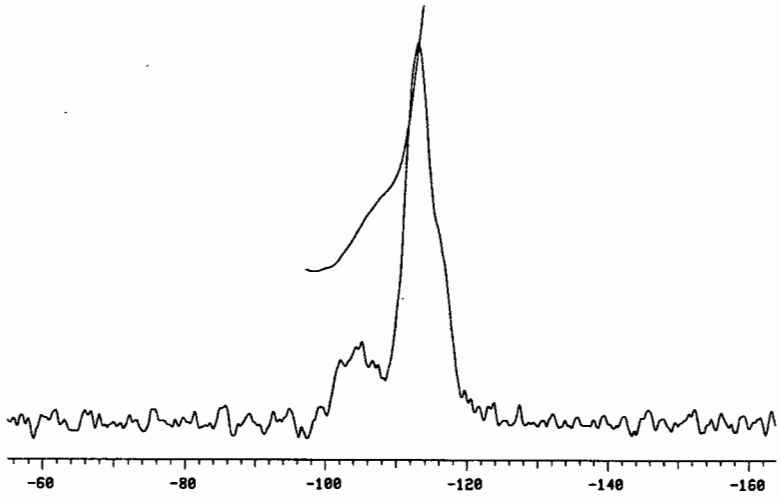

Sample A1

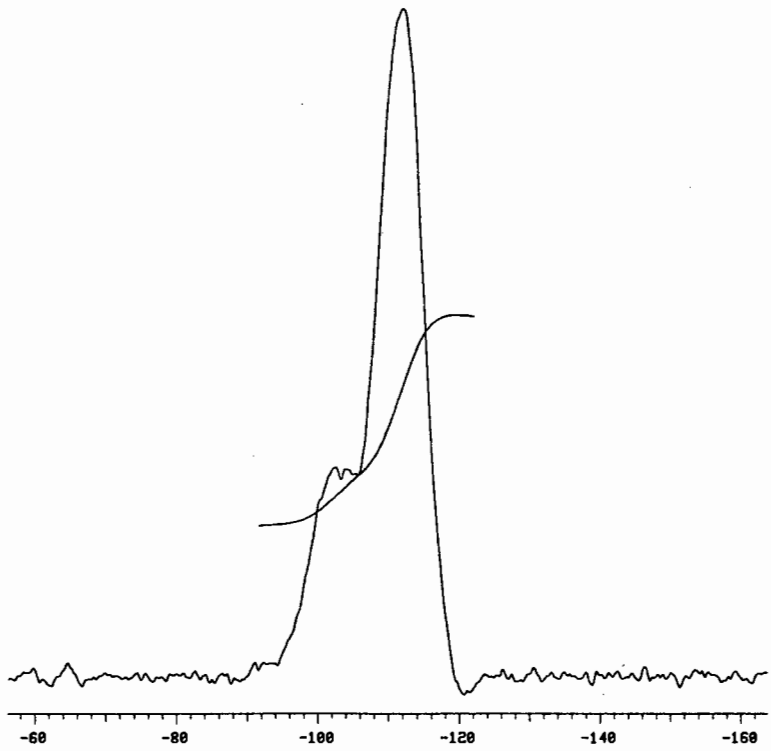

Sample A10

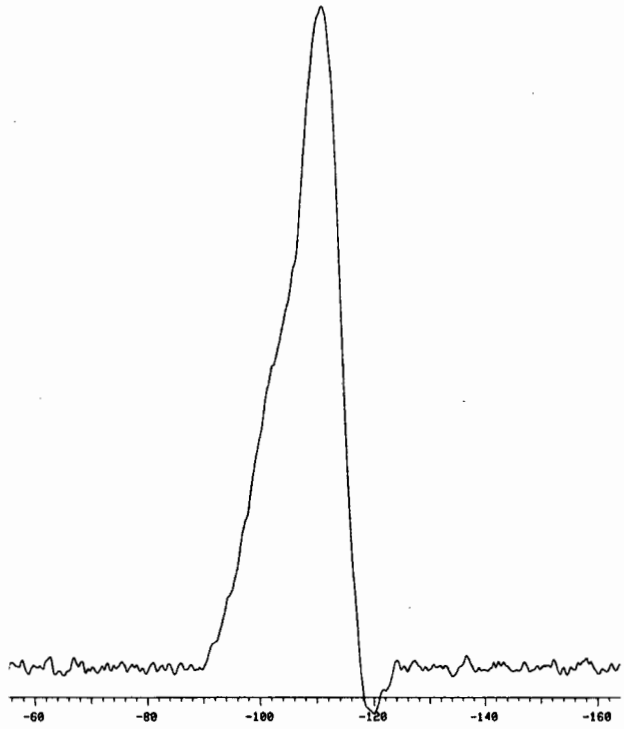

Sample L400/A0.01

APPENDIX G

^{27}Al MAS NMR spectra

^{27}Al MAS NMR Spectra

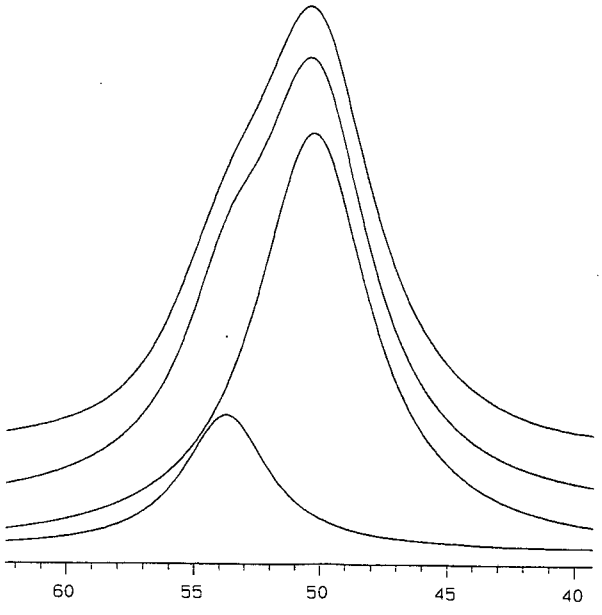

Sample B

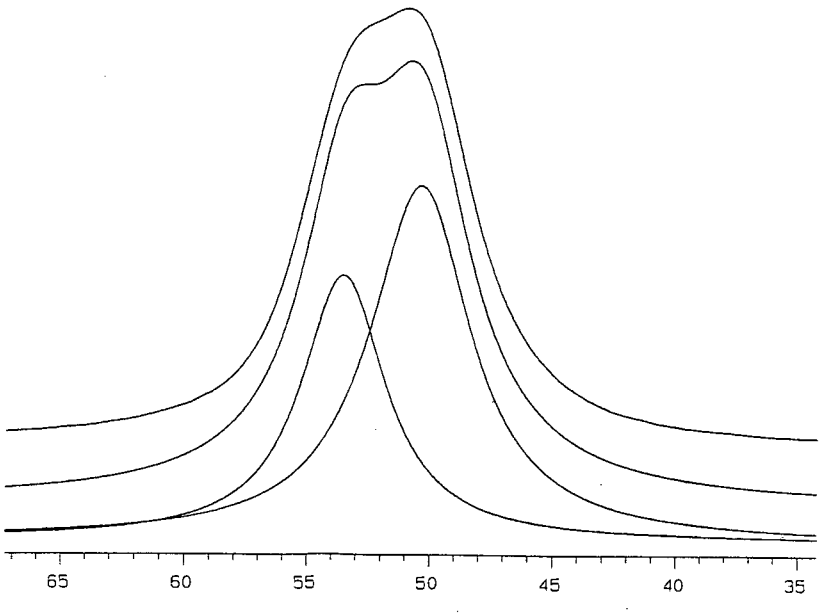

Sample D

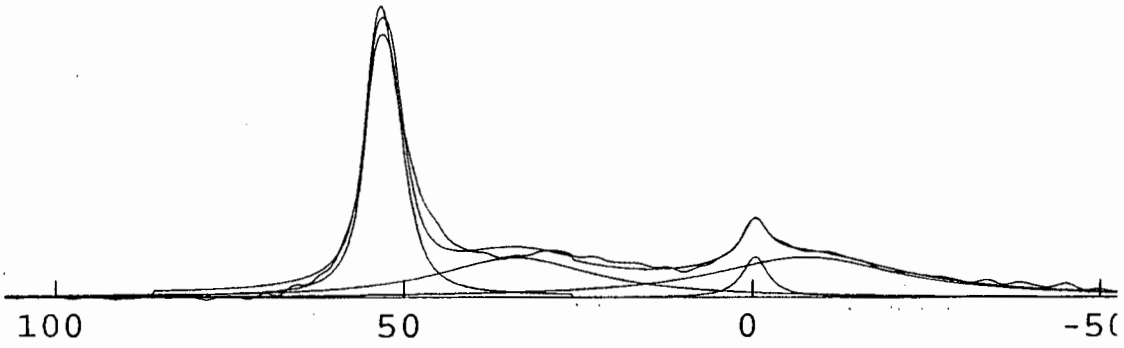

Sample S600

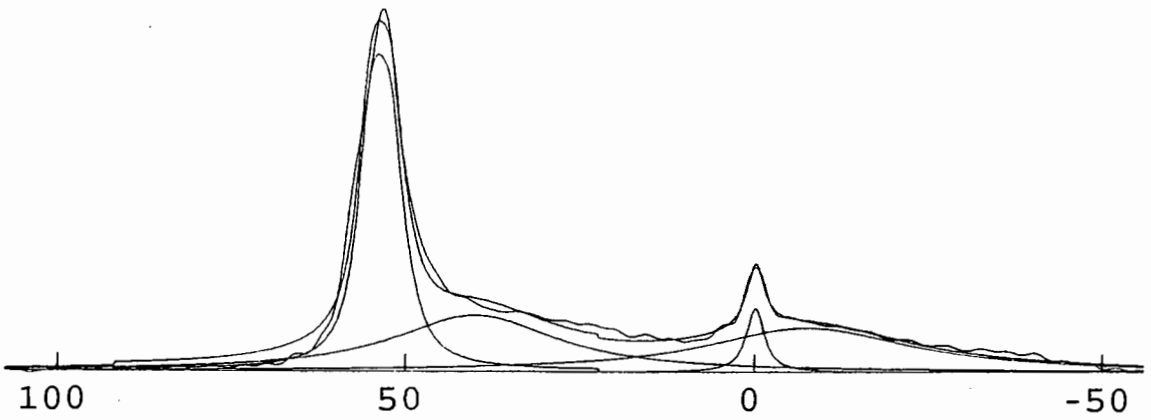

Sample L400

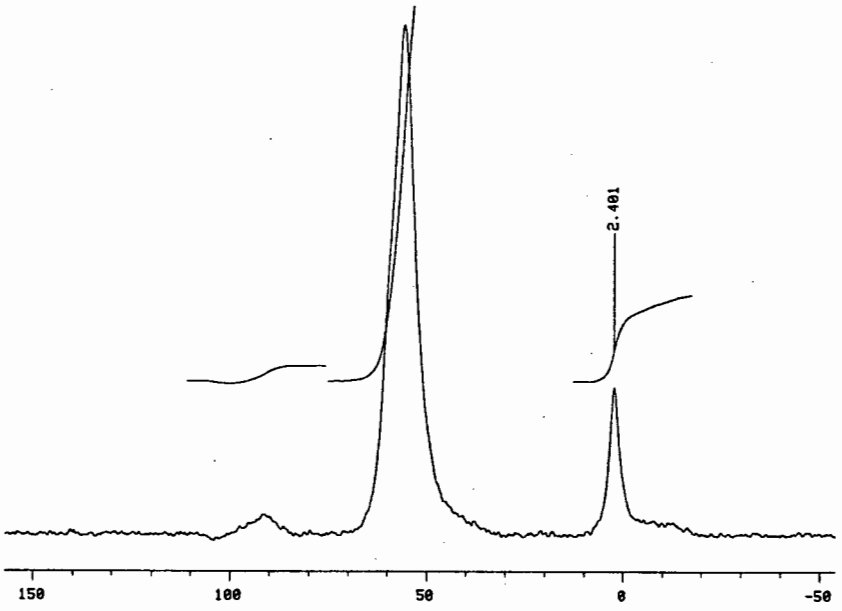

Sample A0.01

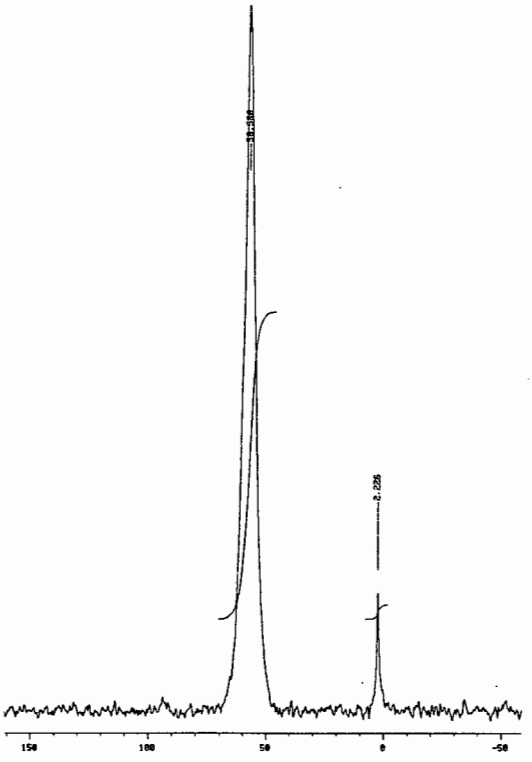

Sample A1

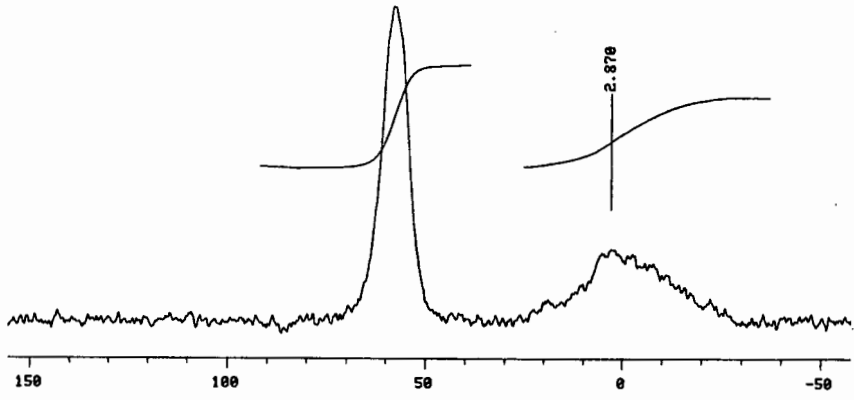

Sample A10

APPENDIX H

Sample calculation of concentration of aluminium species from ^{27}Al MAS NMR and AAS

Sample calculation of concentration of aluminium species from ^{27}Al MAS NMR and AAS (S400)

From AAS, bulk Si/Al ratio (R) = 10.8

The unit cell formula of the sodium form of zeolite Beta is:

$Na_n[Al_nSi_{64-n}O_{128}]$ n<7 (Meier *et al.*, 1996)

Therefore, in a unit cell, Si + Al = 64

$\Rightarrow (R \times Al) + Al = 64$

$\Rightarrow Al \times (R + 1) = 64$

$\Rightarrow$ Al/uc = $64/(R + 1)$

For S400, total Al/uc = $64/(10.8 + 1)$ = 5.4

Table H.1 shows the %area under the peaks corresponding to the different aluminium species present in S400.

Table H.1. %area under peaks assigned to different aluminium species in S400.

Peak position [ppm]	Assignment	%area
57.25	Framework Al	44.16
39.07	EFAl-4/Al-5	29.79
-0.09	EFAl-6	4.30
-7.49	EFAl-x	21.76

Thus,

Framework Al/uc = 0.4416×5.4 = 2.4

(EFAl-4/Al-5)/uc = 0.2979×5.4 = 1.6

EFAl-6/uc = 0.043×5.4 = 0.2

EFAl-x/uc = 0.2176×5.4 = 1.2

APPENDIX I

TPD Spectra

TPD Spectra

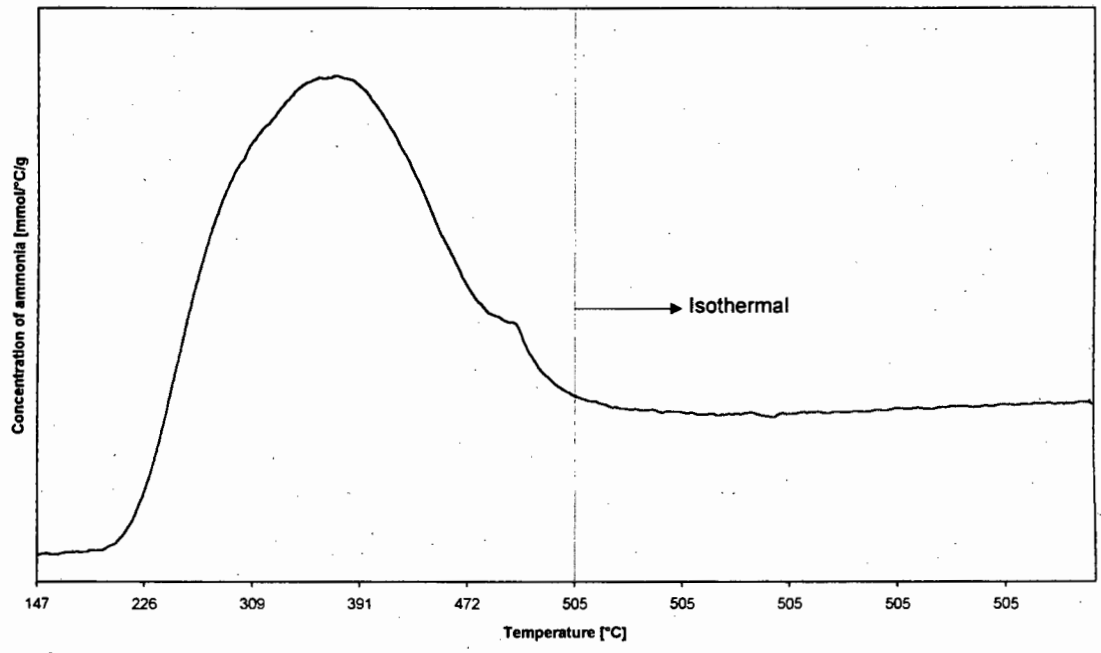

Sample D

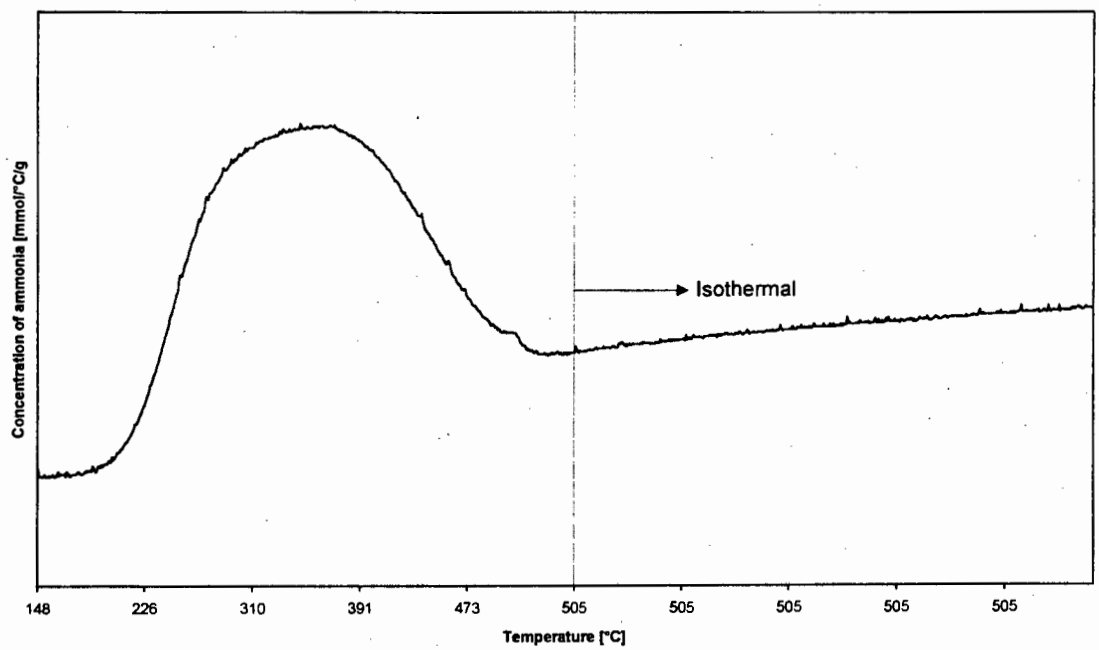

Sample E

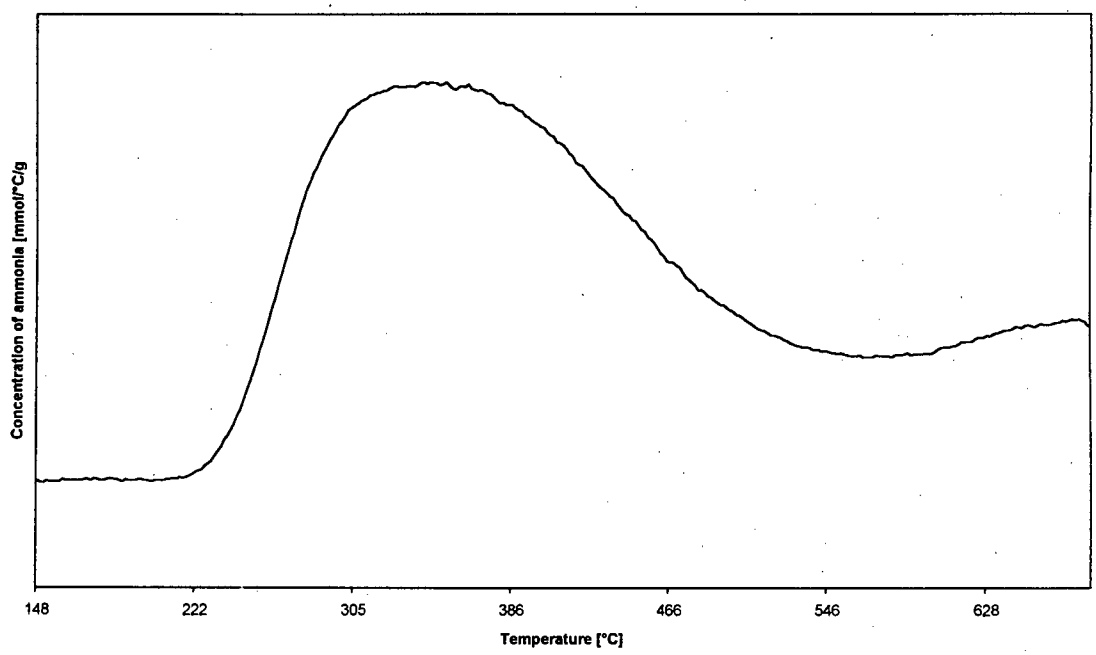

Sample F

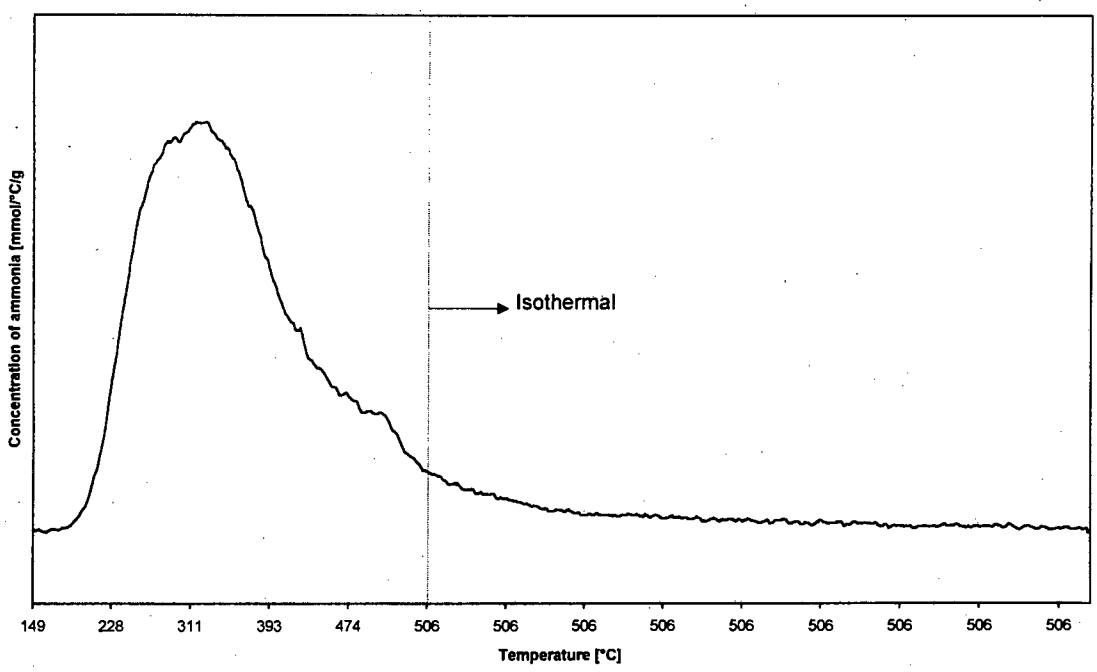

Sample S600

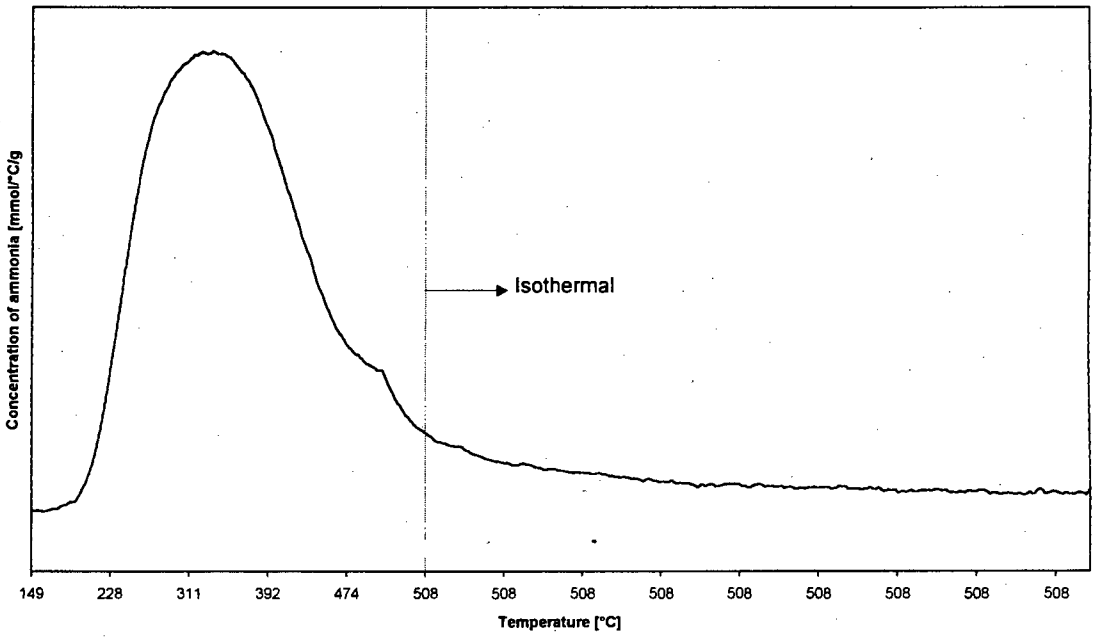
Concentration of ammonia [mmol/°C/g
Isothermal
149
228
311
392
474
508
508
508
508
508
508
508
508
508
Temperature [°C]

Sample L400